

# Insights on the formation and fate of organic nitrates in the atmosphere from field and laboratory observations

Thesis by  
Alexander Pai-chung Teng

In Partial Fulfillment of the Requirements for the  
degree of  
Doctor of Philosophy

CALIFORNIA INSTITUTE OF TECHNOLOGY  
Pasadena, California

2017  
Defended February 22, 2017

© 2017

Alexander Pai-chung Teng  
ORCID: 0000-0002-6434-0501

All rights reserved except where otherwise noted

## ACKNOWLEDGEMENTS

I would like to first acknowledge my advisor, Paul Wennberg. It has been a pleasure working with you, learning from you, and laughing with you! You have provided invaluable guidance, insight, and great opportunities for growth! Thanks for the trip to Korea! Being a grad student in your lab was like being taken on a wild tour of the atmosphere!

I also want to thank John Crouse, whose tireless help, guidance, and mentoring taught me so much about what it means to be a scientist and how to succeed in the field!

Jason St. Clair: thanks for the many words of advice and the many hours spent training me!

Mom, Dad, Grandmom, Mike, Robin, thank you for feeding me and keeping me on track! I made it with all of your food, love, and laughter!

Rebecca, thank you for the unwavering support! You prompted me to start this journey, and I'm glad we finished it together!

## ABSTRACT

Alkenes are oxidized rapidly in the atmosphere by addition of OH and subsequently O<sub>2</sub>, leading to the formation of peroxy radicals. These peroxy radicals react with NO to form organic nitrates through a minor radical-terminating branching pathway. Over large regions of the continental boundary layer, the formation of organic nitrates control tropospheric ozone and the lifetime of NO<sub>x</sub>. Laboratory investigations described herein show that the yield of nitrates through this pathway is larger than previously described for alkenes, and the yield increases with the number of heavy atoms. This result is used to interpret field observations taken over Houston in the summer of 2013. These measurements show that small alkenes still play a large role in ozone production more than a decade after they had been identified as a causal factor.

In further studies, measurements of isoprene hydroxy nitrates (ISOPN) and hydroperoxides, formed from the OH oxidation of isoprene, are used to diagnose the complexities of reversible O<sub>2</sub> addition for allylic hydroxy isoprene radicals. It is shown that over most of the atmosphere, isoprene's peroxy radical isomers are in their equilibrium distribution. In this regime, hydroxy peroxy radical isomers comprise approximately 95% of the radical pool, a much higher fraction than in the nascent (kinetic) distribution. Intramolecular H-shift isomerization from the Z hydroxy peroxy radical isomers produced from OH addition to C<sub>4</sub> is estimated to be 4 s<sup>-1</sup> at 297K. While the Z isomer is initially produced in low yield, it is continually reformed via decomposition of the hydroxy peroxy radicals. As a result, unimolecular chemistry from this isomer contributes as much as half of the atmospheric fate of the entire pool of peroxy radicals formed via addition of OH at C<sub>4</sub>. In contrast, unimolecular chemistry following OH addition at C<sub>1</sub> is slower and less important.

Field observations of alkyl nitrates over the Southeastern United States during the summer over forested environments show that there are still gaps in our understanding of the organic nitrate budget. The formation of isoprene hydroxy nitrates (ISOPN) is shown to be a dominant NO<sub>x</sub> loss pathway during the day.

## PUBLISHED CONTENT AND CONTRIBUTIONS

Teng, A. P., J. D. Crouse, Nguyen T. B., et al. (2017). “Formation and Fate of Organic Nitrates in the Southeastern United States”. In: *In preparation*.

APT participated in the conception of the project, conducted the experiments in collaboration with authors, prepared the data, and wrote the manuscript.

Teng, Alexander P, John D Crouse, and Paul O Wennberg (2017). “Isoprene peroxy radical dynamics”. In: *Journal of the American Chemical Society* 139.15, pp. 5367–5377. DOI: 10.1021/jacs.6b12838. URL: <http://doi.org/10.1021/jacs.6b12838>.

APT participated in the conception of the project, conducted the experiments in collaboration with authors, prepared the data, and wrote the manuscript.

Bates, Kelvin H et al. (2016). “Production and fate of C4 dihydroxycarbonyl compounds from isoprene oxidation”. In: *The Journal of Physical Chemistry A* 120.1, pp. 106–117. DOI: 10.1021/acs.jpca.5b10335. URL: <http://doi.org/10.1021/acs.jpca.5b10335>.

APT participated in performing experiments.

Bela, Megan M et al. (2016). “Wet scavenging of soluble gases in DC3 deep convective storms using WRF-Chem simulations and aircraft observations”. In: *Journal of Geophysical Research: Atmospheres* 121.8, pp. 4233–4257. DOI: 10.1002/2015JD024623. URL: <http://doi.org/10.1002/2015JD024623>.

APT participated in the data collection and data preparation.

Fisher, Jenny A et al. (2016). “Organic nitrate chemistry and its implications for nitrogen budgets in an isoprene-and monoterpene-rich atmosphere: constraints from aircraft (SEAC 4 RS) and ground-based (SOAS) observations in the Southeast US”. In: *Atmospheric Chemistry and Physics* 16.9, pp. 5969–5991. DOI: 10.5194/acp-16-5969-2016. URL: <http://doi.org/10.5194/acp-16-5969-2016>.

APT participated in the data collection and data preparation.

Kaiser, J et al. (2016). “Speciation of OH reactivity above the canopy of an isoprene-dominated forest”. In: *Atmospheric Chemistry and Physics* 16.14, pp. 9349–9359. DOI: 10.5194/acp-16-9349-2016. URL: <http://doi.org/10.5194/acp-16-9349-2016>.

APT participated in the data collection and data preparation.

Nguyen, Tran B, Geoffrey S Tyndall, et al. (2016). “Atmospheric fates of Criegee intermediates in the ozonolysis of isoprene”. In: *Physical Chemistry Chemical Physics* 18.15, pp. 10241–10254. DOI: 10.1039/C6CP00053C. URL: <http://doi.org/10.1039/C6CP00053C>.

APT participated in the data collection and data preparation.

Romer, Paul S et al. (2016). “The lifetime of nitrogen oxides in an isoprene-dominated forest”. In: *Atmospheric Chemistry and Physics* 16.12, pp. 7623–7637. DOI: 10.5194/acp-16-7623-2016. URL: <http://doi.org/10.5194/acp-16-7623-2016>.

APT participated in the data collection and data preparation.

Ayres, BR et al. (2015). “Organic nitrate aerosol formation via NO<sub>3</sub>+ biogenic volatile organic compounds in the southeastern United States”. In: *Atmospheric Chemistry and Physics* 15.23, pp. 13377–13392. DOI: 10.5194/acp-15-13377-2015. URL: <http://doi.org/10.5194/acp-15-13377-2015>.

APT participated in the data collection and data preparation.

Kim, PS et al. (2015). “Sources, seasonality, and trends of southeast US aerosol: an integrated analysis of surface, aircraft, and satellite observations with the GEOS-Chem chemical transport model”. In: *Atmospheric Chemistry and Physics* 15.18, pp. 10411–10433. DOI: 10.5194/acp-15-10411-2015. URL: <http://doi.org/10.5194/acp-15-10411-2015>.

APT participated in the data collection and data preparation.

Nguyen, Tran B, John D Crouse, et al. (2015). “Rapid deposition of oxidized biogenic compounds to a temperate forest”. In: *Proceedings of the National Academy of Sciences* 112.5, E392–E401. DOI: 10.1073/pnas.1418702112. URL: <http://doi.org/10.1073/pnas.1418702112>.

APT participated in the data collection and data preparation.

Schwantes, Rebecca H et al. (2015). “Isoprene NO<sub>3</sub> Oxidation Products from the RO<sub>2</sub>+ HO<sub>2</sub> Pathway”. In: *The Journal of Physical Chemistry A* 119.40, pp. 10158–10171. DOI: 10.1021/acs.jpca.5b06355. URL: <http://doi.org/10.1021/acs.jpca.5b06355>.

APT participated in experimental design, experiment execution, data preparation.

St. Clair, Jason M et al. (2015). “Kinetics and products of the reaction of the first-generation isoprene hydroxy hydroperoxide (ISOPOOH) with OH”. In: *The Journal of Physical Chemistry A* 120.9, pp. 1441–1451. DOI: 10.1021/acs.jpca.5b06532. URL: <http://doi.org/10.1021/acs.jpca.5b06532>.

APT participated in performing experiments.

Teng, A. P., J. D. Crouse, L. Lee, et al. (2015). “Hydroxy nitrate production in the OH-initiated oxidation of alkenes”. In: *Atmospheric Chemistry and Physics* 15.8, pp. 4297–4316. DOI: 10.5194/acp-15-4297-2015. URL: <http://www.atmos-chem-phys.net/15/4297/2015/>.

APT participated in the conception of the project, conducted the experiments in collaboration with authors, prepared the data, and wrote the manuscript.

Wolfe, GM et al. (2015). “Quantifying sources and sinks of reactive gases in the lower atmosphere using airborne flux observations”. In: *Geophysical Research Letters* 42.19, pp. 8231–8240. DOI: 10.1002/2015GL065839. URL: <http://doi.org/10.1002/2015GL065839>.

APT participated in the data collection and data preparation.

Lee, Lance et al. (2014). “On rates and mechanisms of OH and O<sub>3</sub> reactions with isoprene-derived hydroxy nitrates”. In: *The Journal of Physical Chemistry A* 118.9, pp. 1622–1637. DOI: 10.1021/jp4107603. URL: <http://doi.org/10.1021/jp4107603>.

APT participated in the execution of experiments and data preparation.

Nguyen, TB et al. (2014). “Overview of the Focused Isoprene eXperiment at the California Institute of Technology (FIXCIT): mechanistic chamber studies on the oxidation of biogenic compounds”. In: *Atmospheric Chemistry and Physics* 14.24, pp. 13531–13549. DOI: 10.5194/acp-14-13531-2014. URL: <http://doi.org/10.5194/acp-14-13531-2014>.

APT participated in experimental design and execution of experiments.

## TABLE OF CONTENTS

Acknowledgements . . . . .	iii
Abstract . . . . .	iv
Published Content and Contributions . . . . .	v
Table of Contents . . . . .	viii
List of Illustrations . . . . .	ix
List of Tables . . . . .	xviii
Chapter I: Introduction . . . . .	1
Chapter II: Hydroxy nitrate production in the OH-initiated oxidation of alkenes . . . . .	6
2.1 Introduction . . . . .	6
2.2 Materials and methods . . . . .	7
2.3 Results and discussion . . . . .	14
2.4 Atmospheric chemistry implications . . . . .	31
2.5 Conclusion . . . . .	33
2.6 Uncertainties and Box Modeling . . . . .	33
Chapter III: Isoprene peroxy radical dynamics . . . . .	43
3.1 Introduction . . . . .	43
3.2 Experimental Methods . . . . .	46
3.3 Results and Discussion . . . . .	52
3.4 Distribution of Isoprene Peroxy Radicals at Longer $\tau$ . . . . .	55
3.5 Isoprene Peroxy Radical Dynamics in the Atmosphere . . . . .	64
Chapter IV: Formation and Fate of Organic Nitrates in the Southeastern United States . . . . .	70
4.1 Introduction . . . . .	70
4.2 Experimental . . . . .	73
4.3 Results and discussion . . . . .	76
4.4 Conclusions . . . . .	85
4.5 Acknowledgements . . . . .	87
Chapter V: Outlook . . . . .	103
Bibliography . . . . .	106
Appendix A: Supporting Information for Chapter 4: Isoprene Peroxy Radical Dynamics . . . . .	109
Appendix B: Supporting Information for Chapter 5: Formation and Fate of Organic Nitrates in the Southeastern United States . . . . .	151

## LIST OF ILLUSTRATIONS

<i>Number</i>	<i>Page</i>
2.1	
Reaction pathways of alkenes with OH. OH oxidation with alkenes follows two pathways: OH addition ( $f_n$ and $f_{n+1}$ ) and H-abstraction ( $f_{ab}$ , where $f_{ab} = \sum_{n=1}^l f_{abn}$ ). $f_a + f_{ab} = 1$ . Subscripts indicate the carbon number at which either OH addition or abstraction occurs. For alkenes studied in this work at room temperature, the sum of $f_{an}$ and $f_{an+1}$ is much greater than $f_{ab}$ . See text for further discussion of estimations for $f_{ab}$ . . . . .	15
2.2	
$\beta$ -hydroxy nitrate products produced from six alkenes during Exp. 19. The top panel shows the ratio of CIMS hydroxy nitrate (HN) signals to propene HN ( $206 m/z$ ) for ethene HN ( $192 m/z$ , blue), methylpropene HN ( $220 m/z$ , red), 2-methyl,2-butene HN ( $234 m/z$ , teal), 1-hexene HN ( $248 m/z$ , purple), and 1-octene HN ( $276 m/z$ , gold). The bottom panel shows the absolute signal for propene HN ( $206 m/z$ ). The lights were turned on at time = 0, and turned off at 7 min (vertical line), at which point the oxidation stopped. For all compounds other than hydroxy nitrates from 1-octene, a ratio is plotted as a dashed line using averaged data from 3 min after lights until the measurements stopped. For hydroxy nitrates from 1-octene, data after 10 min are averaged. The time lag for hydroxy nitrates from 1-octene arises from wall and sample line equilibration. This suggests that the measured yield is a lower limit. . . . .	16
2.3	
GC-CIMS/TD-LIF chromatogram following Exp. 15. The signals due to individual hydroxy nitrates are determined by integrating the alkyl nitrate peaks (black line, elevated baseline) which co-elute with the individual hydroxy nitrates observed by CIMS, e.g., hydroxy nitrates from 1-butene at $220 m/z$ (blue) and from 1-hexene at $248 m/z$ . Absolute CIMS sensitivities are determined by integrating individual peaks for CIMS signal and TD-LIF signal and dividing. The assigned chemical structures are shown for each alkyl nitrate peak. 17	17

- 2.4 The isomer-averaged branching ratios,  $\alpha$ , derived in this study (blue boxes, data from Table 2.4), compared to previously published nitrate branching ratios (Arey et al., 2001 with pink exes; O'Brien et al., 1998 with green stars). Alkene nitrate yields from O'Brien et al., 1998 have been normalized by  $f_a$  to account for H-abstraction channel in the same fashion as this study. The error weighted fit derived from Fig. 2.4 is shown for hydroxy nitrate branching ratios (black dotted line) from all measured alkenes yields a slope of  $0.045 \pm 0.016$  and intercept of  $-0.11 \pm 0.05$  (errors are  $2\sigma$ ). This fit agrees well with the relationship derived by Arey et al., 2001, who calculated a slope of  $0.0381 \pm 0.0016$  and an intercept of  $-0.073 \pm 0.009$  for *n*-alkanes. 21
- 2.5 Alkoxy H-shift isomerization leading to dihydroxy nitrate formation for 1-hexene. . . . . 22
- 2.6 A chromatographic separation of hydroxy nitrates formed from a set of alkenes in Experiment 19. 192 *m/z* = ethene hydroxy nitrate, 206 *m/z* = propene hydroxy nitrate; 220 *m/z* = methylpropene hydroxy nitrate; 234 *m/z* = 2-methyl 2-butene hydroxy nitrate; 248 *m/z* = 1-hexene hydroxy nitrate; 276 *m/z* = 1-octene hydroxy nitrate. Isomer distributions were determined based on integrating peak areas from chromatograms. The later eluting peaks are prone to tailing and co-elution. In such cases, Gaussian peaks shapes were used to deconvolute co-eluting isomers and the trailing tail was assigned to the later eluting peak. . . . . 23
- 2.7 The measured isomer distribution of propene hydroxy hydroperoxides (blue boxes) as a function of the initial alkene OH reactivity and the initial hydrogen peroxide concentration. The red line represents the alkene OH reactivity regime over which hydroxy hydroperoxide isomer distributions were reported for all alkenes other than propene. The dashed black line represents a kinetic box model simulation designed to study the maximum impact  $RO_2 + RO_2$  chemistry might have on the isomer distributions. See Chapter 2.6 for further details on the kinetic model. . . . . 24

- 2.8 Atmospheric hydroxy nitrate,  $O_3$  and formaldehyde data measured in the Houston plume from the 2013 SEAC4RS campaign. The lower right panel shows how each hydroxy nitrate contributes to the total hydroxy nitrate measured by the Caltech CIMS for the data taken from a flight over Houston on 18 September 2013. As the plane crosses into the Houston plume, hydroxy nitrates derived from anthropogenic emissions are enhanced. The upper right panel shows formaldehyde (black, left axis) and ozone (red, right axis) are strongly correlated with anthropogenically derived hydroxy nitrates. Additionally, the lower bound estimates for the formaldehyde directly attributable to oxidation of each alkene in-plume using the branching ratios derived in this study are shown in colors. For ethene, the contribution is adjusted to produce two formaldehyde molecules after alkoxy decomposition, and uses a decomposition yield of 0.8 to account for glycolaldehyde formation from reaction of the alkoxy radical reaction with  $O_2$ . For isoprene hydroxy nitrate, a branching ratio estimate of 0.12 was used (Paulot et al., 2009). It was assumed that the sum of methyl vinyl ketone hydroxy nitrate (MVKN) and methacrolein hydroxy nitrate (MACRN) are exclusively derived from isoprene hydroxy nitrates with a yield of 1 formaldehyde per each isoprene HN oxidized to form a MVKN or MACRN molecule (Lee et al., 2014), and, therefore, a branching ratio estimate of 0.11 was used. Ozone observations were provided courtesy of Ryerson, Pollack, and Peischl at NOAA ESRL. Formaldehyde observations provided courtesy of Hanisco and Wolfe at NASA. The left panel graphs the flight tracks for this section of the flight colored by the lower bound estimate of formaldehyde formed from oxidation of alkenes. Satellite image courtesy of NASA's AERONET. . . . . 26
- 2.9 A graph showing the  $NO_2$  recovery as a function of temperature. The  $NO_2$  recovery with addition of  $O_2$  in the TD-LIF is shown in red, and in black is  $NO_2$  recovery without addition of  $O_2$ . Conversion of isopropyl nitrate is 100 % in the TD-LIF. . . . . 37
- 2.10 Cold trapping eliminates hydroxy hydroperoxides, removing an interference to the measured acetone. . . . . 39

- 3.1 Isoprene is emitted to the atmosphere in enormous quantities by deciduous trees. Its oxidation by addition of OH radicals (here shown adding to C<sub>4</sub>) initiates a complex dynamical system coupling allylic and peroxy radicals. The impact of this chemistry on atmospheric oxidants and aerosol depends on the fate of the many peroxy radical isomers (RO<sub>2</sub>) formed. Reaction with NO leads to ozone (O<sub>3</sub>) formation; a small, but important, branch yields organic nitrate and, thereby, removes NO<sub>x</sub> from the atmosphere. Reaction with HO<sub>2</sub> leads to hydroxy hydroperoxides (ISOPOOH) and subsequently to aerosol precursors. Finally, the Z- $\delta$  isomers undergo 1,6 H-shift isomerization leading to entirely different products including hydroperoxy aldehydes (HPALDs). As shown in this study, rapid interconversion between the and Z- $\delta$  isomers occurs allowing the H-shift pathway to account for a substantial fraction of the oxidation despite the very low abundance of this RO<sub>2</sub> isomer. This pathway represents a much smaller sink for HO<sub>x</sub> (HO<sub>x</sub>  $\equiv$  OH + HO<sub>2</sub>) than does the pathway forming ISOPOOH. Photo credit: John van der Woude. . . . . 44
- 3.2 Two separate systems of peroxy radicals are formed following OH addition to isoprene. Each of the six peroxy radicals react with NO to form carbonyls and hydroxynitrates or with HO<sub>2</sub> to form hydroperoxides. The Z- $\delta$  isomers also undergo 1,6 H-shift isomerization leading to formation of hydroperoxyaldehydes (HPALDs) and other compounds. Compounds in boxes are separated by gas chromatography and detected using CF<sub>3</sub>O<sup>-</sup> chemical ionization mass spectroscopy. This method is not sensitive to singly functional carbonyls such as methacrolein (MACR) or methyl vinyl ketone (MVK) produced following decomposition of the alkoxy radical products of RO<sub>2</sub> + NO. Parentheses around compounds refers to products resulting from an additional O<sub>2</sub> addition. . . . . 45

- 3.3 The peroxy radical isomer distribution is inferred from measurements of the ISOPN and ISOPOOH isomers. These isomers are separated using gas chromatography and detected as a cluster ion with  $\text{CF}_3\text{O}^-$  observed at  $m/z$  232 and  $m/z$  203, respectively. Shown here is an example chromatogram for ISOPN (experiment conducted at  $\tau_{\text{bimolecular}} = 0.009$  s). The  $\beta$  isomers elute first (1-OH, 2-N, in orange, 4-OH, 3-N in green) followed by the  $\delta$  isomers (*Z* 4-OH, 1-N in pink, *E* 4-OH, 1-N and *Z* 1-OH, 4-N (co-elute) in blue, and *E* 1-OH, 4-N in red). There is approximately 7% conversion of the 1-OH, 2-N to the *E* 1-OH, 4-N isomer during elution through the GC, causing an elevated baseline between these two peaks. The thin black line is the estimated contribution of the total ion signal from this conversion to the ISOPN signal. The last peak (yellow trace) is an unidentified compound. . . . . 50
- 3.4 The ratio of  $\delta$  (red *E*; black *Z*) to  $\beta$  ISOPN isomers formed at 297K shown as a function of the bimolecular lifetime of the  $\text{RO}_2$  radicals for the 1-OH system (top) and the 4-OH system (bottom). The dashed line represents simulation using the kinetic model described in the SI. The red open symbols in the bottom panel are measurements using the 1m megabore RTX-1701 column where the *E* 4-OH, 1-N and *Z* 1-OH, 4-N isomers co-elute. At  $\tau > 10$ s, multiple lines of evidence suggest that this peak is comprised almost entirely of *E* 4-OH, 1-N. The scatter in the points at similar  $\tau_{\text{bimolecular}}$  reflects the challenge in trapping and deconvolution of the ISOPN isomers (the sum of all nitrates is less than 70 pptv). This aspect of the analytical chemistry dominates the uncertainty in the ratio. Data for  $\tau_{\text{bimolecular}} < 0.01$ s is limited due to the challenge of  $\text{NO}_2$  chemistry which becomes important at these very high [NO]; it is not possible to reach this high reactivity with  $[\text{HO}_2]$  because its concentration is limited by self reaction (Eq. 2). . . . . 54

- 3.5 The ratio of the sum of bimolecular products (i.e.  $[\text{ISOPOOH}]/Y_{\text{ISOPOOH}} + [\text{ISOPN}]/Y_{\text{ISOPN}}$ ) produced following addition at  $C_4$  to  $C_1$  decreases with  $\tau_{\text{bimolecular}}$  (blue) reflecting the much faster unimolecular chemistry occurring in the 4-OH system. In red and black, the ratio of the sum of bimolecular and unimolecular products is plotted assuming yields of 100% (red) and 25% (black) for HPALD. To achieve mass closure (black), we find that the unimolecular chemistry must produce HPALD with a yield of  $25 \pm 10\%$  (assuming no error in the HPALD sensitivity). Including this additional source of uncertainty, we estimate an uncertainty of a factor of 2 in the yield. A model incorporating the processes shown in Scheme 1 and simulations using the rates listed in SI Table S7 and S8 are shown as dashed lines. . . . 58
- 3.6 Following 1,6 H-shift to the peroxy radicals (right) and 1,5 H-shift to the alkoxy radicals (left), similar allylic radicals are formed. The measured yield of HPALD (1-OOH, 4-(O)) from the hydroperoxy hydroxyl radical (25%), is, like the yield of  $\text{HC}_5$  (1-OH, 4-(O)) from the dihydroxy radical ( $45 \pm 10\%$ ), less than unity. . . . . 60
- 3.7 The ratio of unimolecular products ( $[\text{HPALD}]/Y_{\text{HPALD}}$ ) to bimolecular products ( $[\beta\text{-ISOPN}]/Y_{\text{ISOPN}} + [\beta\text{-ISOPOOH}]/Y_{\text{ISOPOOH}}$ ) plotted as a function of the total lifetime of the peroxy radicals ( $\tau$ ), where, for the red line,  $\tau$  is approximated as  $\tau = \tau_{\text{bimolecular}} \times \{[\beta\text{ 4-OH Bimolecular}]/[\beta\text{ 1-OH Bimolecular}]/.57\}$  where 0.57 represents the ratio of OH addition at  $C_4$  relative to  $C_1$ . The solid blue line is a fit to the data from the 1-OH system while the red is for the 4-OH system using a least squares method which takes into account uncertainties in both the dependent and independent variables. The ratio  $\tau/\tau_{\text{bimolecular}}$  arises when integrating  $k_{\text{NO}}[\text{NO}] + k_{\text{HO}_2}[\text{HO}_2] d\tau$ , where  $\tau_{\text{bimolecular}}$  is expressed as the inverse of  $k_{\text{NO}}[\text{NO}] + k_{\text{HO}_2}[\text{HO}_2]$ . See SI section 9b for more details. . . . . 61
- 4.1 Organic nitrates formed from the oxidation of isoprene by OH in the presence of NO will produce ISOPN, observed at 232 m/z. Therefore the signal at 232 m/z during the day is most likely dominated by the sum of 1,2 ISOPN and 4,3 ISOPN. Further OH oxidation of these two compounds will yield MACRN and MVKN, observed at 234 m/z (L. Lee et al., 2014a). . . . . 78

- 4.2 Organic nitrates formed from the oxidation of isoprene by  $\text{NO}_3$  radical will produce isoprene carbonyl nitrates (ICN), isoprene nitro-oxy hydroperoxides (ICP), and isoprene hydroxy nitrates (ISOPN). Based on laboratory evidence, these isomers are predominantly  $\delta$ -isomers (the functional groups are at 1 or 4). Therefore ETHLN and PROPNN are produced primarily as a result of the OH oxidation of the products from isoprene +  $\text{NO}_3$  (Alexander P Teng, J. D. Crouse, and P. O. Wennberg, 2017; R. H. Schwantes et al., 2015). . . . . 79
- 4.3 Organic nitrates formed from the oxidation of alkenes by OH in the presence of NO will produce hydroxy nitrates. Pictured above are the dominant isomers (A. Teng et al., 2014). In the case of butadiene only one isomer is expected comprise the majority of products from OH oxidation at the peroxy radical lifetimes found at the site. The signal at each mass is a sum of all isomers. . . . . 80
- 4.4 Time series (left) and diurnal profiles (right) of organic nitrates formed from isoprene with significant enhancements during the day. All times are presented in Central Daylight Time, which was the local time at the SOAS 2013 field site. The diurnal profiles are produced from 30 minute bins, with the black diamond indicating the median, the edge of the rectangles indicating the 25th and 75th percentiles, and the whiskers plotting the non-outlier extremes. . . . . 81
- 4.5 Time series (left) and diurnal profiles (right) of organic nitrates from alkenes besides isoprene with significant enhancements during the day. All times are presented in Central Daylight Time, which was the local time at the SOAS 2013 field site. The diurnal profiles are produced from 30 minute bins, with the black diamond indicating the median, the edge of the rectangles indicating the 25th and 75th percentiles, and the whiskers plotting the non-outlier extremes. . . . . 82

- 4.6 Signals at 316m/z and 300m/z are stable products formed from the oxidation of monoterpenes by NO<sub>3</sub>. The structures responsible for signals at monoterpenes are highly uncertain due to the multiplicity of monoterpenes available for reaction with NO<sub>3</sub>, and the uncertainty of the products formed upon reaction with NO<sub>3</sub>. The site was generally dominated by two monoterpenes:  $\alpha$ -pinene and  $\beta$ -pinene, and so potential structures have been drawn for those two monoterpenes. Chamber studies conducted at Caltech have confirmed that nitro-oxy hydroperoxides are formed from the reaction of  $\alpha$ -pinene and NO<sub>3</sub> and subsequent reaction of this peroxy radical with HO<sub>2</sub>. . . . . 95
- 4.7 Time series (left) and diurnal profiles (right) of organic nitrates with significant enhancements during the night. All times are presented in Central Daylight Time, which was the local time at the SOAS 2013 field site. The diurnal profiles are produced from 30 minute bins, with the black diamond indicating the median, the edge of the rectangles indicating the 25th and 75th percentiles, and the whiskers plotting the non-outlier extremes. . . . . 96
- 4.8 The left pie chart represents the mean contribution to the sum of all nitrogen-containing masses monitored by the Caltech CF<sub>3</sub>O<sup>-</sup> CIMS during the time period of 9AM to 3PM for the entire SOAS campaign. The right pie chart is the same representation but for the time period between 9PM to 3AM. 'Other' category is composed of all compounds listed in Table 4.1 and Table 4.2 that are not called out. . . . . 97
- 4.9 Comparison of (Caltech CF<sub>3</sub>O<sup>-</sup> CIMS organic nitrates + NOAA-GCMS alkyl nitrates + TD-LIF aerosol-phase organic nitrates) and the total alkyl nitrate budget as measured by the Berkeley TD-LIF. On the left are six days over which all measurements were on-line, showing portions where the entire budget was explained by the sum of GCMS, CIMS, and apANs. On the right is the sum of CIMS, GCMS, and apANs plotted against the  $\Sigma$ ANs. The red line is the best fit  $y=0.54x+40$ , with an  $R^2$  of 0.43. . . . . 98
- 4.10 Each different colored flight track shows a flight leg plotted in Figure 4.11 and Figure 4.12. . . . . 99

- 4.11 Speciated organic nitrate measurements are shown for four flight legs from different days. The corresponding flight track for each time series is shown in Figure 4.10. Plotted in stacked solid colors are the speciated organic nitrates as measured by the Caltech CIMS. Pink dots represent the sum of all speciated measurements (Caltech CIMS and the Whole Air Sample measurements) and the aerosol organic nitrate fraction (CU AMS measurements). The dashed black line is the total alkyl nitrate signal in pptv divided by 2 ( $\Sigma$  ANs) as measured by the Berkeley TD-LIF. It is clear that there are significant sources of alkyl nitrates besides the speciated organic nitrates. . . . . 100
- 4.12 Speciated organic nitrate measurements are shown for four flight legs from different days. Each flight leg's corresponding flight track is shown in Figure 4.10. Plotted in stacked solid colors are the speciated organic nitrates as measured by the Caltech CIMS. Pink dots represent the sum of all speciated measurements (Caltech CIMS and the Whole Air Sample measurements) and the aerosol organic nitrate fraction (CU AMS measurements). The dashed black dots are the total alkyl nitrate signal in pptv divided by 2 ( $\Sigma$  ANs) as measured by the Berkeley TD-LIF. It is clear that there are significant sources of alkyl nitrates besides the speciated organic nitrates. . . . . 101
- 4.13 Time series (left) and diurnal profiles (right) of organic nitrates with uncertain sources. All times are presented in Central Daylight Time, which was the local time at the SOAS 2013 field site. The diurnal profiles are produced from 30 minute bins, with the black diamond indicating the median, the edge of the rectangles indicating the 25th and 75th percentiles, and the whiskers plotting the non-outlier extremes. 102
- B.1 The Purdue instrument correlates well to the CIT instrument using just raw, unadjusted data. The modeled data, which uses a kinetic model to estimate the ISOPN isomer distribution and then applies a correction for individual ISOPN isomers, correlates less well with the CIT instrument measurement for ISOPN. . . . . 152

## LIST OF TABLES

<i>Number</i>	<i>Page</i>
2.1 Experiment list. . . . .	9
2.2 Absolute sensitivities for each individual isomer and isomer-averaged sensitivities (bold) were determined by summing peaks in both the CIMS and TD-LIF, and deriving a sensitivity, expressed as normalized counts of analyte ion (normcts) per pptv of analyte. Uncertainties ( $1\sigma$ ) include the 10 % uncertainty from the split ratio and absolute $\text{NO}_2$ determination by the TD-LIF. The measured 1-hexene HN sensitivities are lower than other HNs measured in this study. This may reflect precision errors for this one compound, and thus lead to a high biasing in the HN branching of 1-hexene and 1-octene. Absolute sensitivities for all isomers were determined by summing all peaks in both the CIMS and TD-LIF, and deriving a sensitivity from the total. Uncertainties ( $1\sigma$ ) include the 10 % uncertainty from the split ratio and absolute $\text{NO}_2$ determination by the TD-LIF. The measured 1-hexene HN sensitivities are lower than other HNs measured in this study. This may reflect precision errors for this one compound, and thus lead to a high biasing in the HN branching of 1-hexene and 1-octene. . . . .	18
2.3 Absolute hydroxy nitrate (HN) yields from alkenes at 293 K and 993 hPa. . . . .	20
2.4 $\beta$ HN sensitivities, OH rates, $f_a$ , relative $Y_{\beta\text{HN}}$ , $\alpha_{\text{alkene}}/\alpha_{\text{propene}}$ and branching ratios to form $\beta$ -hydroxy nitrates (HN) at 293 K and 993 hPa.	25
2.5 Isomer distribution for hydroxy nitrates and hydroxy hydroperoxides formed from OH addition to alkenes. . . . .	29
2.6 Box modeling reactions . . . . .	38
3.1 Examples of the oxidation products of isoprene measured in this study.	47
3.2 The fractional abundance of the $\text{RO}_2$ isomers at $\tau_{\text{bimolecular}} < 0.01\text{s}$ inferred from measurements of the ISOPNs. The fractional abundance of <i>Z</i> 1-OH, 4-N and <i>E</i> 4-OH, 1-N ISOPN isomers are estimated from three experiments in which tandem column chromatography successfully separated these two isomers. . . . .	55

- 3.3 The O<sub>2</sub> dissociation rate constant from the  $\delta$  RO<sub>2</sub> radicals ( $k_{\text{RO}_2 \rightarrow \text{R} + \text{O}_2}$ ) determined from kinetic modeling of the inflection point in the ratio of the  $\delta$ : $\beta$  ISOPN as the system transitions from kinetic to thermodynamic control at 297K (see SI). In the last column, the rate constants calculated by Jozef Peeters et al., 2014, are tabulated. Uncertainty in O<sub>2</sub> dissociation rate constant is estimated to be a factor of 2 (see SI). Challenges in separation of the *E* 4-OH and *Z* 1-OH RO<sub>2</sub> isomers limits the ability to separately determine the lifetime of these radicals. 56
- 3.4 Asymptotic yield ratios,  $[E\text{-}\delta]/[\beta]$   $[Z\text{-}\delta]/[\beta]$ , and the calculated free energy difference ( $\Delta G_{\delta\text{-}\beta}$ ). These ratios are estimated from the measured ISOPN isomers at  $\tau_{\text{bimolecular}} > 30$  s. An upper bound for the fractional abundance of *E* 4-OH, 1-N is derived assuming that the co-eluting peak is comprised entirely of *E* 4-OH, 1-N at these long bimolecular lifetimes (Figure 3.3). Free energy differences between the *Z*- $\delta$ -RO<sub>2</sub> and  $\beta$ -RO<sub>2</sub> are estimated from the rate of 1,6 H-shift isomerization as discussed below. In the last column, the rate constants calculated by Peeters et al. are tabulated. . . . . 57
- 3.5 Experimental isomerization rate constants for the 4-OH and 1-OH systems at 297K are compared with those calculated using transition state theory by (Jozef Peeters et al., 2014). The listed experimental uncertainty includes only the fit error from Figure 6. With inclusion of other sources of error, these rates are known to only within a factor of 3.5 (SI section 6c). . . . . 63
- 4.1 Observed nitrogen containing compounds by CF<sub>3</sub>O<sup>-</sup> CIMS by name, abbreviation, monitored *m/z*, and molecular weight. Isobaric compounds cannot be discerned given the mass resolution of the time-of-flight mass spectrometer, i.e. OH oxidation of 1-pentene in the presence of NO to form hydroxy nitrates would also be observed at 234 *m/z*. Given the VOCs measured by other instruments on the site, isobaric compounds contribute only minor amounts to the observed signals. . . . . 78
- 4.2 Significant observed nitrogen-containing *m/z* observed with the CF<sub>3</sub>O<sup>-</sup> CIMS. The molecular weight (m.w.) column is inferred using the molecular weight after subtracting the reagent ion, CF<sub>3</sub>O<sup>-</sup> (85 amu). . . . . 86

*Chapter 1*

## INTRODUCTION

Tropospheric ozone is environmentally important because it helps set the oxidative capacity of the atmosphere. Ozone's photolysis in the presence of water produces hydroxyl radical, the main oxidant in the atmosphere. Ozone also reacts sufficiently quickly with alkenes to initiate their oxidation. Ozone also contributes to oxidative stress of living tissue and at elevated concentrations is implicated in a number of disease burdens. Tropospheric ozone is also one of the most important anthropogenic greenhouse gases. Change in its concentration is calculated to produce 1/5 of the change in the total anthropogenic radiative forcing since the preindustrial era (IPCC, 2007).

Ozone is produced in the troposphere when CO or other volatile organic compounds are photochemically oxidized in the presence of nitrogen oxides. Because of ozone's huge impact, considerable effort has been expended to simulate its current concentrations. The formation of alkyl nitrates significantly impacts gas phase  $\text{NO}_x$ , and thereby influences tropospheric ozone production (see F. Paulot, Henze, and P. O. Wennberg, 2012a

During daytime, alkyl nitrates ( $\text{RONO}_2$ , or interchangeably, organic nitrates) form via a minor chain-terminating branch in the reaction of peroxy radicals with NO. The major branch in this chemistry recycles  $\text{HO}_x$  and produces ozone. The fate of alkyl nitrates is thought to be determined by either 1) deposition leading to loss of atmospheric  $\text{NO}_x$  or 2) further reactions that lead to recycling of  $\text{NO}_x$  or conversion of the organic nitrates to  $\text{HNO}_3$ . Thus,  $\text{RONO}_2$  can serve as both a permanent sink, and as a transport mechanism for  $\text{NO}_x$ .

The current understanding of the formation pathway of alkyl nitrates from peroxy radicals reacting with NO is evolving. There have been many studies detailing the formation of alkyl nitrates from peroxy radicals reacting with NO (Arey et al., 2001; Orlando and Tyndall, 2012). These studies generally find an increasing branching ratio to form alkyl nitrates with increases in pressure, decreases in temperature, and increases in the number of carbon atoms of the peroxy radical. This behavior has been interpreted as increasing stabilization of the peroxy nitrite ( $\text{ROONO}$ ) intermediate, leading to more isomerization to nitrate ( $\text{RONO}_2$ ). The dynamics of this

transition are not well understood (Lohr, Barker, and Shroll, 2003a; Lohr, Barker, and Shroll, 2003b; J. Zhang, Dransfield, and Donahue, 2004).

There has been specific disagreement over the effect of substitution of the peroxy radical on the branching ratio to form alkyl nitrates. As far back as the 1980s, it was reported that the yield from primary and tertiary peroxy radicals is lower than that of secondary peroxy radicals (Arey et al., 2001; Espada et al., 2005; Cassanelli, Fox, and Cox, 2007). Later reports indicate the yield from tertiary nitrates may have been underestimated due to decomposition of tertiary nitrates in analytical systems (Orlando and Tyndall, 2012).

Presented here are a number of studies detailing new laboratory and field investigations into the formation and fate of organic nitrates, particularly from alkenes. These alkenes are both industrially produced and biogenically emitted, and their oxidation in the atmosphere impact local production of ozone significantly.

Chapter 2 describes a laboratory investigation into the formation of hydroxynitrates from the OH initiated oxidation of alkenes. This work began as an investigation into the oxidation kinetics of isoprene hydroxy nitrate (ISOPN) isomers in which novel measurement techniques were employed (gas chromatography coupled with chemical ionization mass spectrometry and thermal dissociation chemiluminescence of alkyl nitrates to  $\text{NO}_2$ ). The investigation quickly expanded to include the products of OH oxidation of alkenes in the presence of NO to form hydroxynitrates when it was noticed the yields of hydroxynitrates from these products was higher than previously reported by J. M. O'Brien et al., 1998; Muthuramu, P B Shepson, and O'Brien, 1993; J. O'Brien et al., 1995.

The results of the laboratory investigation demonstrated that the branching ratio to form hydroxy nitrates could be well parameterized by considering the total number of heavy atoms as the key determinant in the functionally simple monoalkenes. Moreover, for simple  $\beta$  hydroxy peroxy radicals, it is shown that there is a dependence on the substitution of the peroxy radical to the alkyl nitrate branching ratio.

The finding that alkyl nitrates are formed in higher abundance than previously thought implies that alkyl nitrate production has been generally underestimated in previous modeling efforts, and specifically for the Houston-Galveston airshed in the 2000 Texas Air Quality Study (Rosen, 2004). Revised interpretation closed significant gap in the organic nitrate budget where VOC reactivity was dominated by small alkenes. New measurements taken a decade later over the same Houston-

Galveston airshed illustrate that small alkenes still play a significant role oxidant formation more than a decade after the 2000 Texas Air Quality Study identified these compounds as major contributors to photochemical smog in Houston.

The study also demonstrated the first measurements of isomer-resolved hydroxy hydroperoxides for a suite of alkene oxidation products. The results indicate that the reaction between  $HO_2$  and  $\beta$  hydroxy peroxy radicals has close to unity yield to form hydroxy hydroperoxides. Constraints are placed on the OH addition ratios across an unsaturated bond.

Chapter 3 leverages the gas chromatography, chemical ionization techniques developed in Chapter 2 to study isoprene's peroxy radical dynamics. Isoprene is specifically chosen for study due to its outsized role in the atmosphere due to its huge emission by the biosphere. Estimates of biosphere emission are of order 600Tg/yr, a similar magnitude to the entire global methane emission, and roughly ten times the total anthropogenic emission of volatile organic compounds (Guenther, 2006). Importantly, the branching ratios to form alkyl nitrates from the oxidation of isoprene show large variation study to study (Giacopelli et al., 2005; Lockwood et al., 2010; F Paulot et al., 2009; Chen, Hulbert, and Paul B Shepson, 1998; Tuazon and Atkinson, 1990; Sprengnether et al., 2002; Horowitz et al., 2007; Patchen et al., 2007). Moreover, global simulations of tropospheric ozone show strong dependence on this branching ratio and the subsequent fate of ISOPN (Wu et al., 2007; L. Zhang et al., 2010; F. Paulot, Henze, and P. O. Wennberg, 2012b).

In this investigation, we determined that the alkyl nitrate yield from isoprene is  $13 \pm 3\%$  at room temperature and pressure. This yield lies on the higher end of reported laboratory yields, and thereby likely lowers simulated  $O_3$  production where the isoprene photochemical cascade is important. Evidence is shown that the alkyl nitrate yield is independent of  $RO_2$  substitution for isoprene peroxy radicals.

Isoprene oxidation is different from the simple alkenes studied in Chapter 2 because the OH addition forms a resonance-stabilized alkyl radical. For the dominant addition positions (>90%, Lei et al., 2000), this provides two sites for  $O_2$  to add to the molecule, rather than just one for singly unsaturated hydrocarbons. This  $O_2$  addition was thought to be essentially irreversible in the atmosphere, and thus the distribution of peroxy radicals should be based on the energetics of where the alkyl radical is most stabilized. However, it was proposed that the  $O_2$  addition is actually reversible for the given lifetimes of the  $RO_2$  radical in the atmosphere (Peeters, Nguyen, and Vereecken, 2009). Moreover, the distribution of peroxy radicals was predicted to

change drastically between the kinetic (rate of O<sub>2</sub> fragmentation < lifetime of RO<sub>2</sub>) distribution of RO<sub>2</sub> and the thermodynamic (rate of O<sub>2</sub> fragmentation > lifetime of RO<sub>2</sub>).

Chapter 3 delves into the dynamics of O<sub>2</sub> addition and reversal, demonstrating that the nascent kinetic distribution of peroxy radicals is substantially different than the equilibrium distribution. Moreover, this transition from kinetic to equilibrium occurs at peroxy radical lifetimes which generally only exist in urban environments due to elevated NO. Therefore, most of the atmosphere is found to contain isoprene peroxy radicals which are closer to the equilibrium distribution.

The unimolecular channel for isoprene peroxy radicals is shown to be important. Measurements of the subsequent products from the unimolecular channel are shown to produce more than just the hydroperoxy aldehyde, with a significant percentage of this unimolecular channel left unaccounted for.

Chapter 4 delves into field observations of nitrates taken in isoprene-dominated emissions areas in the Southeastern United States. Observations are taken from two separate field campaigns: a ground-based deployment (Southern Oxidant and Aerosol Study 2013), and an airplane campaign (Studies of Emissions, Atmospheric Composition, Clouds and Climate Coupling by Regional Surveys 2013).

Isoprene-derived products are shown to be extremely important in setting the lifetime of NO<sub>x</sub> in these regions due to the formation of ISOPN out competing the OH + NO<sub>2</sub> NO<sub>x</sub> loss pathway. These observations also indicate that the loss pathways of ISOPN are not well accounted for by oxidant oxidation, deposition, or photolysis.

A central question is then explored through further laboratory studies: how is ISOPN being lost in the atmosphere? Specifically, the 1-OH, 2-ONO<sub>2</sub> is targeted for further study due to the analytical observation found in Chapter 3 that this tertiary nitrate hydrolyzes quickly when exposed to liquid water in the gas chromatograph. Successful synthesis of the 1-OH, 2-ONO<sub>2</sub> ISOPN isomer had not yet been reported, likely due to its lability. Synthesis attempts are successful when care is taken to eliminate water.

With a successful synthesis, further laboratory kinetic studies are reported on this isomer. Specifically, the OH and O<sub>3</sub> rate constant are reported and shown to not explain the loss of daytime ISOPN. The 1-OH, 2-ONO<sub>2</sub> ISOPN isomer is shown to readily hydrolyze in D<sub>2</sub>O and in a humidified chamber indicating that heterogeneous hydrolysis may explain the missing loss pathways.

The study presented in Chapter 4 also illuminates gaps in our knowledge pertaining to the organic nitrate budget. Comparison between measured alkyl nitrates and the total alkyl nitrate budget indicate that there is a persistent gap even after including the organic nitrate aerosol fraction. Reasons are explored for this discrepancy.

Chapter 5 summarizes the overall conclusions of this work.

*Chapter 2*HYDROXY NITRATE PRODUCTION IN THE OH-INITIATED  
OXIDATION OF ALKENES

Teng, A. P. et al. (2015). “Hydroxy nitrate production in the OH-initiated oxidation of alkenes”. In: *Atmospheric Chemistry and Physics* 15.8, pp. 4297–4316. DOI: 10.5194/acp-15-4297-2015. URL: <http://www.atmos-chem-phys.net/15/4297/2015/>.

**2.1 Introduction**

The formation of alkyl nitrates is an important process controlling tropospheric oxidants and the lifetime of  $\text{NO}_x$ . During daytime, alkyl nitrates form via a radical chain-terminating branch in the reaction of alkyl peroxy radicals with  $\text{NO}$ . The major branch in this chemistry recycles  $\text{HO}_x$  and produces ozone. The fate of alkyl nitrates is thought to be determined by either (1) deposition leading to loss of atmospheric  $\text{NO}_x$  or (2) further reactions that lead to recycling of  $\text{NO}_x$  or conversion of the organic nitrates to  $\text{HNO}_3$ . Thus,  $\text{RONO}_2$  can serve either as a permanent sink or as a transport mechanism for  $\text{NO}_x$ .

Alkyl nitrates also play an important role in organic aerosol formation (Brown et al., 2009; Rollins et al., 2012). Aerosol nitrates have been observed to form as a result of  $\text{NO}_3$  chemistry, though our understanding of the gas phase mechanisms leading to aerosol nitrate remains incomplete.

Knowledge of the branching ratio of  $\text{RO}_2 + \text{NO}$  to form alkyl nitrates from  $\text{RO}_2$  derived from specific volatile organic compounds (VOCs) is important for diagnosing the role of individual VOCs in ozone and aerosol formation. This knowledge can then guide specific control strategies to mitigate pollution (Ryerson et al., 2003; Rosen, 2004; Farmer et al., 2011).

Many previous studies have reported VOC-specific branching ratios to form alkyl nitrates. These studies suggest that the branching ratios increase with increasing carbon number, increasing pressure, and decreasing temperature (Orlando and Tyn-dall, 2012, and references therein). This behavior has been interpreted as evidence that the lifetime of the  $\text{O-ONO}$  intermediate controls the fraction of the nascent complex that isomerizes onto the  $\text{ONO}_2$  surface. The dynamics that lead from the

peroxynitrite (ROONO) to the nitrate (RONO<sub>2</sub>) is, however, not well understood (Lohr, Barker, and Shroll, 2003; Barker et al., 2003; Zhang et al., 2002).

Alkenes react rapidly by addition of OH and O<sub>2</sub> to form  $\beta$ -hydroxy peroxy radicals. These peroxy radicals react with NO to form  $\beta$ -hydroxy nitrates.

Previous studies have suggested that the branching ratio to form  $\beta$ -hydroxy nitrates from reaction of  $\beta$ -hydroxy peroxy radicals with NO is lower than for peroxy radicals produced from reactions of alkanes of the same carbon number with OH (O'Brien et al., 1998). The lower nitrate branching ratios for  $\beta$ -hydroxy peroxy radicals have been attributed to the  $\beta$ -hydroxy group weakening the O–ONO bond, shortening the lifetime of the OONO complex toward decomposition to NO<sub>2</sub> and thereby reducing the time available to sample the crossing to the nitrate surface (RONO<sub>2</sub>) (Muthuramu, Shepson, and Obrien, 1993; O'Brien et al., 1998; Matsunaga and Ziemann, 2009). Patchen et al., 2007, however, reported the branching ratio to form hydroxy nitrates derived from 1- and 2-butene as larger than previously reported by O'Brien et al., 1998. This study was conducted at 100 torr where RONO<sub>2</sub> yields should be smaller than at atmospheric pressure. Additional studies conducted on alkenes using long-path FT-IR have determined total alkyl nitrate yields similar to those determined for *n*-alkanes. However, these studies provide only upper bounds for branching ratios to RONO<sub>2</sub> due to the possible formation of organic nitrate from RO + NO<sub>2</sub> chemistry Atkinson, Tuazon, and Carter, 1985; Tuazon et al., 1998; Sara M. Aschmann, Arey, and Atkinson, 2010.

In this study, we use CF<sub>3</sub>O<sup>-</sup> CIMS (chemical ionization mass spectrometry) to quantify the hydroxy nitrates yield. In addition, we utilize gas chromatography with both CF<sub>3</sub>O<sup>-</sup> CIMS and thermal dissociation NO<sub>2</sub> laser-induced fluorescence (TD-LIF) to resolve and quantify isomeric distributions of these hydroxy nitrates. The TD-LIF instrument provides independent confirmation that the observed signals are alkyl nitrates and enables secondary calibration of CF<sub>3</sub>O<sup>-</sup> CIMS sensitivity by the TD-LIF for individual  $\beta$ -hydroxy nitrates.

## 2.2 Materials and methods

1-propene (propene) (> 99 %), *d*<sub>6</sub>-propene (> 99 %), 1-butene (but-1-ene) (> 99 %), *cis*-2-butene (*cis*-but-2-ene) (> 99 %), methylpropene (2-methylpropene, isobutylene, isobutene) (> 99 %), 1-pentene (pent-1-ene) (> 98 %), 2-methyl 1-butene (2-methyl but-1-ene) (> 98 %), 2-methyl 2-butene (2-methyl but-2-ene) (> 99 %), isopropyl nitrate (nitric acid, 1-methylethyl ester) (> 99 %), 1-hexene (hex-1-ene)

(> 99 %), 1-octene (oct-1-ene) (> 98 %), and 1,2-butanediol (butane 1,2 diol) (> 98 %) purity were purchased from Sigma Aldrich and used without further purification. Hydrogen peroxide (30 and 50 % by weight in water) was purchased from Sigma Aldrich. Ethene (ethylene) (> 99 %) was purchased from Scott Specialty Gases. A nitric oxide (NO) ( $1994 \pm 20$  ppmv in ultra high purity  $N_2$ ) standard gas tank for chamber experiments was prepared by Matheson. Nitrogen dioxide ( $NO_2$ ) (5 ppmv in ultra high purity  $N_2$ ) gas tank for TD-LIF calibration was prepared by Matheson. Methyl nitrite ( $CH_3ONO$ ) was synthesized, purified, and stored using methods similar to those described by Taylor et al., 1980.

### **Environmental chamber experiments**

The CIMS and thermal dissociation laser-induced fluorescence instrument (TD-LIF) instruments and the Teflon reaction chamber have been described previously (Crouse, Nielsen, et al., 2013; Lee et al., 2014). Briefly, photochemical experiments were conducted in a  $1 \text{ m}^3$  enclosure composed of fluorinated ethylene propylene copolymer (Teflon FEP, Dupont). UV photolysis of hydrogen peroxide ( $H_2O_2$ ) or methyl nitrite ( $CH_3ONO$ ) provided the primary  $HO_x$  source. Experiments to determine the hydroxy nitrate yields were typically conducted with initial mixing ratios of 0.08–2 ppmv of alkene, 0.2–2 ppmv ( $\pm 10$  %) of hydrogen peroxide or 40–200 ppbv methyl nitrite, and 0.5–4 ppmv ( $\pm 5$  %) of NO. Experiments to determine hydroxy hydroperoxide isomeric distributions were conducted with initial mixing ratios of 2–30 ppbv alkene and 2–20 ppmv of hydrogen peroxide. All experiments were performed at ambient pressure, approximately 993 hPa. Table 2.1 provides a complete list of experiments.

Table 2.1: Experiment list.

Expt. #	H <sub>2</sub> O <sub>2</sub> ppmv	NO ppbv	VOC, ppbv	Absolute $\alpha$	Relative $\alpha$	ROOH yield	TD-LIF measurement
1	2	500	propene, 96	ISOPN, 50			x
2	2	500	propene, 93	ISOPN, 38			x
3	2	500	propene, 116	ISOPOOH, 38	x		
4	2	500	propene, 164	ISOPOOH, 50	x		
5	5	500	propene, 143	ISOPOOH, 44	x	CH <sub>3</sub> ONO, 350	
6	500	propene, 156	ISOPOOH, 20	ISOPOOH, 20	x	CH <sub>3</sub> ONO, 370	
7	2.5	1200	propene, 262	1-butene, 183	x	1-pentene, 238	
8	2.5	1100	propene, 270	2-methyl 1-butene, 185	x	1-hexene, 180	
9	2.5	2300	propene, 235	1-hexene, 210	x		
10	2.5	1200	propene, 408	1-hexene, 390	x		
11	2.5	600	propene, 133	1,2 butanediol, 80	x		
12	1.0	600	propene, 162	1,2 butanediol, 490	x		
13	1.0	700	propene, 164	1,2 butanediol, 70	x		
14	600	propene, 122,	propene, 122,	1,2 butanediol, 70	x	CH <sub>3</sub> ONO, 60	
15	2	500	1-butene, 131	1-hexene, 105	x		x
16	2	500	1-butene, 15	<i>cis</i> -2-butene, 120	x		x
17	2	500	ethene, 1096	<i>cis</i> -2-butene, 115	x		x
18	2	500	2-methyl 2-butene, 107		x		x
19	2	500	methylpropene, 342		x		x
20	2.6	propene, 9	propene, 9				x
21	2.6	propene, 8	propene, 8				x
22	2.6	propene, 5	propene, 5				x
23	10.4	propene, 7	propene, 7				x
24	2	propene, 21	propene, 21				x
25	2	propene, 36	propene, 36				x
26	2	propene, 30	propene, 30				x
27	2.7	1-hexene, 5	1-hexene, 5				x
28	2.7	2-methyl 2-butene, 4	2-methyl 2-butene, 4				x
29	2.8	methylpropene, 4	methylpropene, 4				x
30	2.8	1-butene, 7	1-butene, 7				x
31	2	1000	4 <sub>6</sub> -propene, 324				x
32	2	1000	4 <sub>6</sub> -propene, 280				x
33	2	1140	ethene, 963				x
34	0.2	1930	2-methyl 2-butene, 242				x
35	0.2	950	ethene, 2983				x
35	0.2	950	propene, 1418				x
36	0.2	950	2,3 dimethyl 2-butene, 1096				x
36	0.2	950	propene, 1380				x
37	20	2,3-dimethyl 2-butene, 732	2,3-dimethyl 2-butene, 732				x
37	20	methylpropene, 181	methylpropene, 181				x
			methyl vinyl ketone, 1258				x
			<i>cis</i> -2-butene, 674				x
			1-butene, 102				x
			methylpropene, 261				x
			1-octene, 326				x
			methylpropene, 309				x
			1-octene, 314				x
			methacrolein, 902				x

Alkene or CH<sub>3</sub>ONO addition to the environmental chamber was accomplished by first flushing a 500 cm<sup>3</sup> glass bulb with the compound and then filling it to the desired pressure (1–20 hPa). The bulb was then filled with N<sub>2</sub> gas to 993 hPa. If required, the compound was serially diluted by pumping the bulb down to the desired pressure (5–400 hPa) and backfilling again with N<sub>2</sub> to atmospheric pressure. The concentrations of ethene, propene, 1-butene, 2-methyl propene, 2-methyl 2-butene, 2-methyl 1-butene, 1-hexene and 1-octene were determined within the bulb by FT-IR spectroscopy. FT-IR cross sections were obtained from the PNNL (Pacific Northwest National Laboratory) database (Johnson et al., 2002; Sharpe et al., 2004) for all compounds except *cis*-2-butene and *d*<sub>6</sub>-propene. Determinations of the concentrations of *d*<sub>6</sub>-propene and *cis*-2-butene were based on manometry, and checked against GC-FID (gas chromatography flame ionization detector) measurements relative to the other gases added in the same experiment assuming equivalent FID signal per carbon atom. These independent methods agreed to within 3 %.

NO addition was accomplished by evacuating a 500 cm<sup>3</sup> glass bulb, and filling from the standard tank to the desired pressure. NO was added to the enclosure only after at least 0.25 m<sup>3</sup> of air was added to lessen conversion of NO to NO<sub>2</sub> from the reaction of 2NO + O<sub>2</sub>. All pressure measurements were obtained using 13.3 or 1333.3 hPa full scale absolute pressure gauges (MKS Baratron<sup>TM</sup>). H<sub>2</sub>O<sub>2</sub> addition was accomplished by evaporating a known mass of 30 or 50 % by weight H<sub>2</sub>O<sub>2</sub> in water. Concentrations were confirmed by CIMS measurement of hydrogen peroxide in the gas phase.

The composition of the chamber was monitored by sampling from the enclosure at ~ 2000 sccm through a single 4 mm ID perfluoroalkoxy line with instruments sampling in series: (1) ToF-CIMS (Tofwerk, Caltech), (2) Triple Quadripole MS-MS CIMS (Varian, Caltech), (3) GC-FID (HP 5890 II), (4) NO<sub>x</sub> Monitor (Teledyne 200EU), (5) O<sub>3</sub> Monitor (Teledyne 400E). Sampling conducted this way minimizes surface interactions by lowering the residence time of chamber air in the sampling line to < 0.2 s. The sampling configuration in which chamber air passes only through a Teflon sampling line without first entering a gas chromatograph is referred to here as “direct” sampling. The specifics of the CIMS have been described in detail elsewhere (Crounse, McKinney, et al., 2006; Crounse, Paulot, et al., 2011; Crounse, Knap, et al., 2012; Crounse, Nielsen, et al., 2013; Paulot et al., 2013; Clair et al., 2010).

Reaction products were monitored using CF<sub>3</sub>O<sup>-</sup> chemical ionization mass spec-

trometry (CIMS) methods. Multifunctional products from alkene oxidation were detected using  $\text{CF}_3\text{O}^-$  cluster ion signals observed at  $m/z M + 85$  product. The following  $m/z$  were used for hydroxy nitrate determination: ethene, 192; propene, 206;  $d_6$ -propene, 212; 1-butene/*cis*-2-butene/methylpropene, 220; 2-methyl,2-butene/1-pentene/2-methyl 1-butene, 234; 1-hexene 248; 1-octene, 276. For hydroxy hydroperoxides, the following  $m/z$  were used for quantification: propene, 177; 1-butene/methylpropene, 191; 2-methyl 2-butene, 205; 1-hexene, 219. 1,2 butanediol was monitored using signal at  $m/z$  175, and the resulting hydroxycarbonyls were monitored  $m/z$  173.

The alkene concentrations were monitored using an GC-FID (Agilent 5890). Chamber air was sampled into a 10 cm<sup>3</sup> stainless steel sample loop or a 30 cm<sup>3</sup> PFA (perfluoroalkoxy) sample loop using a six-port valve. The sample was transferred to the head of the column in the oven at temperatures between 308 and 373 K, depending on the hydrocarbon. In the case of ethene, samples were cryotrapped with liquid nitrogen on the head of the column. A megabore (0.53 mm) 30 m Plot-Q column (Agilent J & W columns) was used to separate compounds using 7–9 standard cm<sup>3</sup> min<sup>-1</sup> N<sub>2</sub> carrier gas. A suitable temperature ramp was selected for each compound.

### **GC-CIMS/LIF chromatography**

After oxidation, the chamber air was analyzed using GC-CIMS/LIF (gas chromatography  $\text{CF}_3\text{O}^-$  CIMS/TD-LIF). Chamber air is pulled through a Teflon sampling line, through a Teflon three-port valve, and cryofocused at 240–280 K on the head of a 4 m megabore HP 612, a 4 m megabore RTX-1701, or 1 m megabore RTX-1701 column. Columns were held inside a Varian GC oven (CP-3800). Following the GC, the column effluent was split between the ToF-CIMS instrument and the TD-LIF system for the experiments listed in Table 2.1. For all other experiments where the TD-LIF instrument was not used, the column effluent flowed directly to the ToF-CIMS. After a measured flow of chamber air ranging from 30 to 200 standard cm<sup>3</sup> was cryofocused over a length of time ranging from 2 to 12 min by placing the GC column in a cooled (–20 C) isopropanol bath, the three-port valve was switched to allow carrier gas (N<sub>2</sub>) to flow through the GC column. The volume of chamber air cryofocused in this manner was determined by the collection time and the flow rate (inferred from manometry). Carrier gas flow was controlled by a mass flow controller (MKS) at 8.7 standard cm<sup>3</sup> min<sup>-1</sup> N<sub>2</sub>. Temperature program (30 C, hold

0.1 min,  $3\text{ C min}^{-1}$  from 30–60 C,  $10\text{ C min}^{-1}$  to 130 C, hold 3 min) started approximately 2–3 min after cryofocusing. All wetted surfaces in the analytical setup were comprised of Teflon, PEEK, or GC column materials to limit surface interactions.

The TD-LIF system sampled a portion of the GC carrier gas into 400 C oven. Pure  $\text{O}_2$  is added to this flow upstream of the TD oven to ensure complete conversion of  $\text{RONO}_2$  to  $\text{NO}_2$ .  $\text{NO}_2$  is measured using laser-induced fluorescence (Lee et al., 2014). The system was calibrated at the same operating pressure with a standard tank of  $\text{NO}_2$ . The conversion efficiency of the TD-LIF was evaluated with isopropyl nitrate and found to be 100 % (see Chapter 2.6). We assume here that conversion of other  $\text{RONO}_2$  is also 100 %. To the extent the conversion of these hydroxy nitrates to  $\text{NO}_2$  is less than 100 %, the reported branching ratios are biased low.

The ToF-CIMS instrument was operated in the same manner as during the photochemistry with diluted column effluent substituting for the ambient flow. With this split flow configuration, the concurrent elution of alkyl nitrates was monitored by both the ToF-CIMS and TD-LIF instruments, enabling secondary calibration of the CIMS sensitivity by the TD-LIF to the individual alkyl nitrates.

The determination of the split ratio (approximately 10 : 1) between the CIMS and TD-LIF  $\text{NO}_2$  instrument was performed using an isopropyl nitrate standard (80 ppbv in air) prepared in the same fashion as the alkenes described above. The gas standard was both directly sampled from the chamber and following cryo-collecting  $\sim 200\text{ cm}^3$  on an HP 612 column and eluting the peak in the usual GC configuration. The signal level in the TD-LIF instrument was recorded as the GC ramped through its usual temperature program. Signal levels were also compared between direct measurement of  $\sim 80$  ppbv isopropyl nitrate within a Teflon bag into the TD-LIF system and collected for 4 min on a cooled sample loop. A separate check was also conducted with prepared standards of isoprene hydroxy nitrates in which the standard was directly sampled from the chamber and through the GC system. This measurement was problematic due to long equilibration times ( $> 3$  h) resulting from low sampling flow limited by the small diameter tubing in the TD-LIF optimized for GC use. The TD-LIF was also calibrated at the end of each photochemistry experiment with gas standard of 5 ppbv  $\text{NO}_2$  in  $\text{N}_2$  (Matheson) under matching pressure conditions.

### **Experiments to determine hydroxy nitrate branching ratios relative to propene**

Experiments 31–36 (Table 2.1) were conducted to determine the  $\beta$ -hydroxy nitrate yields from alkenes relative to the  $\beta$ -hydroxy nitrate yield from propene. These experiments involved simultaneous oxidation of up to six alkenes. Initial alkene concentrations were determined by FT-IR spectroscopy. The chamber was monitored for at least 20 min to determine the background signals. UV lights were turned on for a period ( $< 10$  min) sufficient to achieve a hydroxy nitrate concentration high enough for quantification while minimizing secondary OH losses of hydroxy nitrates. Less than 10 % of each alkene species was oxidized in each experiment. Experiments were initiated between 292 and 293 K and the temperature rise was no more than 1 K over the course of the experiments. Hydroxy nitrate branching ratios were determined relative to those of propene with the exception of Experiment 31, which measured  $d_6$ -propene hydroxy nitrate branching ratios relative to 1-butene. Accurate GC-FID quantification in these experiments was not possible due to the small change in concentration of each compound.

### **Experiments to determine hydroxy nitrate branching ratios in an absolute manner**

Experiments 1–19 (Table 2.1) were conducted to determine the absolute branching ratios to form  $\beta$ -hydroxy nitrates. Experiments involved addition of 1–3 alkenes, NO, and H<sub>2</sub>O<sub>2</sub> or CH<sub>3</sub>ONO into the chamber. Initial alkene concentrations were determined by FT-IR and confirmed by manometry and GC-FID peak areas. Isoprene hydroxy nitrates or isoprene hydroxy hydroperoxides were also added to the chamber in Experiments 1–7 to measure their OH rate constants relative to propene as described in experiments of Lee et al., 2014; St. Clair et al., 2016. To measure OH exposure, 1,2 butane diol (a reference compound measurable by CIMS) was added to a series of experiments to confirm the alkene decay measured by GC-FID. In these experiments, UV lights were turned on until a significant and quantifiable decay of hydrocarbon was observed ( $> 15$  %) on the GC-FID. Experiments were initiated between 292 and 293 K, and the temperature increased by at most 7 K after the lights were turned on.

## Experiments to determine hydroxy hydroperoxide isomer distributions

Experiments 20–30 (Table 2.1) were conducted to determine the hydroxy hydroperoxide isomer distributions. Experiments involved addition of 1–3 alkenes and  $\text{H}_2\text{O}_2$ . Initial alkene concentrations were determined by FT-IR spectroscopy. UV lights were turned on until a measurable concentration of hydroxy hydroperoxides was produced. Less than 10 % of each alkene species was oxidized in each experiment as indicated by GC-FID signal areas.

## Post-experiment GC-CIMS/TD-LIF monitoring

Following each experiment, products were analyzed by GC-CIMS/TD-LIF or GC-CIMS. At least three replicate GC runs were conducted. Transmission through the CIMS portion of the GC-CIMS/TD-LIF was measured by comparing the direct sampling measurement to the integrated chromatogram signal for a given  $m/z$ . The integrations were corrected by blank GC runs (less than 3 % signal in all cases over the elution time of the hydroxy nitrate peaks). The transmission was determined by the ratio of the direct sampling and the total chromatogram signals after taking into account the sampling flow-rate differences.

## 2.3 Results and discussion

The following analysis procedure was used to calculate branching ratios from the experimental data:

1.  $\beta$ -hydroxy nitrate CIMS sensitivities are determined from simultaneous measurement of hydroxy nitrates by cryofocused gas chromatography.
2. The fraction of the reaction of OH that proceeds via addition,  $f_a$ , is estimated from previously reported kinetic data on alkenes. This allows normalization of subsequent measurements of the yields of  $\beta$ -hydroxy nitrates,  $Y_{\beta\text{HN}}$ , to produce branching ratios,  $\alpha$ .
3. Branching ratios to form hydroxy nitrates,  $\alpha$ , from alkenes relative to  $\alpha_{\text{HN\_propene}}$  are determined through experimental data. These results allow direct comparison of the dependence of  $\alpha$  on structure.  $\alpha$  is well described by a linear relationship:  $\alpha = m \times N + b$ , where  $\alpha$  is isomer-averaged branching ratio, and  $N$  is the number of heavy atoms in the peroxy radical (not counting the peroxy radical oxygens).

- The absolute branching ratios,  $\alpha$ , are determined using absolute quantification of alkene and hydroxy nitrate concentrations. The dependence of  $\alpha$  on the number of heavy atoms,  $N$ , is derived.
- The entire absolute branching ratio data set is used to place all relative nitrate branching ratios on an absolute basis.
- Isomer specific distributions for alkenes are derived using GC chromatograms of hydroxy nitrate isomers.
- The OH addition branching ratios are inferred by analyzing hydroxy hydroperoxide isomer distributions of alkenes oxidized by OH under HO<sub>2</sub>-dominated conditions.
- The dependence of the alkyl nitrate branching ratios on the type (i.e., primary, secondary or tertiary) of  $\beta$ -hydroxy RO<sub>2</sub> radicals is determined by comparing (5) and (6).

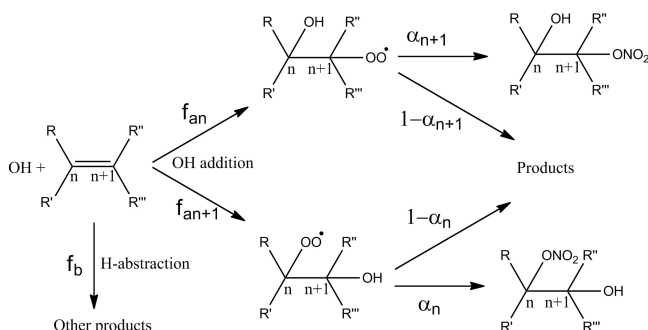


Figure 2.1: Reaction pathways of alkenes with OH. OH oxidation with alkenes follows two pathways: OH addition ( $f_n$  and  $f_{n+1}$ ) and H-abstraction ( $f_{ab}$ , where  $f_{ab} = \sum_{n=1}^l f_{abn}$ ).  $f_a + f_{ab} = 1$ . Subscripts indicate the carbon number at which either OH addition or abstraction occurs. For alkenes studied in this work at room temperature, the sum of  $f_{an}$  and  $f_{an+1}$  is much greater than  $f_{ab}$ . See text for further discussion of estimations for  $f_{ab}$ .

We define the branching ratio ( $\alpha_n$ ) to represent the fraction of RO<sub>2</sub> + NO reaction that produces RONO<sub>2</sub>, where the subscript  $n$  denotes the carbon alpha to the peroxy radical (Fig. 2.1). We define the fraction of OH that adds to carbon  $n$  as  $f_{an}$  out of the total OH + alkene reaction. The total fraction of OH + alkene that proceeds via addition is given as  $f_a = \sum_{n=1}^l f_{an}$ . The total fraction of OH + alkene that proceeds

via H-abstraction is given as  $f_{ab} = \sum_{n=1}^l f_{abn}$ , where the subscript indicates the carbon at which H-abstraction takes place. Therefore  $f_a + f_{ab} = 1$ . The isomer-averaged branching ratio ( $\alpha$  no subscript) to form  $\beta$ -hydroxy nitrates from OH addition to a mono-alkene is then defined in this paper as  $\alpha = f_{an} \times \alpha_{n+1} + f_{an+1} \times \alpha_n$ .

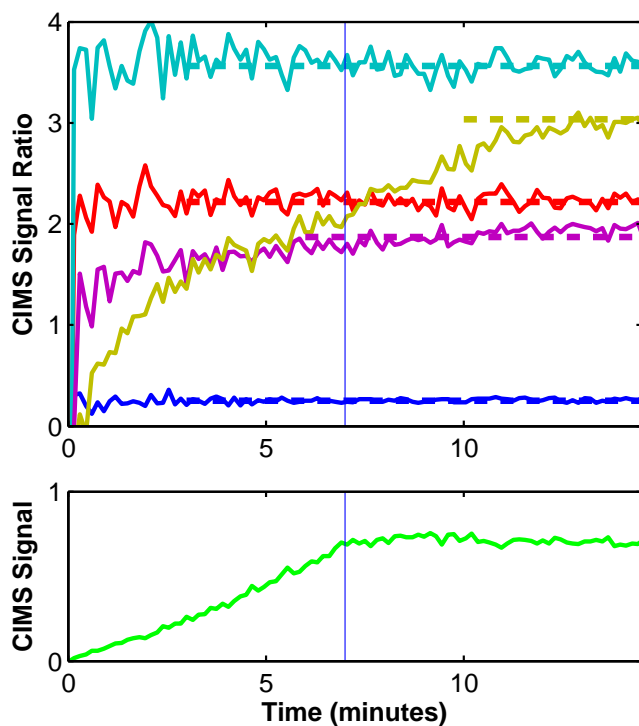


Figure 2.2:  $\beta$ -hydroxy nitrate products produced from six alkenes during Exp. 19. The top panel shows the ratio of CIMS hydroxy nitrate (HN) signals to propene HN ( $206 m/z$ ) for ethene HN ( $192 m/z$ , blue), methylpropene HN ( $220 m/z$ , red), 2-methyl,2-butene HN ( $234 m/z$ , teal), 1-hexene HN ( $248 m/z$ , purple), and 1-octene HN ( $276 m/z$ , gold). The bottom panel shows the absolute signal for propene HN ( $206 m/z$ ). The lights were turned on at time = 0, and turned off at 7 min (vertical line), at which point the oxidation stopped. For all compounds other than hydroxy nitrates from 1-octene, a ratio is plotted as a dashed line using averaged data from 3 min after lights until the measurements stopped. For hydroxy nitrates from 1-octene, data after 10 min are averaged. The time lag for hydroxy nitrates from 1-octene arises from wall and sample line equilibration. This suggests that the measured yield is a lower limit.

Yields of  $\beta$ -hydroxy nitrates ( $Y_{\beta\text{HN}}$ ) are defined as the change in hydroxy nitrate concentration over the change in hydrocarbon (HC):  $Y_{\beta\text{HN}} = -d[\text{HN}]/d[\text{HC}]$ . Hydroxy nitrates produced via H-abstraction and subsequent alkoxy H-shift isomerization result in molecules with different molecular weights from hydroxy nitrates produced by OH addition, and therefore only  $\beta$ -hydroxy nitrates produced via OH addition are

counted in yields. Isomer-averaged branching ratios ( $\alpha$ ) to form  $\beta$ -hydroxy nitrates from  $\beta$ -hydroxy peroxy radicals can be calculated from  $\beta$ -hydroxy nitrate yields by normalizing for the fraction of the alkene reactions with OH that proceed via OH addition:  $\alpha = Y_{\beta\text{HNN}}/(f_a/(f_a + f_{ab})) = Y_{\beta\text{HNN}}/f_a$ . For alkenes studied here,  $f_a$  is greater than 0.75.

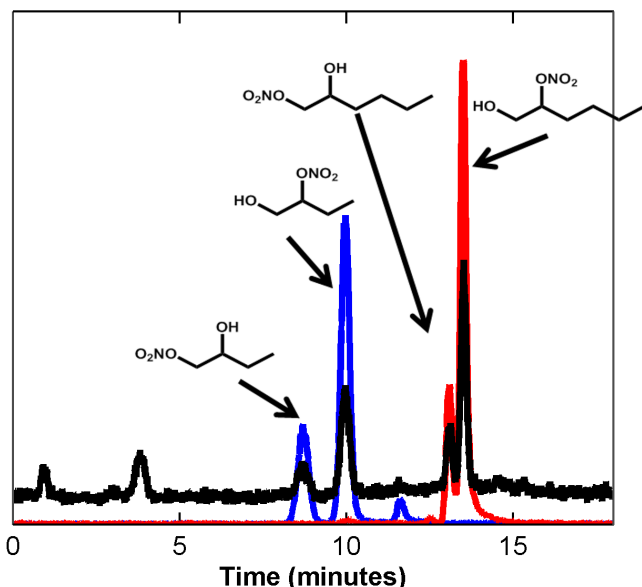


Figure 2.3: GC-CIMS/TD-LIF chromatogram following Exp. 15. The signals due to individual hydroxy nitrates are determined by integrating the alkyl nitrate peaks (black line, elevated baseline) which co-elute with the individual hydroxy nitrates observed by CIMS, e.g., hydroxy nitrates from 1-butene at 220  $m/z$  (blue) and from 1-hexene at 248  $m/z$ . Absolute CIMS sensitivities are determined by integrating individual peaks for CIMS signal and TD-LIF signal and dividing. The assigned chemical structures are shown for each alkyl nitrate peak.

### Determination of CIMS sensitivities by TD-LIF for hydroxy nitrates

CIMS sensitivities were derived from cryofocused gas chromatography and simultaneous measurement of  $\beta$ -hydroxy nitrate compounds by  $\text{CF}_3\text{O}^-$  CIMS and TD-LIF. Discrete gaussian peaks which eluted at the same time in the CIMS and TD-LIF were integrated. The time-integrated normalized ion counts from the CIMS was multiplied by the split ratio between TD-LIF and CIMS instruments then divided by the integrated  $\text{NO}_2$  signal ( $\text{ppbv} \times \text{s}$ ) measured by the TD-LIF to determine a sensitivity in normalized counts ppbv of  $\text{RONO}_2$ . Sensitivities are listed in Table 2.2. An example chromatogram of GC-CIMS/TD-LIF from which sensitivities are derived is shown in Fig. 2.3.

Table 2.2: Absolute sensitivities for each individual isomer and isomer-averaged sensitivities (bold) were determined by summing peaks in both the CIMS and TD-LIF, and deriving a sensitivity, expressed as normalized counts of analyte ion (normcts) per pptv of analyte. Uncertainties ( $1\sigma$ ) include the 10 % uncertainty from the split ratio and absolute  $\text{NO}_2$  determination by the TD-LIF. The measured 1-hexene HN sensitivities are lower than other HNs measured in this study. This may reflect precision errors for this one compound, and thus lead to a high biasing in the HN branching of 1-hexene and 1-octene. Absolute sensitivities for all isomers were determined by summing all peaks in both the CIMS and TD-LIF, and deriving a sensitivity from the total. Uncertainties ( $1\sigma$ ) include the 10 % uncertainty from the split ratio and absolute  $\text{NO}_2$  determination by the TD-LIF. The measured 1-hexene HN sensitivities are lower than other HNs measured in this study. This may reflect precision errors for this one compound, and thus lead to a high biasing in the HN branching of 1-hexene and 1-octene.

Hydroxy nitrates derived from $\text{CF}_3\text{O}^-$ sensitivity	Measured CIMS (normcts pptv <sup>-1</sup> ), 10 <sup>4</sup>
ethene, 1-OH, 2-ONO <sub>2</sub>	<b>3.5 ± 0.4</b>
propene 1-OH, 2-ONO <sub>2</sub>	5.0 ± 1.2
propene 2-OH, 1-ONO <sub>2</sub>	5.0 ± 1.4
propene, both	<b>5.0 ± 1.0</b>
1-butene 1-OH, 2-ONO <sub>2</sub>	3.3 ± 0.5
1-butene 2-OH, 1-ONO <sub>2</sub>	2.9 ± 0.4
1-butene, both	<b>3.1 ± 0.4</b>
<i>cis</i> -2-butene, first diastereomer	2.8 ± 0.4
<i>cis</i> -2-butene, second diastereomer	2.9 ± 0.4
<i>cis</i> -2-butene, both	<b>2.9 ± 0.4</b>
methylpropene 1-OH, 2-ONO <sub>2</sub>	3.9 ± 0.4
methylpropene 2-OH, 1-ONO <sub>2</sub>	3.7 ± 0.8
methylpropene, both	<b>3.8 ± 0.5</b>
2-methyl,2-butene 2-OH, 3-ONO <sub>2</sub>	3.8 ± 0.4
2-methyl,2-butene 3-OH, 2-ONO <sub>2</sub>	3.8 ± 0.5
2-methyl,2-butene, both	<b>3.8 ± 0.4</b>
1-hexene, 1-OH, 2-ONO <sub>2</sub>	2.6 ± 0.3
1-hexene, 2-OH, 1-ONO <sub>2</sub>	2.0 ± 0.4
1-hexene, both	<b>2.4 ± 0.3</b>

### The relative yields of $\beta$ -hydroxy nitrates from alkene oxidation

$\beta$ -hydroxy nitrate branching ratios were measured relative to  $\alpha_{\text{HN,propene}}$  for Experiments 31–36 with the exception of Experiment 31 which measured  $d_6$ -propene relative to 1-butene. With minimal oxidation of total hydrocarbon (< 10 %), the measured CIMS signal of each compound is used to determine the ratio of the yield

of  $\beta$ -hydroxy nitrates, where yield is defined as  $Y = f_{a1} \times \alpha_2 + f_{a2} \times \alpha_1$ :

$$\frac{Y_{\text{HN\_alkene}}}{Y_{\text{HN\_propene}}} = \frac{\text{signal}_{\text{HN\_alkene}}}{\text{signal}_{\text{HN\_propene}}} \cdot \frac{\text{sens}_{\text{HN\_propene}}}{\text{sens}_{\text{HN\_alkene}}} \cdot \frac{k_{\text{OH,propene}}}{k_{\text{OH,alkene}}} \cdot \frac{[\text{propene}]_{\text{avg}}}{[\text{alkene}]_{\text{avg}}}. \quad (2.1)$$

To determine the ratio of the average branching ratios ( $\alpha_{\text{alkene}}/\alpha_{\text{propene}}$ ), we multiply the ratio of the yields by the ratio of the fraction of OH addition ( $f_a$ ):

$$\frac{\alpha_{\text{HN\_alkene}}}{\alpha_{\text{HN\_propene}}} = \frac{Y_{\text{HN\_alkene}}}{Y_{\text{HN\_propene}}} \cdot \frac{f_{a\_propene}}{f_{a\_alkene}}. \quad (2.2)$$

The mean concentrations throughout the experiment were calculated by averaging the initial and final alkene concentrations. The amount of alkene oxidized could not be accurately determined by GC-FID due to the small fractional change in the mixing ratio. Therefore, the loss was estimated iteratively by using the calculated branching ratio for the hydroxy nitrates (see Sect. 3.3 for derivation of absolute branching ratios used in this calculation). The difference in the determination of  $Y_{\beta\text{HN}}$  between using average vs. the initial alkene concentrations was less than 5 % in all cases. CIMS signals from Expt. 19 are shown in Fig. 2.2. Estimates for secondary loss of hydroxy nitrates by reactions with OH for the relative yield experiments ( $k_{\text{OH}}$  estimates from Treves and Ruddich, 2003; and Kwok and Atkinson, 1995) using the method described by Atkinson et al. (1982) result in corrections of < 3 % and are neglected in this subset of experiments. For absolute yield determinations, which involved larger OH exposure, the applied corrections are listed in Table 2.3.

The relative branching ratio data set allows us to directly compare the dependence of  $\alpha$  on structure by reducing the uncertainties associated with the measurement and analysis. The analysis of the relative yield experiments also reduces systematic uncertainty through cancellation of correlated errors associated with determination of total chamber volume and the use of the GC-FID. The relative yield determination relies on the ratio of OH rate constants, the ratio of initial alkene concentrations, the ratio of CIMS HN sensitivities, and the ratio of CIMS HN signals. In each relative yield determination, only the ratio of OH rate constants and ratio of HN sensitivities are determined outside the given experiment.

### Normalizing nitrate yields for H-abstraction

To calculate the branching ratio for reaction of  $\text{RO}_2$  with NO to form  $\beta$ -hydroxy nitrates following addition of OH and  $\text{O}_2$  to alkenes, it is necessary to estimate the

Table 2.3: Absolute hydroxy nitrate (HN) yields from alkenes at 293 K and 993 hPa.

Alkene	$\Delta$ Alkene ppbv/%	HN, ppbv	$k_{\text{OH,HN}}^1$ ( $\times 10^{-11}$ ) ( $\text{cm}^3 \text{ molec}^{-1} \text{ s}^{-1}$ )	$k_w^2$ ( $\times 10^{-6}$ ) ( $\text{s}^{-1}$ )	$F^3$	$F_{\text{temp}}^4$	$Y_{\beta\text{HN}}$ (%)	$f_a^5$	$\alpha$ (%)
ethene	221/21 ( $\pm 2$ )	$2.6 \pm 0.5$	0.3	3.8	1.06	1.02	$1.3 \pm 0.2$	1	$1.3 \pm 0.2$
overall ethene									$1.3 \pm 0.5$
propene	38/32 ( $\pm 3$ )	$1.6 \pm 0.4$	0.6	1.6	1.05	1.01	$4.4 \pm 1$	0.97	$4.6 \pm 1$
propene	60/37 ( $\pm 4$ )	$2.4 \pm 0.6$	0.6	1.6	1.07	1.01	$4.3 \pm 1$	0.97	$4.4 \pm 1$
propene	104/39 ( $\pm 4$ )	$4 \pm 0.8$	0.6	1.6	1.07	1.05	$4.3 \pm 1$	0.97	$4.5 \pm 1$
propene	83/31 ( $\pm 2$ )	$3.7 \pm 0.8$	0.6	1.6	1.05	1.05	$4.7 \pm 1$	0.97	$4.8 \pm 1$
propene	71/18 ( $\pm 2$ )	$2.9 \pm 0.6$	0.6	1.6	1.03	1.04	$4.4 \pm 1$	0.97	$4.1 \pm 1$
propene	68/33 ( $\pm 2$ )	$2.4 \pm 0.5$	0.6	1.6	1.09	1.04	$4.0 \pm 1$	0.97	$4.1 \pm 1$
propene	34/21 ( $\pm 3$ )	$1.2 \pm 0.3$	0.6	1.6	1.03	1.03	$3.7 \pm 1$	0.97	$3.9 \pm 1$
propene	59/36 ( $\pm 4$ )	$2.1 \pm 0.5$	0.6	1.6	1.05	1.06	$4.0 \pm 1$	0.97	$4.1 \pm 1$
propene	42/34 ( $\pm 4$ )	$1.5 \pm 0.4$	0.6	1.6	1.05	1.01	$3.8 \pm 1$	0.97	$3.9 \pm 1$
overall propene									$4.1 \pm 2$
1-butene	71/55 ( $\pm 4$ )	$6.8 \pm 1.2$	0.7	3.7	1.1	1.06	$11 \pm 2$	0.92	$12 \pm 2$
1-butene	78/43 ( $\pm 3$ )	$7.6 \pm 1.3$	0.7	3.7	1.09	1.06	$12 \pm 2$	0.92	$13 \pm 2$
overall 1-butene									$12 \pm 5$
<i>cis</i> -2-butene	85/74 ( $\pm 5$ )	$8.4 \pm 1.3$	0.6	4	1.11	1.06	$12 \pm 2$	0.97	$12 \pm 2$
overall <i>cis</i> -butene									$12 \pm 4$
methylpropene	166/49 ( $\pm 3$ )	$13.7 \pm 1.9$	0.5	6.5	1.05	1.05	$9 \pm 1$	0.97	$9 \pm 1$
overall methylpropene									$9 \pm 3$
2-methyl 1-butene	114/60 ( $\pm 4$ )	$15.5 \pm 3.9$	0.8	2	1.08	1.05	$15 \pm 4$	0.95	$16 \pm 4$
overall 2-methyl 1-butene									$16 \pm 7$
2-methyl 2-butene	66/64 ( $\pm 4$ )	$5.3 \pm 0.8$	0.8	8.3	1.07	1.04	$9 \pm 2$	0.97	$9 \pm 2$
overall 2-methyl 2-butene									$9 \pm 4$
1-pentene	108/44 ( $\pm 3$ )	$12 \pm 3$	0.85	6.7	1.12	1.05	$13 \pm 3$	0.87	$15 \pm 3$
overall 1-pentene									$15 \pm 6$
1-hexene	62/59 ( $\pm 6$ )	$9.2 \pm 1.5$	1	10	1.2	1.06	$19 \pm 3$	0.86	$22 \pm 4$
1-hexene	78/43 ( $\pm 4$ )	$11.8 \pm 1.9$	1	10	1.13	1.07	$18 \pm 3$	0.86	$21 \pm 4$
1-hexene	91/23 ( $\pm 2$ )	$14.6 \pm 2.4$	1	10	1.06	1.06	$18 \pm 3$	0.86	$21 \pm 4$
overall 1-hexene									$21 \pm 8$

<sup>1</sup> Rate constants are from Treves and Ruddich (2003) or estimated based on Treves and Ruddich (2003). <sup>2</sup> All loss rate constants are calculated from post experiment HN signal decay. <sup>3</sup> Correction factor  $F$  accounts for loss of hydroxy nitrates due to wall loss and reaction with OH. This factor was calculated using a modified equation for  $F$  described by Atkinson et al. (1982), where  $k_7 = k_{\text{OH,alkene}} \times [\text{OH}]_{\text{average}}$ , and  $k_{10} = k_{\text{OH,HN}} \times [\text{OH}]_{\text{average}} + k_w$ , where  $[\text{OH}]_{\text{average}}$  is calculated using alkene decay. <sup>4</sup> Correction factor  $F_{\text{temp}}$  accounts for the change in  $\alpha$  in response to temperature variation during the experiment. This factor was estimated using the temperature dependence of  $\alpha$  reported by Arey et al. (2001). <sup>5</sup> See text for more details on estimates for normalization for the fraction of OH + alkene that proceeds via OH addition,  $f_a$ .

fraction of alkene loss,  $f_a$ , that proceeds via this channel. A quantitative determination of  $f_a$  from our experimental data is not possible because  $\text{CF}_3\text{O}^-$  CIMS is insensitive to singly functionalized carbonyl or nitrate compounds formed from the OH H-abstraction channels. The H-abstraction channel by OH has been measured for propene and *cis*-2-butene to be less than 3 %, and for 1-butene to be  $8 \pm 3$  % (Krasnoperov, Butkovskaya, and Le Bras, 2011; Loison et al., 2010). There have, however, been few studies of H-abstraction rates for other alkenes at ambient temperatures.

Using theoretical methods, Pfrang et al., 2006a; Pfrang et al., 2006b predicted

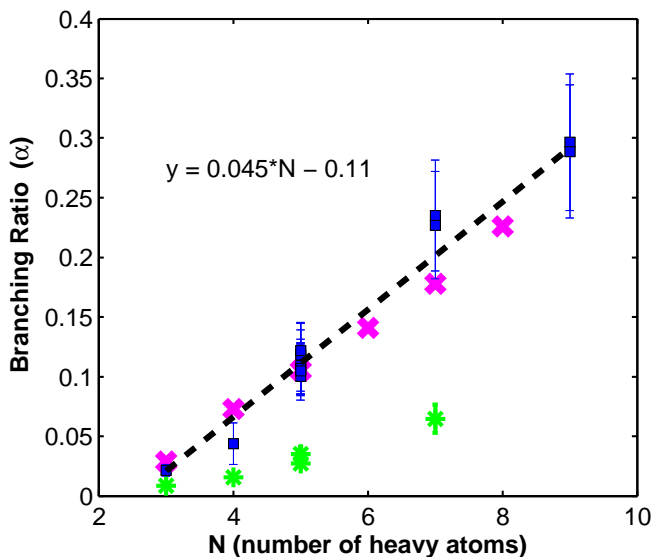


Figure 2.4: The isomer-averaged branching ratios,  $\alpha$ , derived in this study (blue boxes, data from Table 2.4), compared to previously published nitrate branching ratios (Arey et al., 2001 with pink exes; O'Brien et al., 1998 with green stars). Alkene nitrate yields from O'Brien et al., 1998 have been normalized by  $f_a$  to account for H-abstraction channel in the same fashion as this study. The error weighted fit derived from Fig. 2.4 is shown for hydroxy nitrate branching ratios (black dotted line) from all measured alkenes yields a slope of  $0.045 \pm 0.016$  and intercept of  $-0.11 \pm 0.05$  (errors are  $2\sigma$ ). This fit agrees well with the relationship derived by Arey et al., 2001, who calculated a slope of  $0.0381 \pm 0.0016$  and an intercept of  $-0.073 \pm 0.009$  for *n*-alkanes.

that the chain length should not affect the rate of OH addition to 1-alkenes, and therefore, the increasing abstraction rate with size should scale with additional  $\text{CH}_2$  groups. There is, however, disagreement in experimental results about how much the abstraction rate increases with each additional  $\text{CH}_2$ . Sara M Aschmann and Atkinson, 2008 measured OH rate constants for a series of 1-alkenes and found that the OH rate constant increases at a rate of  $2 \times 10^{-12} \text{ cm}_3 \text{ molec}^{-1} \text{ s}^{-1}$  per  $\text{CH}_2$  group, roughly 25 % higher than for *n*-alkanes ( $1.4 \times 10^{-12} \text{ cm}_3 \text{ molec}^{-1} \text{ s}^{-1}$ , determined by Kwok and Atkinson, 1995). For this analysis, we assume that  $f_{ab}$  is 8 % for 1-butene and, because H-abstraction from non-allylic  $\text{CH}_2$  groups is expected to be similar to  $\text{CH}_2$  groups in alkanes, we assume that the abstraction rate increases according to the parameterization suggested by Kwok and Atkinson (1995). This implies 15 % H-abstraction for 1-hexene, and 22 % for 1-octene. Using a rate similar to that reported in Aschmann and Atkinson (2008), the abstraction fraction ( $f_{ab}$ ) for 1-octene would be 28 %.

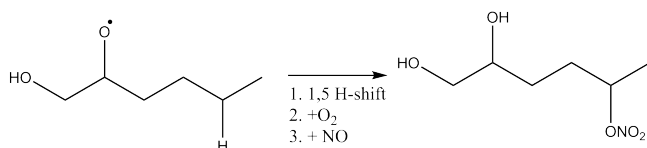


Figure 2.5: Alkoxy H-shift isomerization leading to dihydroxy nitrate formation for 1-hexene.

To estimate abstraction rates for methyl-substituted alkenes, we use an overall  $k_{\text{OH}}$  of  $31.4 \times 10^{-12} \text{ cm}_3\text{molec}^{-1}\text{s}^{-1}$  for 1-butene (Atkinson and Arey, 2003), Kwok and Atkinson's (1995) suggested  $k_{\text{OH}}$  for a  $\text{CH}_3$  group of  $0.14 \times 10^{-12} \text{ cm}_3\text{molec}^{-1}\text{s}^{-1}$ , and an 8% H-abstraction ( $f_{\text{ab}}$ ). We estimate a  $k_{\text{OH,abstraction}}$  rate constant for a secondary allylic  $\text{CH}_2$  group of  $2.4 \times 10^{-12}$ . Using an overall  $k_{\text{OH}}$  of  $26.3 \times 10^{-12} \text{ cm}_3\text{molec}^{-1}\text{s}^{-1}$  for propene (Atkinson and Arey, 2003) and an upper limit of 3% abstraction, we derive an upper limit  $k_{\text{OH,abstraction}}$  rate constant of a primary allylic  $\text{CH}_3$  group of  $0.8 \times 10^{-12} \text{ cm}_3\text{molec}^{-1}\text{s}^{-1}$ . Assuming vinylic hydrogen abstraction rates are negligible, we estimate  $f_{\text{ab}}$  for *cis*-2-butene, methylpropene, 2-methyl 1-butene, 2-methyl 2-butene to all be less than 5%.

### Absolute $\beta$ -hydroxy nitrate yields and branching ratios

The absolute yield of hydroxy nitrates for several of the alkenes was determined in Experiments 1–19. Longer reaction times were necessary to quantify, with sufficient precision, the amount of alkene oxidized. The concentration of hydroxy nitrates at the end of the experiment was determined by measuring the total GC-TD-LIF peak signal which corresponded to a CIMS hydroxy nitrate signal. The initial concentration of alkene was determined by FT-IR and GC-FID, and total loss was determined by the decay in peak area by the GC-FID. In Experiments 11–14, 1,2 butanediol was also added as a reference compound to allow the total loss of alkene to be determined independent of the GC-FID. 1,2 butane diol was monitored using the CIMS at signal  $m/z$  175 by CIMS to determine its decay over time. The ratio of the OH rate constants for 1,2 butanediol to propene is estimated to be  $1.1 \pm 0.1$  from relative rate information from the literature (Atkinson et al., 1982, 1986; Bethel et al., 2001). The alkene decay inferred from the 1,2 butanediol decay was found to match the GC-FID alkene decay within error. The nitrate yield is calculated by dividing the amount of hydroxy nitrates formed by the amount of alkenes reacted.

For each reaction, a secondary loss correction factor,  $F$ , was applied to account for losses of hydroxy nitrates by OH and wall loss using equations derived in Atkinson

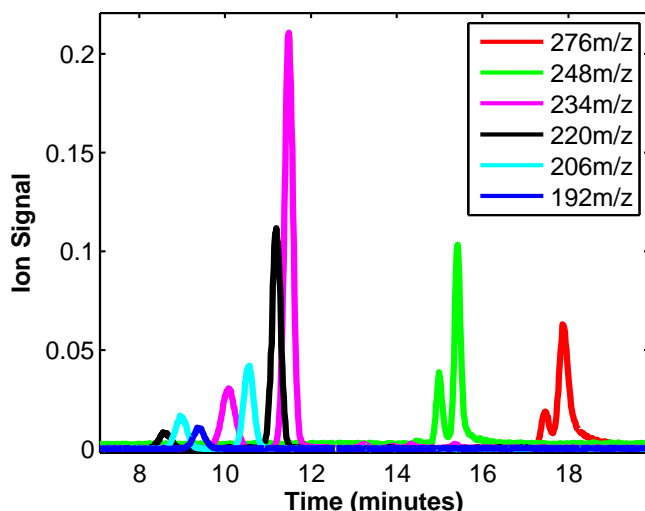


Figure 2.6: A chromatographic separation of hydroxy nitrates formed from a set of alkenes in Experiment 19. 192  $m/z$  = ethene hydroxy nitrate, 206  $m/z$  = propene hydroxy nitrate; 220  $m/z$  = methylpropene hydroxy nitrate; 234  $m/z$  = 2-methyl 2-butene hydroxy nitrate; 248  $m/z$  = 1-hexene hydroxy nitrate; 276  $m/z$  = 1-octene hydroxy nitrate. Isomer distributions were determined based on integrating peak areas from chromatograms. The later eluting peaks are prone to tailing and co-elution. In such cases, Gaussian peaks shapes were used to deconvolute co-eluting isomers and the trailing tail was assigned to the later eluting peak.

et al. (1982), and substituting  $k_7$  by  $k_7 \times \text{OH}$  and  $k_{10}$  by  $k_{10} \times \text{OH} + k_w$ , where  $k_w$  is the experimentally derived first order wall loss rate constant. Rate coefficients for OH + hydroxy nitrates were estimated based on Treves and Ruddich (2003). First order wall loss rate constants were determined by monitoring post-oxidation dark decay over at least an hour and found to be  $\leq 10^{-5} \text{ s}^{-1}$  for all compounds. A second correction factor,  $F_{\text{temp}}$ , was applied to normalize the yields to a single temperature ( $T = 293 \text{ K}$ ) to account for the dependence of the branching ratio on temperature.  $F_{\text{temp}}$  was estimated using the temperature dependence on branching ratio described in Arey et al. (2001).

Branching ratios to form  $\beta$ -hydroxy nitrates were calculated by normalizing the  $\beta$ -hydroxy nitrate by the fraction of OH + alkene reactions estimated to proceed via OH addition ( $\alpha = Y/f_a$ ). See Sect. 3.4 for more details (Table 2.3). The yields increase linearly with size of the molecule.

We find that the branching ratios can be expressed as  $\alpha = (0.045 \pm 0.016) \times N - (0.11 \pm 0.05)$ , where  $N$  is the number of heavy atoms in the peroxy radical (not including the peroxy radical oxygens). The  $\alpha$  derived for 2-methyl 2-butene was

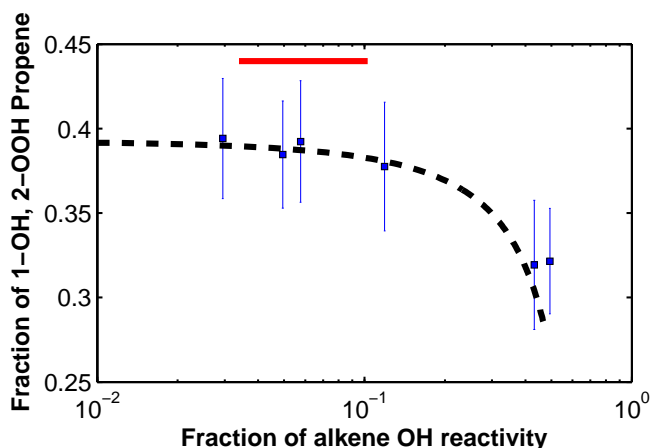


Figure 2.7: The measured isomer distribution of propene hydroxy hydroperoxides (blue boxes) as a function of the initial alkene OH reactivity and the initial hydrogen peroxide concentration. The red line represents the alkene OH reactivity regime over which hydroxy hydroperoxide isomer distributions were reported for all alkenes other than propene. The dashed black line represents a kinetic box model simulation designed to study the maximum impact  $\text{RO}_2 + \text{RO}_2$  chemistry might have on the isomer distributions. See Chapter 2.6 for further details on the kinetic model.

not included in the fit, as it was found to be significantly lower than 1-pentene and 2-methyl 1-butene. Preliminary data from other experiments (not reported here) indicate that  $\alpha$  for another internal alkene, 2,3-dimethyl 2-butene, is also substantially lower than similar carbon number compound 1-hexene. It is unclear why these internal alkenes exhibit significantly lower branching ratios to form alkyl nitrates.

### Hydroxy nitrate branching ratios from relative measurements

To place the relative nitrate yields of the alkenes (3.2) on an absolute basis, we scale the slope of the error weighted fit of the relative branching ratios to match that of the slope of the error weighted fit derived from the observed dependence of the absolute branching ratios on  $N$  derived in Sect. 3.3. Branching ratios to form  $\beta$ -hydroxy nitrates calculated using this method are listed in Table 2.4 and shown in Fig. 2.4.

Table 2.4:  $\beta$  HN sensitivities, OH rates,  $f_a$ , relative  $Y_{\beta\text{HN}}$ ,  $\alpha_{\text{alkene}}/\alpha_{\text{propene}}$  and branching ratios to form  $\beta$ -hydroxy nitrates (HN) at 293 K and 993 hPa.

Alkene	Relative CIMS sensitivity	Relative $k_{\text{OH,alkene}}$	Relative $Y_{\beta\text{HN}}$	OH addition fraction, $f_a^d$	$\alpha_{\text{alkene}}/\alpha_{\text{propene}}$	$\alpha$ (%)	Previously reported $Y_{\text{total } N}$ ( <sup>a</sup> = only $Y_{\beta\text{HN}}$ )
ethene	$0.7 \pm 0.08$	$0.323 \pm 0.04$	$0.51 \pm 0.1$	1	$0.49 \pm 0.1$	$2.2 \pm 0.6$	$0.86 \pm 0.03^a$
ethene	$0.7 \pm 0.08$	$0.323 \pm 0.04$	$0.51 \pm 0.08$	1	$0.49 \pm 0.08$	$2.2 \pm 0.5$	
propene	$1 \pm 0.2$	$1 \pm 0$	$1 \pm 0.2$	0.97	$1 \pm 0.2$	$4.4 \pm 1$	$1.5 \pm 0.1^a$
<i>d</i> <sub>6</sub> -propene	$1 \pm 0.2^c$	$1 \pm 0.07$	$1.5 \pm 0.3$	1	$1.5 \pm 0.3$	$6.6 \pm 2$	
1-butene	$0.62 \pm 0.08$	$1.19 \pm 0.05$	$2.6 \pm 0.4$	0.92	$2.7 \pm 0.4$	$12 \pm 3$	$2.5 \pm 0.2^a$
1-butene	$0.62 \pm 0.08$	$1.19 \pm 0.05$	$2.6 \pm 0.4$	0.92	$2.8 \pm 0.4$	$12 \pm 3$	
1-butene	$0.62 \pm 0.08$	$1.19 \pm 0.05$	$2.6 \pm 0.4$	0.92	$2.8 \pm 0.4$	$12 \pm 3$	
<i>cis</i> -2-butene	$0.58 \pm 0.08$	$2.13 \pm 0.02$	$2.5 \pm 0.4$	0.97	$2.5 \pm 0.4$	$11 \pm 2$	$3.4 \pm 0.5^a$
<i>cis</i> -2-butene	$0.58 \pm 0.08$	$2.13 \pm 0.02$	$2.3 \pm 0.3$	0.97	$2.3 \pm 0.3$	$10 \pm 2$	
methylpropene	$0.76 \pm 0.1$	$1.95 \pm 0.05$	$2.4 \pm 0.4$	0.97	$2.4 \pm 0.4$	$10 \pm 2$	$6 \pm 2.1^b$
methylpropene	$0.76 \pm 0.1$	$1.95 \pm 0.05$	$2.4 \pm 0.5$	0.97	$2.4 \pm 0.5$	$11 \pm 3$	
methylpropene	$0.76 \pm 0.1$	$1.95 \pm 0.05$	$2.4 \pm 0.4$	0.97	$2.4 \pm 0.4$	$11 \pm 2$	
methylpropene	$0.76 \pm 0.1$	$1.95 \pm 0.05$	$2.4 \pm 0.4$	0.97	$2.4 \pm 0.4$	$11 \pm 2$	
2-methyl 2-butene	$0.76 \pm 0.08$	$3.3 \pm 0.04$	$2.5 \pm 0.4$	0.97	$2.5 \pm 0.4$	$11 \pm 2$	$9 \pm 3.1^b$
2-methyl 2-butene	$0.76 \pm 0.08$	$3.3 \pm 0.04$	$2.4 \pm 0.3$	0.97	$2.4 \pm 0.3$	$10 \pm 2$	
1-hexene	$0.48 \pm 0.06$	$1.4 \pm 0.03$	$4.7 \pm 0.8$	0.85	$5.4 \pm 0.9$	$24 \pm 5$	$5.5 \pm 1.0^a$
1-hexene	$0.48 \pm 0.06$	$1.4 \pm 0.03$	$4.6 \pm 0.7$	0.85	$5.2 \pm 0.8$	$23 \pm 5$	
1-octene	$0.48 \pm 0.06^c$	$1.62 \pm 0.05$	$5.5 \pm 0.9$	0.78	$7 \pm 1$	$30 \pm 7$	$13 \pm 4.5^b$
1-octene	$0.48 \pm 0.06^c$	$1.62 \pm 0.05$	$4.8 \pm 0.7$	0.78	$6 \pm 1$	$29 \pm 6$	

<sup>a</sup> O'Brien et al. (1998) only hydroxy nitrate yield; <sup>b</sup> Tuazon et al. (1998); <sup>c</sup> Estimated values. For *d*<sub>6</sub>-propene hydroxy nitrates, the sensitivity is assumed to be the same as propene hydroxy nitrates. For 1-octene hydroxy nitrates, the sensitivity was assumed to be the same as 1-hexene hydroxy nitrates; <sup>d</sup> See the text for how the fraction of reactivity with OH occurring by addition ( $f_a$ ) is estimated.

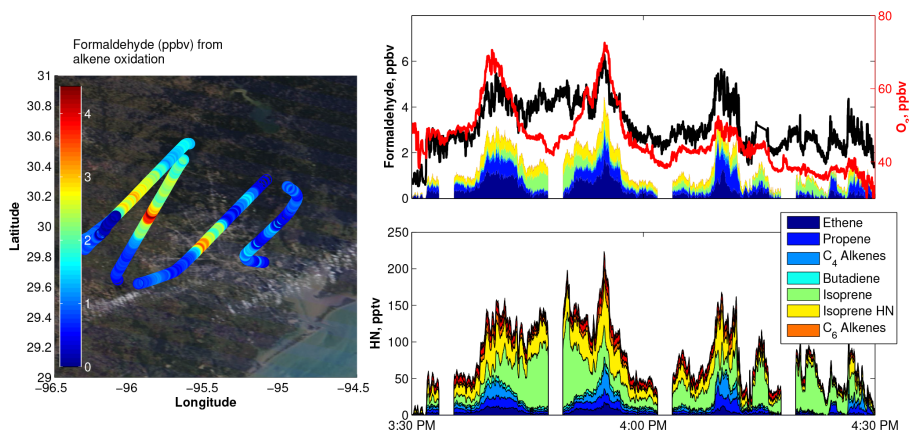


Figure 2.8: Atmospheric hydroxy nitrate,  $O_3$  and formaldehyde data measured in the Houston plume from the 2013 SEAC4RS campaign. The lower right panel shows how each hydroxy nitrate contributes to the total hydroxy nitrate measured by the Caltech CIMS for the data taken from a flight over Houston on 18 September 2013. As the plane crosses into the Houston plume, hydroxy nitrates derived from anthropogenic emissions are enhanced. The upper right panel shows formaldehyde (black, left axis) and ozone (red, right axis) are strongly correlated with anthropogenically derived hydroxy nitrates. Additionally, the lower bound estimates for the formaldehyde directly attributable to oxidation of each alkene in-plume using the branching ratios derived in this study are shown in colors. For ethene, the contribution is adjusted to produce two formaldehyde molecules after alkoxy decomposition, and uses a decomposition yield of 0.8 to account for glycolaldehyde formation from reaction of the alkoxy radical reaction with  $O_2$ . For isoprene hydroxy nitrate, a branching ratio estimate of 0.12 was used (Paulot et al., 2009). It was assumed that the sum of methyl vinyl ketone hydroxy nitrate (MVKN) and methacrolein hydroxy nitrate (MACRN) are exclusively derived from isoprene hydroxy nitrates with a yield of 1 formaldehyde per each isoprene HN oxidized to form a MVKN or MACRN molecule (Lee et al., 2014), and, therefore, a branching ratio estimate of 0.11 was used. Ozone observations were provided courtesy of Ryerson, Pollack, and Peischl at NOAA ESRL. Formaldehyde observations provided courtesy of Hanisco and Wolfe at NASA. The left panel graphs the flight tracks for this section of the flight colored by the lower bound estimate of formaldehyde formed from oxidation of alkenes. Satellite image courtesy of NASA's AERONET.

The method of placing the relative branching ratios on an absolute basis are prone to correlated errors if the two data sets are not independent of each other. We believe the data sets are sufficiently independent for the following reasons: (1) the absolute nitrate yields require a correction for OH, temperature, and wall loss, whereas the relative set does not, (2) the determination of  $\Delta$ alkene relies on GC-FID for the absolute data set while only initial reactant concentration and literature  $k_{OH}$  rate constants for the relative set, (3) the deviations of the data from the best fit

relationships are not well correlated. The two data sets, however, are prone to similar biases in the following ways: (1) initial alkene concentrations were measured by FT-IR and with the same reference spectra in both sets of experiments, (2) sensitivities for  $\beta$ -hydroxy nitrates and absolute  $\beta$ -hydroxy nitrate yields both rely upon GC-TD-LIF data.

As shown in Fig. 2.4, the dependence of the hydroxy nitrate branching ratios from  $\beta$ -hydroxy peroxy radicals on the number of heavy atoms are similar to those observed for peroxy radicals derived from *n*-alkanes (Arey et al., 2001). This suggests that destabilization of the O–ONO bond due to the presence of the  $\beta$ -hydroxy group is likely small.

Deuteration also leads to an increased branching ratio to form nitrates, possibly due to increased O–ONO lifetime resulting from the lower frequency vibrational and rotational modes. The nitrate branching ratio of *d*<sub>6</sub>-propene is a factor of 1.5 times higher than *h*<sub>6</sub>-propene. A similar increase in nitrate branching ratio has been observed for deuterated isoprene (Crouse et al., 2011).

The measured branching ratios to form  $\beta$ -hydroxy nitrates (Table 2.4) are consistent with Tuazon et al. (1998) determinations of total alkyl nitrates formed from methylpropene, *cis*-2-butene, and 2-methyl,2-butene. For the experimental conditions in Tuazon et al. (1998), however, formation of methyl nitrate from CH<sub>3</sub>O + NO<sub>2</sub> may be significant. As the FT-IR nitrate determination includes the sum of all RONO<sub>2</sub> species, these results represent an upper limit to the alkene-derived HN yield. Branching ratios reported here are also consistent with those reported by Patchen et al. (2007) for 1-butene and 2-butene determined by CIMS and calibrated using synthesized standards.

The measurements of the branching ratios reported here are significantly higher than those determined by O'Brien et al. (1998) using gas chromatography with calibration using authentic standards. O'Brien et al. (1998) used a similar GC separation technique followed by thermal dissociation of alkyl nitrates with detection of NO<sub>2</sub> by chemiluminescence. The experimental conditions were quite different than the current study. Initial alkene and oxidant concentrations were 2–3 orders of magnitude higher for most alkenes studied. Based on simulations of the experiments reported in O'Brien et al. (1998), the high initial NO concentrations led to rapid production of copious amounts of NO<sub>2</sub>, which, upon UV illumination forms significant levels of O<sup>3</sup>P for all experiments with initial NO<sub>x</sub> concentrations > 100 ppmv. Our simulations suggest that significant alkene loss in their study was due to oxidation

by O<sup>3</sup>P. This implies a significant underestimation of the branching ratios in the O'Brien et al. (1998) study for all compounds derived from high NO<sub>x</sub> experiments. See the Supplement for further details on this analysis.

### **Nitrate yields from alkoxy isomerization**

In addition to the  $\beta$ -hydroxy nitrates, dihydroxy nitrates are formed from  $\beta$ -hydroxy alkoxy radicals that are able to undergo 1,5 H-shift chemistry (Fig. 2.5). The CIMS sensitivities for these nitrates could not be obtained because they had low transmission through the gas chromatograph. From ambient sampling, the CIMS signal for the dihydroxy nitrates, relative to the  $\beta$ -hydroxy nitrates, are 1-butene, < 2 %, 1-hexene, > 10 %, 1-octene, > 5 %. For 1-butene, an upper limit is provided due to the small amount formed. For the dihydroxy nitrates from 1-hexene and 1-octene, only lower limits are reported as significant uptake to the walls of the chamber was observed.

### **Hydroxy nitrate isomer attribution**

An example GC chromatogram is shown in Fig. 2.6. Transmission through the GC was measured by integrating the entire chromatogram for a given  $m/z$ , dividing by direct sampling signal at that same  $m/z$ , and multiplying by the ratio of the direct sampling flow rate to the cryofocused gas volume. The transmission for all hydroxy nitrate isomers through the GC-CIMS/TD-LIF was measured to be 100 %  $\pm$  5 except for 1-octene hydroxy nitrates (transmission = 92 %  $\pm$  5).

Peaks were assigned from the GC chromatogram for 1-alkenes assuming the 1-OH addition product is the major isomer due to alkyl radical stabilization (i.e.,  $f_{a1} > f_{a2}$ ). In 2-methyl,2-butene, for similar reasons we assume 3-OH addition is formed in higher abundance than 2-OH addition for similar reasons (i.e.,  $f_{a3} > f_{a2}$ ). The individual isomeric distributions derived from gas chromatography are listed in Table 2.5.

Table 2.5: Isomer distribution for hydroxy nitrates and hydroxy hydroperoxides formed from OH addition to alkenes.

Alkene	Product	X = ONO <sub>2</sub> % isomer distribution	X = OOH % isomer distribution	$\alpha_1 : \alpha_2$	Previously reported % distribution	Type of reported distribution
propene	1-X, 2-OH: 2-X, 1-OH	31 ± 7: 69 ± 7	40 ± 3: 60 ± 3	1 : 1.5 <sup>+0.3</sup> <sub>-0.2</sub>	40: 60 <sup>a</sup> 28: 72 <sup>b</sup>	ONO <sub>2</sub> isomers OH branching
1-butene	1-X, 2-OH: 2-X, 1-OH	27 ± 7: 73 ± 7	35 ± 3: 65 ± 3	1 : 1.5 <sup>+0.3</sup> <sub>-0.3</sub>	35: 65 <sup>c</sup> 50: 50 <sup>e</sup> 50: 50 <sup>f</sup> 44: 56 <sup>a</sup>	OH branching OH branching OH branching OH branching RONO <sub>2</sub> isomers
<i>cis</i> -2-butene	2-X, 3-OH [(R,S) and (S,R)]: 2-X, 3-OH [(S,S) and (R,R)]	50 ± 6: 50 ± 6			29: 71 <sup>b</sup> 15: 85 <sup>d</sup>	OH branching OH branching
2-methylpropene	1-X, 2-OH: 2-X, 1-OH	11 ± 3: 89 ± 3	21 ± 2: 79 ± 2	1 : 2.2 <sup>+0.9</sup> <sub>-0.6</sub>	15: 85 <sup>d</sup>	OH branching
2-methyl 2-butene	2-X, 3-OH, 3-methyl: 3-X, 2-OH, 3-methyl	18 ± 10: 82 ± 10	31 ± 6: 69 ± 6	1 : 2.0 <sup>+2.4</sup> <sub>-0.7</sub>	44: 66 <sup>d</sup>	OH branching
1-hexene	1-X, 2-OH: 2-X, 1-OH	28 ± 7: 72 ± 7	30 <sup>+23</sup> <sub>-14</sub> : 70 <sup>+14</sup> <sub>-23</sub>	1 : 1.1 <sup>+0.9</sup> <sub>-0.8</sub>	42: 58 <sup>a</sup>	RONO <sub>2</sub> isomers
1-octene	1-X, 2-OH: 2-X, 1-OH	14 ± 15: 86 ± 15				
1-alkene (C <sub>14</sub> to C <sub>17</sub> )	1-X, 2-OH: 2-X, 1-OH					
2-methyl 1-alkene (C <sub>15</sub> )	1-X, 2-OH: 2-X, 1-OH				30: 70 <sup>g</sup> 10: 90 <sup>g</sup>	RONO <sub>2</sub> isomers RONO <sub>2</sub> isomers

<sup>a</sup> O'Brien et al. (1998), <sup>b</sup> Loison et al. (2010), <sup>c</sup> Cvetanovic (1976), <sup>d</sup> Peeters et al. (2007), <sup>e</sup> Feltham et al. (2000), <sup>f</sup> Krasnoperov

et al. (2011), <sup>g</sup> Matsunaga and Ziemann et al. (2009, 2010).

### Hydroxy nitrate branching ratios depend on RO<sub>2</sub> substitution

There is significant disagreement in the literature on the dependence of the yield of nitrates from RO<sub>2</sub> + NO with the nature of R. A central question in this debate is whether the yields of nitrates from primary, secondary, and tertiary peroxy radicals are different (Orlando and Tyndall, 2012).

To determine the branching ratios of  $\beta$ -hydroxy alkyl nitrates from specific  $\beta$ -hydroxy peroxy radicals ( $\alpha_1$  and  $\alpha_2$ ), it is necessary to know the fraction of OH adding to each carbon ( $f_{a1}$  and  $f_{a2}$ ). To estimate these fractions, we measured the isomer distribution of  $\beta$ -hydroxy hydroperoxides formed from the reaction of RO<sub>2</sub> with HO<sub>2</sub>. For these peroxy radicals, we assume that the yield of hydroperoxides from RO<sub>2</sub> + HO<sub>2</sub> reaction is unity (Raventos-Duran et al., 2007; Hasson et al., 2004; Spittler et al., 2000; Wallington and Japar, 1990a, b). We further assume that the CIMS sensitivity is the same for both isomers. With these assumptions, the ratio of the signal of the hydroxy hydroperoxides to hydroxy nitrate isomers provides an estimate of the difference in nitrate branching ratios for the individual RO<sub>2</sub> isomers.

The hydroxy hydroperoxide isomer distributions are listed in Table 2.5. It is difficult to ensure that the fate of peroxy radicals (RO<sub>2</sub>) react only with HO<sub>2</sub> because the self reaction of HO<sub>2</sub> limits its abundance. There are, therefore, other reaction pathways that must be considered when interpreting the isomer distribution of hydroxy hydroperoxides, namely: RO<sub>2</sub> + NO; RO<sub>2</sub> H-shift isomerization, RO<sub>2</sub> + wall, and RO<sub>2</sub> + RO<sub>2</sub>. RO<sub>2</sub> + NO reactions should not disturb the ROOH isomeric distribution unless the RO<sub>2</sub> + NO reaction rate constant differs between peroxy radicals. We did not detect products resulting from RO<sub>2</sub> H-shift isomerization, nor do we expect for these compounds to undergo H-shift isomerizations given the RO<sub>2</sub> lifetimes (estimated to be < 0.2 s) in these experiments. For similar reasons, RO<sub>2</sub> + wall is not expected to be a large contribution, as the mixing time of our chamber (approximately 5 min) is 2 orders of magnitude slower than the RO<sub>2</sub> lifetime.

RO<sub>2</sub> + RO<sub>2</sub> chemistry will likely perturb the ROOH isomeric distribution due to the strong dependence of peroxy radical self-reaction rates on the alkyl substitution of R (Orlando and Tyndall, 2012, and references therein). We determined the isomer distribution sensitivity to RO<sub>2</sub> + RO<sub>2</sub> chemistry with propene by varying the ratio of HO<sub>2</sub> to RO<sub>2</sub> and measuring the subsequent hydroxy hydroperoxide isomer distribution. This was accomplished by increasing the ratio of hydrogen peroxide to initial alkene concentration (and thus the ratio of HO<sub>2</sub> to RO<sub>2</sub>) at a given light flux ( $j_{H_2O_2} \approx 2 \times 10^{-6} s^{-1}$ ). Conditions where the propene hydroperoxide isomer ratios

reached a plateau were noted, and ratios of the remaining hydroperoxides alkenes were measured at these conditions (see Fig. 2.7).

The inferred ratio of  $f_{a1}$  and  $f_{a2}$  is in reasonable agreement with the experimental findings of Cvetanovic (1976) (unpublished, as reported by Peeters et al., 2007), Matsunaga and Ziemann (2009, 2010), Loison et al. (2010), and Peeters et al. (2007) which all found OH addition favors formation of more stable alkyl radicals. In contrast, Krasnoperov et al. (2011) suggested OH addition is equally distributed for propene.

Based on the  $f_{a1}$  and  $f_{a2}$  and hydroxy nitrate isomer distributions, we find that, for a given compound, the lesser substituted peroxy radical has a lower nitrate branching ratio than the higher substituted peroxy radical. This result is consistent across all compounds studied except 1-hexene, where uncertainty stemming from losses in the GC is large. This finding is in contrast to studies of simple peroxy radicals where  $\alpha$  for primary and tertiary radicals have been found to be either equal to or less than  $\alpha$  of secondary radicals (Arey et al., 2001; Espada et al., 2005; Cassanelli et al., 2007). Tyndall and Orlando (2012) cautioned that tertiary nitrates may have been underestimated in these studies due to losses of tertiary nitrates in gas chromatography.

A single  $\text{RO}_2 + \text{HO}_2$  experiment (Experiment 37) was conducted with methylpropene to determine whether the assumption of unity yield of hydroxy hydroperoxides was valid. For methylpropene, the yield of acetone was found to be  $< 5\%$  as determined by GC-FID and proton transfer reaction MS. Only an upper bound for acetone production could be estimated due to significant signal interference by hydroxy hydroperoxides to the acetone signal in the GC-FID (see Chapter 2.6).

## 2.4 Atmospheric chemistry implications

Measurements of alkyl nitrates in the atmosphere have been used extensively to diagnose ozone and aerosol formation (Rosen et al., 2004; Farmer et al., 2011; Perring et al., 2013). The development of methods described here for speciating these nitrates enables new opportunities to evaluate the role of individual compounds towards oxidant formation in urban regions.

The rate of ozone production from an individual VOC precursor can be estimated from the rate of alkyl nitrate formation. For small molecules where alkoxy chemistry leads to fragmentation, approximately two ozone molecules are formed for each VOC-derived peroxy radical that reacts with NO. In addition, this chemistry yields

reactive aldehydes that can lead to further oxidant production.

Neglecting entrainment or deposition and assuming an average alkyl nitrate branching ratio for the VOC mixture  $\ll 1$ , yields the following relationship (Rosen et al., 2004; Farmer et al., 2011; Perring et al., 2013):

$$\frac{\Delta O_3}{\Delta \text{ANs}} \approx \frac{P_{O_3}}{P_{\text{ANs}}} \approx \frac{2(1 - \alpha)}{\alpha} \approx \frac{2}{\alpha} \quad (2.3)$$

In this study, the hydroxy nitrate branching ratios,  $\alpha$ , are determined for a suite of alkenes. With this knowledge, we can estimate how much ozone (and, for terminal alkenes, how much formaldehyde) is produced for every alkyl nitrate formed. Recent research flights conducted over Houston as a part of the 2013 NASA SEAC4RS campaign provide an illustration of how measurements of hydroxy nitrates can be used to apportion the role of individual VOC precursors in oxidant formation.

Previous field studies in the Houston–Galveston airshed have yielded contradictory conclusions on the causes for the high ozone episodes experienced in the region. TexAQS I (2000) indicated the direct emission of ethene, propene, butadiene, and butenes were associated with rapid ozone production (Daum et al., 2003; Ryerson et al., 2003; Wert et al., 2003; Zhang et al., 2004). Subsequently, however, data from TexAQS II (2005-6) indicated that primary or secondary emissions of formaldehyde and nitrous acid might contribute significantly to ozone production (Olaguer et al., 2009). Rappengluck et al. (2010) and Buzcu et al. (2011), for example, concluded that a quarter or more of the measured formaldehyde is directly emitted from vehicles. In contrast, Parrish et al. (2012) suggested that greater than 90% of the formaldehyde is produced via alkene oxidation. The disagreement on the source of formaldehyde has significant implications for ozone mitigation strategies (Olaguer et al., 2014).

Shown in Fig. 2.8 are Caltech CIMS measurements of hydroxy nitrates above Houston obtained during SEAC4RS flight of 18 September 2013. During this flight, the NASA DC8 aircraft traversed Houston repeatedly sampling plumes of elevated ozone and formaldehyde. The measured hydroxy nitrates are highly correlated with elevated ozone and formaldehyde. Using Eq. (3), we find that the oxidation of small alkenes explains a large fraction of these enhancements. This finding is consistent with the earlier analysis of Rosen et al. (2004), and we suggest that, a decade later, small alkenes from petrochemical emissions remain a significant contributor to oxidant formation in Houston.

## 2.5 Conclusion

$\beta$ -hydroxy nitrate branching ratios for reactions of NO with RO<sub>2</sub> derived from the OH addition to linear and methyl-substituted alkenes are reported. Measurements of the hydroxy hydroperoxide isomer distributions from HO<sub>2</sub>-dominated oxidation of propene, 1-butene, 2-methyl 2-butene, methylpropene, and 1-hexene suggest that there is a significant difference in nitrate branching ratio, and that these branching ratios increase with increasing substitution (primary < secondary < tertiary). We recommend the overall  $\beta$ -hydroxy nitrate branching ratio from  $\beta$ -hydroxy peroxy radicals produced from C<sub>2</sub> to C<sub>8</sub> monoalkenes to be  $\alpha = (0.045 \pm 0.016) \times N - (0.11 \pm 0.05)$ , where  $N$  is the total number of heavy atoms (for alkenes,  $N$  is the total number of carbon atoms plus 1 for the OH that adds), and listed errors are  $2\sigma$ . The branching ratio dependence on the number of heavy atoms is found to be the same (within error) to that derived for  $n$ -alkanes (Arey et al., 2001).

## 2.6 Uncertainties and Box Modeling

### Uncertainties

The following is a description of the uncertainties associated with each step in the analysis presented here.

1. The determination of CIMS sensitivities for  $\beta$ -hydroxy nitrate compounds.
2. The relative determination of  $\alpha$ .
3. The absolute determination of  $\alpha$ .
4. The hydroxy nitrate isomer distributions.
5. The hydroxy hydroperoxide isomer distributions.

### CIMS sensitivities derived from TD-LIF measurements

The uncertainties associated with determination of the CIMS sensitivity include the following: assumption that the conversion of  $\beta$ -hydroxy nitrates is 100% in the TD-LIF; uncertainty in the split ratio of eluent flow between the CF<sub>3</sub>O<sup>-</sup> CIMS and TD-LIF; uncertainty in the absolute sensitivity to NO<sub>2</sub> in the TD-LIF; and integration errors associated with determining a baseline for trailing peaks in both the CF<sub>3</sub>O<sup>-</sup> CIMS and the TD-LIF chromatograms. Uncertainty in the conversion of hydroxy nitrates in the TD-LIF is discussed in Appendix A. Combined errors for the split flow ratio and absolute NO<sub>2</sub> determination are 10%. Reproducibility of sensitivity from

repeat chromatograms had errors than  $< 5\%$ , except for propene ( $< 15\%$ ), which was signal-to-noise limited. It is possible that co-eluting compounds detectable in the TD-LIF but not the  $\text{CF}_3\text{O}^-$  CIMS would bias the CIMS sensitivity low. For hydroxy nitrates from  $d_6$ -propene and 1-octene, the CIMS measurement was assumed to have the same absolute sensitivity as hydroxy nitrates from propene and 1-hexene, respectively. These were estimated to have an additional uncertainty of  $3\%$ .

### **Relative determination of $\alpha$**

Uncertainty in the estimate of the hydroxy nitrate branching ratios relative to  $\alpha_{\text{HN\_propene}}$  from Eq. (2) are determined by the relative uncertainties associated with the direct sampling CIMS measurement, the determination of CIMS sensitivities, the ratio of the OH reaction rate constants from the literature, uncertainties associated with determining the relative initial concentrations and the relative ratio of the secondary loss rates. Relative uncertainties in the  $k_{\text{OH}}$  rate constants were taken from Atkinson et al. (1983, 1986), and Aschmann and Atkinson (2008), and are reported to be  $< 6\%$ . The  $k_{\text{OH}}$  rate for  $d_6$ -propene was taken to be the same as  $k_{\text{OH}}$  for propene (Stuhl et al., 1998). PNNL spectral database IR cross sections were used to determine alkene gas concentrations, with an associated uncertainty of  $2\%$ . For compounds with no published IR cross sections, the GC-FID signal was used to corroborate the pressure measurement. This contributes an additional  $3\%$  uncertainty. Uncertainties in the CIMS quantification of hydroxy nitrates include background signal subtraction, signal to noise level, and equilibration-related time lags associated with lower volatility compounds. The combination of these uncertainties are estimated to be lower than  $10\%$  for all compounds. Additional uncertainty in sensitivity for  $d_6$ -propene and 1-octene hydroxy nitrates was assumed to be  $3\%$  because HNs derived from those compounds were not calibrated using the GC-TD-LIF technique.

### **Absolute determination of $\alpha$**

As compared to the determination of  $\alpha$  relative to  $\alpha_{\text{HN\_propene}}$ , the absolute determination of  $\alpha$  includes significant additional uncertainty associated with determining the total change in alkene concentration, the correction factors,  $F$  and  $F_{\text{temp}}$ , which account for secondary losses of hydroxy nitrates and the effect of increasing temperature from prolonged UV illumination of the chamber. The total change in alkene concentration includes uncertainty from the determination of total cham-

ber volume (3 %) and the GC-FID to quantify alkene loss (tabulated from repeat GC-FID measurements, and listed in Table 2.2). Secondary losses and temperature effects are tabulated in Table 2.2, and their uncertainties are taken to be half their total correction value. To determine an overall estimate for the branching ratio for a given compound, a reproducibility uncertainty (20 %, estimated from the standard deviation of the propene experiments) was added to the average of multiple experiments.

### ***β*-hydroxy nitrate isomer distributions**

Uncertainty estimates include uncertainty propagation from the CIMS sensitivity determination by TD-LIF for individual isomers, reproducibility of peak integration ( $\pm 2$  % for all compounds), discriminatory losses in the GC for 1-octene, and peak deconvolution for 2-methyl 2-butene HN isomers (an additional 7 %). For all compounds listed, the GC transmission is found to be  $100 \pm 5$  %, except for 1-hexene RONO<sub>2</sub>, which had a transmission of  $92 \pm 5$  %, which was assigned an additional error from this potentially discriminatory loss.

### ***β*-hydroxy hydroperoxide isomer distributions**

Uncertainty in the isomer distribution contain contributions from the reproducibility in GC peak integrations, and discriminatory losses through the GC. Uncertainties in the GC peak integrations are  $< 4$  % for all compounds, with an extra uncertainty of  $< 5$  % assigned to 2-methyl 2-butene arising from peak deconvolution of an assumed Gaussian peak shape. For all compounds listed, the GC transmission is found to be  $100 \pm 5$  %, except for 1-hexene derived ROOH, which had a transmission of 50 %. It is unclear for this compound whether the losses through the GC discriminated between the isomers, and therefore the uncertainties for this isomer distribution are large. Uncertainty from the impact of RO<sub>2</sub> + RO<sub>2</sub> was determined to be negligible given that the distribution for propene hydroxy hydroperoxides plateaus at the experimental conditions in this work (Fig. 2.7). Further evidence for the negligible impact of RO<sub>2</sub> + RO<sub>2</sub> is the lack of signals from dihydroxy and hydroxycarbonyl compounds in the CIMS observations. Experiments 25 and 26, conducted at higher ratios of alkene to hydrogen peroxide, had distinct dihydroxy and hydroxy carbonyl signals. The potential impact of RO<sub>2</sub> + RO<sub>2</sub> was also estimated through kinetic box modeling in which the primary RO<sub>2</sub> was allowed to react at a fast rate equivalent to peroxyacetyl radicals. The kinetic box modeling results, shown in Fig. 2.7, suggests that the impact of RO<sub>2</sub> + RO<sub>2</sub> on the isomer distribution should be minimal over

the experimental conditions. See Chapter 2.6 for a full description of the box model used. The uncertainty estimates do not take into account potential differences in the CIMS sensitivity for specific isomers as isomers were assumed to have the same sensitivity. For hydroxy nitrate isomers, aside from the 1-hexene HN, all isomers were determined to have very similar sensitivities.

### **Conversion efficiency in the TD-LIF**

The conversion efficiency of the TD-LIF instrument was evaluated with isopropyl nitrate. A known concentration of isopropyl nitrate was prepared in helium and sampled by the TD-LIF instrument. Oxygen addition upstream of the TD-LIF oven was increased until the  $\text{NO}_2$  signal downstream of the oven reached a plateau. This level was equal to the concentration of isopropyl nitrate (Fig. 2.9).

The conversion of  $\text{RONO}_2$  in the GC-CIMS/TD-LIF was also evaluated with isopropyl nitrate. A known amount of isopropyl nitrate was added into the chamber filled with air and sampled directly into the TD-LIF, bypassing the GC. A known volume of chamber air was then cryofocused onto the head of the GC column and analyzed in the same way described in Sect. 2. The signal from direct sampling and GC sampling agreed with the gravimetric determination to better than 10 %.

The conversion of the TD-LIF was also evaluated with isoprene hydroxy nitrates (ISOPN). The ISOPN concentrations were measured directly with TD-LIF after addition of only ISOPN into the chamber. This measurement was, however, problematic due to long equilibration times ( $> 3$  h) resulting from low sampling flow and small diameter tubing in the TD-LIF optimized for GC use. The sensitivity as determined by this measurement was 10–30 % greater than the sensitivity determined through the GC for ISOPN compounds. Full equilibration of ISOPN in the direct sampling lines of the TD-LIF was never reached given the limited sampling time available for experiments. Direct sampling of the alkene-derived hydroxy nitrates discussed in this paper was not possible because authentic standards for these compounds were not available, and post-oxidation chamber air contains non-negligible levels of  $\text{NO}_2$ . Additionally, it has been observed that high concentrations of hydrogen peroxide perturbs the measurements of nitrates and  $\text{NO}_2$  in the TD-LIF, particularly in the presence of  $\text{NO}$ . Using a GC to separate hydrogen peroxide,  $\text{NO}_2$  and  $\text{NO}$  allowed measurements of hydroxy nitrate yields without these interferences.

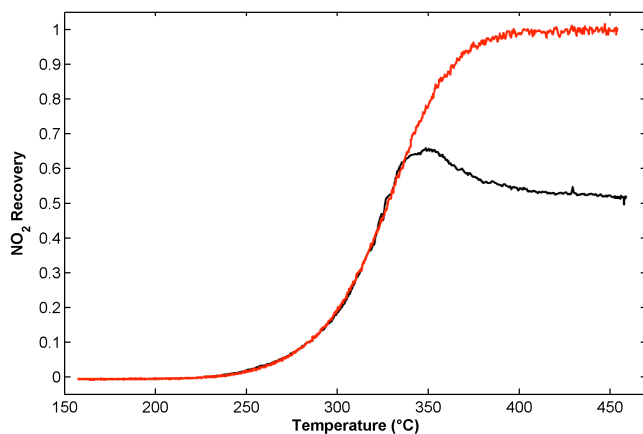


Figure 2.9: A graph showing the  $\text{NO}_2$  recovery as a function of temperature. The  $\text{NO}_2$  recovery with addition of  $\text{O}_2$  in the TD-LIF is shown in red, and in black is  $\text{NO}_2$  recovery without addition of  $\text{O}_2$ . Conversion of isopropyl nitrate is 100 % in the TD-LIF.

### Kinetic box modeling for hydroxy hydroperoxide isomer distribution

A kinetic box model of simplified chemistry in the hydroxy hydroperoxide yield experiments was used to understand the maximum potential impact of  $\text{RO}_2 + \text{RO}_2$  reactions on the isomer distribution of hydroxy hydroperoxides. In the simplified chemistry only primary peroxy radicals self reactions are considered to occur with a fast reaction rate constant equivalent to the self reaction of peroxyacetyl radical (Atkinson et al., 2007). A rate constant for the  $\text{RO}_2 + \text{HO}_2$  of  $1 \times 10^{-11} \text{ cm}^3 \text{ molec}^{-1} \text{ s}^{-1}$  (slightly slower than the IUPAC (International Union of Pure and Applied Chemistry) recommended rate constant for hydroxy-ethene  $\text{RO}_2 + \text{HO}_2$ ; Atkinson et al., 2007) is assumed. The products of  $\text{RO}_2 + \text{RO}_2$  were assumed to be chain terminating to minimize subsequent production of  $\text{HO}_2$ . The model used the measured ratio of primary to secondary peroxides from propene of 0.39 : 0.61. Table 2.6 lists the considered reactions and accompanying rate constants. The box model was initialized with 2.5 ppmv  $\text{H}_2\text{O}_2$  and propene concentrations varying from 1 to 150 ppbv. The box model was run for 10 min, the approximate length of UV exposure for each hydroxy hydroperoxide isomer run.

The model runs suggests that at the ratio of initial alkene OH reactivity to hydrogen peroxide concentration used in this study, the hydroxy hydroperoxide isomer distribution are unaffected by  $\text{RO}_2 + \text{RO}_2$  chemistry.

Table 2.6: Box modeling reactions

Reactions	Rate constants	
$H_2O_2 + hv \rightarrow OH + OH$	$2 \times 10^{-6}$	
$H_2O_2 + OH \rightarrow HO_2 + H_2O$	$1.8 \times 10^{-12}$	
$HO_2 + HO_2 \rightarrow H_2O_2$	$2.5 \times 10^{-12}$	
$OH + alkene \rightarrow 0.4primRO_2 + 0.6secRO_2$	$2.63 \times 10^{-11}$	All rate constant
$primRO_2 + primRO_2 \rightarrow \text{products}$	$1.6 \times 10^{-11}$	
$primRO_2 + HO_2 \rightarrow primROOH$	$1 \times 10^{-11}$	
$secRO_2 + HO_2 \rightarrow secROOH$	$1 \times 10^{-11}$	

units are in  $\text{cm}^3 \text{molec}^{-1} \text{s}^{-1}$  except for  $H_2O_2 + hv$ , which is in  $\text{s}^{-1}$ .

### Measurement of $\text{HO}_x$ recycling for methylpropene

Acetone measurements in the GC-FID were used to infer the yield of  $\text{HO}_x$  recycling for  $\text{RO}_2 + \text{HO}_2$  reactions occurring after OH and  $\text{O}_2$  additions to methylpropene. These observations were significantly impacted by methylpropene derived hydroxy hydroperoxides decomposing into acetone in the stainless steel sample loop. Similar decomposition of hydroxy hydroperoxides into carbonyls has been noted in other analytical instrumentation, particularly from isoprene-derived hydroxy hydroperoxides decomposing into methacrolein and methyl vinyl ketone (Liu et al., 2013; Rivera et al., 2014). In order to measure the true acetone signal, a portion of the Teflon sample line was placed in a  $-50\text{C}$  isopropanol bath, a temperature that was sufficiently low to completely trap the hydroxy hydroperoxides while not retaining acetone. Blank GC runs with zero air were run until a negligible acetone signals were measured, at which point cold trapped samples of chamber air were analyzed. The result of removing hydroxy hydroperoxides while retaining acetone is shown in Fig. 2.2, where the true acetone signal is shown to be low for Experiment 37.

The measurement of acetone was also confirmed with on-line measurements from the triple quadrupole CIMS instrument operated in positive mode with proton-transfer ionization. The predominant reagent ion in this mode is the protonated double cluster of water,  $\text{H}_2\text{OH}_3\text{O}^+$ . It was confirmed by measuring methylpropene-derived hydroxy hydroperoxides that this particular sampling and ionization method did not yield ions of protonated acetone from these hydroxy hydroperoxides in any significant yield.

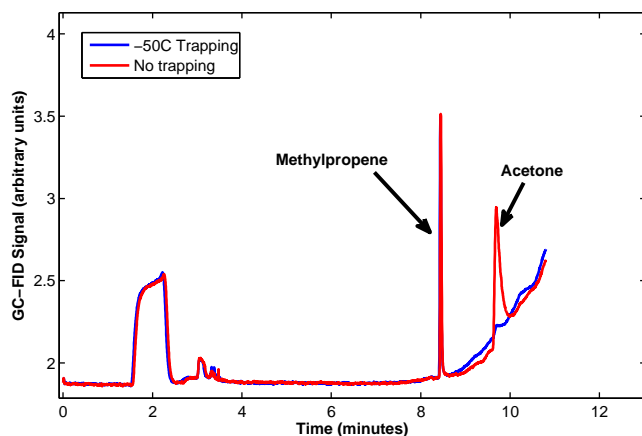


Figure 2.10: Cold trapping eliminates hydroxy hydroperoxides, removing an interference to the measured acetone.

## References

- Arey, Janet et al. (2001). "Alkyl nitrate, hydroxyalkyl nitrate, and hydroxycarbonyl formation from the NO<sub>x</sub>-air photooxidations of C5-C8 n-alkanes". In: *The Journal of Physical Chemistry A* 105.6, pp. 1020–1027.
- Aschmann, Sara M., Janet Arey, and Roger Atkinson (2010). "Kinetics and products of the reactions of OH radicals with 4,4-dimethyl-1-pentene and 3,3-dimethylbutanal at 296 ± 2 K". In: *Journal of Physical Chemistry A* 114.18, pp. 5810–5816. ISSN: 10895639. DOI: 10.1021/jp101893g. URL: <http://pubs.acs.org/doi/abs/10.1021/jp101893g>.
- Aschmann, Sara M and Roger Atkinson (2008). "Rate constants for the gas-phase reactions of OH radicals with E-7-tetradecene, 2-methyl-1-tridecene and the C7–C14 1-alkenes at 295 ± 1 K". In: *Physical Chemistry Chemical Physics* 10.28, p. 4159. ISSN: 1463-9076. DOI: 10.1039/b803527j. URL: <http://www.ncbi.nlm.nih.gov/pubmed/18612520><http://xlink.rsc.org/?DOI=b803527j>.
- Atkinson, Roger, Ernesto C. Tuazon, and William P L Carter (1985). "Extent of H atom abstraction from the reaction of the OH radical with 1-butene under atmospheric conditions". In: *International Journal of Chemical Kinetics* 17.7, pp. 725–734. ISSN: 10974601. DOI: 10.1002/kin.550170703. URL: <http://onlinelibrary.wiley.com/doi/10.1002/kin.550170703/full>.
- Barker, John R et al. (2003). "Modeling the organic nitrate yields in the reaction of alkyl peroxy radicals with nitric oxide. 2. Reaction simulations". In: *The Journal of Physical Chemistry A* 107.38, pp. 7434–7444.
- Brown, S. S. et al. (2009). "Nocturnal isoprene oxidation over the Northeast United States in summer and its impact on reactive nitrogen partitioning and secondary

- organic aerosol”. In: *Atmospheric Chemistry and Physics* 9.9, pp. 3027–3042. ISSN: 16807316. DOI: 10.5194/acp-9-3027-2009.
- Clair, Jason M St et al. (2010). “Chemical ionization tandem mass spectrometer for the in situ measurement of methyl hydrogen peroxide”. In: *Review of Scientific Instruments* 81.9, p. 094102.
- Crounse, John D, Hasse C Knap, et al. (2012). “Atmospheric fate of methacrolein. 1. Peroxy radical isomerization following addition of OH and O<sub>2</sub>”. In: *The Journal of Physical Chemistry A* 116.24, pp. 5756–5762.
- Crounse, John D, Karna A McKinney, et al. (2006). “Measurement of gas-phase hydroperoxides by chemical ionization mass spectrometry”. In: *Analytical chemistry* 78.19, pp. 6726–6732.
- Crounse, John D, Lasse B Nielsen, et al. (2013). “Autoxidation of Organic Compounds in the Atmosphere”. In: *The Journal of Physical Chemistry Letters* 4.20, pp. 3513–3520.
- Crounse, John D, Fabien Paulot, et al. (2011). “Peroxy radical isomerization in the oxidation of isoprene”. In: *Physical Chemistry Chemical Physics* 13.30, pp. 13607–13613. ISSN: 1463-9076. DOI: 10.1039/c1cp21330j. URL: <http://dx.doi.org/10.1039/C1CP21330J>.
- Farmer, D. K. et al. (2011). “Impact of organic nitrates on urban ozone production”. In: *Atmospheric Chemistry and Physics* 11.9, pp. 4085–4094. ISSN: 16807316. DOI: 10.5194/acp-11-4085-2011. URL: <http://www.atmos-chem-phys.net/11/4085/2011/>.
- Johnson, Timothy J et al. (2002). “Removing aperture-induced artifacts from Fourier transform infrared intensity values.” In: *Applied optics* 41.15, pp. 2831–9. ISSN: 0003-6935. DOI: <http://dx.doi.org/10.1364/AO.41.002831>. URL: <http://www.ncbi.nlm.nih.gov/pubmed/12027170>.
- Krasnoperov, Lev N., Nadezhda Butkovskaya, and Georges Le Bras (2011). “Branching ratios in the hydroxyl reaction with propene”. In: *Journal of Physical Chemistry A* 115.12, pp. 2498–2508. ISSN: 10895639. DOI: 10.1021/jp107178n. URL: <http://pubs.acs.org/doi/abs/10.1021/jp107178n>.
- Lee, Lance et al. (2014). “On rates and mechanisms of OH and O<sub>3</sub> reactions with isoprene-derived hydroxy nitrates”. In: *The Journal of Physical Chemistry A* 118.9, pp. 1622–1637. DOI: 10.1021/jp4107603. URL: <http://doi.org/10.1021/jp4107603>.
- Lohr, Lawrence L, John R Barker, and Robert M Shroll (2003). “Modeling the organic nitrate yields in the reaction of alkyl peroxy radicals with nitric oxide. 1. Electronic structure calculations and thermochemistry”. In: *The Journal of Physical Chemistry A* 107.38, pp. 7429–7433.

- Loison, Jean Christophe et al. (2010). "Gas-phase kinetics of hydroxyl radical reactions with C<sub>3</sub>H<sub>6</sub> and C<sub>4</sub>H<sub>8</sub>: Product branching ratios and OH addition site-specificity". In: *Journal of Physical Chemistry A* 114.51, pp. 13326–13336. ISSN: 10895639. DOI: 10.1021/jp107217w. URL: <http://pubs.acs.org/doi/abs/10.1021/jp107217w>.
- Matsunaga, Aiko and Paul J. Ziemann (2009). "Yields of  $\beta$ -hydroxynitrates and dihydroxynitrates in aerosol formed from OH radical-initiated reactions of linear alkenes in the presence of NO<sub>x</sub>". In: *Journal of Physical Chemistry A* 113.3, pp. 599–606. ISSN: 10895639. DOI: 10.1021/jp807764d. URL: <http://pubs.acs.org/doi/abs/10.1021/jp807764d>.
- Muthuramu, K, P B Shepson, and J M O'Brien (1993). "Preparation, Analysis, and Atmospheric Production Of Multifunctional Organic Nitrates". In: *Environ. Sci. Technol.* 27, pp. 1117–1124. ISSN: 0013936X. DOI: 10.1021/es00043a010. URL: <http://pubs.acs.org/doi/pdf/10.1021/es00043a010>.
- O'Brien, Jason M et al. (1998). "Determination of the hydroxy nitrate yields from the reaction of C<sub>2</sub>-C<sub>6</sub> alkenes with OH in the presence of NO". In: *The Journal of Physical Chemistry A* 102.45, pp. 8903–8908.
- Orlando, John J and Geoffrey S Tyndall (2012). "Laboratory studies of organic peroxy radical chemistry: an overview with emphasis on recent issues of atmospheric significance". In: *Chemical Society Reviews* 41.19, pp. 6294–6317.
- Patchen, Amie K et al. (2007). "Direct kinetics study of the product-forming channels of the reaction of isoprene-derived hydroxyperoxy radicals with NO". In: *International Journal of Chemical Kinetics* 39.6, pp. 353–361.
- Paulot, Fabien et al. (2013). "Unexpected Epoxide Formation in the". In: *Science* 325.2009, pp. 730–733. ISSN: 0036-8075. DOI: 10.1126/science.1172910. URL: <http://www.ncbi.nlm.nih.gov/pubmed/19661425%20http://www.sciencemag.org/cgi/doi/10.1126/science.1172910>.
- Pfrang, Christian et al. (2006a). "Correlations for gas-phase reactions of NO<sub>3</sub>, OH and O<sub>3</sub> with alkenes: An update". In: *Atmospheric Environment* 40.6, pp. 1170–1179. ISSN: 13522310. DOI: 10.1016/j.atmosenv.2005.10.019. URL: <http://linkinghub.elsevier.com/retrieve/pii/S1352231005009751>.
- (2006b). "Structure-activity relations (SARs) for gas-phase reactions of NO<sub>3</sub>, OH and O<sub>3</sub> with alkenes: An update". In: *Atmospheric Environment* 40.6, pp. 1180–1186. ISSN: 13522310. DOI: 10.1016/j.atmosenv.2005.09.080. URL: <http://linkinghub.elsevier.com/retrieve/pii/S1352231005009763>.
- Rollins, AW et al. (2012). "Evidence for NO<sub>x</sub> control over nighttime SOA formation". In: *Science* 337.6099, pp. 1210–1212.
- Rosen, R. S. (2004). "Observations of total alkyl nitrates during Texas Air Quality Study 2000: Implications for O<sub>3</sub> and alkyl nitrate photochemistry". In: *Journal of Geophysical Research* 109.D7, p. D07303. ISSN: 0148-0227. DOI: 10.1029/2003JD004227. URL: <http://doi.wiley.com/10.1029/2003JD004227>.

- Ryerson, T. B. et al. (2003). “Effect of petrochemical industrial emissions of reactive alkenes and NO<sub>x</sub> on tropospheric ozone formation in Houston, Texas”. In: *Journal of Geophysical Research* 108.D8, pp. 4249–4273. ISSN: 0148-0227. DOI: 10.1029/2002JD003070. URL: <http://www.agu.org/pubs/crossref/2003/2002JD003070.shtml%7B%5C%7D5Cnhttp://www.agu.org/journals/jd/jd0308/2002JD003070/2002JD003070.pdf>.
- Sharpe, S.N. et al. (2004). “Gas Phase Database for Quantitative Infrared Spectroscopy”. In: *Applied Spectroscopy* 58.12, pp. 1452–1461. ISSN: 0003-7028. DOI: 10.1366/0003702042641281. arXiv: arXiv:1011.1669v3.
- St. Clair, Jason M. et al. (2016). “Kinetics and Products of the Reaction of the First-Generation Isoprene Hydroxy Hydroperoxide (ISOPOOH) with OH”. In: *Journal of Physical Chemistry A* 120.9, pp. 1441–1451. ISSN: 15205215. DOI: 10.1021/acs.jpca.5b06532. URL: <http://pubs.acs.org/doi/10.1021/acs.jpca.5b06532%7B%5C%7D5Cnhttp://dx.doi.org/10.1021/acs.jpca.5b06532%20http://pubs.acs.org/doi/abs/10.1021/acs.jpca.5b06532>.
- Taylor, W.D. et al. (1980). “Atmospheric photodissociation lifetimes for nitromethane, methyl nitrite, and methyl nitrate”. In: *International Journal of Chemical Kinetics* 12.4, pp. 231–240. ISSN: 10974601. DOI: 10.1002/kin.550120404. URL: <http://doi.wiley.com/10.1002/kin.550120404>.
- Tuazon, Ernesto C. et al. (1998). “Products of the gas-phase reactions of a series of methyl-substituted ethenes with the OH radical”. In: *Environmental Science and Technology* 32.14, pp. 2106–2112. ISSN: 0013936X. DOI: 10.1021/es980153a. URL: <http://pubs.acs.org/doi/abs/10.1021/es980153a>.
- Zhang, Dan et al. (2002). “Hydroxy peroxy nitrites and nitrates from OH initiated reactions of isoprene”. In: *Journal of the American Chemical Society* 124.32, pp. 9600–9605.

*Chapter 3*

## ISOPRENE PEROXY RADICAL DYNAMICS

Teng, Alexander P, John D Crouse, and Paul O Wennberg (2017). “Isoprene peroxy radical dynamics”. In: *Journal of the American Chemical Society* 139.15, pp. 5367–5377. DOI: 10.1021/jacs.6b12838. URL: <http://doi.org/10.1021/jacs.6b12838>.

**3.1 Introduction**

2-methyl-1,3-butadiene, ( $C_5H_8$ , isoprene), is emitted to the atmosphere primarily by deciduous trees(Sharkey, Wiberley, and Donohue, 2007). The subsequent oxidation of isoprene by the hydroxyl radical (OH) substantially alters atmospheric composition globally. This chemistry leads to poor air quality in regions with large emissions of nitrogen oxides ( $NO_x \equiv NO + NO_2$ ), reduces ozone in regions without, and can increase organic aerosol, albeit in uncertain amounts(Chameides et al., 1988; F. Paulot, D. K. Henze, and P. O. Wennberg, 2012; Claeys, 2004).

Owing to its importance in atmospheric photochemistry, the oxidation of isoprene by OH has been studied extensively over the past decades. Despite this attention, isoprene chemistry continues to offer surprises as this complex photochemistry is probed using new theoretical and experimental methods(Orlando and G. S. Tyndall, 2012). The rich organic peroxy ( $RO_2$ ) chemistry results from isoprene’s conjugated alkene motif.

As with other alkenes, the reaction of isoprene with OH proceeds at nearly the gas kinetic limit and almost entirely by addition. Owing to the enhanced stability of allylic radicals, addition occurs almost entirely at the terminal carbons (e.g  $C_4$  in Scheme 1). As discussed in the SI Section 2c, OH addition to carbons 2 and 3 represents a very small fraction of the reactivity.

Following addition of OH, oxygen adds to the allyl radical yielding hydroxy peroxy radicals. In contrast to other simple alkyl radicals, the formation of the allyl radical in isoprene adds significant complexity to the subsequent peroxy radical chemistry. Due to resonance, oxygen can add either  $\beta$  or  $\delta$  to the hydroxy group; for the  $\delta$  hydroxy peroxy radicals both *E* and *Z* isomers form (The *Z*  $\delta$  isomer formed following addition at  $C_4$  is shown in Figure 3.3, Scheme 1 shows all isomers). Due



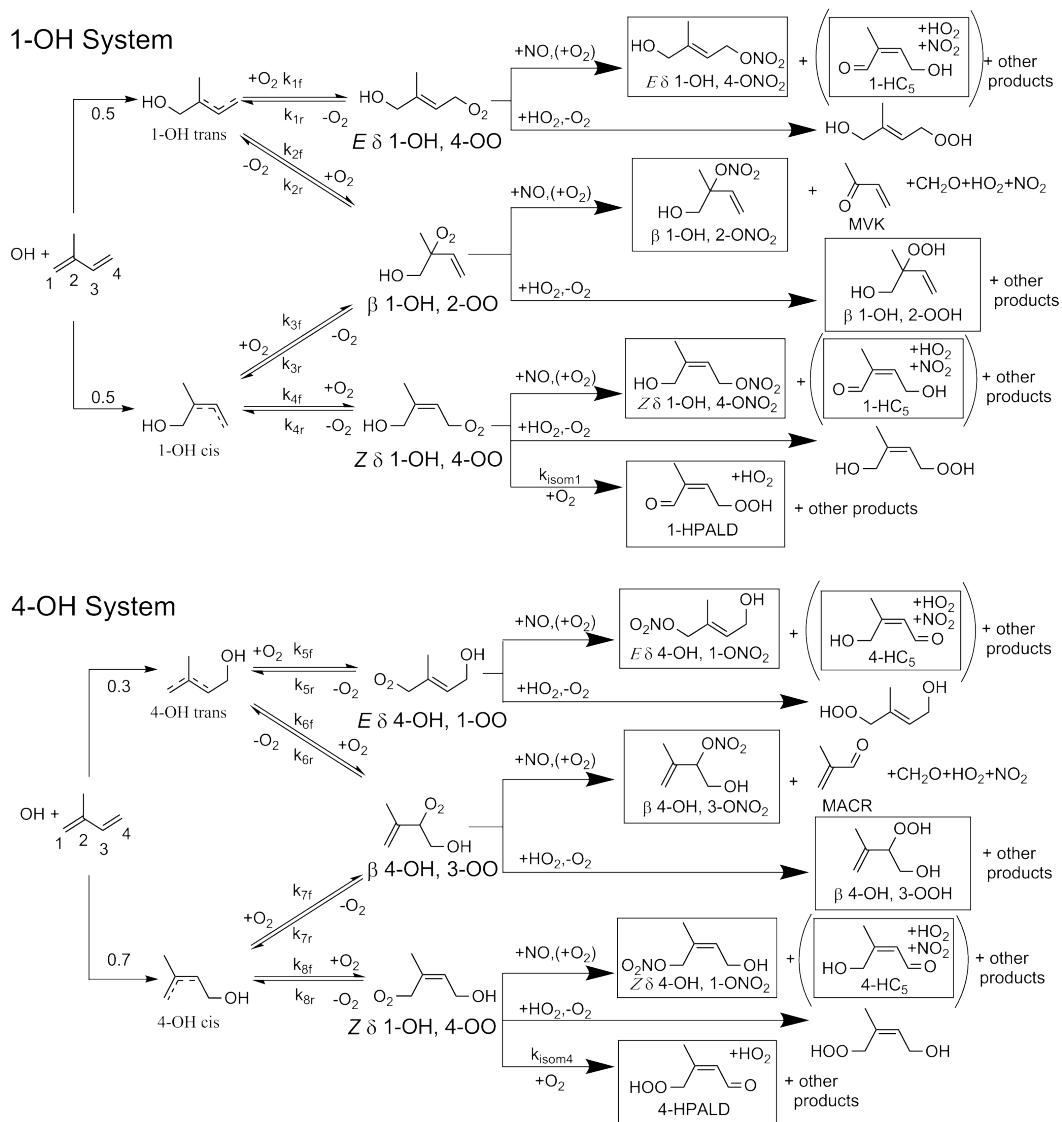


Figure 3.2: Two separate systems of peroxy radicals are formed following OH addition to isoprene. Each of the six peroxy radicals react with NO to form carbonyls and hydroxynitrates or with HO<sub>2</sub> to form hydroperoxides. The Z-δ isomers also undergo 1,6 H-shift isomerization leading to formation of hydroperoxyaldehydes (HPALDs) and other compounds. Compounds in boxes are separated by gas chromatography and detected using CF<sub>3</sub>O<sup>-</sup> chemical ionization mass spectroscopy. This method is not sensitive to singly functional carbonyls such as methacrolein (MACR) or methyl vinyl ketone (MVK) produced following decomposition of the alkoxy radical products of RO<sub>2</sub> + NO. Parentheses around compounds refers to products resulting from an additional O<sub>2</sub> addition.

non-allylic peroxy radicals (~17 kcal/mol vs. ~25-30 kcal/mol)(Benson, 1965; Ruiz et al., 1981). As a result of the low BDE, we show below that the peroxy radicals

decompose on time scales faster than they react via intra- or bi-molecular processes in the atmosphere. As discussed in the seminal paper by J Peeters, T L Nguyen, and L Vereecken, 2009, the result is a highly dynamic system of allylic and peroxy radicals leading to formation of distinctly different products that depend on both the concentrations of bimolecular reaction partners (*e.g.* NO and HO<sub>2</sub>) and the rate of intramolecular 1,6 H-shift chemistry (Scheme 1).

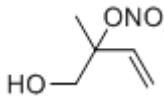
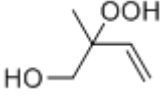
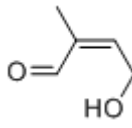
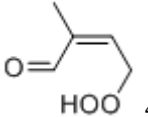
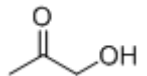
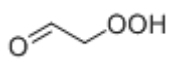
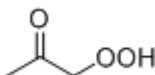
In this study, we probe the peroxy radical dynamics of the isoprene system using newly developed methods that enable measurement of isomer-specific yields of many of the stable end products (Table 1). By varying the concentrations of NO and HO<sub>2</sub> and thus the bimolecular lifetime of the peroxy radicals, we observe changing yields of specific hydroxy nitrate and hydroxy hydroperoxide isomers as well as compounds formed via intramolecular 1,6 H-shift chemistry. These data constrain the kinetics and thermodynamics in this complex system. While we focus our discussion on the isoprene peroxy radicals, we also provide additional constraints on the broader chemistry of isoprene. In addition, the behavior of the isoprene system is also compared with that of butadiene and 2,3-dimethylbutadiene (see SI Section 10).

### 3.2 Experimental Methods

The environmental chamber has been described previously and only study-specific details are provided here (St. Clair, McCabe, et al., 2010; St. Clair, Rivera-Rios, et al., 2016; A. P. Teng et al., 2015; K. H. Bates et al., 2014; John D Crouse et al., 2011a; John D Crouse, Nielsen, et al., 2013; F. Paulot, J. D. Crouse, et al., 2009). All experiments are conducted in a 0.85 m<sup>3</sup> chamber made of fluorinated ethylene propylene (Teflon-FEP, DuPont) with one port for the introduction of reagents and sampling. The experimental chamber is placed inside a room with reflective surfaces and a bank of eight UV lights (Sylvania F40/350BL,  $\lambda_{\text{peak}} = 350$  nm). During each experiment, approximately 1 std L min<sup>-1</sup> (P=1 atm, T=273.15K) of sample flow is drawn from the chamber via a 6.35 mm O.D. PFA tube, (residence time in sample line <0.2 s). For all experiments described in the body of this manuscript, the chamber temperature is 297±2 K and the pressure is 993±5 hPa. Additional experiments performed at elevated temperature are described in the SI Section 7.

A gas chromatograph with a flame ionization detector (GC-FID, Hewlett Packard 5890 series II Plus) is used to measure isoprene and other alkenes. Measurements of the multifunctional nitrates and peroxides are made using CF<sub>3</sub>O<sup>-</sup> chemical ionization

Table 3.1: Examples of the oxidation products of isoprene measured in this study.

Compound	Example isomer
Isoprene Hydroxy Nitrates (ISOPN)	 1-OH, 2-N
Isoprene Hydroxy Hydroperoxides (ISOPOOH)	 1-OH, 2-OOH
Isoprene Hydroxy Carbonyls (HC <sub>5</sub> )	 4-OH, 1-(O)
Isoprene Hydroperoxy Aldehydes (HPALD)	 4-OOH, 1-(O)
Glycolaldehyde (GLYC)	
Hydroxy acetone (HAc)	
Hydroperoxy Acetaldehyde (HPACET)	
Hydroperoxy Acetone (HPAC)	

mass spectrometry (CIMS)<sup>14,15</sup>.  $\text{CF}_3\text{O}^-$  selectively ionizes analytes by generally forming either cluster ions ( $m/z = \text{analyte mass} + 85$ ) or fluoride transfer ions ( $m/z = \text{analyte mass} + 19$ ). The time-of-flight CIMS mass spectrometer (ToF-CIMS) provide data for  $m/z = 19$  to  $m/z = 396$  at 1 AMU resolution. Compounds measured in this study are listed in Table 3.1. Chromatographic separation of individual isomers of isoprene-derived VOC products is novel and described in more detail below and in the SI Sections 2 – 5.

The chamber was prepared for each experiment with multiple flushes of clean dry air from a purge gas generator (Perkin, Model 75-52). Next, a known amount (~800 std L) of this clean, dry air was added for each experiment using a mass flow controller (MKS).

Photolysis of methyl nitrite ( $\text{CH}_3\text{ONO}$ ), synthesized, purified, and stored using the methods similar to those described by Taylor et al., 1980, is used to produce OH.  $\text{CH}_3\text{ONO}$ , stored in a glass trap submerged in liquid nitrogen, is warmed to

allow release of ~15 hPa CH<sub>3</sub>ONO vapor into an evacuated 500 cm<sup>3</sup> glass bulb. The contents of the bulb are then discarded, and the bulb is re-filled in the same manner to the desired pressure (1-200 hPa). If necessary, dilution of the CH<sub>3</sub>ONO is accomplished by subsequently filling the bulb to 993 hPa with pure N<sub>2</sub>, then pumping the bulb down to the desired pressure (1-200 hPa). The contents of the bulb are then transferred to the experimental chamber.

Isoprene (>98%), methylpropene (2-methylpropene) (> 99 %), butadiene (buta-1,3-diene) (>99%), 1-hexene (hex-1-ene) (> 99 %), 1,2-butanediol (butane 1,2 diol) (> 98 %) were purchased from Sigma Aldrich and are used without further purification. Isoprene is added to the chamber by first adding approximately 0.5 cm<sup>3</sup> liquid isoprene to a small glass tube (vapor pressure is ~600 hPa at 20 C). The contents of the tube are expanded into an evacuated 500 cm<sup>3</sup> bulb. The bulb is then evacuated, discarding its contents, and refilled to the desired pressure (1-200 hPa). If necessary, a dilution of the bulb is accomplished in the same method as CH<sub>3</sub>ONO described above. The contents of the bulb are then transferred to the experimental chamber. The purity and concentration are confirmed by FT-IR (using cross sections provided by Sharpe et al., 2004).

For a subset of the experiments, a constant ratio of isoprene, butadiene and methylpropene is used. A 5L clean gas cylinder was evacuated and filled with the desired partial pressures of isoprene (120 hPa), butadiene (240 hPa), and methylpropene (260 hPa). The tank is then filled to approximately  $1 \times 10^7$  hPa with ultra high purity N<sub>2</sub> (Sigma Aldrich, 99.999%). Additions of this mixture to the experimental chamber is performed in a fashion analogous to that described for CH<sub>3</sub>ONO.

For some experiments, nitric oxide (NO) or nitrogen dioxide (NO<sub>2</sub>) is added before beginning oxidation. In these experiments a 500 cm<sup>3</sup> or 6000 cm<sup>3</sup> glass bulb is filled from a primary standard tank containing either 1993±20 ppmv NO in N<sub>2</sub> (Matheson) or 4%±0.1% NO<sub>2</sub> in N<sub>2</sub> (Matheson) to the desired pressure (1-900 hPa). In the case of NO addition, special care is taken to minimize conversion losses of NO to NO<sub>2</sub>. The glass bulb is filled to ~1100 hPa with high purity N<sub>2</sub> to minimize NO reaction with O<sub>2</sub> while transferring to the experimental chamber. For the same reason, the contents of the glass bulb are only transferred when the experimental bag contains greater than 0.4 m<sup>3</sup> air (the rate of conversion of NO to NO<sub>2</sub> scales as [O<sub>2</sub>][NO]<sup>2</sup>).

Hydrogen peroxide (50% by weight in H<sub>2</sub>O, Sigma Aldrich) is added to the chamber by weighing an aliquot in a glass vial and then flowing 20 std L min<sup>-1</sup> clean air through the vial into the experimental chamber until the droplet completely evaporated (~10

min). The glass vial is then reweighed to confirm complete evaporation. Butanediol is added to the experimental chamber by placing a droplet into a glass vial, and flowing clean air through the vial for a set period of time.

Upon illumination, photochemistry is initiated. The desired light flux for each experiment is achieved by energizing 1-8 UV lights. For longer peroxy radical lifetimes, a single UV light is used and all direct UV light is blocked such that only photons scattered off the back reflector contributed to the light flux. For most experiments, photochemistry is limited to oxidation of less than 10% of the initial isoprene to minimize secondary losses of products. At longer bimolecular lifetimes, experiments require 12-20 hours of oxidation time (depending on experimental conditions). Wall loss is measured and accounted for in each experiment by measuring concentrations of products for 1-3 hours after oxidation is completed. Measured wall loss rate constants for ISOPN are generally  $1-3 \times 10^{-6} \text{ s}^{-1}$  at the low end, and are as high as  $1 \times 10^{-5} \text{ s}^{-1}$  for  $\text{H}_2\text{O}_2$ .

After oxidation, the chamber air is analyzed using gas chromatography CIMS (GC-CIMS)(A. P. Teng et al., 2015; Lee et al., 2014b; T. Nguyen et al., 2014). In brief, chamber air is pulled through a Teflon sampling line, through a Teflon three-port valve, and cryofocused onto the head of a 1 m megabore Restek RTX-1701 column by placing the column into a cooled isopropanol bath held at the desired temperature (250-273K). An example chromatogram from this setup is shown in Figure 3.3. For a subset of experiments, a 2 m Restek RTX-200 column followed by a 0.35 m Restek RTX-1701 column is used to quantitatively separate co-eluting ISOPN isomers. The dual column setup is inspired from the work of Mills et al., 2016, who demonstrated a successful separation of *E* 4-OH, 1-N and *Z* 1-OH, 4-N isomers using the RTX-200 column phase. Inert PEEK fittings are used to connect the Teflon tubing to the GC column. Columns are held inside a Varian GC oven (CP-3800). After analytes from a known volume of chamber air (typically 200-2000  $\text{std cm}^3$ ) are cryofocused on the head of the column, the oven temperature is ramped. Nitrogen carrier gas flow is controlled by a mass flow controller (MKS) at  $9 \text{ std cm}^3 \text{ min}^{-1}$ . The temperature program is controlled during the chromatographic separation as follows: 30 C, hold 0.1 min,  $+3 \text{ C min}^{-1}$  until 60 C, then  $+10 \text{ C min}^{-1}$  until 130 C, hold 3 min. All wetted surfaces in the analytical setup are comprised of Teflon, PEEK, or GC column materials to limit surface losses. Special care is taken to avoid liquid water formation while cryofocusing to minimize the hydrolysis and isomerization of the isoprene hydroxy nitrates (see SI Section 2b).

The isomer specific product distributions are determined by subtracting a baseline and fitting the chromatograms using Gaussian peak shapes for the eluting compounds (Figure 3.3). See SI Sections 2-5 for more information on peak assignments. Isomer specific sensitivities for the isoprene-derived hydroxy nitrates (ISOPN) are measured using the setup described in Lee et al., 2014b in which the separated isomers eluting from the GC are simultaneously measured by  $\text{CF}_3\text{O}^-$  CIMS and thermal-dissociation laser-induced fluorescence (TD-LIF)  $\text{NO}_2$  measurement. The CIMS is 6% more sensitive to the  $\beta$  ISOPN isomers (1-OH, 2-N and 4-OH, 3-N) than the  $\delta$  isomers (1-OH, 4-N and 4-OH, 1-N). CIMS sensitivities for the other compounds measured here for which pure compounds are not available, are estimated from the calculated ion-molecule collision rate (See SI Section 1)(Su and Chesnavich, 1982).

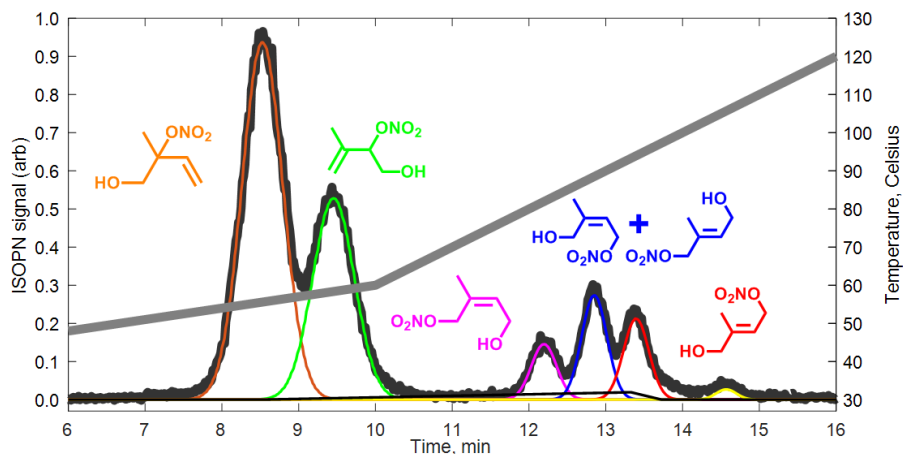


Figure 3.3: The peroxy radical isomer distribution is inferred from measurements of the ISOPN and ISOPOOH isomers. These isomers are separated using gas chromatography and detected as a cluster ion with  $\text{CF}_3\text{O}^-$  observed at  $m/z$  232 and  $m/z$  203, respectively. Shown here is an example chromatogram for ISOPN (experiment conducted at  $\tau_{\text{bimolecular}} = 0.009$  s). The  $\beta$  isomers elute first (1-OH, 2-N, in orange, 4-OH, 3-N in green) followed by the  $\delta$  isomers (*Z* 4-OH, 1-N in pink, *E* 4-OH, 1-N and *Z* 1-OH, 4-N (co-elute) in blue, and *E* 1-OH, 4-N in red). There is approximately 7% conversion of the 1-OH, 2-N to the *E* 1-OH, 4-N isomer during elution through the GC, causing an elevated baseline between these two peaks. The thin black line is the estimated contribution of the total ion signal from this conversion to the ISOPN signal. The last peak (yellow trace) is an unidentified compound.

### Calculation of Peroxy Radical Bimolecular Lifetime

The lifetime of the peroxy radicals with respect to bimolecular chemistry is estimated using recommended rate coefficients for  $\text{HO}_2 + \text{HO}_2$ ,  $\text{ISOPO}_2 + \text{HO}_2$ ,  $\text{ISOPO}_2 + \text{NO}$  and the yields of ISOPN and ISOPOOH. In all experiments, the concentrations of  $\text{HO}_2$  and  $\text{NO}$  levels are sufficiently high, relative to  $\text{ISOPO}_2$ , that the self-reaction of  $\text{ISOPO}_2$  is negligible. The bimolecular peroxy radical lifetime for these experiments is thus controlled by  $[\text{NO}]$  and  $[\text{HO}_2]$ :

$$\tau_{\text{bimolecular}} = \frac{1}{k_{\text{ISOPO}_2+\text{NO}}[\text{NO}] + k_{\text{ISOPO}_2+\text{HO}_2}[\text{HO}_2]} \quad (3.1)$$

Following John D Crouse et al., 2011b, the concentration of  $\text{HO}_2$  is estimated from the measured rate of hydrogen peroxide production ( $P_{\text{H}_2\text{O}_2}$ ) and the concentration of water measured by CIMS during each experiment:

$$P_{\text{H}_2\text{O}_2} = k_{\text{H}_2\text{O}_2} \times [\text{HO}_2]^2 \quad (3.2)$$

$$[\text{HO}_2] = \sqrt{\frac{P_{\text{H}_2\text{O}_2}}{k_{\text{H}_2\text{O}_2}}} \quad (3.3)$$

The rate constant for the  $\text{HO}_2$  self-reaction rate is calculated as (R. Atkinson et al., 2006):

$$k_{\text{HO}_2+\text{HO}_2} = \left( 2.2 \times 10^{-13} \exp\left(\frac{600}{T}\right) + 1.9 \times 10^{-33} [M] \exp\left(\frac{980}{T}\right) \right) \times \left( 1 + 1.4 \times 10^{-21} [\text{H}_2\text{O}] \exp\left(\frac{2200}{T}\right) \right) \quad (3.4)$$

For the experiments where  $\text{NO}$  is added, we use the measured  $[\text{NO}]$ . For those without added  $\text{NO}$ , as we do not have an instrument capable of accurately quantifying the low abundance of  $[\text{NO}]$  in the presence of  $\text{CH}_3\text{NO}$  ( $\sim 10$ - $100$  pptv), we infer  $[\text{NO}]$  from the ratio of the observed production rate of  $[\text{ISOPN}]$  and  $[\text{ISOPOOH}]$ ,  $P_{\text{ISOPN}}$  and  $P_{\text{ISOPOOH}}$ , respectively:

$$P_{\text{ISOPN}} = Y_{\text{ISOPN}} \times k_{\text{ISOP}O_2+\text{NO}} \times [\text{NO}] \times [\text{RO}_2] \quad (3.5)$$

$$P_{\text{ISOPOOH}} = Y_{\text{ISOPOOH}} \times k_{\text{ISOP}O_2+\text{HO}_2} \times [\text{HO}_2] \times [\text{RO}_2] \quad (3.6)$$

$$[\text{NO}] = \frac{P_{\text{ISOPN}}}{P_{\text{ISOPOOH}}} \frac{Y_{\text{ISOPOOH}}}{Y_{\text{ISOPN}}} \frac{k_{\text{ISOP}O_2+\text{HO}_2}}{k_{\text{ISOP}O_2+\text{NO}}} [\text{HO}_2] \quad (3.7)$$

The yield of hydroperoxides,  $Y_{\text{ISOPOOH}}$ , is taken to be 95% (Liu et al., 2013; F. Paulot, J. D. Crouse, et al., 2009) while the yield of hydroxynitrates,  $Y_{\text{ISOPN}}$ , is determined here to be 13±2% at 297K (see SI Section 2d). For the  $k_{\text{ISOP}O_2+\text{NO}}$ , the IUPAC recommended rate constant value of  $8.6 \times 10^{-12} \text{ cm}^3 \text{ molec}^{-1} \text{ s}^{-1}$  is used;  $k_{\text{ISOP}O_2+\text{HO}_2} = 1.7 \times 10^{-11} \text{ cm}^3 \text{ molec}^{-1} \text{ s}^{-1}$  (Boyd et al., 2003). Finally,  $\tau_{\text{bimolecular}}$  is calculated by substituting Equation ( 2 ) and Equation (7) into Equation ( 1).

For experiments in which NO is added, it is present at sufficiently high concentrations that HO<sub>2</sub> chemistry is not important (formation of HO<sub>2</sub>-derived products such as peroxy nitric acid, hydrogen peroxide, or isoprene hydroxy hydroperoxides is not observed). For these experiments, the concentration of NO at the start of the experiment is determined by manometry.

### 3.3 Results and Discussion

The aim of this study is to follow the evolution of the abundance of the individual isoprene hydroxy peroxy radical isomers as a function of their lifetime. Because we are unable to observe these radicals directly, we infer their distribution using measurements of distinct reaction products. In particular, using gas chromatography we measure the CIMS signals arising from the individual isomers of ISOPN and HC<sub>5</sub> compounds produced via NO chemistry, ISOPOOH produced from HO<sub>2</sub> chemistry, and HPALDs and other products of the 1,6 H-shift chemistry from the Z- $\delta$  hydroxy peroxy isomers (Scheme 1).

To relate the time-dependent distribution of the peroxy radical concentrations to the measured concentrations of the stable end products, we must consider whether either the hydroperoxide and nitrate yields, analytical transmission, or the NO and HO<sub>2</sub> reaction rates differ between the peroxy radical isomers. As described in the SI Section 2d, we find that the nitrate yields from  $\delta$  and  $\beta$  peroxy isomers are similar (differences <10%). The  $\delta$  and  $\beta$  nitrates have been shown to have 100% transmission through the GC (Lee et al., 2014a), For ISOPOOH, however, we find that the measured ratio of  $\delta$  to  $\beta$  isomers is ~50% lower than the equivalent ratio

of the ISOPN. The ISOPOOH yield has been shown to be nearly 100% (Harvard), and we do not expect the rate coefficients to vary. Thus, this difference is likely due to poor transmission of the  $\delta$  ISOPOOH isomers. This is not surprising as these fragile  $\delta$  ISOPOOH elute at relatively high temperature through the GC column (see SI). It is possible, however, that some of the difference reflects real differences in yields of the ISOPN. Comparing the ratio of 1-OH,2-N / 4-OH,3-N with 1-OH,2-OOH / 4-OH,3-OOH for equivalent bimolecular lifetimes, we find the ISOPN ratio is generally  $\sim 10\%$  higher than the ISOPOOH ratio, perhaps reflecting a somewhat larger nitrate yield from the tertiary RO<sub>2</sub> than the secondary RO<sub>2</sub> (consistent with trends of nitrate yields with structure observed in other studies (A. P. Teng et al., 2015; Cassanelli, Fox, and Cox, 2007)).

In the following analysis, we assume that the reaction rate coefficients and yields of ISOPN from ISOPO<sub>2</sub> + NO are identical for all peroxy radical isomers. For ISOPOOH, we assume that the rates and yields from ISOPO<sub>2</sub> + HO<sub>2</sub> are identical for the two  $\beta$  isomers. With these assumptions, a link is made between the measured abundances of the ISOPN and ISOPOOH isomers and the time-weighted average of ISOPO<sub>2</sub> isomers that produced them.

### **OH Addition to Isoprene**

From the ISOPN isomer distribution at very short RO<sub>2</sub> lifetimes ( $\tau_{\text{bimolecular}} < 0.01$  s) and the further constraint that the carbon atom to which OH adds does not depend on the peroxy radical lifetime, the measured isomer distributions of ISOPOOH, ISOPN, and HPALD imply a ratio of  $0.57 \pm 0.03$  ( $1 \sigma$ ) for OH addition at C<sub>4</sub> to C<sub>1</sub>. OH addition at C<sub>1</sub> is likely favored by the relative stability of the subsequent allylic radical (formation of an allylic radical with tertiary character favored over a radical with secondary character). This apportionment of OH addition rates at C<sub>1</sub> and C<sub>4</sub> is also consistent with the relative reaction rate constants for the OH addition reactions with butadiene, isoprene, and 2,3 dimethyl 1,3 butadiene (0.7:1:1.2) (Roger Atkinson and Arey, 2003). OH addition to C<sub>2</sub> and C<sub>3</sub> is likely minor (see SI section 2b).

### **Relative Rates of O<sub>2</sub> Addition to Isoprene Hydroxy Allylic Radicals**

In the limit where bimolecular RO<sub>2</sub> chemistry is much faster than the thermalized O<sub>2</sub> dissociation rate from the peroxy radicals, the distribution of products reflects the *cis* to *trans* ratio of OH-isoprene allylic radical adducts and the relative rates of O<sub>2</sub> addition to these radicals at the  $\beta$  and  $\delta$  positions (hereafter, the ‘kinetic limit’). As shown in Figure 3.4, when the RO<sub>2</sub> radicals react faster than  $100 \text{ s}^{-1}$  ( $\tau_{\text{bimolecular}}$

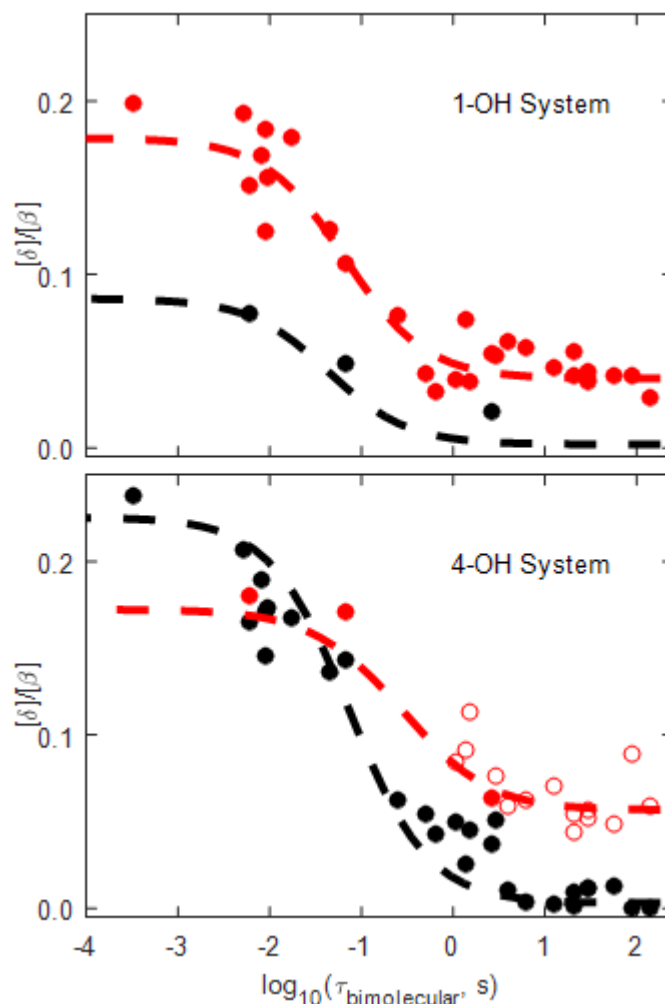


Figure 3.4: The ratio of  $\delta$  (red *E*; black *Z*) to  $\beta$  ISOPN isomers formed at 297K shown as a function of the bimolecular lifetime of the  $\text{RO}_2$  radicals for the 1-OH system (top) and the 4-OH system (bottom). The dashed line represents simulation using the kinetic model described in the SI. The red open symbols in the bottom panel are measurements using the 1m megabore RTX-1701 column where the *E* 4-OH, 1-N and *Z* 1-OH, 4-N isomers co-elute. At  $\tau > 10\text{s}$ , multiple lines of evidence suggest that this peak is comprised almost entirely of *E* 4-OH, 1-N. The scatter in the points at similar  $\tau_{\text{bimolecular}}$  reflects the challenge in trapping and deconvolution of the ISOPN isomers (the sum of all nitrates is less than 70 pptv). This aspect of the analytical chemistry dominates the uncertainty in the ratio. Data for  $\tau_{\text{bimolecular}} < 0.01\text{s}$  is limited due to the challenge of  $\text{NO}_2$  chemistry which becomes important at these very high  $[\text{NO}]$ ; it is not possible to reach this high reactivity with  $[\text{HO}_2]$  because its concentration is limited by self reaction (Eq. 2).

$< 0.01\text{s}$ ), the isomer distribution is independent of the  $\text{RO}_2$  lifetime.

In the kinetic limit, a weighted average of the 1- and 4-OH systems yields a  $\beta$  to  $\delta$  isomer ratio of 3:1 suggesting that  $O_2$  addition is substantially favored at  $\beta$  positions. The ratio is higher in the 1-system than in the 4-system. For butadiene and dimethylbutadiene, this ratio is 2:1 and 4:1, respectively (See SI). Thus, preferential  $O_2$  addition occurs to the allyl radical site with higher substitution (tertiary>secondary>primary) (see SI Section 10 for more information). Table 3.2 lists the fractional abundance of each isomer in the kinetic limit. To estimate the  $O_2$  addition rate constants from this distribution requires knowledge of both the total  $O_2$  addition rate constants and the ratio of the thermalized *cis* to *trans* allyl radicals formed after OH addition neither of which is known experimentally (the ratios shown in Scheme 1 are those calculated by J Peeters, T L Nguyen, and L Vereecken, 2009. That the *E* and *Z* isomers are produced with comparable yield is somewhat of a surprise as Peeters *et al* calculate that rate constant for formation of the *E* isomers ( $k_{1f}$ ,  $k_{5f}$ ) should be hindered by a small barrier for  $O_2$  addition to the *trans*-allylic radicals.

Table 3.2: The fractional abundance of the  $RO_2$  isomers at  $\tau_{\text{bimolecular}} < 0.01$  s inferred from measurements of the ISOPNs. The fractional abundance of *Z* 1-OH, 4-N and *E* 4-OH, 1-N ISOPN isomers are estimated from three experiments in which tandem column chromatography successfully separated these two isomers.

Isomer	Fractional abundance
$\beta$ 1-OH, 2-OO	$0.50 \pm 0.04$
<i>Z</i> $\delta$ 1-OH, 4-OO	$0.04 \pm 0.02$
<i>E</i> $\delta$ 1-OH, 4-OO	$0.09 \pm 0.03$
$\beta$ 4-OH, 3-OO	$0.26 \pm 0.03$
<i>Z</i> $\delta$ 4-OH, 1-OO	$0.06 \pm 0.015$
<i>E</i> $\delta$ 4-OH, 1-OO	$0.05 \pm 0.02$

### 3.4 Distribution of Isoprene Peroxy Radicals at Longer $\tau$

The  $\delta$ : $\beta$  ratio declines rapidly as  $\tau_{\text{bimolecular}}$  exceeds 0.01 s. Because OH adds to isoprene irreversibly for temperatures relevant to the atmosphere (and these experiments), the 1- and 4-OH systems produced by addition at  $C_1$  and  $C_4$  evolve independently. The inflection point ( $\tau_{\text{bimolecular}} \sim 0.1$  s) occurs when the rate of  $O_2$  dissociation from the  $\delta$   $RO_2$  isomers becomes competitive with the rate of bimolecular and intramolecular chemistry (Scheme 1).

The rate constant of  $O_2$  dissociation for the  $\delta$  peroxy radicals is faster than calculated by Jozef Peeters et al., 2014 (Table 3.3). This may reflect error in the calculated thermochemistry (e.g. the  $\delta$   $RO_2$  isomers are less stable with respect to the allyl

Table 3.3: The O<sub>2</sub> dissociation rate constant from the  $\delta$  RO<sub>2</sub> radicals ( $k_{\text{RO}_2 \rightarrow \text{R} + \text{O}_2}$ ) determined from kinetic modeling of the inflection point in the ratio of the  $\delta$ : $\beta$  ISOPN as the system transitions from kinetic to thermodynamic control at 297K (see SI). In the last column, the rate constants calculated by Jozef Peeters et al., 2014, are tabulated. Uncertainty in O<sub>2</sub> dissociation rate constant is estimated to be a factor of 2 (see SI). Challenges in separation of the *E* 4-OH and *Z* 1-OH RO<sub>2</sub> isomers limits the ability to separately determine the lifetime of these radicals.

$\delta$ isomer	$k_{\text{RO}_2 \rightarrow \text{R} + \text{O}_2}, \text{ s}^{-1}$ (experiment)	$k_{\text{RO}_2 \rightarrow \text{R} + \text{O}_2}, \text{ s}^{-1}$ (theory)
<i>E</i> 1-OH, 4-O <sub>2</sub>	16	4.0
<i>Z</i> 4-OH, 1-O <sub>2</sub>	10	0.7

\*A lower level quantum method was used to calculate the *E*  $\delta$  thermochemistry

radical than calculated). Because Peeters *et al*'s estimate of the dissociation rate constant is derived from a combination of the calculated thermochemistry and an assumed but uncertain O<sub>2</sub> addition rate constant, it is possible that the error lies in the addition rate constant (Jenkin et al., 1993; R. Y. Zhang et al., 2000; Ghosh et al., 2010). Regardless of the origin of the error, the key finding for the isoprene system dynamics is that the peroxy radicals are equilibrated at much *shorter* bimolecular lifetimes than anticipated (Jozef Peeters et al., 2014). This is especially important for calculation of the abundance of the *Z*- $\delta$  peroxy radicals that undergo unimolecular 1,6 H-shift chemistry.

The *E*  $\delta$  to  $\beta$  ratio asymptotes at  $\sim 0.05$  in both the 1- and 4-OH systems for  $\tau_{\text{bimolecular}} > 30$  s (Figure 3.4) representing a near steady-state distribution of the *E*  $\delta$  and  $\beta$  peroxy radicals. At these long lifetimes, the rate of O<sub>2</sub> dissociation from the  $\delta$  peroxy radicals vastly exceeds the rate of bimolecular loss and so the  $\delta$  to  $\beta$  ratio is determined by the relative thermodynamic stability of the *E*  $\delta$  and  $\beta$  peroxy radicals.

The difference in the free energies ( $\Delta G$ ) between related  $\delta$  RO<sub>2</sub> isomers and their corresponding  $\beta$  isomers are calculated from  $\delta$  to  $\beta$  ratio of the ISOPN isomers. The steady-state distribution and estimated thermochemistry for the *E*- $\delta$  4-OH, 1-O<sub>2</sub> isomer in Table 3.4 assumes that the co-eluting ISOPN is composed entirely of this isomer (see below). The free energy differences between  $\beta$  and *E*- $\delta$  isomers are similar to those calculated by Jozef Peeters et al., 2014.

There is little direct constraint on the fractional abundance of the *Z*  $\delta$  RO<sub>2</sub> isomers because of the very small concentrations of these nitrates produced for  $\tau_{\text{bimolecular}} > 1$  s. As discussed below, we instead use observations of products resulting from the

Table 3.4: Assymptotic yield ratios,  $[E-\delta]/[\beta]$   $[Z-\delta]/[\beta]$ , and the calculated free energy difference ( $\Delta G \delta-\beta$ ). These ratios are estimated from the measured ISOPN isomers at  $\tau_{\text{bimolecular}} > 30$  s. An upper bound for the fractional abundance of *E* 4-OH, 1-N is derived assuming that the co-eluting peak is comprised entirely of *E* 4-OH, 1-N at these long bimolecular lifetimes (Figure 3.3). Free energy differences between the *Z*- $\delta$ -RO<sub>2</sub> and  $\beta$ -RO<sub>2</sub> are estimated from the rate of 1,6 H-shift isomerization as discussed below. In the last column, the rate constants calculated by Peeters et al. are tabulated.

$\delta$ Isomer	$[\delta]/[\beta]$	$\Delta G$ (297K) (kcal/mol) (Measured ratio)	$\Delta G$ (297K) (kcal/mol) (calculated from 1,6 H-shift rate)	$\Delta G$ (297K), (kcal/mol) Theory(Jozef Peeters et al., 2014)
<i>E</i> 1-OH, 4-O <sub>2</sub>	0.04±0.01	1.9±0.1		2.4*
<i>Z</i> 1-OH, 4-O <sub>2</sub>	< 0.01	>2.7	3.9±1.0	2.6 ± 0.2
<i>Z</i> 4-OH, 1-O <sub>2</sub>	< 0.01	>2.7	3.4±1.0	2.5 ± 0.2
<i>E</i> 4-OH, 1-O <sub>2</sub>	≤0.06±0.02	≥1.6±0.2	1.6±0.2	2.0*

1,6 H-shift chemistry to provide constraints on the abundance of the *Z* isomers.

### The Rates and Products of the 1,6 RO<sub>2</sub> H-shifts

Based on quantum calculations, J Peeters, T L Nguyen, and L Vereecken, 2009 proposed that 1,6 H-shift chemistry of the *Z*  $\delta$  RO<sub>2</sub> isomers (Scheme 1) leading to formation of HPALD is competitive with bimolecular reactions of these radicals in the atmosphere. As a result of the continued re-population of the *Z*  $\delta$  RO<sub>2</sub> following decomposition of the  $\beta$  RO<sub>2</sub>, they suggested that the 1,6 H-shift channels would represent the most prevalent pathway for oxidation of isoprene in nature (J Peeters, T L Nguyen, and L Vereecken, 2009). In 2011, John D Crouse et al., 2011b reported, however, that the rate of HPALD production from isoprene oxidation by OH at RO<sub>2</sub> lifetimes similar to those found in nature was significantly smaller than calculated by Peeters. From measurements of the production rate of the sum of the two HPALDs, the data from Crouse *et al.* were unable to address whether the difference with theory resulted from an overestimate of the 1,6 H-shift rate constants ( $k_{\text{isom}}$ ) or from an overestimate of the fraction of the RO<sub>2</sub> in the *Z*  $\delta$  isomers ( $F_Z$ ), or from a combination thereof. Additionally, both studies (Peeters *et al.* 2009 and Crouse *et al.* 2011) assumed an HPALD yield of 100% from the 1,6 RO<sub>2</sub> 1,6 H-shift, a parameter directly affecting the comparison of experimentally inferred 1,6 H-shift rates with theory. Indeed, soon after publication of Crouse *et al.* 2011, it was

recognized that some of the difference between the experiment and theory was due to the fact that the HPALD yield is significantly smaller than unity (John D Crouse et al., 2011b; Thanh Lam Nguyen, Luc Vereecken, and Jozef Peeters, 2010).

With isomer-specific abundance measurements, 1,6 H-shift chemistry can now be described in much more detail. While the HPALD signal observed in this study is consistent with that described by John D Crouse et al., 2011b (see SI section 6d), these new observations provide constraints on the HPALD yield,  $k_{\text{isom}}$ , and  $F_Z$  independently in each system.

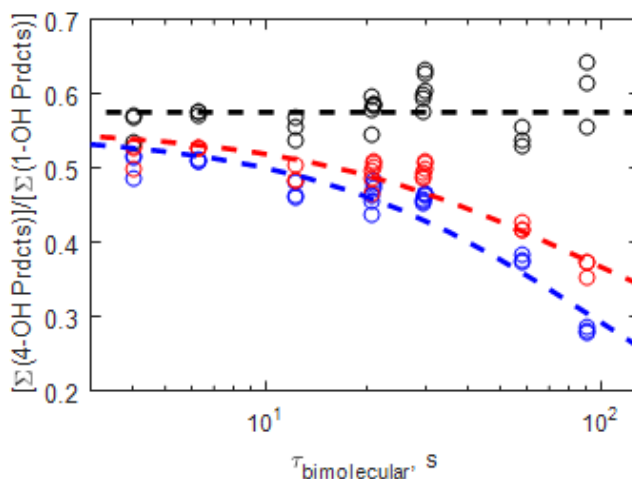


Figure 3.5: The ratio of the sum of bimolecular products (i.e.  $[\text{ISOPOOH}]/Y_{\text{ISOPOOH}} + [\text{ISOPN}]/Y_{\text{ISOPN}}$ ) produced following addition at  $C_4$  to  $C_1$  decreases with  $\tau_{\text{bimolecular}}$  (blue) reflecting the much faster unimolecular chemistry occurring in the 4-OH system. In red and black, the ratio of the sum of bimolecular and unimolecular products is plotted assuming yields of 100% (red) and 25% (black) for HPALD. To achieve mass closure (black), we find that the unimolecular chemistry must produce HPALD with a yield of  $25 \pm 10\%$  (assuming no error in the HPALD sensitivity). Including this additional source of uncertainty, we estimate an uncertainty of a factor of 2 in the yield. A model incorporating the processes shown in Scheme 1 and simulations using the rates listed in SI Table S7 and S8 are shown as dashed lines.

As the 1- and 4-OH systems evolve independently, the ratio of the yields of the hydroperoxides (nitrates) from the two systems is a measure of the relative time,  $\tau$ , (where  $1/\tau = 1/\tau_{\text{unimolecular}} + 1/\tau_{\text{bimolecular}}$ ) that each has to interact with  $\text{HO}_2$  ( $\text{NO}$ ). In the limit where only bimolecular chemistry is important,  $\tau$  in both the 1- and 4-OH systems is  $\tau_{\text{bimolecular}}$  and the ratio of both the hydroperoxide and nitrate will be the ratio of OH addition at  $C_4$  vs  $C_1$  (0.57). Plotted in blue in Figure 3.5 is the

ratio of the sum of the bimolecular products in the 4-OH system to those in the 1-OH system plotted as a function of  $\tau_{\text{bimolecular}}$ . Values different than 0.57 represent the differences in  $\tau$  in the 1- and 4-OH systems that result from intramolecular chemistry from the Z- $\delta$  RO<sub>2</sub> isomers ( $k_{\text{isom}}$ , Scheme 1). For example, at  $\tau_{\text{bimolecular}} = 60$  s the yield of hydroperoxides and hydroxynitrates produced in the 4-OH system is fully one third smaller than that in the 1-OH system reflecting a significantly shorter  $\tau$  in the 4-OH peroxy radicals (*e.g.*, much shorter  $\tau_{\text{unimolecular}}$  for 4-OH peroxy radicals).

The divergence in  $\tau$  between the 1- and 4-OH systems reflects almost entirely the intramolecular chemistry occurring following OH addition at C<sub>4</sub>. At  $\tau_{\text{bimolecular}} = 30$ s, for example, the fraction of the chemistry proceeding to HPALD in the 1-OH system is more than an order of magnitude smaller than in the 4-OH system (only the Z- $\delta$  isomers can isomerize to form HPALDs and other products). Assuming that the yield of HPALD following 1,6 H-shift is the same in the 1- and 4-OH systems, we find that the HPALD yield must be ~25% to achieve mass balance (Figure 3.5). The yield is uncertain to about a factor of two due primarily to uncertainty in the CIMS sensitivity for these compounds (see SI section 6).

It is not surprising that the yield of HPALD following the hydrogen shift should be significantly less than unity. The 1,6 H-shifts produce allylic radicals that have significant radical character at two carbon centers (Figure 3.6). While O<sub>2</sub> addition  $\alpha$  to the OH group will lead to the formation of HPALD via HO<sub>2</sub> elimination, addition of O<sub>2</sub> at the  $\gamma$  position does not. As discussed in the SI section 6b, we find additional products, most likely produced from the addition of O<sub>2</sub> at the  $\gamma$  position, that together constitute a similar yield to HPALD. Nominally 1/3 of the products are unaccounted for reflecting either error in our calibration and/or formation of products to which we are insensitive or that have sufficiently low vapor pressure that they are lost from the gas phase. For example, the reader is referred to a recent paper by Krechmer et al., 2015 where CF<sub>3</sub>O<sup>-</sup> CIMS measurements did not observe highly-oxidized, low vapor pressure organic compounds detected using the NO<sub>3</sub><sup>-</sup> anion.

The chemistry following 1,6 H-shift to the peroxy radicals is likely similar to that following 1,5 H-shift to  $\delta$  alkoxy radicals (formed in the reaction of the  $\delta$  peroxy radicals with NO - see SI section 5b). For the alkoxy radicals, both Z and E isomers yield the same allyl radical products because these radicals interconvert rapidly through an epoxide intermediate (V. S. Nguyen and Jozef Peeters, 2015). Thus, both E and Z  $\delta$  alkoxy radicals produce the same dihydroxy allyl radicals (example

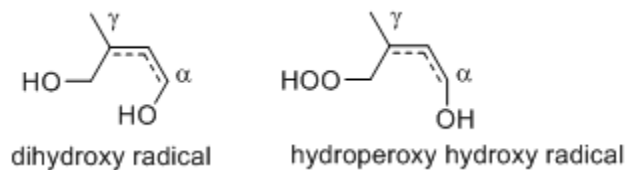


Figure 3.6: Following 1,6 H-shift to the peroxy radicals (right) and 1,5 H-shift to the alkoxy radicals (left), similar allylic radicals are formed. The measured yield of HPALD (1-OOH, 4-(O)) from the hydroperoxy hydroxyl radical (25%), is, like the yield of HC<sub>5</sub> (1-OH, 4-(O)) from the dihydroxy radical ( $45 \pm 10\%$ ), less than unity.

from 4-OH system shown in Figure 3.6). For the alkoxy chemistry the aldehyde yield, estimated from the ratio of HC<sub>5</sub> to the sum of the  $\delta$  ISOPN in the high [NO] experiments where both are well constrained, is  $45 \pm 10\%$  in both 1-OH and 4-OH systems. Given the similarities, we expect that the yield of HPALDs in the 1-OH system is also similar to that of the 4-OH system.

In Figure 3.7, the ratio of unimolecular to bimolecular products is plotted as a function of the lifetime of the peroxy radicals in the 1-OH (blue) and 4-OH (red) systems. The  $\beta$  products represent  $\sim 95\%$  of all bimolecular products for these  $\tau$  (Figure 3.4), a much larger fraction than in the kinetic limit. For the 1-OH system, we assume that  $\tau = \tau_{\text{bimolecular}}$ , consistent with the finding that, even at  $\tau_{\text{bimolecular}} = 60$  s, HPALD (1-OOH, 4-(O)) represents only a few percent of the bimolecular products. To estimate  $\tau$  in the 4-OH system, we scale  $\tau_{\text{bimolecular}}$  by the ratio of the yields of the hydroperoxides in the 4- and 1-OH systems ( $\tau = \tau_{\text{bimolecular}} \times \{[4\text{-OH}, 3\text{-OOH}]/[1\text{-OH}, 2\text{-OOH}]/.57\}$  where 0.57 represents the ratio of OH addition at C<sub>4</sub> relative to C<sub>1</sub>). As expected, the ratio of unimolecular to bimolecular products increases linearly with  $\tau$ . A significant intercept exists, however, in both the 1- and 4-OH systems.

Because the lifetime of the  $\delta$  peroxy radicals is very short ( $\sim 0.1$ s) (Figure 3.4; Table 3.3), for  $\tau > 2$ s the fraction of the peroxy radicals in the Z- $\delta$  isomers will be at steady state ( $F_{Z,ss}$ ) and so the slope calculated in Figure 3.7 is equal to  $F_{Z,ss} \times k_{\text{isom}}$  where:

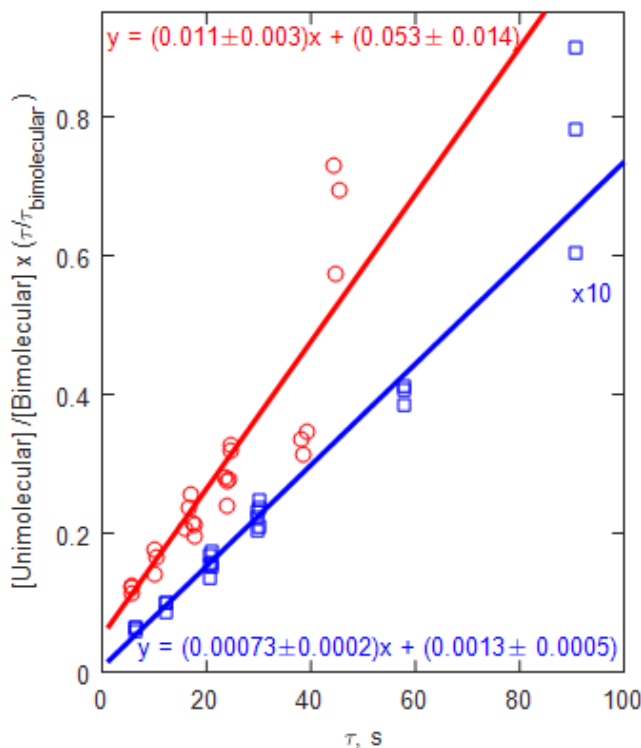


Figure 3.7: The ratio of unimolecular products ( $[\text{HPALD}]/Y_{\text{HPALD}}$ ) to bimolecular products ( $[\beta\text{-ISOPN}]/Y_{\text{ISOPN}} + [\beta\text{-ISOPHOH}]/Y_{\text{ISOPHOH}}$ ) plotted as a function of the total lifetime of the peroxy radicals ( $\tau$ ), where, for the red line,  $\tau$  is approximated as  $\tau = \tau_{\text{bimolecular}} \times \{[\beta\text{ 4-OH Bimolecular}]/[\beta\text{ 1-OH Bimolecular}]/.57\}$  where 0.57 represents the ratio of OH addition at  $C_4$  relative to  $C_1$ . The solid blue line is a fit to the data from the 1-OH system while the red is for the 4-OH system using a least squares method which takes into account uncertainties in both the dependent and independent variables. The ratio  $\tau/\tau_{\text{bimolecular}}$  arises when integrating  $k_{\text{NO}}[\text{NO}] + k_{\text{HO}_2}[\text{HO}_2] d\tau$ , where  $\tau_{\text{bimolecular}}$  is expressed as the inverse of  $k_{\text{NO}}[\text{NO}] + k_{\text{HO}_2}[\text{HO}_2]$ . See SI section 9b for more details.

$$F_{Z,ss,1-OH} = \frac{k_{3r} \frac{k_{4f}}{k_{3f} + k_{4f}}}{k_{4r} \frac{k_{3f}}{k_{3f} + k_{4f}} + k_{isom1} + \frac{1}{\tau_{bi}}} \quad (3.8)$$

$$F_{Z,ss,4-OH} = \frac{k_{7r} \frac{k_{8f}}{k_{7f} + k_{8f}}}{k_{8r} \frac{k_{7f}}{k_{7f} + k_{8f}} + k_{isom4} + \frac{1}{\tau_{bi}}} \quad (3.9)$$

Note that these equations assume that the only significant pathway for converting between the  $\beta$  and  $Z \delta \text{RO}_2$  isomers passes through the allylic radicals (see SI Section 6e for further details).

Because the  $\beta$  isomers are such a large fraction of the total and because the isomerization and bimolecular chemistry are much slower than the loss of  $O_2$  from the  $\delta$  isomers at these  $\tau$  (i.e.  $k_{4r} \times (k_{3f}/(k_{3f}+k_{4f})) \gg k_{isom1} + 1/\tau_{bimolecular}$ ), for the 1-OH system, the RHS of equation 8 is just the ratio of the rates that interconvert the beta and Z-delta isomers, e.g. at steady-state these two isomers are in thermal equilibrium:

$$F_{Z,ss,1-OH} \approx F_{Z,equilibrium,1-OH} = e^{\frac{-(G_\delta - G_\beta)}{RT}} \quad (3.10)$$

Thus, the slope in Figure 3.7 for the 1-OH system is equal to  $F_{Z,equilibrium,1-OH} \times k_{isom1}$ . Unfortunately, as discussed earlier we cannot constrain  $F_Z$  for this system directly from measurement of the ISOPN isomers and, therefore, from the slope in Figure 3.7 only determine the product  $F_{Z,equilibrium,1-OH} \times k_{isom1}$ .

An estimate of  $k_{isom}$  can, however, be determined from the intercept shown in Figure 3.7. This intercept represents the fraction of the initial (kinetically produced) Z  $\delta$  isomers (Table 3.1) that undergo isomerization,  $F_{isom}$ :

$$F_{isom1} = k_{isom1} \times \frac{1}{k_{4r} \frac{k_{3f}}{k_{3f}+k_{4f}} + k_{isom1} + \frac{1}{\tau_{bimolecular}}} \quad (3.11)$$

$$F_{isom4} = k_{isom4} \times \frac{1}{k_{8r} \frac{k_{7f}}{k_{7f}+k_{8f}} + k_{isom4} + \frac{1}{\tau_{bimolecular}}} \quad (3.12)$$

The quotients on the right hand side of Eqn. 11 and Eqn. 12 are the lifetime of the initially produced Z -  $\delta$  peroxy radicals, *i.e.* the inflection points shown in the black curves in Figure 3.4.

From the intercept, we find that only  $\sim 2\%$  of the nascent Z -  $\delta$  population isomerizes in the 1-OH system by the time the system approaches steady-state. In the 4-OH system, however, this fraction is nearly 1/3. To minimize the uncertainty in constraining the intercept, we limit the analysis to data where  $\tau_{bimolecular} > 5s$ . For this subset of the data, the lifetime of the initially produced Z  $\delta$  isomers is shorter than  $\tau_{bimolecular}$ . In addition, in the 1-OH system, the loss of  $O_2$  occurs much faster than  $k_{isom1}$  so:

$$F_{isom1} = \frac{k_{isom1}}{k_{4r} \frac{k_{3f}}{k_{3f}+k_{4f}}} \quad (3.13)$$

$$F_{isom4} = \frac{k_{isom4}}{k_{8r} \frac{k_{7f}}{k_{7f}+k_{8f}} + k_{isom4}} \quad (3.14)$$

In Table 3.4, estimates of the  $k_{isom}$  rate constants are tabulated. These are derived from the intercept from Figure 3.7,  $F_Z$  (kinetic) from Table 3.2, and the lifetime of the initially produced  $Z$ - $\delta$  peroxy radicals isomers (from kinetic modeling of data shown in Figure 3.4 and the SI). As discussed in the SI section 6, due to uncertainty in each of these terms, the rate constants are uncertain to a factor of 3.5.

Table 3.5: Experimental isomerization rate constants for the 4-OH and 1-OH systems at 297K are compared with those calculated using transition state theory by (Jozef Peeters et al., 2014). The listed experimental uncertainty includes only the fit error from Figure 6. With inclusion of other sources of error, these rates are known to only within a factor of 3.5 (SI section 6c).

	Rate constant ( $s^{-1}$ ) Experiment (297K)	Rate constant ( $s^{-1}$ ) Calculated (297K)
$k_{isom1}$	$0.36 \pm 0.15$	$0.49 \pm 0.32$
$k_{isom4}$	$3.7 \pm 1.5$	$5.4 \pm 3.3$

Using these constraints on  $k_{isom}$ , we estimate from the slope in Figure 3.7 that  $F_{Z,ss,1-OH} = 0.0020$  and  $F_{Z,ss,4-OH} = 0.0028$ . Thus,  $F_{Z,thermo,1-OH} = 0.0020$  and  $F_{Z,thermo,4-OH} = 0.004$  (for 4-OH, the relationship between  $F_{Z,ss}$  and  $F_{Z,thermo}$  is given by the ratio of  $k_{8r} \frac{k_{7f}}{k_{7f}+k_{8f}} + k_{isom4}$  to  $k_{8r} \frac{k_{7f}}{k_{7f}+k_{8f}}$ ).  $F_{Z,ss,4-OH}$  is consistent with the measured ratio  $Z$   $\delta$  ISOPN to  $\beta$  ISOPN ( $0.006 \pm 0.005$ ). The associated free energy differences (Table 3.4) are estimated to be accurate to 1 kcal/mol (see SI). While both  $F_{Z,thermo}$  and  $k_{isom}$  are individually quite uncertain, the product of these two terms is much less so ( $\pm 50\%$ ). It is this product that determines the net rate of isomerization in each system needed for atmospheric simulations.

The 297K rate constants for the isomerization are remarkably close to those calculated using multi-conformer transition state theory (TST) (Table 3.4). The temperature dependence of the rate coefficient (see SI) for the 4-OH system is also consistent with the calculated isomerization barrier. For the 1-OH system, however, the increase in the rate with temperature is much faster than calculated and the pre-exponential term is unphysically large. While it is possible that simply reflects

analytical uncertainty, we note that Peeters et al. calculated that  $\Delta E$  for dissociation of the Z  $\delta$  peroxy radicals in the 1-OH system is nearly the same as the  $\Delta E$  of the transition state for the 1,6 H-shift. Our finding that the rate of O<sub>2</sub> dissociation is much faster than Peeters calculated (Table 3.3) along with the finding that the Z  $\delta$  isomers are less stable with respect to the  $\beta$  RO<sub>2</sub> isomers than calculated suggests that the barrier for dissociation of O<sub>2</sub> from the Z  $\delta$  RO<sub>2</sub> may be submerged vis-à-vis the H-shift chemistry. If correct, the fundamental assumption of TST that the reactant is distributed according to Boltzmann statistics may not hold and a more sophisticated kinetic model would be required to calculate the rate constant.

### 3.5 Isoprene Peroxy Radical Dynamics in the Atmosphere

The majority of isoprene is oxidized in remote environments where the peroxy radical bimolecular lifetimes are long (10s to 100s of seconds). As shown in Figure 3.4, the peroxy radical distribution under these conditions will be determined primarily by thermodynamic stability of these radicals and the rate of unimolecular chemistry. Note that even at relatively short lifetimes, some isomerization occurs due to (relatively)  $k_{\text{isom}}$  and the much larger fraction of the Z-delta isomers produced initially. The interesting aspect of this finding is that it is possible to simply parameterize the product yields provided that the temperature and lifetimes are known, substantially simplifying the description of the chemistry in the context of the atmosphere (see SI section 6e and Figures S23 and S24). The change in the peroxy radical distribution to the kinetic regime occurs only where NO is above 10 ppb (e.g., only in urban centers or in NO<sub>x</sub> plumes from power plants and biomass burning will the distribution be sensitive to the initial kinetic distribution).

Because the  $\beta$  and  $\delta$  ISOPN isomers are oxidized at significantly different rates and with different fractions returning NO<sub>x</sub> to the atmosphere, the RO<sub>2</sub> distribution alters how the formation of ISOPN affects NO<sub>x</sub> and thereby O<sub>3</sub> (F Paulot, D. Henze, and P. Wennberg, 2012). From this work, greater than 90% of the ISOPN isomers produced in the OH chemistry produced in the atmosphere will be present as  $\beta$  isomers. For typical atmospheric condition (e.g.  $\tau_{\text{bimolecular}} = 100$  s; Pressure = 1 Atm; Temp = 300K), >50% of the 4-OH system exits through the isomerization channel minimizing the formation of 4-OH, 3-O<sub>2</sub> bimolecular products. Thus a single isomer - the 1-OH 2-NO<sub>2</sub> - will contribute >75% of the total yield of ISOPN. This isomer reacts with OH at the slowest rate of all ISOPN isomers, and is rapidly hydrolyzed in water to form HNO<sub>3</sub> and C<sub>5</sub> diols. As a result, the NO<sub>x</sub> loss to HNO<sub>3</sub> via formation of ISOPN is likely efficient (Fabien Paulot et al., 2013; Lee et al.,

2014b; Xie et al., 2013; F. Paulot, D. K. Henze, and P. O. Wennberg, 2012).

The increasing abundance of  $\beta$  RO<sub>2</sub> isomers with RO<sub>2</sub> lifetime implies that the NO chemistry will result in methyl vinyl ketone yields ~20% higher and much lower HC<sub>5</sub> yields in the atmosphere than predicted from laboratory studies conducted at shorter peroxy radical lifetimes (see SI section 2e). The methacrolein yields will be more variable due to loss of the 4-OH peroxy radicals via isomerization.

1,6 H-shift isomerization of the isoprene peroxy radicals is important in the atmosphere. The fraction of isoprene peroxy radicals following this channel, however, depends on local NO, HO<sub>2</sub>, and temperature. At 100s bimolecular lifetime, nearly half of the 4-OH system will exit through the unimolecular channel at 300 K. In contrast, only a small fraction, 7%, from the 1-OH system will follow this pathway.

Not all of the carbon in the unimolecular channel is accounted for by HPALD and other measured products (see SI Section 6 for more detail). Approximately 30% is unaccounted for and, if composed of low volatility products, this chemistry would represent an important source of organic aerosol.

Previous studies have invoked the unimolecular channels as potential source of missing HO<sub>x</sub> regeneration in forested settings (J Peeters, T L Nguyen, and L Vereecken, 2009; Taraborrelli et al., 2012; Fuchs et al., 2013). The results from this study suggest that the 1,6 H-shift chemistry is less efficient than calculated using the rates suggested by Peeters, 2014. Without a full accounting of the products and their photochemistry, however, it isn't possible to fully characterize the impact on OH levels.

In SI section 8 we provide temperature dependent rate coefficients for the all processes listed in Scheme 1 along with simulations of the full dataset obtained in this study. A more simplified scheme that captures this complex chemistry with sufficient fidelity for inclusion in global simulations will be forthcoming in a future publication.

## References

- Atkinson, Roger and Janet Arey (2003). "Atmospheric Degradation of Volatile Organic Compounds Atmospheric Degradation of Volatile Organic Compounds". In: *Chemical Reviews* 103, pp. 4605–4638. ISSN: 0009-2665. DOI: 10.1021/cr0206420.
- Atkinson, R. et al. (2006). "Evaluated kinetic and photochemical data for atmospheric chemistry: Volume II – gas phase reactions of organic species". In: *At-*

- ospheric Chemistry and Physics* 6.11, pp. 3625–4055. ISSN: {1680-7316}. DOI: 10.5194/acp-6-3625-2006. arXiv: acp/2004-4-1461 [1680-7324]. URL: <http://www.atmos-chem-phys.net/6/3625/2006/>.
- Bates, Kelvin H. et al. (2014). “Gas phase production and loss of isoprene epoxydiols”. In: *Journal of Physical Chemistry A* 118.7, pp. 1237–1246. ISSN: 10895639. DOI: 10.1021/jp4107958.
- Benson, Sidney W (1965). “Effects of Resonance and Structure on the Thermochemistry of Organic Peroxy Radicals and the Kinetics of Combustion Reactions”. In: *J. Am. Chem. Soc.* 8.5, pp. 972–979. ISSN: 0002-7863. DOI: 10.1021/ic50027a046. URL: <http://pubs.acs.org/doi/abs/10.1021/ja01083a006>.
- Boyd, Andrew A. et al. (2003). “Rate constants for RO<sub>2</sub> + HO<sub>2</sub> reactions measured under a large excess of HO<sub>2</sub>”. In: *Journal of Physical Chemistry A* 107.6, pp. 818–821. ISSN: 10895639. DOI: 10.1021/jp026581r. URL: <http://pubs.acs.org/doi/abs/10.1021/jp026581r>.
- Cassanelli, Paola, David J Fox, and R Anthony Cox (2007). “Temperature dependence of pentyl nitrate formation from the reaction of pentyl peroxy radicals with NO”. In: *Physical Chemistry Chemical Physics* 9.31, pp. 4332–4337. ISSN: 14639076. DOI: DOI10.1039/b700285h. URL: <http://xlink.rsc.org/?DOI=b700285h>.
- Chameides, W. et al. (1988). “The role of biogenic hydrocarbons in urban photochemical smog: Atlanta as a case study”. In: *Science* 241.4872, pp. 1473–1475. ISSN: 0036-8075. DOI: 10.1126/science.3420404. URL: <http://www.jstor.org.ezp-prod1.hul.harvard.edu/stable/1702675%20http://www.sciencemag.org/cgi/doi/10.1126/science.3420404>.
- Claeys, M. (2004). “Formation of Secondary Organic Aerosols Through Photooxidation of Isoprene”. In: *Science* 303.5661, pp. 1173–1176. ISSN: 0036-8075. DOI: 10.1126/science.1092805. URL: <http://www.sciencemag.org/cgi/doi/10.1126/science.1092805>.
- Crouse, John D, Lasse B Nielsen, et al. (2013). “Autoxidation of Organic Compounds in the Atmosphere”. In: *The Journal of Physical Chemistry Letters* 4.20, pp. 3513–3520.
- Crouse, John D et al. (2011a). “Peroxy radical isomerization in the oxidation of isoprene”. In: *Physical Chemistry Chemical Physics* 13.30, pp. 13607–13613.
- (2011b). “Peroxy radical isomerization in the oxidation of isoprene”. In: *Physical Chemistry Chemical Physics* 13.30, pp. 13607–13613. ISSN: 1463-9076. DOI: 10.1039/c1cp21330j. URL: <http://dx.doi.org/10.1039/C1CP21330J>.
- Fuchs, H. et al. (2013). “Experimental evidence for efficient hydroxyl radical regeneration in isoprene oxidation”. In: *Nature Geoscience* 6.October, pp. 10–13. ISSN: 1752-0894. DOI: 10.1038/ngeo1964. URL: <http://www.nature.com/doi/10.1038/ngeo1964>.

- Ghosh, Buddhadeb et al. (2010). "OH initiated oxidation of 1,3-butadiene in the presence of O<sub>2</sub> and NO". In: *Chemical Physics Letters* 494.1-3, pp. 8–13. ISSN: 00092614. DOI: 10.1016/j.cplett.2010.05.056. URL: <http://linkinghub.elsevier.com/retrieve/pii/S0009261410007207>.
- Jenkin, Michael E. et al. (1993). "Kinetics and product study of the self-reactions of allyl and allyl peroxy radicals at 296 K". In: *Journal of the Chemical Society, Faraday Transactions* 89.3, pp. 433–446. ISSN: 0956-5000. DOI: 10.1039/ft9938900433. URL: <http://xlink.rsc.org/?DOI=ft9938900433>.
- Krechmer, Jordan E. et al. (2015). "Formation of Low Volatility Organic Compounds and Secondary Organic Aerosol from Isoprene Hydroxyhydroperoxide Low-NO Oxidation". In: *Environmental Science & Technology* 49.17, pp. 10330–10339. ISSN: 0013-936X. DOI: 10.1021/acs.est.5b02031. URL: <http://pubs.acs.org/doi/10.1021/acs.est.5b02031>.
- Lee, Lance et al. (2014a). "On Rates and Mechanisms of OH and O<sub>3</sub> Reactions with Isoprene-Derived Hydroxy Nitrates". In: *The Journal of Physical Chemistry A*.
- (2014b). "On rates and mechanisms of OH and O<sub>3</sub> reactions with isoprene-derived hydroxy nitrates". In: *The Journal of Physical Chemistry A* 118.9, pp. 1622–1637. DOI: 10.1021/jp4107603. URL: <http://doi.org/10.1021/jp4107603>.
- Liu, Y. J. et al. (2013). "Production of methyl vinyl ketone and methacrolein via the hydroperoxyl pathway of isoprene oxidation". In: *Atmospheric Chemistry and Physics* 13.11, pp. 5715–5730. ISSN: 16807324. DOI: 10.5194/acp-13-5715-2013. URL: <http://www.atmos-chem-phys.net/13/5715/2013/>.
- Mills, Graham P. et al. (2016). "Measurement of isoprene nitrates by GCMS". In: *Atmospheric Measurement Techniques* 9.9, pp. 4533–4545. ISSN: 18678548. DOI: 10.5194/amt-9-4533-2016. URL: <http://www.atmos-meas-tech-discuss.net/amt-2016-23/%20http://www.atmos-meas-tech.net/9/4533/2016/>.
- Nguyen, TB et al. (2014). "Overview of the Focused Isoprene eXperiment at the California Institute of Technology (FIXCIT): mechanistic chamber studies on the oxidation of biogenic compounds". In: *Atmospheric Chemistry and Physics* 14.24, pp. 13531–13549. DOI: 10.5194/acp-14-13531-2014. URL: <http://doi.org/10.5194/acp-14-13531-2014>.
- Nguyen, Thanh Lam, Luc Vereecken, and Jozef Peeters (2010). "HO<sub>x</sub> regeneration in the oxidation of isoprene III: Theoretical study of the key isomerisation of the Z-??-hydroxy-peroxy isoprene radicals". In: *ChemPhysChem* 11.18, pp. 3996–4001. ISSN: 14394235. DOI: 10.1002/cphc.201000480. URL: <http://doi.wiley.com/10.1002/cphc.201000480>.
- Nguyen, Vinh Son and Jozef Peeters (2015). "Fast (E)-(Z) Isomerization Mechanisms of Substituted Allyloxy Radicals in Isoprene Oxidation". In: *Journal of Physical Chemistry A* 119.28, pp. 7270–7276. ISSN: 15205215. DOI: 10.1021/jp512057t. URL: <http://pubs.acs.org/doi/abs/10.1021/jp512057t>.

- Orlando, John J. and Geoffrey S. Tyndall (2012). "Laboratory studies of organic peroxy radical chemistry: an overview with emphasis on recent issues of atmospheric significance". In: *Chemical Society Reviews* 41.19, p. 6294. ISSN: 0306-0012. DOI: 10.1039/c2cs35166h. arXiv: arXiv:1011.1669v3. URL: <http://www.ncbi.nlm.nih.gov/pubmed/22847633>.
- Paulot, F., J. D. Crouse, et al. (2009). "Isoprene photooxidation: new insights into the production of acids and organic nitrates". In: *Atmospheric Chemistry and Physics* 9.4, pp. 1479–1501. ISSN: 1680-7324. DOI: 10.5194/acp-9-1479-2009.
- Paulot, F., D. K. Henze, and P. O. Wennberg (2012). "Impact of the isoprene photochemical cascade on tropical ozone". In: *Atmospheric Chemistry and Physics* 12.3, pp. 1307–1325. ISSN: 16807316. DOI: 10.5194/acp-12-1307-2012. URL: <http://www.atmos-chem-phys.net/12/1307/2012/>.
- Paulot, F, DK Henze, and PO Wennberg (2012). "Impact of the isoprene photochemical cascade on tropical ozone". In: *Atmospheric Chemistry and Physics* 12.3, pp. 1307–1325.
- Paulot, Fabien et al. (2013). "Unexpected Epoxide Formation in the". In: *Science* 325.2009, pp. 730–733. ISSN: 0036-8075. DOI: 10.1126/science.1172910. URL: <http://www.ncbi.nlm.nih.gov/pubmed/19661425> <http://www.sciencemag.org/cgi/doi/10.1126/science.1172910>.
- Peeters, J, T L Nguyen, and L Vereecken (2009). "HOx radical regeneration in the oxidation of isoprene". In: *Physical Chemistry Chemical Physics* 11.28, p. 5935. ISSN: 1463-9076. DOI: 10.1039/b908511d. URL: <http://www.ncbi.nlm.nih.gov/pubmed/19588016> <http://xlink.rsc.org/?DOI=b908511d>.
- Peeters, Jozef et al. (2014). "Hydroxyl radical recycling in isoprene oxidation driven by hydrogen bonding and hydrogen tunneling: The upgraded LIM1 mechanism". In: *Journal of Physical Chemistry A* 118.38, pp. 8625–8643. ISSN: 15205215. DOI: 10.1021/jp5033146. URL: <http://pubs.acs.org/doi/abs/10.1021/jp5033146>.
- Ruiz, Rennie P. et al. (1981). "Direct observation of the equilibrium between allyl radicals, oxygen, and allylperoxy radicals". In: *The Journal of Physical Chemistry* 85.12, pp. 1622–1624. ISSN: 0022-3654. DOI: 10.1021/j150612a003. URL: <http://pubs.acs.org/doi/abs/10.1021/j150612a003>.
- Sharkey, T. D., A. E. Wiberley, and A. R. Donohue (2007). "Isoprene Emission from Plants: Why and How". In: *Annals of Botany* 101.1, pp. 5–18. ISSN: 0305-7364. DOI: 10.1093/aob/mcm240. URL: <https://academic.oup.com/aob/article-lookup/doi/10.1093/aob/mcm240>.
- Sharpe, S.N. et al. (2004). "Gas Phase Database for Quantitative Infrared Spectroscopy". In: *Applied Spectroscopy* 58.12, pp. 1452–1461. ISSN: 0003-7028. DOI: 10.1366/0003702042641281. arXiv: arXiv:1011.1669v3.

- St. Clair, Jason M., David C. McCabe, et al. (2010). "Chemical ionization tandem mass spectrometer for the in situ measurement of methyl hydrogen peroxide". In: *Review of Scientific Instruments* 81.9, p. 94102. ISSN: 00346748. DOI: 10.1063/1.3480552. URL: <http://link.aip.org/link/RSINAK/v81/i9/p094102/s1%7B%5C%7Dagg=doi>.
- St. Clair, Jason M., Jean C. Rivera-Rios, et al. (2016). "Kinetics and Products of the Reaction of the First-Generation Isoprene Hydroxy Hydroperoxide (ISOPOOH) with OH". In: *Journal of Physical Chemistry A* 120.9, pp. 1441–1451. ISSN: 15205215. DOI: 10.1021/acs.jpca.5b06532. URL: <http://pubs.acs.org/doi/10.1021/acs.jpca.5b06532%7B%5C%7D5Cnhttp://dx.doi.org/10.1021/acs.jpca.5b06532%20http://pubs.acs.org/doi/abs/10.1021/acs.jpca.5b06532>.
- Su, Timothy and Walter J. Chesnavich (1982). "Parametrization of the ion–polar molecule collision rate constant by trajectory calculations". In: *The Journal of Chemical Physics* 76.10, pp. 5183–5185. ISSN: 0021-9606. DOI: 10.1063/1.442828. URL: <http://scitation.aip.org/content/aip/journal/jcp/76/10/10.1063/1.442828%7B%5C%7D5Cnhttp://scitation.aip.org/docserver/fulltext/aip/journal/jcp/76/10/1.442828.pdf?expires=1439474997%7B%5C%7Ddid=id%7B%5C%7Daccname=2106620%7B%5C%7Dchecksum=5818A6668BFC7B4E287E4F32D36C6934>.
- Taraborrelli, D. et al. (2012). "Hydroxyl radical buffered by isoprene oxidation over tropical forests". In: *Nature Geoscience* 5.4, pp. 300–300. ISSN: 1752-0894. DOI: 10.1038/ngeo1433. URL: <http://dx.doi.org/10.1038/ngeo1405>.
- Taylor, W. D. et al. (1980). "Atmospheric photodissociation lifetimes for nitromethane, methyl nitrite, and methyl nitrate". In: *International Journal of Chemical Kinetics* 12.4, pp. 231–240. ISSN: 10974601. DOI: 10.1002/kin.550120404. URL: <http://doi.wiley.com/10.1002/kin.550120404>.
- Teng, A. P. et al. (2015). "Hydroxy nitrate production in the OH-initiated oxidation of alkenes". In: *Atmospheric Chemistry and Physics* 15.8, pp. 4297–4316. DOI: 10.5194/acp-15-4297-2015. URL: <http://www.atmos-chem-phys.net/15/4297/2015/>.
- Xie, Y. et al. (2013). "Understanding the impact of recent advances in isoprene photooxidation on simulations of regional air quality". In: *Atmospheric Chemistry and Physics* 13.16, pp. 8439–8455. ISSN: 16807316. DOI: 10.5194/acp-13-8439-2013. URL: <http://www.atmos-chem-phys.net/13/8439/2013/>.
- Zhang, R Y et al. (2000). "Kinetic studies of OH-initiated reactions of isoprene". In: *Journal of Geophysical Research-Atmospheres* 105.D20, pp. 24627–24635. ISSN: 0148-0227. DOI: 10.1029/2000JD900330. URL: <http://doi.wiley.com/10.1029/2000JD900330>.

*Chapter 4*FORMATION AND FATE OF ORGANIC NITRATES IN THE  
SOUTHEASTERN UNITED STATES

Teng, A. P. et al. (2017). "Formation and Fate of Organic Nitrates in the Southeastern United States". In: *In preparation*.

**4.1 Introduction**

Over much of the remote continental boundary layer, atmospheric  $\text{NO}_x$  losses are determined not only by the formation rate of nitric acid but also by the formation of organic nitrates ( $\text{RONO}_2$ ) from biogenic precursors such as isoprene, methyl butenol, and terpenes (Browne and R. Cohen, 2012; Browne, K.-E. Min, et al., 2013; Browne, Wooldridge, et al., 2014; Fisher et al., 2016; G. Wolfe et al., 2015; P. S. Romer et al., 2016; B. H. Lee et al., 2016). Once formed, these organic nitrates either 1) deposit, likely leading to loss of atmospheric  $\text{NO}_y$  or 2) are oxidized further to other organic nitrates, release  $\text{NO}_x$  or to  $\text{HNO}_3$ . Thus, depending on their fate, formation of  $\text{RONO}_2$  species leads to a permanent atmospheric loss or a transportable reservoir for  $\text{NO}_x$ .

Organic nitrates are formed in the troposphere predominantly via two processes: in a minor branching pathway when peroxy radicals reacting with  $\text{NO}$ , or via  $\text{NO}_3$  radical addition to alkenes. The importance of these reactions (in particular isoprene oxidation) to global tropospheric oxidant levels has been recognized previously (Horowitz et al., 2007; Ito, Sillman, and Penner, 2007; F Paulot, Henze, and P. Wennberg, 2012). It is therefore important to understand the efficiency of nitrate formation and the subsequent fate of these compounds.

Much of our understanding of nitrate formation efficiency from the  $\text{RO}_2 + \text{NO}$  and  $\text{NO}_3$  pathways results from laboratory studies. For  $\text{RO}_2 + \text{NO}$ , nitrate formation proceeds through a poorly understood peroxyxynitrite isomerization reaction (D. Zhang et al., 2002; Lohr, Barker, and Shroll, 2003; J. Zhang, Dransfield, and Donahue, 2004; Barker et al., 2003). General trends have been established, however, which show that the yields of organic nitrates from peroxyxynitrites increase with the size of the peroxy radical, decrease with temperature, and increase with pressure (Orlando and G. S. Tyndall, 2012). Measured branching ratios to form organic nitrates from

isoprene oxidation have varied between 4-15% (Tuazon and Atkinson, 1990; Chen, Hulbert, and Paul B Shepson, 1998; Stevens et al., 1999; Sprengnether et al., 2002; Patchen et al., 2007; F Paulot, J. Crouse, et al., 2009; Lockwood et al., 2010; Alexander P Teng, J. D. Crouse, and P. O. Wennberg, 2017). Organic nitrate branching ratios produced in the oxidation of alkenes by OH have shown branching ratios half that of similarly sized alkanes (e.g. (J. M. O'Brien et al., 1998)), recent laboratory evidence suggests, however, that the yields (including from isoprene) are similar to those from alkane oxidation (A. P. Teng et al., 2015; Alexander P Teng, J. D. Crouse, and P. O. Wennberg, 2017). Thus, the formation of nitrates from alkenes play a larger role than previously recognized (A. P. Teng et al., 2015; Rindelaub, K. M. McAvey, and P. B. Shepson, 2014; Alexander P Teng, J. D. Crouse, and P. O. Wennberg, 2017). Yields of organic nitrates via oxidation of unsaturated VOCs by NO<sub>3</sub> are generally higher. For example, laboratory studies on isoprene oxidation by NO<sub>3</sub> show yields of organic nitrates which vary between 65-90% (Ian Barnes et al., 1990; Berndt and Böge, 1997; Perring et al., 2009; A. W. Rollins, Kiendler-Scharr, et al., 2009; A. J. Kwan et al., 2012; R. H. Schwantes et al., 2015). Organic nitrate yields from monoterpene oxidation by NO<sub>3</sub> depend significantly on the monoterpene oxidized, ranging from low yields of 10-20% for  $\alpha$ -pinene to 40-105% for  $\beta$ -pinene (Wängberg, I Barnes, and Becker, 1997; Hallquist et al., 1999; Spittler et al., 2006; Fry, Kiendler-Scharr, A. Rollins, Wooldridge, et al., 2009; Perraud et al., 2010; C. M. Boyd et al., 2015; Ayres et al., 2015a).

There is significant evidence that the formation of organic nitrates from NO<sub>3</sub> oxidation contributes to a large portion of secondary organic aerosol mass (A. Rollins et al., 2012; Fry, Draper, et al., 2013; Ayres et al., 2015b; C. M. Boyd et al., 2015; Xu et al., 2015; B. H. Lee et al., 2016). The resulting products of NO<sub>3</sub> oxidation, particularly of monoterpenes, creates highly functionalized, low vapor pressure compounds which contribute significantly to the secondary organic aerosol burden in the Southeastern United States (Xu et al., 2015; B. H. Lee et al., 2016). While the fate of the organic nitrate fraction in the particle-phase is not well understood, field and laboratory observations show evidence for the importance of conversion of organic nitrates to nitric acid in the particle phase (D. A. Day et al., 2010; L. M. Russell, Bahadur, and Ziemann, 2011; Darer et al., 2011; K. Hu, Darer, and Elrod, 2011; Shang Liu et al., 2012; Rindelaub, K. M. McAvey, and P. B. Shepson, 2014; C. M. Boyd et al., 2015; P. S. Romer et al., 2016).

The fate of peroxy radicals formed following addition of NO<sub>3</sub> to alkenes is not

well constrained due to uncertainty in the rate constants for  $\text{RO}_2$  (S. S. Brown and Stutz, 2012). There are four general fates for these  $\text{RO}_2$  radicals: reaction with  $\text{NO}_3$ ,  $\text{HO}_2$ ,  $\text{RO}_2$  or H-shift isomerization. Atmospheric simulations have reached opposite conclusions as to the fate of these peroxy radicals, particularly at night. Some studies suggest that  $\text{RO}_2 + \text{NO}_3$  is the most important reaction, while others conclude that  $\text{RO}_2 + \text{HO}_2$  is important (Kirchner and Stockwell, 1996; Bey, Aumont, and Toupance, 2001; Xie et al., 2013). A recent investigation using formaldehyde to reach an equitable distribution of  $\text{NO}_3$  has found that for isoprene,  $\text{RO}_2 + \text{HO}_2$  results in substantial production of hydroperoxides (R. H. Schwantes et al., 2015). Laboratory investigations of beta-pinene indicate that the fate of  $\text{RO}_2 + \text{HO}_2$  or  $\text{RO}_2 + \text{NO}_3$  will be dominated by secondary organic aerosol formation (C. M. Boyd et al., 2015). For many forested environments where  $\text{NO}_3$  concentrations cannot build due to the fast reaction with monoterpenes, the only available fate for a peroxy radical at night will be reaction with  $\text{HO}_2$  or  $\text{RO}_2$  (Ayres et al., 2015b). Other recent investigations and theoretical modeling have cited the importance of peroxy radical lifetimes in setting the potential fate of peroxy radicals and, in contrast to the similar chemistry following addition of OH (Peeters, T. L. Nguyen, and Vereecken, 2009; J. D. Crouse, Fabien Paulot, et al., 2011; J. D. Crouse, Nielsen, et al., 2013; G. M. Wolfe et al., 2012; Alexander P Teng, J. D. Crouse, and P. O. Wennberg, 2017), no one has studied the influence of peroxy radical lifetime following addition of  $\text{NO}_3$ .

Speciation of multifunctional nitrates allows identification of specific precursor alkenes, and therefore apportionment of the importance of each alkene to oxidant budgets. While measurements of speciated simple alkane-derived nitrates is routine, multifunctional organic nitrates have only recently been reported due to the difficulty of analysis. Previous studies have measured ambient concentrations of isoprene-derived nitrates at two forested sites in Michigan and Tennessee using a gas chromatography separation followed by conversion of organic nitrates to  $\text{NO}_2$  by pyrolysis and detection by chemiluminescence (Grossenbacher, Couch, et al., 2001; Grossenbacher, Barket Jr, et al., 2004). This technique was also used to measure hydroxy nitrates derived from alkenes at a rural site in Ontario (J. O'Brien et al., 1995). A preconcentration, solvent desorption technique followed by HPLC and GCMS technique has also been used previously to measure hydroxy nitrates from atop a wooded hill in Germany and over the Atlantic Ocean (Kastler and K Ballschmiter, 1998; Fischer, Kastler, and Karlheinz Ballschmiter, 2000). More recently, the Caltech  $\text{CF}_3\text{O}^-$ -CIMS instrument has been used to measure hydroxy nitrate concentrations at a forested site in the Sierra Nevadas. These measurements

showed biogenically-derived organic nitrates constituted two thirds of the total alkyl nitrate budget, confirming the importance of biogenically derived organic nitrates to the  $\text{NO}_y$  budget (Beaver et al., 2012). More recent measurements have been taken in the Southeastern United States from both ground and aircraft instruments, which have measured speciated gas and particle phase organic nitrates (B. H. Lee et al., 2016).

In this paper, we present ground-based measurements of speciated organic nitrates derived from ethene, propene, isoprene, and monoterpenes from the Caltech  $\text{CF}_3\text{O}^-$  CIMS over a forested site in the southeastern United States and across the broader region observed from the NASA's DC8 aircraft. We compare these measurements to the total alkyl nitrates ( $\Sigma\text{AN}$ ) as measured by the Berkeley Thermal Dissociation Laser Induced Fluorescence (TD-LIF) to understand the impact of biogenic emissions on the oxidant budget.

## 4.2 Experimental

### Sample Description

The ground-based observations and measurements presented here were obtained during the Southern Oxidant and Aerosol Study (SOAS) at the Centreville ("CTR") Southeastern Aerosol Research and Characterization Study (SEARCH) location managed by the Electric Power Research Institute (Latitude 32.90289 Longitude - 87.24968) for the U.S. Environmental Protection Agency. The site was chosen, in part, for the high concentration of local biogenic emissions. The instruments reported in this paper were collocated on top of a 20m tall stainless steel walk up tower as described by (T. B. Nguyen et al., 2015b). Several meters away from the tower to the east, west, and north directions was a temperate forest (Talladega National Forest). To the south of the tower was a grassy field. The type of vegetation nearby the tower included needle-leaf coniferous (shortleaf, longleaf, and loblolly pine), and broad-leaf deciduous (primarily oak, sweetgum, and hickory) tree species. Average canopy height in 2013 was 10m.

The aircraft observations and measurements presented here were obtained during the Southern Oxidant and Aerosol Study ((T. B. Nguyen et al., 2015b)) and the Studies of Emissions and Atmospheric Composition, Clouds, and Climate Coupling by Regional Surveys (SEAC4RS, (Toon et al., 2016)).

## Instrumentation

Multifunctional speciated organic nitrates were quantified using the Caltech  $\text{CF}_3\text{O}^-$  time-of-flight mass spectrometer (ToFwerks/Caltech) (J. D. Crouse, McKinney, et al., 2006; F Paulot, J. Crouse, et al., 2009; Clair et al., 2010; T. B. Nguyen et al., 2015a; L. Lee et al., 2014b; Alexander P Teng, J. D. Crouse, and P. O. Wennberg, 2017; A. P. Teng et al., 2015). In brief, this ionization chemistry is selective for multifunctional organic nitrates, acidic species, peroxides, and multifunctional carbonyls and alcohols. The ground-based set up was described fully by (T. B. Nguyen et al., 2015a). For SEAC4RS, the instrument setup was similar to that described by (J. D. Crouse, McKinney, et al., 2006) and (Clair et al., 2010).

At SOAS, instrumental backgrounds were measured every thirty minutes by scrubbing the analytes using a two-stage filter containing palladium coated alumina pellets and sodium bicarbonate treated nylon wool. This passes ambient water vapor while scrubbing ambient analytes (Spencer et al., 2011). To determine ambient concentrations, an interpolation between these background signals was subtracted from ambient signals.

The  $\text{CF}_3\text{O}^-$  CIMS technique measures nitrates at the  $m/z$  of the parent molecule + 85 ( $\text{CF}_3\text{O}^-$ ). Using  $\text{CF}_3\text{O}^-$ , no significant fragmentation has been noted for any nitrate molecules aiding significantly in identification of measured analytes. Experimentally-derived sensitivities have been determined using a secondary calibration source for ethanal nitrate (ETHLN), propanone nitrate (PROPNN), isoprene hydroxy nitrates (ISOPN) and methyl vinyl ketone nitrates (MVKN), and are all found to be within 25% of each other (L. Lee et al., 2014a). For those organic nitrate compounds for which experimentally derived sensitivities are not available, a sensitivity equal to the isoprene  $\beta$  hydroxy nitrates was applied. This sensitivity is on the upper end of all of the nitrates and therefore potentially underestimates ambient concentrations. The estimated uncertainty for the CIMS concentrations presented here are  $\pm 20\%$  compounds for which sensitivity is known, and 40% for compounds for which the sensitivity is unknown.

The experimentally-derived sensitivities are 25% smaller than estimated from calculated dipole moments and polarizabilities as used by Fabien Paulot et al., 2013 and Beaver et al., 2012. Using the sensitivities determined by L. Lee et al., 2014a increases the speciated alkyl nitrates reported in Beaver et al., 2012 such that they account for nearly the entire measured alkyl nitrate budget at the forested site in the Sierra Nevadas.

The measured signal at any given  $m/z$  is a sum of the target compound and a small signal from the naturally occurring  $^{13}\text{C}$  isotope signal produced from the species at the  $m/z - 1$  amu. The size of the contribution increases with the presumed number of carbons atoms in a molecule. We corrected for this by subtracting from the signal at the  $m/z$  of the nitrate 1.1 % times the number of carbons that produce signal at  $m/z - 1$ . For the nitrates presented here, this correction was only applied to two compounds: 1) ethanal nitrate signal, observed at  $m/z$  190, due to the large ambient signal observed at  $m/z$  189 (a known product of IEPOX oxidation, (K. H. Bates et al., 2014), and 2) propanone nitrate, observed at  $m/z$  204, due to the large ambient signal observed at  $m/z$  203 (a known signal for the sum of ISOPOOH and IEPOX). For the other nitrate signals reported, the isotopologues at  $m/z - 1$  signals were too small to contribute significantly.

Gas- and particle-phase alkyl nitrate (AN) measurements were made by the University of California Berkeley using a thermal dissociation laser-induced fluorescence (TD-LIF) instrument as described elsewhere (D. Day et al., 2002; A. W. Rollins, Smith, et al., 2010). The instrument operates four channels: 1)  $\text{NO}_2$ , 2)  $\text{NO}_2 + \Sigma\text{PNs}$ , 3)  $\text{NO}_2 + \Sigma\text{PNs} + \Sigma\text{ANs}$ , 4) aerosol-phase alkyl nitrates only. Channels 2 and 3 pass flow through ovens set at characteristic temperatures to completely dissociate reactive nitrogen classes into  $\text{NO}_2$  and a companion radical. The aerosol phase alkyl nitrate channel passes ambient air through a gas-phase denuder which traps all gas-phase compounds including  $\text{NO}_2$  (A. Rollins et al., 2012) while allowing >85 % of particles with an aerodynamic diameter above 100 nm to pass through to the oven for conversion to and subsequent detection of  $\text{NO}_2$ .

At CTR, a suite of VOCs were measured by the NOAA Tropospheric Airborne Chromatograph for Oxy-hydrocarbons and Hydrocarbons gas chromatograph and electron ionization mass spectrometer (TACOH-GCMS) sampling system. Ambient air was sampled for five minutes every thirty minutes through a 40m Teflon tube, cryotrapped by liquid nitrogen in a sample loop, and then thermally desorbed into the head of a gas chromatography column. Compounds were identified by retention time and by matching mass spectral fragmentation pattern against a NIST library. On the DC8, a similar suite of VOCs were measured by the UC-Irvine from bottled air collected periodically during flight.

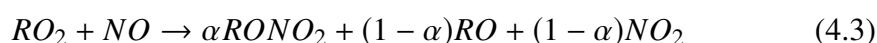
### 4.3 Results and discussion

#### Daytime $\text{NO}_x$ loss is dominated by isoprene

During the daytime, the main gas phase  $\text{NO}_x$  loss pathway in urban atmospheres is generally considered:



However, further away from elevated urban  $\text{NO}_x$  emissions, the the formation of organic nitrates becomes a dominant gas phase  $\text{NO}_x$  loss pathway (Browne and R. Cohen, 2012; Browne, K.-E. Min, et al., 2013).



The impact of any VOC on instantaneous  $\text{NO}_x$  loss depends on its concentration, OH rate constant, the likelihood that the subsequent peroxy radical will react with NO, and the branching ratio ( $\alpha$ ) to form an organic nitrate after reaction with NO. The instantaneous gas-phase  $\text{NO}_x$  loss is given by:

$$\frac{d[\text{NO}_x]_{\text{loss,NO}_2}}{dt} = k_{\text{OH,NO}_2 \rightarrow \text{HNO}_3} [\text{NO}_2] [\text{OH}] \quad (4.6)$$

$$\frac{d[\text{NO}_x]_{\text{loss,VOC}}}{dt} = k_{\text{OH,VOC}} [\text{OH}] [\text{VOC}] \times \frac{k_{\text{NO,RO}_2} [\text{NO}]}{k_{\text{NO,RO}_2} [\text{NO}] + k_{\text{HO}_2,\text{RO}_2} [\text{HO}_2] + k_{\text{isom}}} \quad (4.7)$$

Approximately 80% of  $\text{NO}_x$  loss is accounted for by nitrate formation from isoprene and terpenes across the campaign, with the remainder accounted for by  $\text{OH} + \text{NO}_2$ . A small fraction of the  $\text{NO}_x$  losses (less than 2%) are in reactive small alkenes and alkanes (ethene, propene, methyl vinyl ketone, ethane, propane, butanes, pentanes, hexane, decane). The distribution of  $\text{NO}_x$  losses reported here are similar to those observed for a Boreal forest in Canada (Browne, K.-E. Min, et al., 2013), and imply that BVOC-derived organic nitrates may play an outsized role in setting  $\text{NO}_x$  lifetime and ozone production efficiency over regions with high biogenic emissions depending on their fate.

### **Daytime organic nitrates at CTR: sources, time series, and diurnal profiles**

Names, abbreviations, signals, and molecular weights of observed organic nitrates are listed in Table 4.1. During the day, oxidation by OH in the presence of NO is generally responsible for organic nitrate formation. The Caltech CIMS is only sensitive to multifunctional nitrates and therefore predominantly measures products from precursors which can undergo OH or NO<sub>3</sub> addition (to unsaturated bonds) to produce multifunctional compounds. Daytime peak concentrations of isoprene ranged from 2ppbv to 10ppbv. Daytime concentrations of speciated organic nitrates are dominated by ISOPN, much like the BEARPEX 2009 environment (Xiong et al., 2015; Beaver et al., 2012). There are eight possible peroxy isomers that can form following OH addition to isoprene, but recent laboratory studies have shown that at peroxy radical lifetimes  $\gg 1$ s two peroxy isomers dominate following OH addition (Figure 4.1) (Alexander P Teng, J. D. Crouse, and P. O. Wennberg, 2017). This dramatically simplifies the subsequent ISOPN chemistry, as the two isomers predominantly oxidize to MVKN and MACRN, which CIMS monitors as one signal at 234m/z (L. Lee et al., 2014a). This MVKN+MACRN signal also has a contribution from methvyl vinyl ketone and methacrolein OH oxidation in the presence of NO. This additional source of MACRN and MVKN is minimal, as laboratory investigations have shown (J. D. Crouse, Knap, et al., 2012; Praske et al., 2014). There are two other nitrates observed during the day which can be attributed to isoprene oxidation products: ETHLN and PROPNN. These products are derived from OH oxidation of  $\delta$ -isoprene nitrate isomers as shown in Figure 4.2. These  $\delta$ -isoprene nitrate are predicted to form predominantly from NO<sub>3</sub> radical oxidation (R. H. Schwantes et al., 2015).

In addition to isoprene, other alkenes were also present at the SOAS site. Ethene, propene, butadiene, and C<sub>4</sub>-enes (1-butene, 2-butene, and methylpropene) had measurable daytime concentrations and therefore form hydroxy nitrates from OH oxidation in the presence of NO as shown in Figure 4.3. Unlike isoprene, which has a light-dependent biogenic emission profile, these alkenes seemed to be predominantly anthropogenic in origin as their concentrations correlated well with anthropogenic tracers, and reached daily peak concentrations at night. Previous studies have noted that these alkenes, with the exception of butadiene, also have light-dependent biogenic emission profiles (AH Goldstein et al., 1996; Lamanna and A. H. Goldstein, 1999). Their daytime concentrations were generally 60-100pptv.

Time series and average diurnal profiles for each of the nitrates discussed above are

Table 4.1: Observed nitrogen containing compounds by  $\text{CF}_3\text{O}^-$  CIMS by name, abbreviation, monitored  $m/z$ , and molecular weight. Isobaric compounds cannot be discerned given the mass resolution of the time-of-flight mass spectrometer, i.e. OH oxidation of 1-pentene in the presence of NO to form hydroxy nitrates would also be observed at 234  $m/z$ . Given the VOCs measured by other instruments on the site, isobaric compounds contribute only minor amounts to the observed signals.

name	abbrev.	$m/z$	m.w.
Ethanal nitrate	ETHNL	190	105
Nitro-oxy ethanol	-	192	107
Propanone nitrate	PROPNN	204	119
Nitro-oxy propanol	-	206	121
Nitro-oxy butenol	-	218	133
Nitro-oxy butanol	-	220	235
Isoprene carbonyl nitrate	ICN	230	145
Isoprene hydroxy nitrate	ISOPN	232	147
Methacrolein and methyl vinyl ketone hydroxy nitrates	MACRN and MVKN	234	149
Isoprene nitro-oxy hydroperoxide and Isoprene nitro-oxy hydroxy epoxide	ICP	248	163
Monoterpene hydroxy nitrate	$\text{C}_{10}\text{H}_{17}\text{NO}_4$	300	215
Monoterpene nitro-oxy hydroperoxide	$\text{C}_{10}\text{H}_{17}\text{NO}_5$	316	231

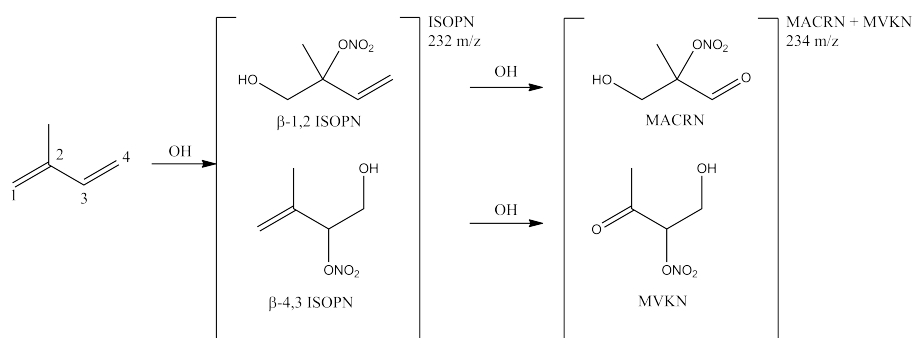


Figure 4.1: Organic nitrates formed from the oxidation of isoprene by OH in the presence of NO will produce ISOPN, observed at 232  $m/z$ . Therefore the signal at 232  $m/z$  during the day is most likely dominated by the sum of 1,2 ISOPN and 4,3 ISOPN. Further OH oxidation of these two compounds will yield MACRN and MVKN, observed at 234  $m/z$  (L. Lee et al., 2014a).

shown in Figure 4.4 and 4.5. All data is presented in Central Daylight Time (CDT). The time series of nitrates shows dramatic variation in daytime peaks due to variation in biogenic precursor emissions. Warm and sunny days generally had much higher emissions of isoprene and subsequently had higher concentrations of isoprene-derived nitrates. Diurnal profiles for isoprene-derived daytime nitrates increase after sunrise. Daily late morning peaks for daytime isoprene-derived nitrates has been attributed to downward mixing of the nocturnal residual layer (Beaver et al., 2012; Xiong et al., 2015). After this peak, ISOPN and MVKN+MACRN generally had

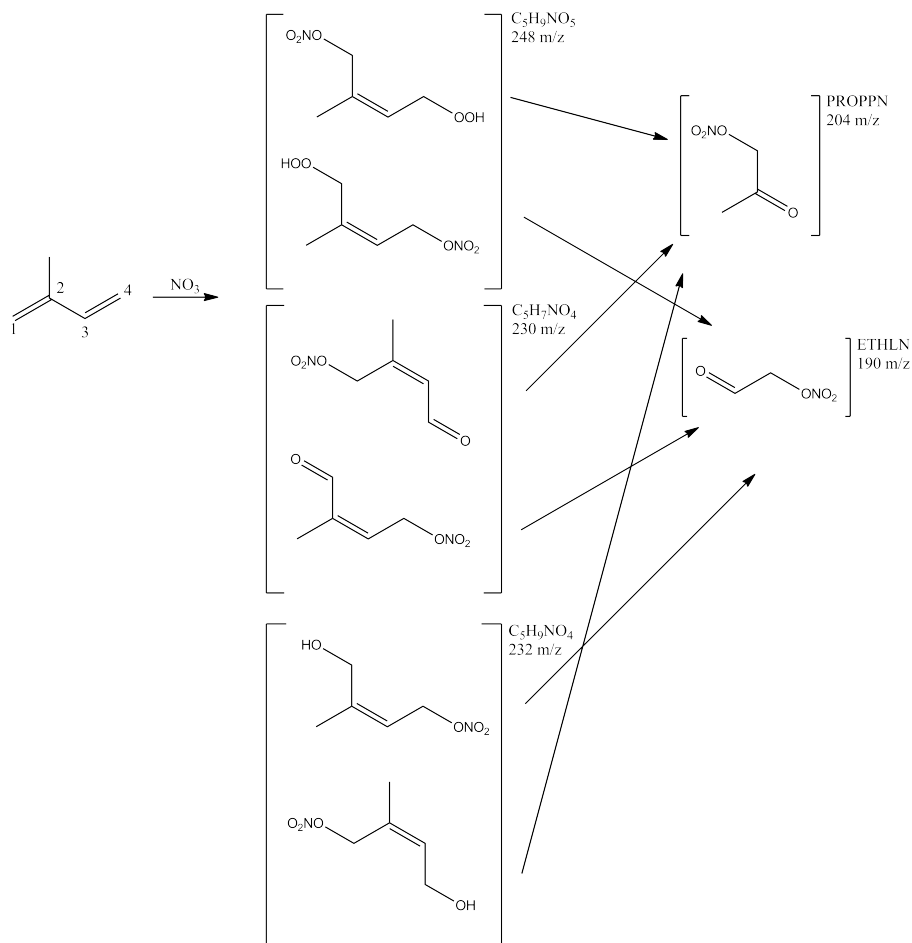


Figure 4.2: Organic nitrates formed from the oxidation of isoprene by  $\text{NO}_3$  radical will produce isoprene carbonyl nitrates (ICN), isoprene nitro-oxy hydroperoxides (ICP), and isoprene hydroxy nitrates (ISOPN). Based on laboratory evidence, these isomers are predominantly  $\delta$ -isomers (the functional groups are at 1 or 4). Therefore ETHLN and PROPNN are produced primarily as a result of the OH oxidation of the products from isoprene +  $\text{NO}_3$  (Alexander P Teng, J. D. Crouse, and P. O. Wennberg, 2017; R. H. Schwantes et al., 2015).

sustained concentrations throughout the day, whereas ETHLN concentrations, and to a lesser extent PROPNN concentrations, decreased as the day progressed. This difference indicates that ETHLN and PROPNN may not have a sustained source during the day, but rather are produced during the day from nighttime products. Often, but not always, ISOPN and MVKN+MACRN concentrations did not fall to zero during the night. This diurnal profile for ISOPN matches simulations updated with recent laboratory measurements of reaction rates with ozone and OH (L. Lee et al., 2014a). Other alkene-derived nitrates did not display such prominent late

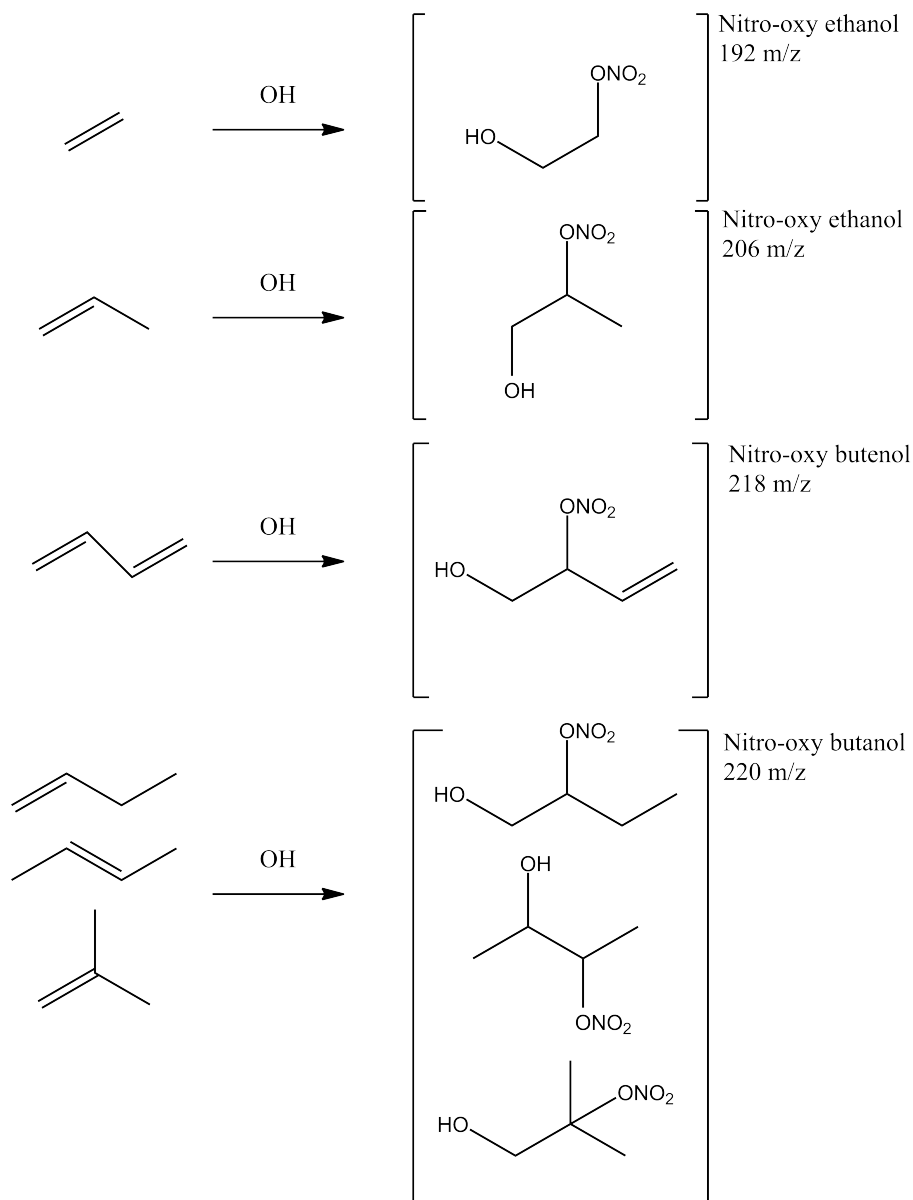


Figure 4.3: Organic nitrates formed from the oxidation of alkenes by OH in the presence of NO will produce hydroxy nitrates. Pictured above are the dominant isomers (A. Teng et al., 2014). In the case of butadiene only one isomer is expected comprise the majority of products from OH oxidation at the peroxy radical lifetimes found at the site. The signal at each mass is a sum of all isomers.

morning peaks which may indicate they are not produced in abundance in the residual nocturnal boundary layer.

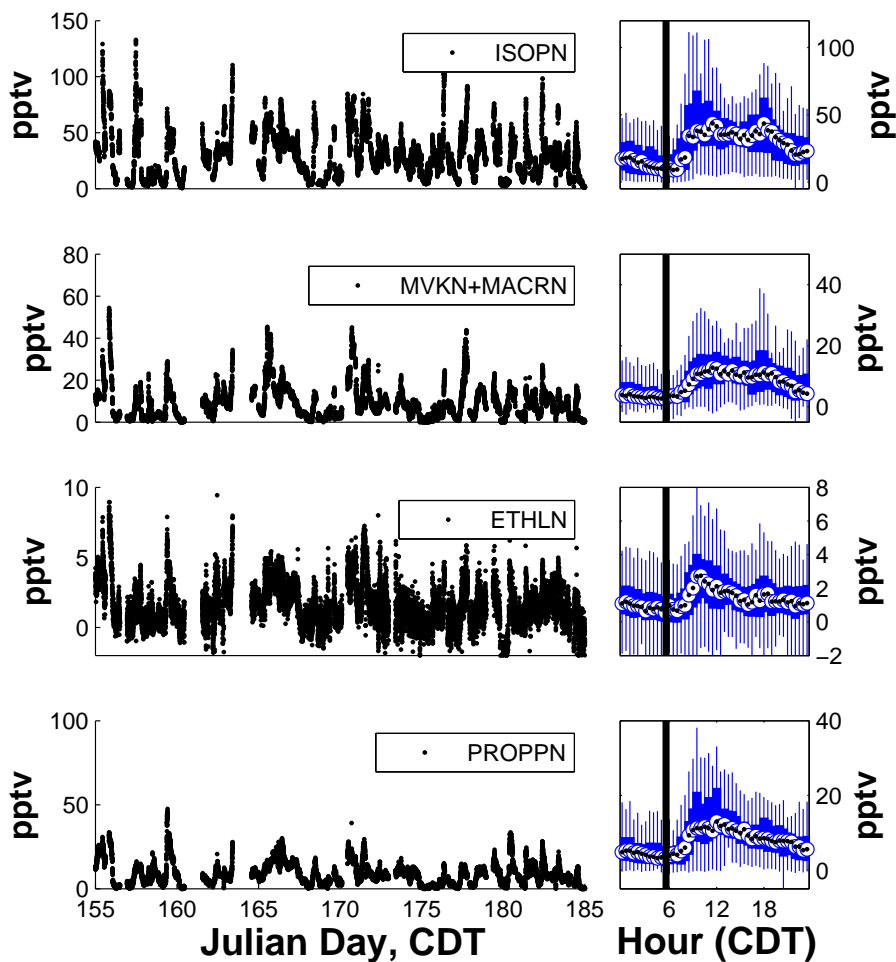


Figure 4.4: Time series (left) and diurnal profiles (right) of organic nitrates formed from isoprene with significant enhancements during the day. All times are presented in Central Daylight Time, which was the local time at the SOAS 2013 field site. The diurnal profiles are produced from 30 minute bins, with the black diamond indicating the median, the edge of the rectangles indicating the 25th and 75th percentiles, and the whiskers plotting the non-outlier extremes.

#### Nighttime organic nitrates: sources, time series, and diurnal profiles

Observed nighttime nitrates are a mixture of isoprene-derived and monoterpene-derived nitrates. Emissions of isoprene are light dependent but are not completely oxidized during the day allowing some isoprene oxidation to occur at night. Monoterpene emissions as well are higher during the day. However, their emissions are generally temperature dependent, and due to the shallower nocturnal boundary layer and lower reactive losses at night their concentrations can often be higher at night. As shown in Figure 4.2, observed isoprene-derived nitrates at night include both

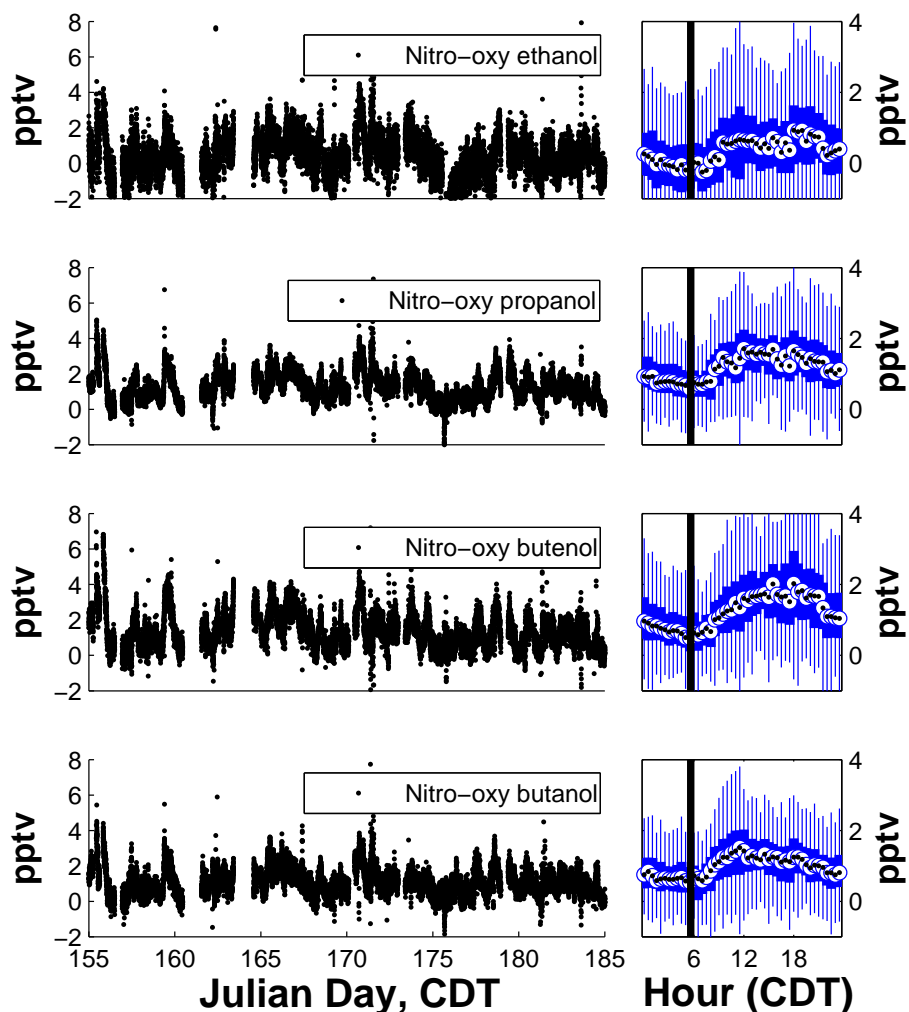


Figure 4.5: Time series (left) and diurnal profiles (right) of organic nitrates from alkenes besides isoprene with significant enhancements during the day. All times are presented in Central Daylight Time, which was the local time at the SOAS 2013 field site. The diurnal profiles are produced from 30 minute bins, with the black diamond indicating the median, the edge of the rectangles indicating the 25th and 75th percentiles, and the whiskers plotting the non-outlier extremes.

carbonyl nitrates (ICN), hydroxy nitrates (ISOPN), and nitro-oxy hydroperoxides (INP). Signals that correspond to monoterpene derived nitro-oxy hydroperoxides and hydroxy nitrates were observed as well. There were six observed monoterpenes which were measured at the SOAS 2013 field site, of which only the following five could have contributed to the monoterpene-derived nitrates:  $\alpha$ -pinene,  $\beta$ -pinene, camphene, myrcene, and limonene. The sixth monoterpene, para-cymene, has a much slow reaction with  $\text{NO}_3$ . Figure 4.6 shows four examples of potential

monoterpene-derived nitrates.

Time series and average diurnal profiles for each of the nitrates discussed above are shown in Figure 4.7. These compounds generally increase in concentration before sunset and continue to accumulate throughout the night, reaching a peak before sunrise, at which point their concentration rapidly decreases. At sunrise, the boundary layer begins to increase in height, leading to a much larger mixing volume, while also switching the main oxidant chemistry from  $\text{NO}_3$  to OH radical. Therefore the quick decline in concentration is most likely due to a strong dilution component and a minor loss pathway to OH radical. The signal which corresponds to INP had a slightly different diurnal profile. It generally increased during the night, but often had a significant peak during the day. Loss simulations of  $\text{NO}_3$  at the SOAS field site shows that a significant fraction of nitrate radical is lost to isoprene during the day (Ayres et al., 2015b), and therefore these daytime peaks are likely attributable to INP formation from oxidation of isoprene by  $\text{NO}_3$  during the day.

The fate of peroxy radicals at night is not well constrained in part by laboratory studies or ambient measurements (Kirchner and Stockwell, 1996; Bey, Aumont, and Toupance, 2001; S. S. Brown and Stutz, 2012). The nitrates present at night indicate that neither peroxy radical reaction with  $\text{HO}_2$  or  $\text{RO}_2$  can be neglected in the nocturnal boundary layer. Figure 4.8 shows that an almost equal concentration of INP (formed exclusively from  $\text{HO}_2$  pathway) and ICN (formed from either peroxy radical reaction with another  $\text{RO}_2$  or  $\text{NO}_3$ ) (A. J. Kwan et al., 2012; R. H. Schwantes et al., 2015). The monoterpene signal for nitro-oxy hydroperoxide  $\text{C}_{10}\text{H}_{17}\text{NO}_5$  (likely derived from peroxy radical reaction with  $\text{HO}_2$ ) is also roughly equivalent to that of the monoterpene hydroxy nitrate  $\text{C}_{10}\text{H}_{17}\text{NO}_4$  (possibly formed from peroxy radical reaction with  $\text{RO}_2$ ). Taken together, these measurements show strong evidence for the production of nitro-oxy peroxides at night, and therefore the importance of  $\text{RO}_2 + \text{HO}_2$  in the nighttime atmosphere in forested environments.

#### **Alkyl nitrates budget at the SOAS CTR site**

Previous measurements of speciated gas-phase organic nitrates measured by the Caltech CIMS over a forested site showed the entire budget of alkyl nitrates ( $\Sigma\text{ANs}$ ) could be explained by the biogenically-derived nitrates (Beaver et al., 2012). The SOAS 2013 study provides a unique opportunity to assess how universal this finding is for forested environments. A comparison between  $\Sigma\text{ANs}$ , and the sum of aerosol phase organic nitrates, speciated multifunctional nitrates by the NOAA GC-MS and

Caltech CIMS is shown in Figure 4.9. Unfortunately, aerosol phase organic nitrates and  $\text{CF}_3\text{O}^-$  CIMS measurements only overlapped between JD 179 and 185. Over those six days, however, the speciated CIMS nitrates + NOAA-GCMS alkyl nitrates + aerosol-phase alkyl nitrates (apANs) explained only 57% of the  $\Sigma\text{AN}$  signal. The unexplained fraction of alkyl nitrates was not constant throughout the measurement period as shown by the varying gap on JD 180, 182, and 183.

It is unclear what compounds make up the unexplained budget of alkyl nitrates. Single functional nitrate compounds are generally well measured by GC-MS techniques and do not generally comprise a large fraction of the alkyl nitrate budget over forested regions (Beaver et al., 2012). Methyl nitrate was not measured due to an interference in the chromatography at the site, so it is possible but unlikely that methyl nitrate was the source of discrepancy, as it would have to have 5-20x higher concentration to ethyl or propyl nitrate to explain the gap. Dinitrates are even-massed and therefore would not be included in our budget analysis. It is possible that there is a significant source of dinitrates at the site, though the gap does not have a clear diurnal trend. Anthropogenic tracers (toluene, PAHs) or biomass burning tracers (HCN) do not track well with the gap, nor does humidity or temperature.

One difference between the BEARPEX 2009 and SOAS 2013 is the large abundance of aerosol phase organic nitrates. The budget is often dominated by the aerosol-phase alkyl nitrates (Ayres et al., 2015b; B. H. Lee et al., 2016). Lab studies have shown much higher secondary organic aerosol yields from  $\text{NO}_3$  chemistry compared to OH chemistry, particularly for limonene and  $\beta$ -pinene (Spittler et al., 2006; Ng et al., 2008; Fry, Kiendler-Scharr, A. Rollins, Wooldridge, et al., 2009; A. W. Rollins, Kiendler-Scharr, et al., 2009; Fry, Kiendler-Scharr, A. Rollins, Brauers, et al., 2011; Ayres et al., 2015b; C. M. Boyd et al., 2015). Due to the large presence of hydroperoxides in nighttime chemistry, it is possible much of the aerosol-phase organic nitrates produced at night also have hydroperoxide functionality. This is a potentially large source of oxidant to the aerosol and may play a significant role in aerosol aging.

### **Alkyl nitrates budget over the Southeastern United States**

Measurements of speciated alkyl nitrates cannot explain the total alkyl nitrate ( $\Sigma\text{ANs}$ ) in the boundary layer over the entire Southeastern United States. The speciated alkyl nitrates from the Caltech CIMS explain generally explain much less than a third of the total ANs (shown in Figure 4.11, Figure 4.12 with flight tracks shown

in Figure 4.10). Given the measured VOCs, it is expected that biogenically-derived organic nitrates should dominate the budget for all of the flights shown. It is unclear to what extent the signal measured by the Berkeley TD-LIF includes aerosol phase organic nitrates, and therefore some of this gap may be attributable to organic nitrates that have been taken up onto the aerosol phase. The AMS measures a response from organic nitrates in the aerosol phase, though this measurement is hampered by the lack of representative calibration standards for ambient aerosols and potential thermal decomposition of organic nitrates (Farmer et al., 2010). The reported aerosol phase organic nitrates (below 1  $\mu\text{m}$  in diameter) do not explain the gap and are approximately equal to or less than total speciated organic nitrates measured by the Caltech CIMS. Similarly, simple alkyl nitrates speciated by the Whole Air Sampler which include methyl nitrate account for only 40-100pptv, and also do not account for the gap.

#### **Unidentified nitrates from CIMS**

As at the SOAS 2013 field site, as at BEARPEX 2009, a significant concentration of nitrogen-containing, unidentified masses were measured. Table 4.2 lists the masses included in the 'Other' category, and their maximum concentration measured over the entire campaign. Figure 4.8 shows the average contribution of nitrates measured by CIMS. Approximately 20% is contributed to the total speciated organic nitrates measured by CIMS. Figure 4.13 shows a subset of time series and average diurnal profiles for a subset of the unidentified compounds. Signals that most closely correlate with ISOPN are 250m/z, 260m/z and 262m/z. Signal at 264m/z peaks during the early morning and falls off during the day similarly to ETHLN and PROPNN, suggesting that it may be a short lived photo-oxidation product of a compound produced at night. Signals that most closely match  $\text{NO}_3$  oxidation profiles include m/z at 244, 246, 270, and 314. A compound with signal at 314 m/z implies a molecular weight of 229amu, and is most likely derived from monoterpene oxidation. Chamber studies conducted as part of FIX-CIT have shown a similar signal in the OH and  $\text{NO}_3$  oxidation of  $\alpha$ -pinene and  $\beta$ -pinene (T. Nguyen et al., 2014; Xu et al., 2015).

#### **4.4 Conclusions**

Speciation of multifunctional organic nitrates explains a substantial portion of the total alkyl nitrates as measured over a forested region in the southeastern United States during the summer. In contrast to a similar study in the Sierra Nevadas over

Table 4.2: Significant observed nitrogen-containing  $m/z$  observed with the  $\text{CF}_3\text{O}^-$  CIMS. The molecular weight (m.w.) column is inferred using the molecular weight after subtracting the reagent ion,  $\text{CF}_3\text{O}^-$  (85 amu).

$m/z$	m.w.	max ppt
222	137	5
224	139	3
244	159	18
246	161	10
250	165	14
260	175	4
262	177	6
264	179	7
266	181	2
270	185	7
272	187	2
278	193	2
290	205	3
292	207	1
298	215	1
302	217	4
304	219	3
318	233	2
330	245	2
332	247	3
336	251	5

a Ponderosa pine forest, a significant fraction of the total alkyl nitrate budget was comprised of aerosol phase organic nitrates. A diurnal profile of the aerosol phase organic nitrates shows substantial enhancement of organic nitrates in the aerosol phase at night. This coincides with the diurnal profile of a suite of biogenically-derived organic nitrates from  $\text{NO}_3$  oxidation, indicating biogenic precursors are most likely important in the production of secondary organic aerosol mass at night. The measurements also indicate a significant presence of peroxides formed from  $\text{NO}_3$  oxidation, demonstrating that  $\text{RO}_2 + \text{HO}_2$  is an important fate for peroxy radicals at night. These measurements highlight the overall importance of biogenic precursors to the total alkyl nitrate budget.

We also report the first diurnal profiles for nitro-oxy ethanol, nitro-oxy propanol, and nitro-oxy butanol. These are derived from ethene, propene, and  $\text{C}_4$ -enes, which are most likely anthropogenic in origin at the SOAS 2013 field site.

#### 4.5 Acknowledgements

We thank the organizers and committee members of the SOAS campaign: A.G. Carlton, A.H. Goldstein, J.L. Jimenez, R.W. Pinder, J. de Gouw, B.J. Turpin, and A.B. Guenther. We acknowledge funding from the National Science Foundation (NSF) under grant AGS-1240604. Financial and logistical support for SOAS was provided by the NSF, the Earth Observing Laboratory at the National Center for Atmospheric Research, the personnel at Atmospheric Research and Analysis, and the Electric Power Research Institute. The authors would like to thank K. Duffey, P. Romer, P.W. Woolridge and R.C. Cohen for TD-LIF alkyl nitrate data. The authors also acknowledge P.A. Feiner and W.H. Brune for providing OH and HO<sub>2</sub> measurements. The authors would also like to thank A. Koss, K. Olson, A.H. Goldstein, and J. de Gouw for providing VOC data. The authors also acknowledge D. Day, P. Campuzano-Jost and J.L. Jimenez for AMS data. The authors would also like to acknowledge S. Meinardi, B. Barletta, and D. Blake for VOC data during the SEAC4RS campaign.

#### References

- Ayres, BR et al. (2015a). “Organic nitrate aerosol formation via NO<sub>3</sub>+ biogenic volatile organic compounds in the southeastern United States”. In: *Atmospheric Chemistry and Physics* 15.23, pp. 13377–13392. DOI: 10.5194/acp-15-13377-2015. URL: <http://doi.org/10.5194/acp-15-13377-2015>.
- (2015b). “Organic nitrate aerosol formation via NO<sub>3</sub>+ biogenic volatile organic compounds in the southeastern United States”. In: *Atmospheric Chemistry and Physics* 15.23, pp. 13377–13392.
- Barker, John R et al. (2003). “Modeling the organic nitrate yields in the reaction of alkyl peroxy radicals with nitric oxide. 2. Reaction simulations”. In: *The Journal of Physical Chemistry A* 107.38, pp. 7434–7444.
- Barnes, Ian et al. (1990). “Kinetics and products of the reactions of nitrate radical with monoalkenes, dialkenes, and monoterpenes”. In: *Journal of Physical Chemistry* 94.6, pp. 2413–2419.
- Bates, Kelvin Hamilton et al. (2014). “Gas Phase Production and Loss of Isoprene Epoxydiols”. In: *The Journal of Physical Chemistry A*.
- Beaver, MR et al. (2012). “Importance of biogenic precursors to the budget of organic nitrates: observations of multifunctional organic nitrates by CIMS and TD-LIF during BEARPEX 2009”. In: *Atmospheric Chemistry and Physics* 12.13, pp. 5773–5785.

- Berndt, Torsten and Olaf Böge (1997). "Gas-phase reaction of NO<sub>3</sub> radicals with isoprene: a kinetic and mechanistic study". In: *International journal of chemical kinetics* 29.10, pp. 755–765.
- Bey, Isabelle, Bernard Aumont, and Gérard Toupance (2001). "A modeling study of the nighttime radical chemistry in the lower continental troposphere: 1. Development of a detailed chemical mechanism including nighttime chemistry". In: *Journal of Geophysical Research: Atmospheres (1984–2012)* 106.D9, pp. 9959–9990.
- Boyd, C. M. et al. (2015). "Secondary organic aerosol formation from the  $\beta$ -pinene+NO<sub>3</sub> system: effect of humidity and peroxy radical fate". In: *Atmospheric Chemistry and Physics* 15.13, pp. 7497–7522. DOI: 10.5194/acp-15-7497-2015. URL: <http://www.atmos-chem-phys.net/15/7497/2015/>.
- Brown, Steven S and Jochen Stutz (2012). "Nighttime radical observations and chemistry". In: *Chemical Society Reviews* 41.19, pp. 6405–6447.
- Browne, EC and RC Cohen (2012). "Effects of biogenic nitrate chemistry on the NO<sub>x</sub> lifetime in remote continental regions". In: *Atmospheric Chemistry and Physics* 12.24, pp. 11917–11932.
- Browne, EC, K-E Min, et al. (2013). "Observations of total RONO<sub>2</sub> over the boreal forest: NO<sub>x</sub> sinks and HNO<sub>3</sub> sources". In: *Atmospheric Chemistry and Physics* 13.9, pp. 4543–4562.
- Browne, EC, PJ Wooldridge, et al. (2014). "On the role of monoterpene chemistry in the remote continental boundary layer". In: *Atmospheric Chemistry and Physics* 14.3, pp. 1225–1238.
- Chen, Xiaohui, David Hulbert, and Paul B Shepson (1998). "Measurement of the organic nitrate yield from OH reaction with isoprene". In: *Journal of Geophysical Research: Atmospheres (1984–2012)* 103.D19, pp. 25563–25568.
- Clair, Jason M St et al. (2010). "Chemical ionization tandem mass spectrometer for the in situ measurement of methyl hydrogen peroxide". In: *Review of Scientific Instruments* 81.9, p. 094102.
- Crounse, John D, Hasse C Knap, et al. (2012). "Atmospheric fate of methacrolein. 1. Peroxy radical isomerization following addition of OH and O<sub>2</sub>". In: *The Journal of Physical Chemistry A* 116.24, pp. 5756–5762.
- Crounse, John D, Karena A McKinney, et al. (2006). "Measurement of gas-phase hydroperoxides by chemical ionization mass spectrometry". In: *Analytical chemistry* 78.19, pp. 6726–6732.
- Crounse, John D, Lasse B Nielsen, et al. (2013). "Autoxidation of Organic Compounds in the Atmosphere". In: *The Journal of Physical Chemistry Letters* 4.20, pp. 3513–3520.

- Crounse, John D, Fabien Paulot, et al. (2011). "Peroxy radical isomerization in the oxidation of isoprene". In: *Physical Chemistry Chemical Physics* 13.30, pp. 13607–13613.
- Darer, Adam I et al. (2011). "Formation and stability of atmospherically relevant isoprene-derived organosulfates and organonitrates". In: *Environmental science & technology* 45.5, pp. 1895–1902.
- Day, DA et al. (2002). "A thermal dissociation laser-induced fluorescence instrument for in situ detection of NO<sub>2</sub>, peroxy nitrates, alkyl nitrates, and HNO<sub>3</sub>". In: *Journal of Geophysical Research: Atmospheres (1984–2012)* 107.D6, ACH–4.
- Day, Douglas A et al. (2010). "Organonitrate group concentrations in submicron particles with high nitrate and organic fractions in coastal southern California". In: *Atmospheric Environment* 44.16, pp. 1970–1979.
- Farmer, DK et al. (2010). "Response of an aerosol mass spectrometer to organonitrates and organosulfates and implications for atmospheric chemistry". In: *Proceedings of the National Academy of Sciences* 107.15, pp. 6670–6675.
- Fischer, Ralf G, Jürgen Kastler, and Karlheinz Ballschmiter (2000). "Levels and pattern of alkyl nitrates, multifunctional alkyl nitrates, and halocarbons in the air over the Atlantic Ocean". In: *Journal of Geophysical Research: Atmospheres (1984–2012)* 105.D11, pp. 14473–14494.
- Fisher, Jenny A et al. (2016). "Organic nitrate chemistry and its implications for nitrogen budgets in an isoprene-and monoterpene-rich atmosphere: constraints from aircraft (SEAC 4 RS) and ground-based (SOAS) observations in the Southeast US". In: *Atmospheric Chemistry and Physics* 16.9, pp. 5969–5991. DOI: 10.5194/acp-16-5969-2016. URL: <http://doi.org/10.5194/acp-16-5969-2016>.
- Fry, JL, DC Draper, et al. (2013). "Observations of gas-and aerosol-phase organic nitrates at BEACHON-RoMBAS 2011". In: *Atmospheric Chemistry and Physics* 13.17, pp. 8585–8605.
- Fry, JL, A Kiendler-Scharr, AW Rollins, T Brauers, et al. (2011). "SOA from limonene: role of NO<sub>3</sub> in its generation and degradation". In: *Atmospheric Chemistry and Physics* 11.8, pp. 3879–3894.
- Fry, JL, A Kiendler-Scharr, AW Rollins, PJ Wooldridge, et al. (2009). "Organic nitrate and secondary organic aerosol yield from NO<sub>3</sub> oxidation of  $\beta$ -pinene evaluated using a gas-phase kinetics/aerosol partitioning model". In: *Atmospheric Chemistry and Physics* 9.4, pp. 1431–1449.
- Goldstein, AH et al. (1996). "Emissions of ethene, propene, and 1-butene by a midlatitude forest". In: *Journal of Geophysical Research: Atmospheres (1984–2012)* 101.D4, pp. 9149–9157.

- Grossenbacher, John W, Dennis J Barket Jr, et al. (2004). “A comparison of isoprene nitrate concentrations at two forest-impacted sites”. In: *Journal of Geophysical Research: Atmospheres (1984–2012)* 109.D11.
- Grossenbacher, John W, Tara Couch, et al. (2001). “Measurements of isoprene nitrates above a forest canopy”. In: *Journal of Geophysical Research: Atmospheres (1984–2012)* 106.D20, pp. 24429–24438.
- Hallquist, Mattias et al. (1999). “Aerosol and product yields from NO<sub>3</sub> radical-initiated oxidation of selected monoterpenes”. In: *Environmental science & technology* 33.4, pp. 553–559.
- Horowitz, Larry W. et al. (2007). “Observational constraints on the chemistry of isoprene nitrates over the eastern United States”. In: *Journal of Geophysical Research Atmospheres* 112.12, D12S08. ISSN: 01480227. DOI: 10.1029/2006JD007747. URL: <http://doi.wiley.com/10.1029/2006JD007747>.
- Hu, KS, Adam I Darer, and Matthew J Elrod (2011). “Thermodynamics and kinetics of the hydrolysis of atmospherically relevant organonitrates and organosulfates”. In: *Atmospheric Chemistry and Physics* 11.16, pp. 8307–8320.
- Ito, Akinori, Sanford Sillman, and Joyce E Penner (2007). “Effects of additional nonmethane volatile organic compounds, organic nitrates, and direct emissions of oxygenated organic species on global tropospheric chemistry”. In: *Journal of Geophysical Research: Atmospheres (1984–2012)* 112.D6.
- Kastler, Jürgen and K Ballschmiter (1998). “Bifunctional alkyl nitrates—trace constituents of the atmosphere”. In: *Fresenius’ journal of analytical chemistry* 360.7-8, pp. 812–816.
- Kirchner, Frank and William R Stockwell (1996). “Effect of peroxy radical reactions on the predicted concentrations of ozone, nitrogenous compounds, and radicals”. In: *Journal of Geophysical Research: Atmospheres (1984–2012)* 101.D15, pp. 21007–21022.
- Kwan, A. J. et al. (2012). “Peroxy radical chemistry and OH radical production during the NO<sub>3</sub>-initiated oxidation of isoprene”. In: *Atmospheric Chemistry and Physics* 12.16, pp. 7499–7515. DOI: 10.5194/acp-12-7499-2012. URL: <http://www.atmos-chem-phys.net/12/7499/2012/>.
- Lamanna, Mark S and Allen H Goldstein (1999). “In situ measurements of C<sub>2</sub>-C<sub>10</sub> volatile organic compounds above a Sierra Nevada ponderosa pine plantation”. In: *Journal of Geophysical Research: Atmospheres (1984–2012)* 104.D17, pp. 21247–21262.
- Lee, Ben H et al. (2016). “Highly functionalized organic nitrates in the southeast United States: Contribution to secondary organic aerosol and reactive nitrogen budgets”. In: *Proceedings of the National Academy of Sciences* 113.6, pp. 1516–1521.

- Lee, Lance et al. (2014a). “On Rates and Mechanisms of OH and O<sub>3</sub> Reactions with Isoprene-Derived Hydroxy Nitrates”. In: *The Journal of Physical Chemistry A*.
- (2014b). “On rates and mechanisms of OH and O<sub>3</sub> reactions with isoprene-derived hydroxy nitrates”. In: *The Journal of Physical Chemistry A* 118.9, pp. 1622–1637. DOI: 10.1021/jp4107603. URL: <http://doi.org/10.1021/jp4107603>.
- Liu, Shang et al. (2012). “Hydrolysis of organonitrate functional groups in aerosol particles”. In: *Aerosol Science and Technology* 46.12, pp. 1359–1369.
- Lockwood, AL et al. (2010). “Isoprene nitrates: preparation, separation, identification, yields, and atmospheric chemistry”. In: *Atmospheric Chemistry and Physics* 10.13, pp. 6169–6178.
- Lohr, Lawrence L, John R Barker, and Robert M Shroll (2003). “Modeling the organic nitrate yields in the reaction of alkyl peroxy radicals with nitric oxide. 1. Electronic structure calculations and thermochemistry”. In: *The Journal of Physical Chemistry A* 107.38, pp. 7429–7433.
- Ng, NL et al. (2008). “Secondary organic aerosol (SOA) formation from reaction of isoprene with nitrate radicals (NO<sub>3</sub>)”. In: *Atmospheric Chemistry and Physics* 8.14, pp. 4117–4140.
- Nguyen, TB et al. (2014). “Overview of the Focused Isoprene eXperiment at the California Institute of Technology (FIXCIT): mechanistic chamber studies on the oxidation of biogenic compounds”. In: *Atmospheric Chemistry and Physics* 14.24, pp. 13531–13549.
- Nguyen, Tran B et al. (2015a). “Rapid deposition of oxidized biogenic compounds to a temperate forest”. In: *Proceedings of the National Academy of Sciences*, p. 201418702.
- (2015b). “Rapid deposition of oxidized biogenic compounds to a temperate forest”. In: *Proceedings of the National Academy of Sciences* 112.5, E392–E401. DOI: 10.1073/pnas.1418702112. URL: <http://doi.org/10.1073/pnas.1418702112>.
- O’Brien, Jason M et al. (1998). “Determination of the hydroxy nitrate yields from the reaction of C<sub>2</sub>-C<sub>6</sub> alkenes with OH in the presence of NO”. In: *The Journal of Physical Chemistry A* 102.45, pp. 8903–8908.
- O’Brien, JM et al. (1995). “Measurements of alkyl and multifunctional organic nitrates at a rural site in Ontario”. In: *Journal of Geophysical Research: Atmospheres (1984–2012)* 100.D11, pp. 22795–22804.
- Orlando, John J and Geoffrey S Tyndall (2012). “Laboratory studies of organic peroxy radical chemistry: an overview with emphasis on recent issues of atmospheric significance”. In: *Chemical Society Reviews* 41.19, pp. 6294–6317.
- Patchen, Amie K et al. (2007). “Direct kinetics study of the product-forming channels of the reaction of isoprene-derived hydroxyperoxy radicals with NO”. In: *International Journal of Chemical Kinetics* 39.6, pp. 353–361.

- Paulot, F, JD Crouse, et al. (2009). "Isoprene photooxidation: new insights into the production of acids and organic nitrates". In: *Atmospheric Chemistry and Physics* 9.4, pp. 1479–1501.
- Paulot, F, DK Henze, and PO Wennberg (2012). "Impact of the isoprene photochemical cascade on tropical ozone". In: *Atmospheric Chemistry and Physics* 12.3, pp. 1307–1325.
- Paulot, Fabien et al. (2013). "Unexpected Epoxide Formation in the". In: *Science* 325.2009, pp. 730–733. ISSN: 0036-8075. DOI: 10.1126/science.1172910. URL: <http://www.ncbi.nlm.nih.gov/pubmed/19661425> <http://www.sciencemag.org/cgi/doi/10.1126/science.1172910>.
- Peeters, Jozef, Thanh Lam Nguyen, and Luc Vereecken (2009). "HOx radical regeneration in the oxidation of isoprene". In: *Physical Chemistry Chemical Physics* 11.28, pp. 5935–5939.
- Perraud, Veronique et al. (2010). "Identification of organic nitrates in the NO<sub>3</sub> radical initiated oxidation of  $\alpha$ -pinene by atmospheric pressure chemical ionization mass spectrometry". In: *Environmental science & technology* 44.15, pp. 5887–5893.
- Perring, AE et al. (2009). "A product study of the isoprene+ NO<sub>3</sub> reaction". In: *Atmospheric Chemistry and Physics* 9.14, pp. 4945–4956.
- Praske, Eric et al. (2014). "Atmospheric Fate of Methyl Vinyl Ketone: Peroxy Radical Reactions with NO and HO<sub>2</sub>". In: *The Journal of Physical Chemistry A*.
- Rindelaub, J. D., K. M. McAvey, and P. B. Shepson (2014). "Determination of  $\alpha$ -pinene-derived organic nitrate yields: particle phase partitioning and hydrolysis". In: *Atmospheric Chemistry and Physics Discussions* 14.3, pp. 3301–3335. DOI: 10.5194/acpd-14-3301-2014. URL: <http://www.atmos-chem-phys-discuss.net/14/3301/2014/>.
- Rollins, Andrew W, A Kiendler-Scharr, et al. (2009). "Isoprene oxidation by nitrate radical: alkyl nitrate and secondary organic aerosol yields". In: *Atmospheric Chemistry and Physics* 9.18, pp. 6685–6703.
- Rollins, Andrew W, Jared D Smith, et al. (2010). "Real time in situ detection of organic nitrates in atmospheric aerosols". In: *Environmental science & technology* 44.14, pp. 5540–5545.
- Rollins, AW et al. (2012). "Evidence for NO<sub>x</sub> control over nighttime SOA formation". In: *Science* 337.6099, pp. 1210–1212.
- Romer, P. S. et al. (2016). "The lifetime of nitrogen oxides in an isoprene-dominated forest". In: *Atmospheric Chemistry and Physics* 16.12, pp. 7623–7637. DOI: 10.5194/acp-16-7623-2016. URL: <http://www.atmos-chem-phys.net/16/7623/2016/>.

- Russell, Lynn M, Ranjit Bahadur, and Paul J Ziemann (2011). "Identifying organic aerosol sources by comparing functional group composition in chamber and atmospheric particles". In: *Proceedings of the National Academy of Sciences* 108.9, pp. 3516–3521.
- Schwantes, Rebecca H et al. (2015). "Isoprene NO<sub>3</sub> Oxidation Products from the RO<sub>2</sub>+ HO<sub>2</sub> Pathway". In: *The Journal of Physical Chemistry A* 119.40, pp. 10158–10171. DOI: 10.1021/acs.jpca.5b06355. URL: <http://doi.org/10.1021/acs.jpca.5b06355>.
- Spencer, KM et al. (2011). "Quantification of hydroxyacetone and glycolaldehyde using chemical ionization mass spectrometry". In: *Atmospheric Chemistry and Physics Discussions* 11.8, pp. 23619–23653.
- Spittler, M et al. (2006). "Reactions of NO<sub>3</sub> radicals with limonene and  $\alpha$ -pinene: Product and SOA formation". In: *Atmospheric Environment* 40, pp. 116–127.
- Sprengnether, Michele et al. (2002). "Product analysis of the OH oxidation of isoprene and 1, 3-butadiene in the presence of NO". In: *Journal of Geophysical Research: Atmospheres (1984–2012)* 107.D15, ACH–8.
- Stevens, P et al. (1999). "Measurements of the kinetics of the OH-initiated oxidation of isoprene: Radical propagation in the OH+ isoprene+ O<sub>2</sub>+ NO reaction system". In: *International journal of chemical kinetics* 31.9, pp. 637–643.
- Teng, A. P. et al. (2015). "Hydroxy nitrate production in the OH-initiated oxidation of alkenes". In: *Atmospheric Chemistry and Physics* 15.8, pp. 4297–4316. DOI: 10.5194/acp-15-4297-2015. URL: <http://www.atmos-chem-phys.net/15/4297/2015/>.
- Teng, Alexander P, John D Crouse, and Paul O Wennberg (2017). "Isoprene peroxy radical dynamics". In: *Journal of the American Chemical Society* 139.15, pp. 5367–5377. DOI: 10.1021/jacs.6b12838. URL: <http://doi.org/10.1021/jacs.6b12838>.
- Teng, AP et al. (2014). "Hydroxy nitrate production in the OH-initiated oxidation of alkenes". In: *Atmospheric Chemistry and Physics Discussions* 14.5, pp. 6721–6757.
- Toon, Owen B et al. (2016). "Planning, implementation, and scientific goals of the Studies of Emissions and Atmospheric Composition, Clouds and Climate Coupling by Regional Surveys (SEAC4RS) field mission". In: *Journal of Geophysical Research: Atmospheres* 121.9, pp. 4967–5009.
- Tuazon, Ernesto C and Roger Atkinson (1990). "A product study of the gas-phase reaction of Isoprene with the OH radical in the presence of NO<sub>x</sub>". In: *International Journal of Chemical Kinetics* 22.12, pp. 1221–1236.

- Wängberg, I, I Barnes, and KH Becker (1997). “Product and mechanistic study of the reaction of NO<sub>3</sub> radicals with  $\alpha$ -pinene”. In: *Environmental science & technology* 31.7, pp. 2130–2135.
- Wolfe, Glenn M et al. (2012). “Photolysis, OH reactivity and ozone reactivity of a proxy for isoprene-derived hydroperoxyenals (HPALDs)”. In: *Physical Chemistry Chemical Physics* 14.20, pp. 7276–7286.
- Wolfe, GM et al. (2015). “Quantifying sources and sinks of reactive gases in the lower atmosphere using airborne flux observations”. In: *Geophysical Research Letters* 42.19, pp. 8231–8240. DOI: 10.1002/2015GL065839. URL: <http://doi.org/10.1002/2015GL065839>.
- Xie, Y et al. (2013). “Understanding the impact of recent advances in isoprene photooxidation on simulations of regional air quality”. In: *Atmospheric Chemistry and Physics* 13.16, pp. 8439–8455.
- Xiong, F et al. (2015). “Observation of isoprene hydroxynitrates in the southeastern United States and implications for the fate of NO<sub>x</sub>”. In: *Atmospheric Chemistry and Physics* 15.19, pp. 11257–11272.
- Xu, Lu et al. (2015). “Effects of anthropogenic emissions on aerosol formation from isoprene and monoterpenes in the southeastern United States”. In: *Proceedings of the National Academy of Sciences* 112.1, pp. 37–42.
- Zhang, Dan et al. (2002). “Hydroxy peroxy nitrites and nitrates from OH initiated reactions of isoprene”. In: *Journal of the American Chemical Society* 124.32, pp. 9600–9605.
- Zhang, Jieyuan, Tim Dransfield, and Neil M Donahue (2004). “On the mechanism for nitrate formation via the peroxy radical+ NO reaction”. In: *The Journal of Physical Chemistry A* 108.42, pp. 9082–9095.

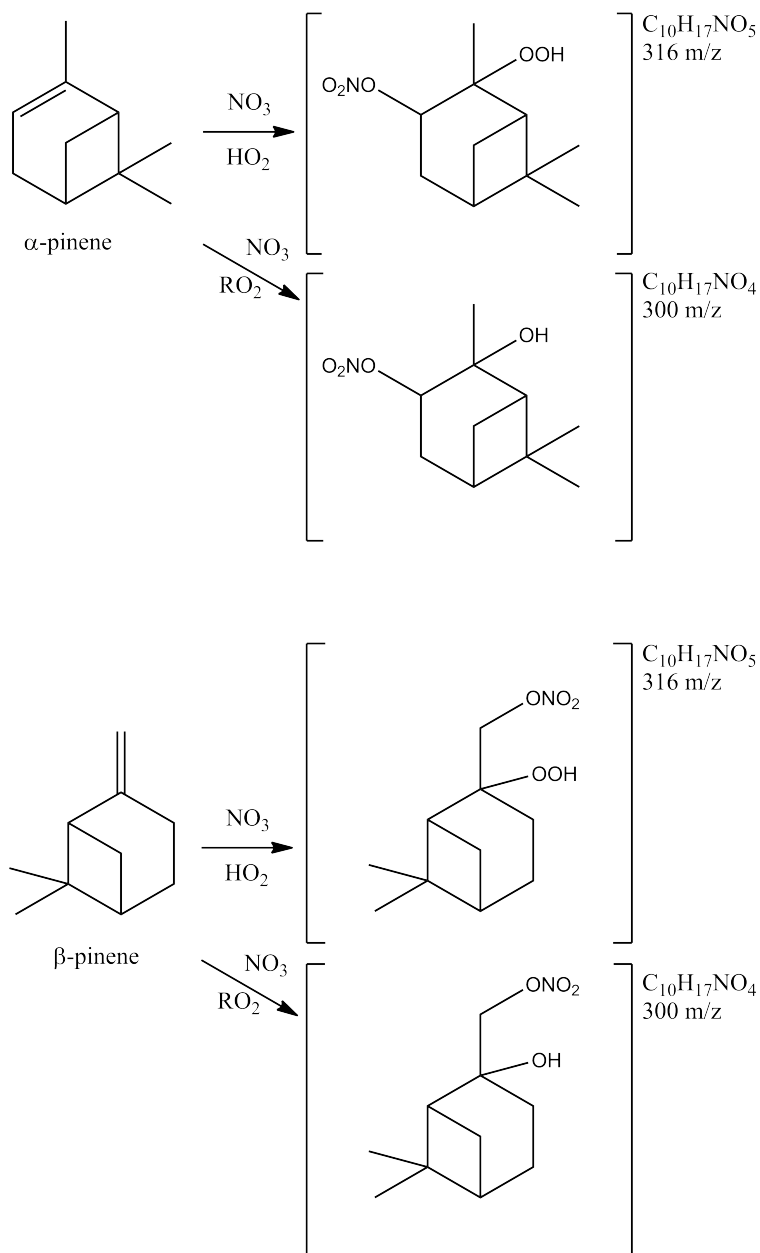


Figure 4.6: Signals at 316 $m/z$  and 300 $m/z$  are stable products formed from the oxidation of monoterpenes by  $\text{NO}_3$ . The structures responsible for signals at monoterpenes are highly uncertain due to the multiplicity of monoterpenes available for reaction with  $\text{NO}_3$ , and the uncertainty of the products formed upon reaction with  $\text{NO}_3$ . The site was generally dominated by two monoterpenes:  $\alpha$ -pinene and  $\beta$ -pinene, and so potential structures have been drawn for those two monoterpenes. Chamber studies conducted at Caltech have confirmed that nitro-oxy hydroperoxides are formed from the reaction of  $\alpha$ -pinene and  $\text{NO}_3$  and subsequent reaction of this peroxy radical with  $\text{HO}_2$ .

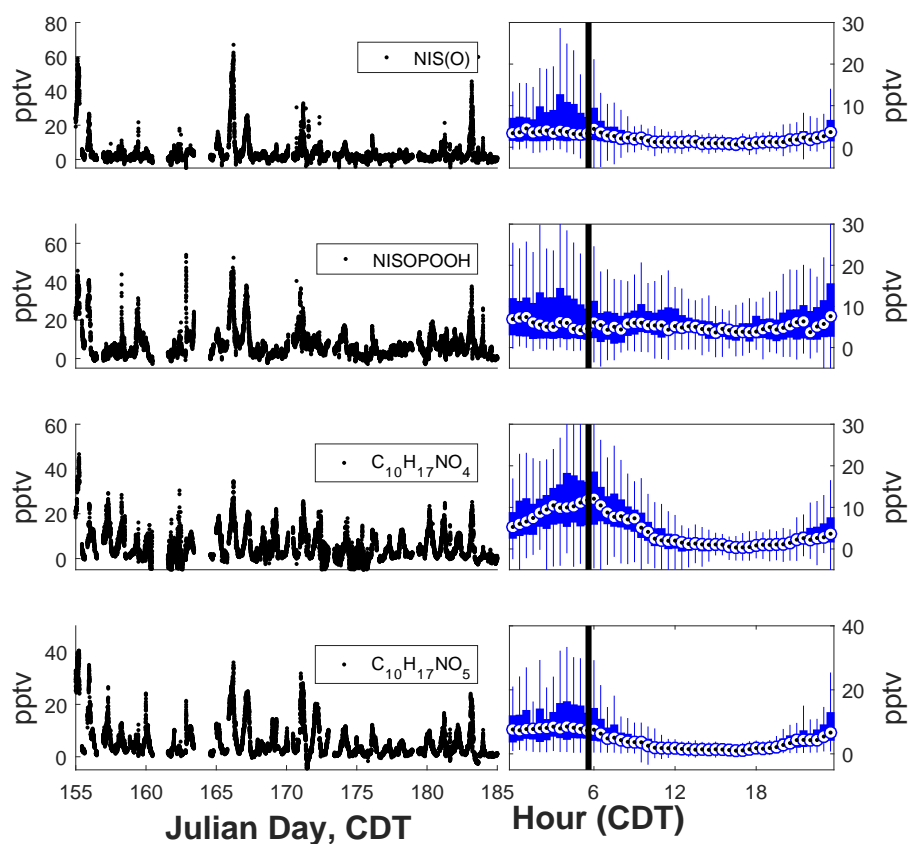


Figure 4.7: Time series (left) and diurnal profiles (right) of organic nitrates with significant enhancements during the night. All times are presented in Central Daylight Time, which was the local time at the SOAS 2013 field site. The diurnal profiles are produced from 30 minute bins, with the black diamond indicating the median, the edge of the rectangles indicating the 25th and 75th percentiles, and the whiskers plotting the non-outlier extremes.

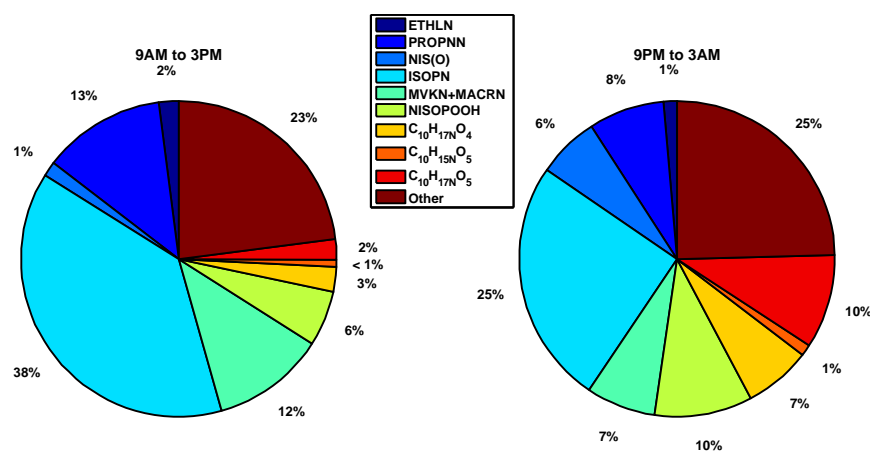


Figure 4.8: The left pie chart represents the mean contribution to the sum of all nitrogen-containing masses monitored by the Caltech  $CF_3O^-$  CIMS during the time period of 9AM to 3PM for the entire SOAS campaign. The right pie chart is the same representation but for the time period between 9PM to 3AM. 'Other' category is composed of all compounds listed in Table 4.1 and Table 4.2 that are not called out.

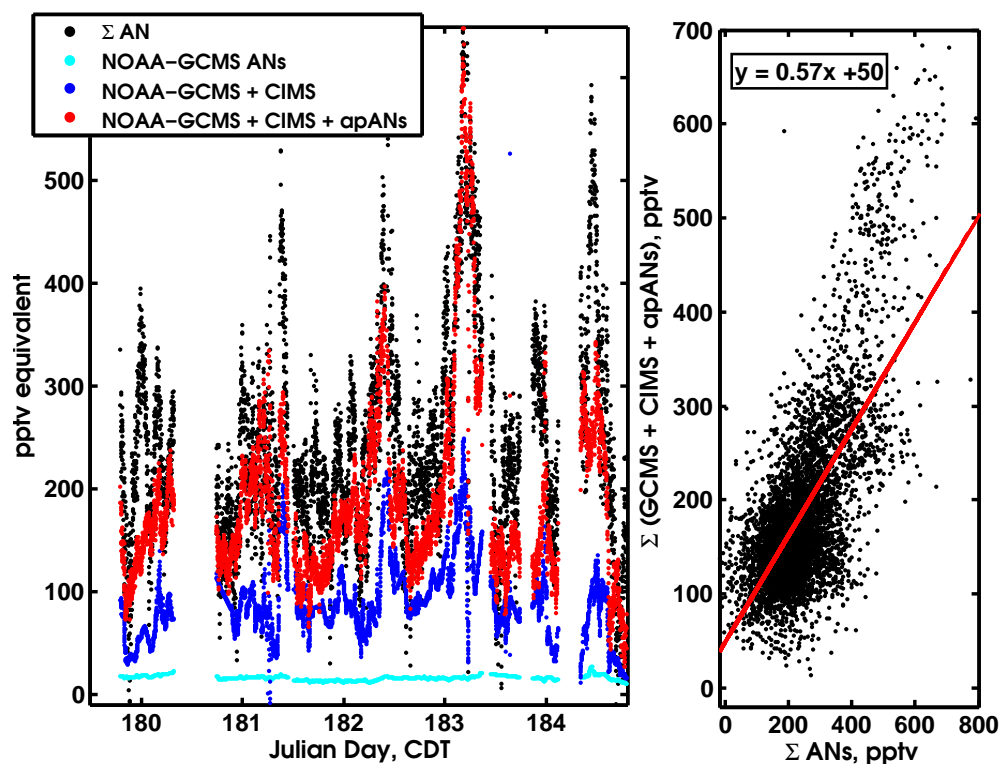


Figure 4.9: Comparison of (Caltech  $\text{CF}_3\text{O}^-$  CIMS organic nitrates + NOAA-GCMS alkyl nitrates + TD-LIF aerosol-phase organic nitrates) and the total alkyl nitrate budget as measured by the Berkeley TD-LIF. On the left are six days over which all measurements were on-line, showing portions where the entire budget was explained by the sum of GCMS, CIMS, and apANs. On the right is the sum of CIMS, GCMS, and apANs plotted against the  $\Sigma$ ANs. The red line is the best fit  $y=0.54 + 40$ , with an  $R^2$  of 0.43.

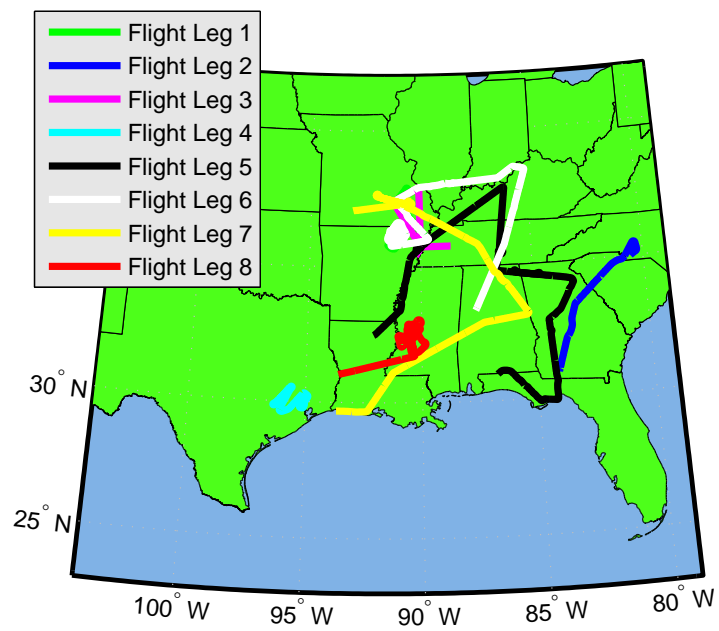


Figure 4.10: Each different colored flight track shows a flight leg plotted in Figure 4.11 and Figure 4.12.

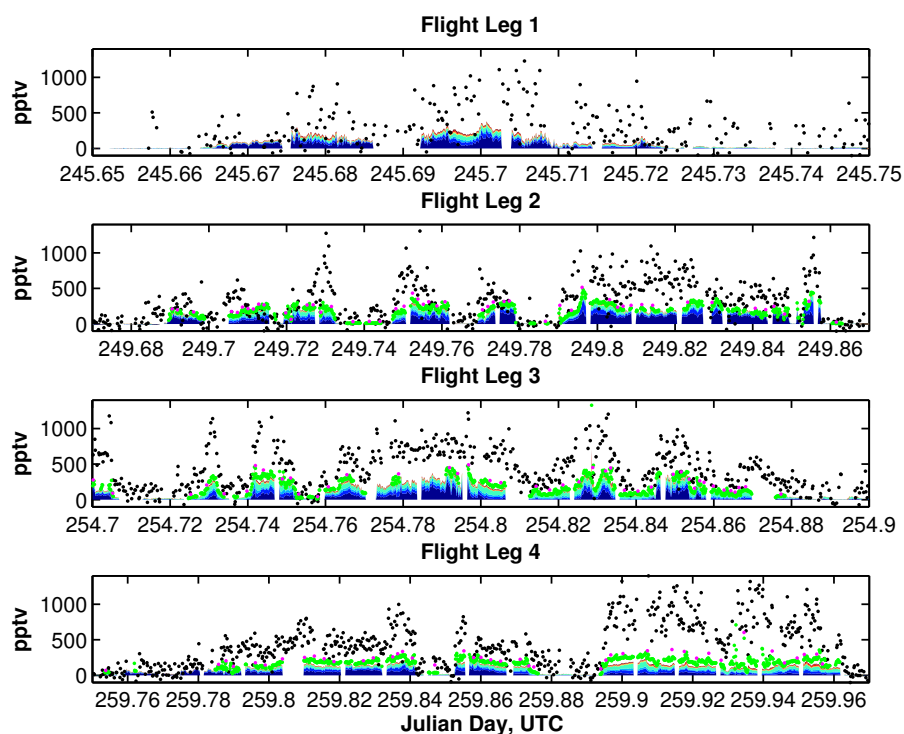


Figure 4.11: Speciated organic nitrate measurements are shown for four flight legs from different days. The corresponding flight track for each time series is shown in Figure 4.10. Plotted in stacked solid colors are the speciated organic nitrates as measured by the Caltech CIMS. Pink dots represent the sum of all speciated measurements (Caltech CIMS and the Whole Air Sample measurements) and the aerosol organic nitrate fraction (CU AMS measurements). The dashed black line is the total alkyl nitrate signal in pptv divided by 2 ( $\Sigma$  ANs) as measured by the Berkeley TD-LIF. It is clear that there are significant sources of alkyl nitrates besides the speciated organic nitrates.

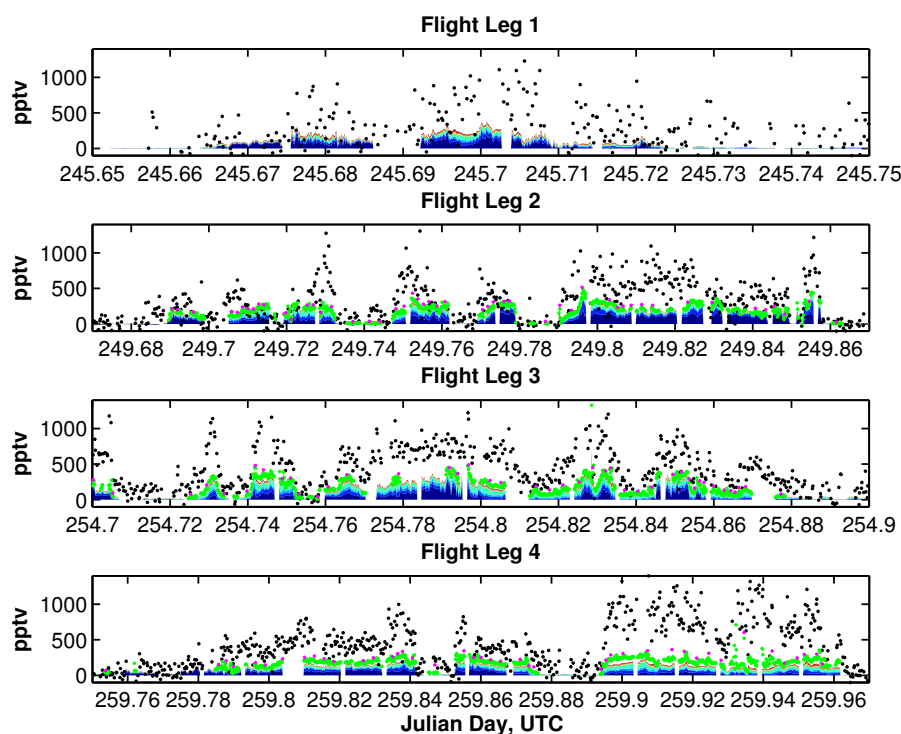


Figure 4.12: Speciated organic nitrate measurements are shown for four flight legs from different days. Each flight leg's corresponding flight track is shown in Figure 4.10. Plotted in stacked solid colors are the speciated organic nitrates as measured by the Caltech CIMS. Pink dots represent the sum of all speciated measurements (Caltech CIMS and the Whole Air Sample measurements) and the aerosol organic nitrate fraction (CU AMS measurements). The dashed black dots are the total alkyl nitrate signal in pptv divided by 2 ( $\Sigma$  ANs) as measured by the Berkeley TD-LIF. It is clear that there are significant sources of alkyl nitrates besides the speciated organic nitrates.

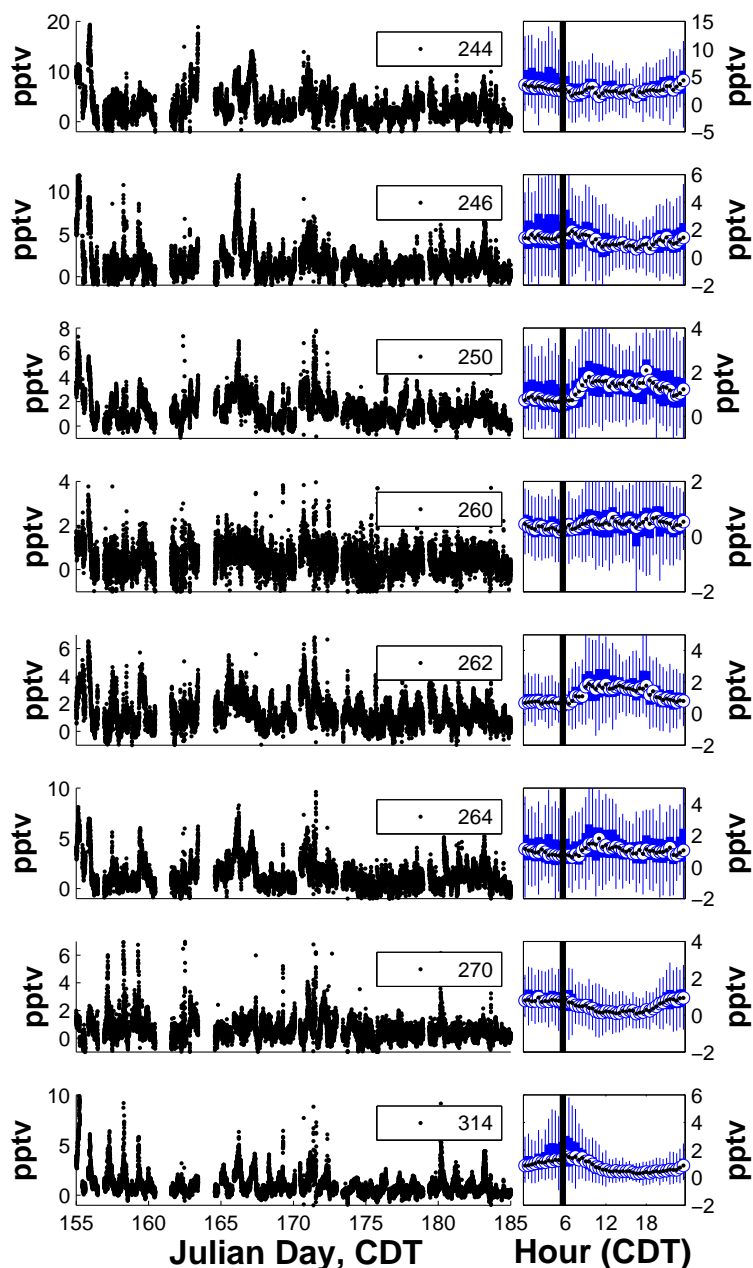


Figure 4.13: Time series (left) and diurnal profiles (right) of organic nitrates with uncertain sources. All times are presented in Central Daylight Time, which was the local time at the SOAS 2013 field site. The diurnal profiles are produced from 30 minute bins, with the black diamond indicating the median, the edge of the rectangles indicating the 25th and 75th percentiles, and the whiskers plotting the non-outlier extremes.

*Chapter 5*

## OUTLOOK

This work describes both laboratory and field investigations performed to better understand the formation and fate of organic nitrates in the troposphere. There are, however, major lines of investigation left in the understanding of the chemistry mechanisms and atmospheric implications.

A major question left open in Chapter 3: what are the products missing in the unimolecular channel? A significant fraction of the carbon is unaccounted for, and further studies should be attempted to understand what these products are, what their likely impact on HO<sub>x</sub> recycling might be, and perhaps most importantly, whether they are a significant contributor to secondary organic aerosol formation.

Another line of inquiry left open in Chapter 3 is the yield of carbonyls from NO and HO<sub>2</sub> chemistry. The work assumes that the branching ratio to form organic nitrates is independent of RO<sub>2</sub> substitution, and presents evidence for this, but without direct measurements of the carbonyls which make up the bulk of the carbon chemistry, it is difficult to definitively conclude this is the case. Simultaneous measurements of methyl vinyl ketones, methacrolein, and formaldehyde are difficult due to the decomposition of isoprene hydroxy nitrates and isoprene hydroxy hydroperoxides interfering in both PTR-MS and gas chromatography measurements.

A continuously stirred tank reactor may provide an easy way to measure product yields at precise and low NO (10 ppbv to hundreds of ppt) levels, overcoming a significant uncertainty in Chapter 3. Conducted together with measurements of carbonyls where the instrumental interferences are overcome with cold trapping techniques (Liu et al., 2013).

Chapter 4 also did not answer the main question, which was whether or not heterogeneous hydrolysis explains the short lifetime of ISOPN. GC-CIMS data taken at PROPHET during the summer 2016 should directly answer this question. The main lines of evidence would be to show that 1) the 1,2 ISOPN isomer is present in significantly lower concentrations relative to the hydroxy hydroperoxides and the 4,3 ISOPN isomer, 2) that the relative concentration of the 1,2 ISOPN is somehow related to a heterogeneous loss process such as cloud water scavenging, aerosols, or humidity.

Further laboratory studies might also be required. For heterogeneous hydrolysis to be important, a Henry's law constant and a hydrolysis rate are required to estimate the heterogeneous loss in the atmosphere. Attempts were made to measure the Henry's law constant for the 1,2 ISOPN isomer in 1-octanol, and the 4,3 ISOPN isomer in water. The main uncertainty was the concentration in the liquid after equilibration.

Similarly, attempts were made to measure the hydrolysis rate using many methods to mix on shorter timescales and measure the results. The most promising method attempted was a plug flow reactor set up in which the reaction time of the ISOPN isomers in H<sub>2</sub>O could be varied across two orders of magnitude using syringe pumps. This result failed mainly due to uneven mixing between the two syringe pumps. A microfluidics device which mixed droplets for variable lengths of time before analysis would be an interesting technique to measure the hydrolysis rate constant.

Chapter 4 also discusses the significant gap in the organic nitrate budget in forested environments. B. H. Lee et al., 2016 study observed significant highly functionalized, high mass nitrates in both the gas and aerosol phase. These compounds make up a significant fraction of the aerosol organic nitrate, and likely begin as gas phase compounds. It is possible that these compounds explain the significant gap between speciated and total organic nitrates measured at the SOAS site. The mechanism for the formation of these compounds is still not known, and with some of the dinitrates measured by B. H. Lee et al., 2016 containing only 5 carbons, potentially implying their source as isoprene.

This also dovetails with the lack of significant studies investigating monoterpene and sesquiterpene oxidation at atmospherically relevant peroxy radical lifetimes. For those compounds with significantly lower bond dissociation energies for the peroxy radicals, reversible O<sub>2</sub> addition is possible, but likely the largest impact of longer peroxy radicals is the ability to react through unimolecular channels.

Nighttime oxidation is not well studied at atmospherically relevant conditions for biogenically dominated VOCs. At the SOAS site, NO<sub>3</sub> was titrated to lower than measurable concentration, and HO<sub>2</sub> and NO (lower than measurable levels due to titration by O<sub>3</sub>) concentrations indicate that a peroxy radical lifetime is likely an order of magnitude longer than during the day. One question is what the effect of such long peroxy radical lifetimes might be. Is it possible that a peroxy radical at night lives long enough to react heterogeneously? Is it possible that the main

reaction partners are in fact other peroxy radicals? New experimental techniques need to be pioneered to properly explore these dynamics.

There continue to be significant gaps in our understanding of the oxidative mechanisms volatile organic compounds undergo in the atmosphere.



- 5C%7D%7B%5C\_%7Duser=687336%7B%5C%7D%7B%5C\_%7DcoverDate=08/11/2000%7B%5C%7D%7B%5C\_%7Dalid=1172426822%7B%5C%7D%7B%5C\_%7Drdoc=1%7B%5C%7D%7B%5C\_%7Dfmt=high%7B%5C%7D%7B%5C\_%7Dorig=search%7B%5C%7D.
- Liu, Y. J. et al. (2013). “Production of methyl vinyl ketone and methacrolein via the hydroperoxyl pathway of isoprene oxidation”. In: *Atmospheric Chemistry and Physics* 13.11, pp. 5715–5730. ISSN: 16807324. DOI: 10.5194/acp-13-5715-2013. URL: <http://www.atmos-chem-phys.net/13/5715/2013/>.
- Lockwood, AL et al. (2010). “Isoprene nitrates: preparation, separation, identification, yields, and atmospheric chemistry”. In: *Atmospheric Chemistry and Physics* 10.13, pp. 6169–6178.
- Lohr, Lawrence L., John R. Barker, and Robert M. Shroll (2003a). “Modeling the Organic Nitrate Yields in the Reaction of Alkyl Peroxy Radicals with Nitric Oxide. 1. Electronic Structure Calculations and Thermochemistry”. In: *Journal of Physical Chemistry A* 107.38, pp. 7429–7433. ISSN: 10895639. DOI: 10.1021/jp034637r. URL: <http://pubs.acs.org/doi/abs/10.1021/jp034637r>.
- (2003b). “Modeling the Organic Nitrate Yields in the Reaction of Alkyl Peroxy Radicals with Nitric Oxide. 1. Electronic Structure Calculations and Thermochemistry”. In: *Journal of Physical Chemistry A* 107.38, pp. 7429–7433. ISSN: 10895639. DOI: 10.1021/jp034637r. URL: <http://pubs.acs.org/doi/abs/10.1021/jp034638j>.
- Muthuramu, K, P B Shepson, and J M O'Brien (1993). “Preparation, Analysis, And Atmospheric Production Of Multifunctional Organic Nitrates”. In: *Environ. Sci. Technol.* 27, pp. 1117–1124. ISSN: 0013936X. DOI: 10.1021/es00043a010. URL: <http://pubs.acs.org/doi/pdf/10.1021/es00043a010>.
- O'Brien, Jason M et al. (1998). “Determination of the hydroxy nitrate yields from the reaction of C2-C6 alkenes with OH in the presence of NO”. In: *The Journal of Physical Chemistry A* 102.45, pp. 8903–8908.
- O'Brien, JM et al. (1995). “Measurements of alkyl and multifunctional organic nitrates at a rural site in Ontario”. In: *Journal of Geophysical Research: Atmospheres (1984–2012)* 100.D11, pp. 22795–22804.
- Orlando, John J and Geoffrey S Tyndall (2012). “Laboratory studies of organic peroxy radical chemistry: an overview with emphasis on recent issues of atmospheric significance”. In: *Chemical Society Reviews* 41.19, pp. 6294–6317.
- Patchen, Amie K et al. (2007). “Direct kinetics study of the product-forming channels of the reaction of isoprene-derived hydroxyperoxy radicals with NO”. In: *International Journal of Chemical Kinetics* 39.6, pp. 353–361.
- Paulot, F., D. K. Henze, and P. O. Wennberg (2012a). “Impact of the isoprene photochemical cascade on tropical ozone”. In: *Atmospheric Chemistry and Physics* 12.3, pp. 1307–1325. ISSN: 16807316. DOI: 10.5194/acp-12-1307-2012. URL: <http://www.atmos-chem-phys-discuss.net/11/25605/2011/>.

- Paulot, F., D. K. Henze, and P. O. Wennberg (2012b). "Impact of the isoprene photochemical cascade on tropical ozone". In: *Atmospheric Chemistry and Physics* 12.3, pp. 1307–1325. ISSN: 16807316. DOI: 10.5194/acp-12-1307-2012. URL: <http://www.atmos-chem-phys.net/12/1307/2012/>.
- Paulot, F et al. (2009). "Isoprene photooxidation: new insights into the production of acids and organic nitrates". In: *Atmospheric Chemistry and Physics* 9.4, pp. 1479–1501.
- Peeters, Jozef, Thanh Lam Nguyen, and Luc Vereecken (2009). "HOx radical regeneration in the oxidation of isoprene". In: *Physical Chemistry Chemical Physics* 11.28, pp. 5935–5939.
- Rosen, R. S. (2004). "Observations of total alkyl nitrates during Texas Air Quality Study 2000: Implications for O<sub>3</sub> and alkyl nitrate photochemistry". In: *Journal of Geophysical Research* 109.D7, p. D07303. ISSN: 0148-0227. DOI: 10.1029/2003JD004227. URL: <http://doi.wiley.com/10.1029/2003JD004227>.
- Sprengnether, Michele et al. (2002). "Product analysis of the OH oxidation of isoprene and 1, 3-butadiene in the presence of NO". In: *Journal of Geophysical Research: Atmospheres (1984–2012)* 107.D15, ACH–8.
- Teng, Alexander P, John D Crouse, and Paul O Wennberg (2017). "Isoprene peroxy radical dynamics". In: *Journal of the American Chemical Society* 139.15, pp. 5367–5377. DOI: 10.1021/jacs.6b12838. URL: <http://doi.org/10.1021/jacs.6b12838>.
- Tuazon, Ernesto C. and Roger Atkinson (1990). "A product study of the gasphase reaction of Isoprene with the OH radical in the presence of NO<sub>x</sub>". In: *International Journal of Chemical Kinetics* 22.12, pp. 1221–1236. ISSN: 10974601. DOI: 10.1002/kin.550221202.
- Wu, Shiliang et al. (2007). "Why are there large differences between models in global budgets of tropospheric ozone?" In: *Journal of Geophysical Research: Atmospheres (1984–2012)* 112.D5.
- Xiong, F et al. (2015). "Observation of isoprene hydroxynitrates in the southeastern United States and implications for the fate of NO<sub>x</sub>". In: *Atmospheric Chemistry and Physics* 15.19, pp. 11257–11272.
- Zhang, Jieyuan, Tim Dransfield, and Neil M Donahue (2004). "On the mechanism for nitrate formation via the peroxy radical+ NO reaction". In: *The Journal of Physical Chemistry A* 108.42, pp. 9082–9095.
- Zhang, L. et al. (2010). "Intercomparison methods for satellite measurements of atmospheric composition: Application to tropospheric ozone from TES and OMI". In: *Atmospheric Chemistry and Physics* 10.10, pp. 4725–4739. ISSN: 16807316. DOI: 10.5194/acp-10-4725-2010. URL: <http://www.atmos-chem-phys.net/10/4725/2010/>.

*Appendix A***SUPPORTING INFORMATION FOR CHAPTER 4: ISOPRENE  
PEROXY RADICAL DYNAMICS**

# Isoprene Peroxy Radical Dynamics

Alexander P. Teng<sup>1</sup>, John D. Crouse<sup>1</sup>, Paul O. Wennberg<sup>1,2</sup>

<sup>1</sup>Division of Geological and Planetary Sciences, California Institute of Technology, Pasadena, California 91125, United States

<sup>2</sup>Division of Engineering and Applied Science, California Institute of Technology, Pasadena, California 91125, United States

## Supplementary Information

### Table of Contents

	<b>Page</b>
1. CIMS Sensitivity	S2
2. ISOPN ( $m/z$ 232)	S3
a. GC elution assignment	S3
b. Isomer interconversion in GC	S4
i. Chromatographic separation	S4
ii. Hydrolysis	S6
c. ISOPN formation from OH addition at C <sub>2</sub> and C <sub>3</sub>	S7
d. ISOPN yield	S8
e. Implied methacrolein and methyl vinyl ketone yields	S11
3. ISOPHOH ( $m/z$ 203)	S12
a. GC elution assignment	S12
4. HPALD and other compounds ( $m/z$ 201)	S13
a. GC elution assignment	S13
b. Identity of early eluting compounds	S14
5. HC <sub>5</sub> ( $m/z$ 185)	S15
a. GC elution assignment	S15
b. HC <sub>5</sub> yield and schemes	S16
6. Unimolecular H-shift of the Z $\delta$ peroxy radicals	S18
a. HPALD yield	S21
b. Yield of other products	S22
c. Uncertainties in the rate of peroxy radical H-shift chemistry	S23
d. Comparison with bulk isomerization rate from Crouse <i>et al.</i> , 2011	S24
e. Derivation of a linear approximation of products vs. $\tau$	S26
7. Experiments constraining $k_{2r}$	S27
8. Temperature dependence of the RO <sub>2</sub> kinetics.	S28
9. Isoprene oxidation: Additional simulations	S32
a. Comparison with Peeters <i>et al.</i> , 2014	S36
10. 1,3 Butadiene and 2,3 Dimethylbutadiene oxidation	S39
11. References	S41

## 1. CIMS Sensitivities

For ISOPN, the sensitivity has been measured using a CIMS/TD-LIF technique described by Lee *et al.*<sup>1</sup> The CIMS sensitivity for ISOPOOH, HC<sub>5</sub>, and HPALD relative to that of ISOPN is estimated using the ratio of the ion-molecule collision rates calculated according to Crouse *et al.*<sup>2</sup> and Paulot *et al.*<sup>3</sup> The sensitivity determined via the ion collision rate is multiplied by the percentage of the total ion signal from this molecule occurring at the observed  $m/z$ . This is not always unity due to fragmentation. This fraction is diagnosed by presence of other (fragment) ions in the chromatograms. For example, for ISOPOOH the fraction of product ions observed at the simple cluster ion ( $m/z$  203) is 0.5 (see section 3a). For HPAC, HPACET, and compounds of molecular weight 116 and 132, a CIMS sensitivity of  $2.0 \times 10^{-4}$  normalized counts per pptv (nmcts / pptv) is used. To obtain the concentration of each molecule in the flow tube, the normalized counts (determined by dividing the signal at all masses by the reagent ion signal ( $^{13}\text{CF}_3\text{O}^-$  and its cluster with  $\text{H}_2\text{O}$  and  $\text{H}_2\text{O}_2$  ( $m/z$  86 +  $m/z$  104 +  $m/z$  120  $\approx$  70,000 ion counts per second))) is divided by the sensitivity. For example, 1 pptv of ISOPN in the instrument flow tube produces  $\sim$ 25 ion counts per second at  $m/z$  232. In Table S1, the sensitivities are given for the simple  $\text{CF}_3\text{O}^-$  cluster ( $m/z$  as indicated).

**Table S1** – List of compound names, measured mass to charge ratios ( $m/z$ ), and sensitivities used in this study to convert from the signal measured at the  $m/z$  listed in column 2 to concentration of the compound listed in column 1. nmcts is the ion count rate at the noted  $m/z$  normalized by that of the reagent ions ( $^{13}\text{CF}_3\text{O}^-$  and its clusters with water and hydrogen peroxide).

Compound	$m/z$	Sensitivity ( $\times 10^{-4}$ nmcts pptv $^{-1}$ )
ISOPN	232	3.6
ISOPOOH	203	1.6
HPALD	201	2.8
HC <sub>5</sub>	185	4.5
HPAC	161	2.0
HPACET	175	2.0
MW 116	201	2.0
MW 132	217	2.0

## 2. ISOPN ( $m/z$ 232)

### 2a. GC Elution Assignments

The ISOPN elution order is assigned using authentic standards. Synthesis, purification and identification of several ISOPN isomers (4-OH, 3-N; *E* 1-OH, 4-N; *Z* 1-OH, 4-N) are described previously.<sup>1</sup> Synthesis, purification and identification of the 1-OH isomers is accomplished using a new synthesis approach that will be described in a forthcoming paper. The order of the elution of the ISOPN isomers on the RTX 1701 column (Restek) follows these rules: more substituted OH groups elute earlier, more substituted ONO<sub>2</sub> groups elute earlier, and *Z* isomers elute before *E* isomers.

There is an unidentified peak at  $m/z$  232 that elutes at the end of the separation (Figure 2 (main body), 14.5 minute elution time). This peak represents ~2% of the total ISOPN signal independent of RO<sub>2</sub> lifetimes. ISOPN isomer distributions analyzed at higher temperature and pressure GC programs show a much smaller signal at this peak, indicating it is thermally labile. It is possible this peak is not a nitrate functionality, but rather a nitro product of a minor branching channel in which the reactive intermediate 1-OH, 2-OONO\* undergoes an isomerization (Figure S1).

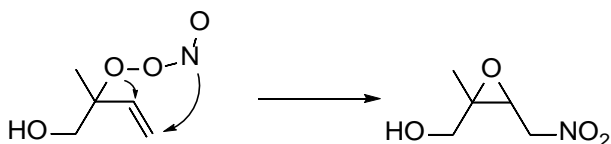


**Figure S1** – Possible isomerization mechanism to form unidentified  $m/z$  232 peak that elutes at 13.5 min in Figure S2 (14.5 min Figure 2, main body).

## 2b. Isomer Interconversion

A major challenge to the gas chromatographic analysis of ISOPN is loss and interconversion of the 1-OH, 2-N isomer to *E* 1-OH, 4-N during chromatographic separation. It also hydrolyzes quickly when water vapor is co-condensed.

### 2.b.i. Chromatographic separation

1-OH, 2-N ISOPN converts to the *E* 1-OH, 4-N isomer along the GC column. This produces an elevated baseline between the  $\beta$  and  $\delta$  peaks (Figure S2). This interconversion is sensitive to temperature and pressure in the column. Elution of the 1-OH, 2-N ISOPN under higher temperatures and higher pressures increases this conversion. To accurately determine the yields of 1-OH, 2-N and *E* 1-OH, 4-N isomer ISOPN it is, therefore, necessary to minimize and account for any interconversion.

The interconversion is confirmed through three experiments. In the first, oxidation of 1-OH, 2-OOH ISOPOOH by OH with an initial concentration of 15 ppmv NO is performed. In this experiment, 1-OH, 2-N ISOPN is produced by reaction of NO with the peroxy radical formed following H-abstraction of the peroxide H. The high NO concentration results in a peroxy radical lifetime too short to allow significant decomposition of the nascent RO<sub>2</sub>. In this experiment, GC analysis of the ISOPN shows a long, flat tailing peak after 1-OH, 2-N ISOPN which ends at the elution time of *E* 1-OH, 4-N isomer.

A second experiment to confirm the 1-OH, 2-N ISOPN interconversion during the GC utilized a heterogeneous reaction where 1-OH, 2-OOH ISOPOOH is trapped on the column, and gas-phase HONO (few hundred ppbv in air) is passed over the trapped peroxide. The HONO converts the 1-OH, 2-OOH to 1-OH, 2-N ISOPN. The chromatogram shows a similar long tail that ends at the elution time of the *E* 1-OH, 4-N ISOPN is observed.

The third test comes from a GC analysis after an ozone oxidation experiment of ISOPN isomers in which  $\delta$  isomers are preferentially reacted away (the  $\delta$  isomers' ozone rate constants are two orders of magnitude larger than that of the  $\beta$  isomers), leaving only 1-OH, 2-N and 4-OH, 3-N.<sup>1</sup> These chromatograms contain elevated baselines. A control analysis where only the 4-OH, 3-N isomer is analyzed by gas chromatography shows no elevated baseline.

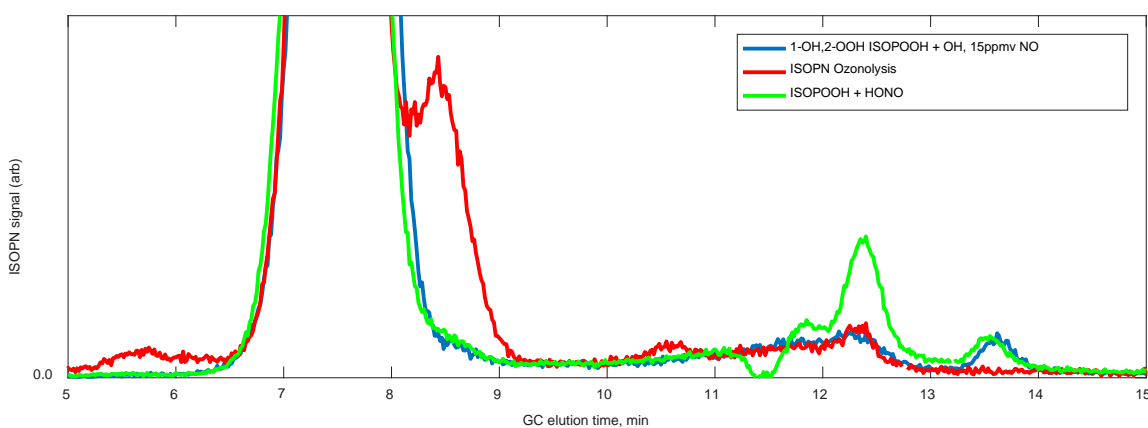


**Figure S2** – Chromatogram of  $m/z$  232 (ISOPN) illustrate the slow elevated baseline resulting from conversion of the  $\beta$  1-OH, 2-N to *E* 1-OH, 4-N on the column. The small dip in the green trace at 11.5 minutes is due to the large signal peak at 233  $m/z$  that temporarily increases the baseline and artificially reduces signal to zero temporarily.

In all three experiments, the baseline increases nearly linearly until the elution time of *E* 1-OH, 4-N. For all of the experiments listed in this study, the operating conditions for the chromatography are the same, and therefore the absolute amount of conversion is a

function only of the amount of 1-OH, 2-N trapped. A correction is modeled using these three experiments.

### **2.b.ii. Hydrolysis**

The 1-OH, 2-N isomer hydrolyzes when water vapor is co-condensed on the column. The chromatograms shown in Figure S3 are sequential samples from the same chamber experiment. Shown in blue is the chromatogram obtained when the trapping temperature is cold enough to collect H<sub>2</sub>O. In this experiment, a significant fraction of the 1-OH, 2-N isomer is converted to the *E* 1-OH, 4-N isomer. In addition, the expected product of hydrolysis, the 1-OH, 2-OH isoprene diol, is produced. For the data shown in the main body of this study, we scrupulously avoided trapping water on the GC column.

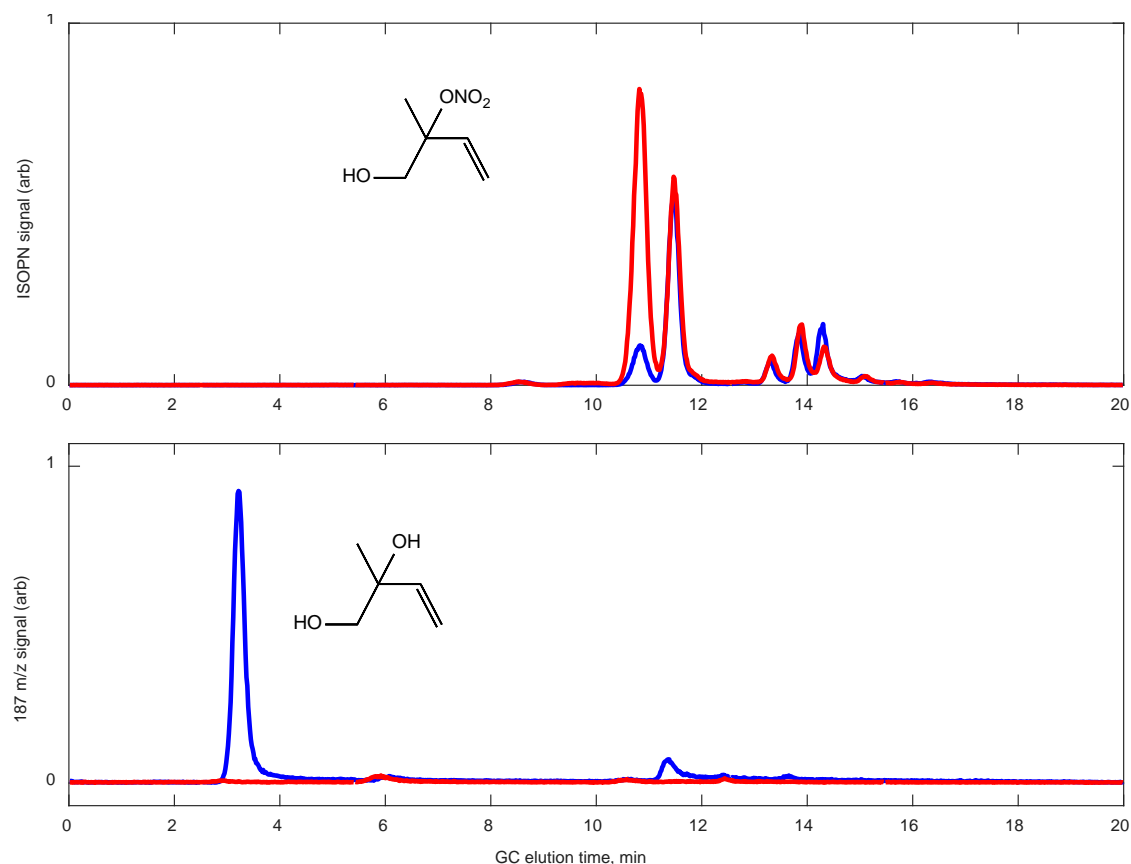


**Figure S3** – Two chromatograms, taken sequentially from the same experimental chamber showing the effect of co-trapping water with ISOPN. The only difference between the operating conditions is the trap temperature (red = -20C, and blue = -45C).

## 2c. ISOPN formation from OH addition at C<sub>2</sub> and C<sub>3</sub>

Previous studies have calculated that OH adds to isoprene at the C<sub>2</sub> and C<sub>3</sub> centers 4-7% of the time.<sup>4-6</sup> A synthetic standard of 2-OH, 1-N isomer (that would be produced from internal OH addition at C<sub>2</sub>, O<sub>2</sub> addition to C<sub>1</sub>, and subsequent reaction with NO), elutes before the 1-OH, 2-N isomer in the gas chromatographic analysis. The 3-OH, 4-N should, likewise, elute before the 4-OH, 3-N peak. Assigning chromatographic *m/z* 232 peaks eluting before 1-OH, 2-N (at RO<sub>2</sub> lifetimes < 0.01 s), to products arising from OH addition to C<sub>2</sub> and C<sub>3</sub> suggests a combined contribution of <1.5% to the signal from all hydroxy nitrates formed. Thus, there is little evidence for addition at C<sub>2</sub> or C<sub>3</sub> from measurements of the β

ISOPN isomers. It is possible, however, that the OH addition at C<sub>2</sub> and C<sub>3</sub> results in products not identified in this study due to a unimolecular chemistry occurring before O<sub>2</sub> addition to the OH-isoprene adduct.<sup>7</sup>

## 2d. ISOPN Yield

The isoprene nitrate yield is measured in chamber experiments in which isoprene, CH<sub>3</sub>ONO, and NO are added to the chamber. Loss of isoprene is measured using GC-FID. Here, a PFA sampling loop on a PEEK 6-way valve connected to a 30 m PLOT-Q column in a GC-FID (Hewlett Packard 5890 series II Plus) chromatographically separates and measures isoprene from other products of the oxidation chemistry. The sampling loop is maintained at room temperature. Details of the chamber set up are described in the Methods section, and experimental conditions and results are listed in Table S2. The yield is corrected for loss by OH (F<sub>corr</sub>) using the measured isomer distribution and appropriate OH rate constants (Table S3).

The reported yield is corrected to 297 K using the measured temperature increase due to the heating by the UV lamps as described in Teng *et al.*<sup>8</sup> The sensitivity of ISOPN isomers for CF<sub>3</sub>O<sup>•</sup> are determined from the same experimental setup for isoprene nitrates as described in Teng *et al.*<sup>8</sup> The sensitivity for all ISOPN isomers is within +-7% of the mean.

**Table S2** – Experimental conditions and resulting yields for yield of ISOPN from isoprene + OH in the presence of air and NO at 297 K and 993 hPa. The calculated yield is higher by  $F_{\text{corr}}$  than the ratio of ISOPN measured / Isoprene loss due to photooxidation of the ISOPNs.

Exp	[Isoprene] <sub>o</sub> (ppbv)	[NO] <sub>o</sub> (ppbv)	[Isoprene] lost (ppbv)	[ISOPN] measured (ppbv)	$F_{\text{corr}}$	ISOPN Yield (%)
1	181	535	49	7.1	1.08	16 ± 3
2	24.0	490	4.1	0.5	1.04	13 ± 2
3	227	612	63	7.3	1.08	12 ± 2
4	171	504	21	2.7	1.03	14 ± 2
5	180	623	23	3.0	1.03	13 ± 2
6	199	550	43	4.2	1.05	10 ± 2
<b>Average:</b>						<b>13 ± 2</b>

**Table S3** – Isomer distributions and OH rate constants used to correct yield calculations. Rate constants for 4-OH, 3-N, Z 1-OH, 4-N, and E 1-OH, 4-N are taken from Lee *et al.*<sup>1</sup> The rate constant for the 1-OH, 2-N, Z 4-OH, 1-N and E 4-OH, 1-N were determined as part of this study, with estimated uncertainties of ±30%.

Isomer	Isomer Distribution	$k_{\text{OH}}$ ( $\text{cm}^3 \text{molec}^{-1} \text{s}^{-1}$ )
1-OH, 2-N	0.50	$3.0 \times 10^{-11}$
4-OH, 3-N	0.26	$4.2 \times 10^{-11}$
Z 4-OH, 1-N	0.06	$8 \times 10^{-11}$
E 4-OH, 1-N	0.05	$8 \times 10^{-11}$
Z 1-OH, 4-N	0.04	$11 \times 10^{-11}$
E 1-OH, 4-N	0.09	$11 \times 10^{-11}$

A set of experiments was conducted to evaluate whether the hydroxy nitrate yield varies between isomers. A constant ratio of isoprene and 1-hexene, or isoprene and methylpropene is oxidized at two different levels of initial NO concentration. A FEP pillow bag (0.2 m<sup>3</sup>) is filled by flowing N<sub>2</sub> over liquid isoprene, and then a liquid standard of 1-hexene. For methyl propene, a glass bulb of desired pressure (20 hPa) was transferred to the pillow bag. In each case, the pillow bag concentration is then checked by FT-IR, and two evacuated bulbs are filled to the desired pressure (~900 hPa). The two bulbs are used in back-to-back oxidation experiments at differing NO concentrations. The experimental conditions for both experiments are as follows: ~120 ppbv isoprene, ~140 ppbv 1-hexene, ~80 ppbv CH<sub>3</sub>ONO. For the high NO experiment, 620 ppbv NO is added to the chamber. For

the lower NO experiment, 13 ppbv NO is added to the chamber. The extent of the reaction is terminated with <10% isoprene oxidized to minimize secondary OH losses.

The ratio of the hydroxy nitrate signals after oxidation period (Figure S4), indicate the ratio of ISOPN to 1-hexene-derived hydroxy nitrate (1-hexane HN) formed remains constant despite the difference in the ISOPN distribution (Figure S5). Given the precision of the results, however, we cannot rule out a  $\sim 10\%$  difference in the average yields of the  $\delta$  and  $\beta$  ISOPN isomers.

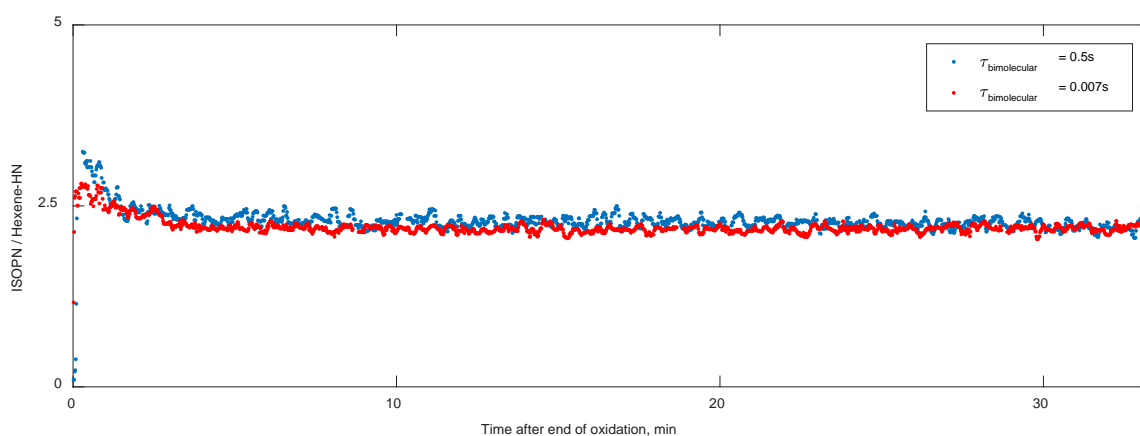


**Figure S4** – The ratio of signals for  $m/z$  232 (ISOPN) to  $m/z$  248 (1-hexene derived hydroxy nitrate) produced during isoprene and 1-hexene + OH oxidation experiments at two different  $RO_2$  lifetimes. The relative yields of ISOPN to 1-hexene HN do not change significantly over experiments with different  $RO_2$  lifetimes.

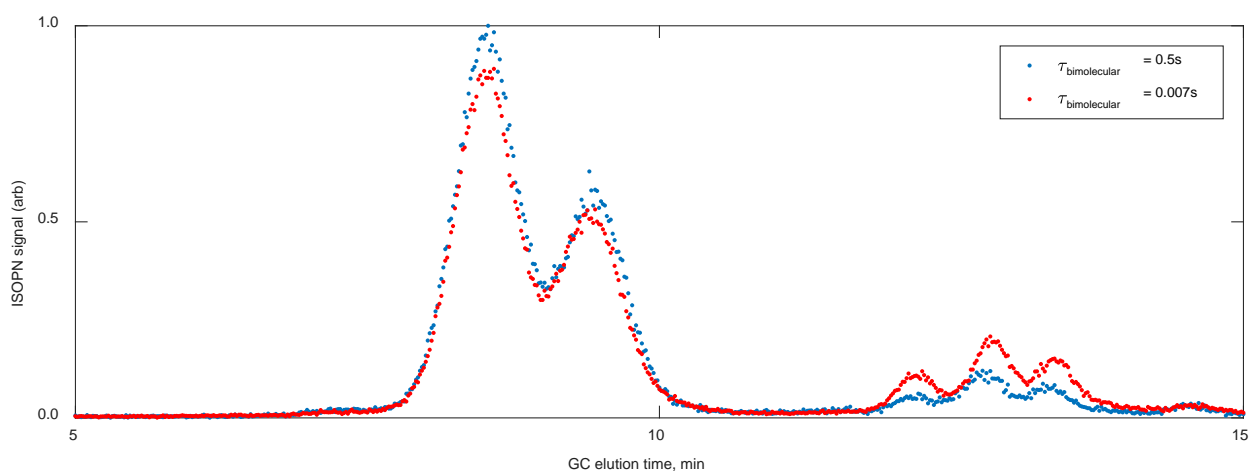


**Figure S5** – GC chromatograms for  $m/z$  232 (ISOPN) for the two experiments of differing bimolecular  $RO_2$  lifetimes shown in Figure S4. Signals are normalized to the integral of the peak areas.

## 2e. Implied Methacrolein and Methyl Vinyl Ketone yields

The varying distribution of peroxy radicals shown in Table 2 (main body) will map into peroxy radical lifetime dependent yields for methacrolein and methyl vinyl ketone produced via reaction with NO. Accounting for the 13% yield of hydroxy nitrates, the expected yields of MVK and MACR should be 87% of the fractional abundance of the 1-OH, 2-O<sub>2</sub> and 4-OH, 3-O<sub>2</sub> isomers, respectively. The previously reported yields of methyl vinyl ketone and methacrolein at very short RO<sub>2</sub> lifetimes (Table S4) can be compared with our estimate for the yields of 43% and 23%, respectively, in the kinetic limit. The yields are expected to increase as the  $\beta$  fraction increases and then fall as H-shift chemistry becomes important. The yields reported by Spregnether *et al.*<sup>9</sup> agree most closely with the measured kinetic limit distribution. In the equilibrium regime, Liu *et al.*<sup>10</sup> report MVK and MACR yields higher than other studies, albeit statistically indistinguishable from the Spregnether study. For their conditions ( $\tau_{\text{bimolecular}}=5$  s), simulations using the data presented in this study would suggest yields of 53 and 27%. Further study of the methacrolein and methyl vinyl ketone yields from the ISOP<sub>2</sub> + NO channel at atmospherically relevant lifetimes is warranted.

**Table S4** – The reported yields of methyl vinyl ketone and methacrolein from isoprene oxidation by OH from reaction of the peroxy radicals with NO (previous studies). The total  $\beta$  RO<sub>2</sub> fraction is calculated from the measured yields. The bimolecular lifetime is calculated from the reported NO concentration. For those cases where NO concentration is only reported at the start of an experiment, the bimolecular lifetime is calculated from the initial value.

Citation	MVK yield (%)	MACR yield (%)	Implied $\beta$ RO <sub>2</sub> Fraction (%)	$\tau_{[\text{NO}]}$ , s
Tuazon and Atkinson <sup>11</sup>	29 ± 7	21 ± 5	57	6x10 <sup>-4</sup>
	33 ± 7 <sup>a</sup>	24 ± 5 <sup>a</sup>	65	
Paulson <i>et al.</i> <sup>12</sup>	35.5 ± 4	25 ± 3	70	7x10 <sup>-4</sup>
Miyoshi <i>et al.</i> <sup>13</sup>	32 ± 5	22 ± 2	62	~6x10 <sup>-4</sup>
Ruppert <i>et al.</i> <sup>14</sup>	31 ± 3	20 ± 2	59	2x10 <sup>-3</sup>
Sprengnether <i>et al.</i> <sup>9</sup>	44 ± 6	28 ± 4	83	~1.5x10 <sup>-4</sup>
Karl <i>et al.</i> <sup>15</sup>	41 ± 3	27 ± 3 <sup>b</sup>	78	8-20 <sup>d</sup>
Galloway <i>et al.</i> <sup>16</sup>	30.4 ± 1.3	22.0 ± 0.6	60	~1x10 <sup>-2</sup>
Liu <i>et al.</i> <sup>10</sup>	44.5 ± 5.5 <sup>c</sup>	31.8 ± 4.2 <sup>c</sup>	88	5

<sup>a</sup> corrected for O(<sup>3</sup>P) reaction as communicated to Paulson (1992).

<sup>b</sup> result influenced by H-shift isomerization.

<sup>c</sup> assumes that 93% of the peroxy radicals react with NO.

<sup>d</sup> HO<sub>2</sub> likely contributes to this chemistry, however no measurements were made of the HO<sub>2</sub> concentrations.

### 3. ISOPOOH (*m/z* 203)

#### 3a. GC elution assignments

Peak assignments for  $\beta$  ISOPOOH isomers (1-OH, 2-OOH and 4-OH, 3-OOH) are based on authentic standard synthesis (Figure S6).<sup>17,18</sup> No evidence of internal OH addition products is present in the *m/z* 203 chromatograms. There is a group of small peaks eluting after the  $\beta$  ISOPOOH isomers, tentatively identified as the  $\delta$  ISOPOOH isomers. GC analysis of synthesized standard *Z* 4-OH, 1-OOH elutes within the group of peaks tentatively identified as the  $\delta$  ISOPOOH isomers, but with a transmission of only ~50%. It is likely that the other  $\delta$  isomers have similarly low transmission.

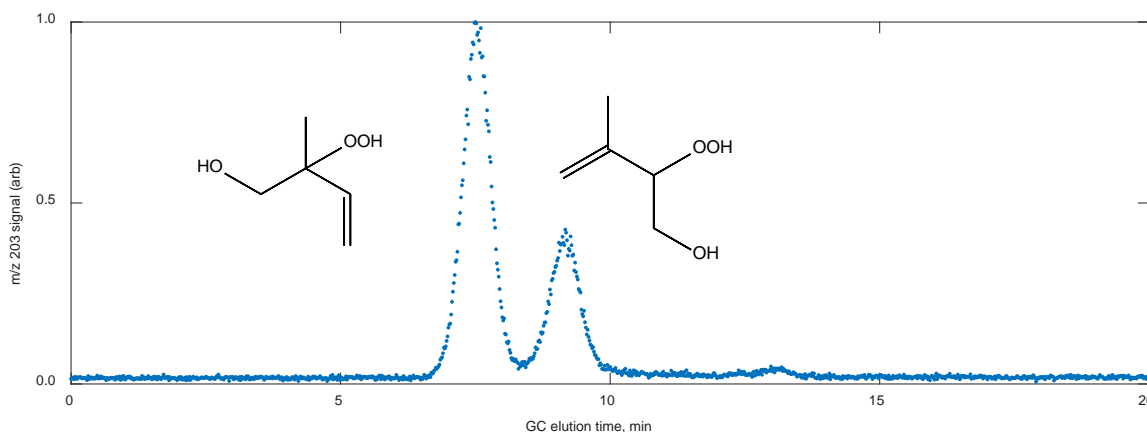


**Figure S6** – Chromatogram for  $m/z$  203 (ISOPPOOH).  $\delta$  ISOPPOOH isomers (between 11 and 15 minutes) do not have 100% transmission through the GC column.

#### 4. HPALD and other compounds ( $m/z$ 201)

##### 4a. GC Peak assignments

Four main peaks are observed at  $m/z$  201, corresponding to the mass of a  $\text{CF}_3\text{O}^-$  cluster ion with a neutral species of mass 116 AMU (Figure S7). MS/MS on the bulk  $m/z$  201 signal yields an  $m/z$  63 fragment ion with similar yield to that observed from  $\text{ISOPPOOH}\cdot\text{CF}_3\text{O}^-$  ions<sup>2</sup>. The +1 isotope signal observed at  $m/z$  202 (arising primarily from  $^{13}\text{C}$ ) indicates the isomers observed at  $m/z$  201 are composed primarily of 5 carbon compounds. The relative yield (compared to ISOPPOOH and ISOPN products) of all four  $m/z$  201 peaks increases as the bimolecular lifetime increases. The latter two  $m/z$  201 peaks elute at temperatures in excess of the  $\text{HC}_5$  compounds, as would be expected for the  $\delta$  hydroperoxy aldehydes, and are assigned as such. Specific identification of the two latter peaks is based on their relative amounts. The HPALD derived from the 4-OH ISOP $\text{O}_2$  unimolecular channel is formed at a faster bulk rate than the 1-OH ISOP $\text{O}_2$  unimolecular channel (main body, Figure 4). However, as discussed in the main text, the yields of HPALDs from both unimolecular channels are uncertain. Nevertheless, the later eluting peak is assigned to arise from the HPALD derived from the 4-OH system and the second to

last peak is assigned to the HPALD derived from the 1-OH system, as the reverse assignment would require very disparate HPALD yields between the two systems, and this is deemed unlikely, consistent with that found for HC<sub>5</sub>.

#### **4b. Identity of early eluting compounds**

The identities of the first two peaks observed in the  $m/z$  201 chromatogram are unknown. They comprise approximately 30% of the total  $m/z$  201 signal at all RO<sub>2</sub> lifetimes. At higher temperatures, the second peak grows larger than the first, consistent with assignment to the unimolecular channel in the 1-OH peroxy radical system.

It is unlikely these are heterogeneously produced cyclic peroxy hemiacetal rearrangement products of the HPALDs, as their concentration does not increase significantly for several hours over which GC analyses are conducted after minute-long oxidation experiments. These peaks are also not formed in the GC from the major HPALD peaks, as these compounds did not reappear in an experiment in which only later eluting HPALD peaks are cold trapped, evaporated back into a pillow bag, and re-analyzed by GC.

Because the identity of the compounds giving rise to the two early-eluting  $m/z$  201 peaks is unknown, we cannot estimate the CIMS sensitivity. For this analysis, we've assumed a generic sensitivity for the early eluting  $m/z$  201 peaks as listed in Table S1. It is unlikely that the sensitivity is more than a factor of two higher as the dipole moment would have to substantially exceed that of all similar molecules; a lower sensitivity cannot, however, be ruled out.

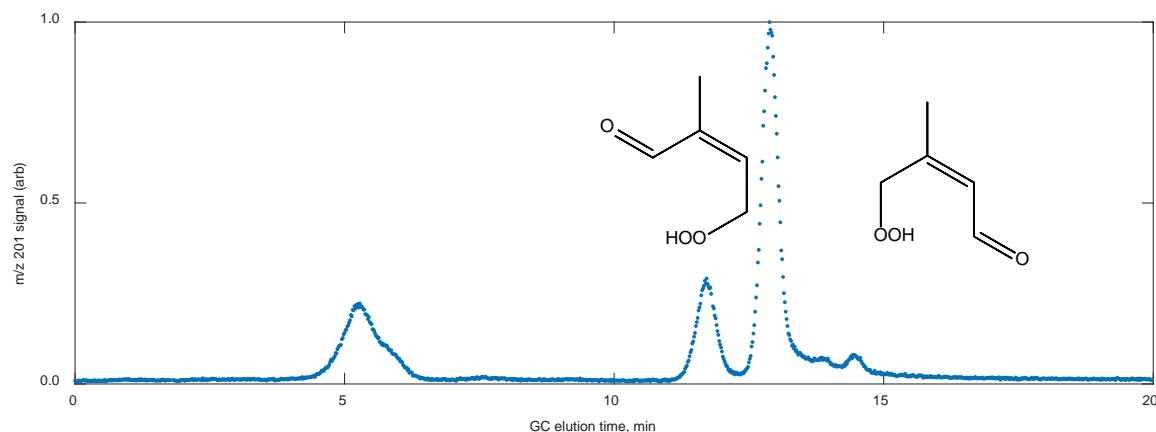


**Figure S7** – Chromatogram for  $m/z$  201 (HPALDs) and two other unidentified compounds are separated.

## 5. HC<sub>5</sub> ( $m/z$ 185)

### 5a. GC Peak Assignments for C<sub>5</sub> Hydroxy Carbonyls (HC<sub>5</sub>, $m/z$ 185)

There are only two major peaks observed in the chromatogram of the C<sub>5</sub> hydroxy carbonyls (HC<sub>5</sub>,  $m/z$  185, Figure S8). The identification of the elution order relies on OH oxidation experiments of 1-OH, 2-OOH and 4-OH, 3-OOH where OH abstracts the peroxide hydrogen to form either the 1-OH or 4-OH peroxy radical systems. These peroxy radicals decompose and reform producing the  $\delta$  isomers. In the experiment oxidizing 1-OH, 2-OOH we observe only the first HC<sub>5</sub> peak; the second peak is produced in the oxidation of 4-OH, 3-OOH. This finding gives further confidence in our assignments for the HPALDs elution order.

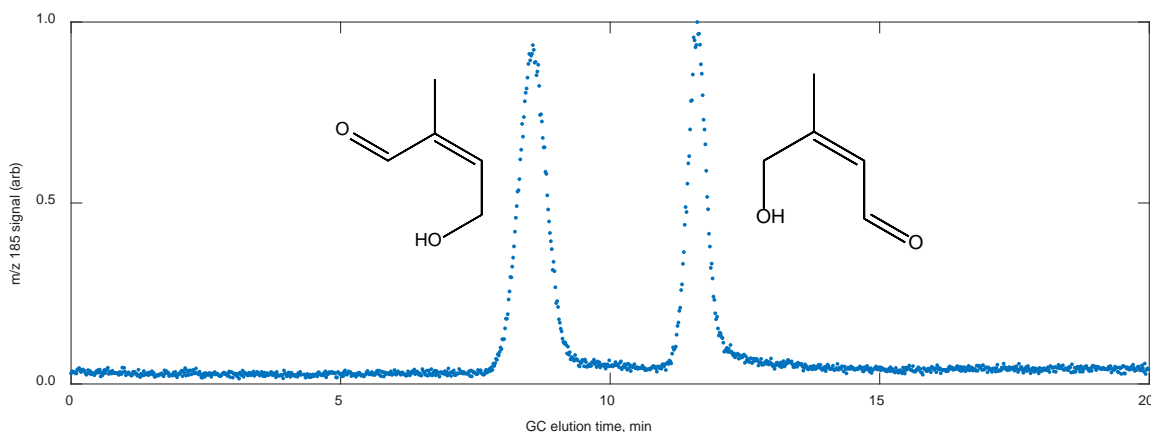


**Figure S8** – Chromatogram for  $m/z$  185 ( $\text{HC}_5$ ) which separates the two isomers, one from the 1-OH and 4-OH system.

## 5b. $\text{HC}_5$ Yields and schemes

H-shift chemistry following reaction of the  $\delta$  peroxy radicals with NO (Scheme 1, main text) gives rise to allylic radicals similar to those that yield the HPALDs. Theoretical calculations have shown that the  $E$   $\delta$  and  $Z$   $\delta$  hydroxy alkoxy radicals interconvert rapidly through an epoxide intermediate<sup>19</sup>. Because the rate of H-shift from the hydrogen  $\alpha$  to the OH group in the  $Z$   $\delta$  isomer is much faster than conversion of the  $E$   $\delta$  alkoxy to  $\text{HC}_5$  via reaction with  $\text{O}_2$ , Peeters *et al.*<sup>19</sup> suggested that only the  $Z$   $\delta$  isomers of  $\text{HC}_5$  will form. The  $\text{HC}_5$  chromatograms indicate that this is the case: there are only two isomers of  $\text{HC}_5$  one each from the 1-OH and 4-OH systems. Thus, the entire pool of  $\delta$  alkoxy radicals will produce the dihydroxy allylic radicals.

The chemistry following H-shift to the  $\delta$  alkoxy radical (produced via reaction of the  $\delta$  peroxy radical with NO) mimics that following H-shift to  $Z$   $\delta$  peroxy radical. As with the allylic radicals formed following H-shift  $\text{RO}_2$  chemistry, there are two positions for  $\text{O}_2$  addition. Addition of  $\text{O}_2$   $\alpha$  to the OH group will yield  $\text{HC}_5$ . The ratio of  $[\text{HC}_5]$  to  $[\delta \text{ ISOPN}]$  is consistent with an  $\text{HC}_5$  yield of  $45\% \pm 10\%$  in both 1-OH and 4-OH systems.



## 6. Unimolecular H-shift of the Z- $\delta$ Peroxy Radicals

Following H-shift from the Z- $\delta$  peroxy radicals, HPALDs are formed from the hydroperoxy hydroxy allylic radical reacting with O<sub>2</sub> at C<sub>1</sub> (1-OH system) or C<sub>4</sub> (4-OH system). As with HC<sub>5</sub>, however, the yield is not unity. Some of the additional products have been previously identified (hydroperoxy acetaldehyde, hydroperoxy acetone).<sup>2</sup> Several additional (yet unknown) products are observed here: a molecular weight 132 compound and two additional compounds of molecular weight 116 (same as HPALD) discussed in section 4b. It is unclear how these compounds form.

Proposed pathways to form HPALD compounds are shown below (Figures S11 and S12). Relative to the OH addition, O<sub>2</sub> addition can occur at the  $\alpha$  position, which will eliminate HO<sub>2</sub> forming HPALDs. Oxygen addition at the  $\gamma$  position will produce two isomers, one in which the enolic hydrogen is *cis* to the peroxy radical, and another in which it is *trans*. With no obvious unimolecular chemistry, the *trans* peroxy radicals may dissociate within the lifetime of bimolecular chemistry. For the *cis* peroxy radical, the enolic H-shift is calculated to be very fast ( $\sim 10^6$  s<sup>-1</sup>) outrunning any other chemistry<sup>20,21</sup>. This produces an alkyl radical to which oxygen can add. The resulting peroxy radical will undergo rapid H-shifts with the other peroxides<sup>22</sup>, with the fastest exit channel likely being a unimolecular H-shift from the aldehydic hydrogen. This can either result in prompt decomposition to yield CO, OH, and a dihydroperoxy carbonyl, or another oxygen can add, again yielding multiple peroxy radicals from rapid H-shift between the peroxides. The hydrogen  $\alpha$  to the primary peroxide or the secondary peroxide are the only two available unimolecular exit channels, and are likely fast, yielding a highly substituted and oxygenated peracid.

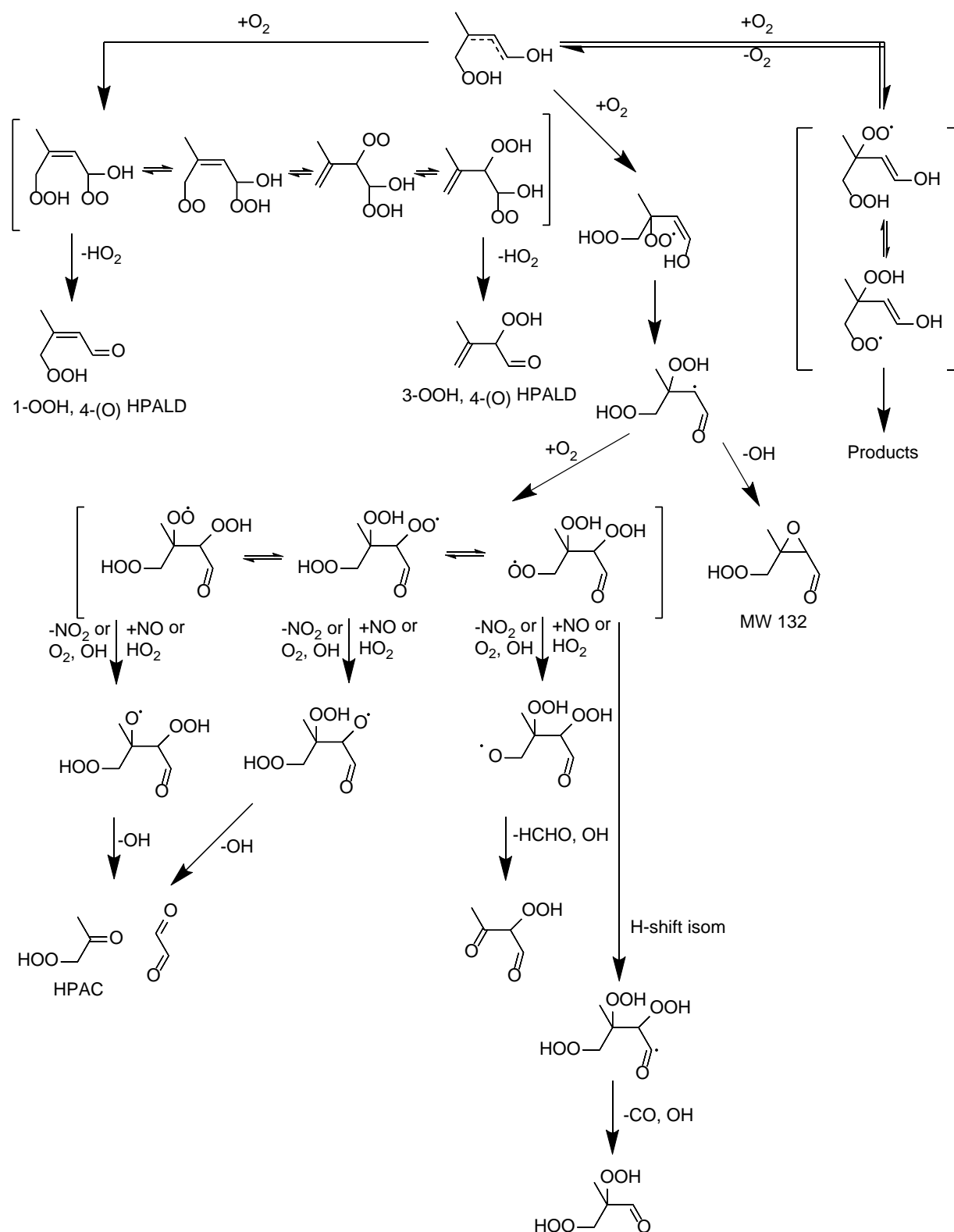


**Figure S11** – Chemistry following H-shift chemistry in the 4-OH peroxy radical system. Calculations suggest that the H-shifts leading to the  $\beta$  peroxy carbonyls (shown on the left) are much slower than  $\text{HO}_2$  elimination. The  $\text{C}_4$  dihydroxy peroxy carbonyl compound shown at the very bottom of the figure is not detected by  $\text{CF}_3\text{O}^\cdot$ , indicating it either does not form, fragments to form indiscriminate ions, or is lost to the walls.



## 6a. Yield of HPALD

A lower bound for the fraction of the peroxy radicals undergoing H-shift isomerization following addition of OH at C<sub>4</sub>,  $F_{\text{isom}4}$ , is approximated by  $1 - 1.74 \cdot [4\text{-OH}, 3\text{-OOH}] / ([1\text{-OH}, 2\text{-OOH}])$  where 1.74 is the ratio of OH addition at C<sub>1</sub> relative to C<sub>4</sub>. The ratio of unimolecular to bimolecular products can then be expressed as  $F_{\text{isom}} / (1 - F_{\text{isom}})$ . To the degree that errors in the calibration for 4-OH, 3-OOH and 1-OH, 2-OOH are correlated, this estimate for  $F_{\text{isom}4}$  is most sensitive to error in the calculated  $\tau_{\text{bimolecular}}$ . Most of the error in  $\tau_{\text{bimolecular}}$  in turn comes from error in  $P_{\text{H}_2\text{O}_2}$  (e.g. the H<sub>2</sub>O<sub>2</sub> sensitivity and  $k_{\text{H}_2\text{O}_2+\text{H}_2\text{O}_2}$ ). The H<sub>2</sub>O<sub>2</sub> sensitivity is accurate to 30% (so  $k_{\text{H}_2\text{O}_2+\text{H}_2\text{O}_2} \times [\text{H}_2\text{O}_2]$  is accurate to 15% +uncertainty in  $k_{\text{H}_2\text{O}_2+\text{H}_2\text{O}_2}$  [20%]). Thus, we estimate that  $k_{\text{bimolecular}}$  (where  $k_{\text{bimolecular}}$  is defined as  $1/\tau_{\text{bimolecular}}$ ) is accurate to 35%.

With this estimate for  $F_{\text{isom}}$ , we can derive the  $Y_{\text{HPALD}}$ . As shown in Figure S13,  $Y_{\text{HPALD}}$  is derived from the slope of relationship of  $[4\text{-HPALD}] / ([\text{ISOPN}] / Y_{\text{ISOPN}} + [\text{ISOPOOH}] / Y_{\text{ISOPOOH}})$  versus  $F_{\text{isom}} / (1 - F_{\text{isom}})$ . Accounting for the small influence of isomerization in the 1-OH system, we find that  $Y_{\text{HPALD}}$  is 25%.

From simple mass balance (adding HPALD to the other compounds assigned to H-shift RO<sub>2</sub> chemistry – see below),  $Y_{\text{HPALD}}$  is unlikely to be more than two times higher. From 1) HPALD calibration uncertainty and 2) uncertainty in  $k_{\text{bimolecular}}$  (35%), and considering that the HC<sub>5</sub> yield is 45% (with its own calibration uncertainty), we suggest that  $Y_{\text{HPALD}}$  cannot be less than 15%. Thus, we estimate that the yield of HPALD is within a factor of two of 25%.

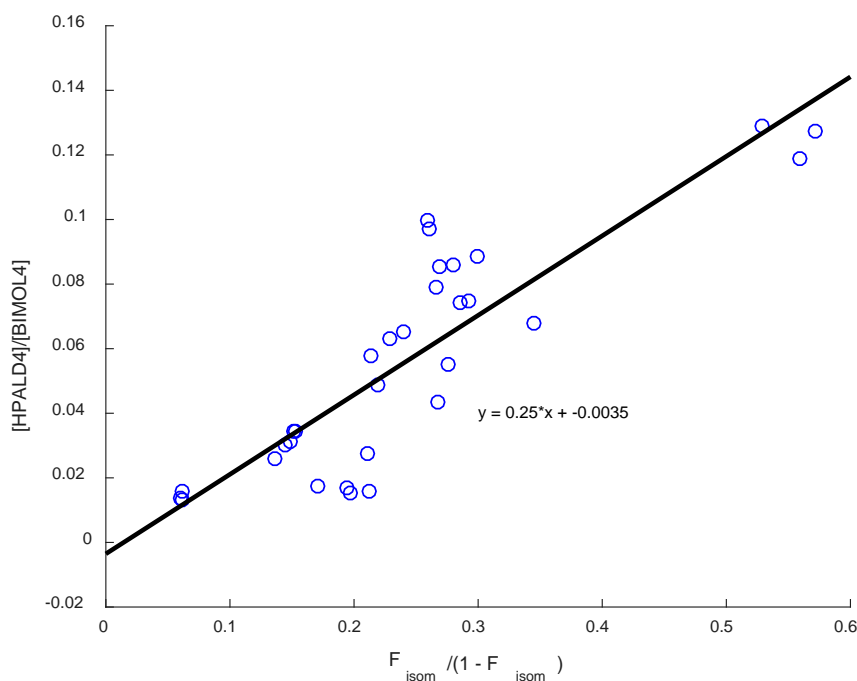


**Figure S13** –  $F_{\text{isom}}$  at 297K is estimated by first calculating the total bimolecular products divided by their respective yields, i.e.  $[\text{BIMOL1}] = [1\text{-OH, 2-ONO}_2 \text{ ISOPN}]/Y_{\text{ISOPN}} + [1\text{-OH, 2-OOH}]/Y_{\text{ISOPOOH}}$ ,  $[\text{BIMOL4}] = [4\text{-OH, 3-ONO}_2 \text{ ISOPN}]/Y_{\text{ISOPN}} + [4\text{-OH, 3-OOH}]/Y_{\text{ISOPOOH}}$ . The  $F_{\text{isom}}$  is then given as  $1 - [\text{BIMOL4}]/[\text{BIMOL1}] * (0.635/0.365)$ . Data is only plotted for  $\tau_{\text{bimolecular}}$  between 1s and 40s. A least squares fit is shown above, with a slope of 0.25, the derived estimate for  $Y_{\text{HPALD}}$ .

## 6b. Yield of Other Products.

Yields of the observed unimolecular products are shown in Table S5. Yields for HPALDs are discussed above. Yields for compounds other than the HPALDs are derived from their production rate divided by that of HPALD using the sensitivities from Table S1 (Figure S14).

**Table S5** – Yields (%) of unimolecular products at 297 K.

Compound	Z 1-OH, 4-O <sub>2</sub>	Z 4-OH, 1-O <sub>2</sub>
HPALD	25	25
HPACET	8.2	
HPAC	16	
MW 116	15	
MW 132	3.5	
Total	68	

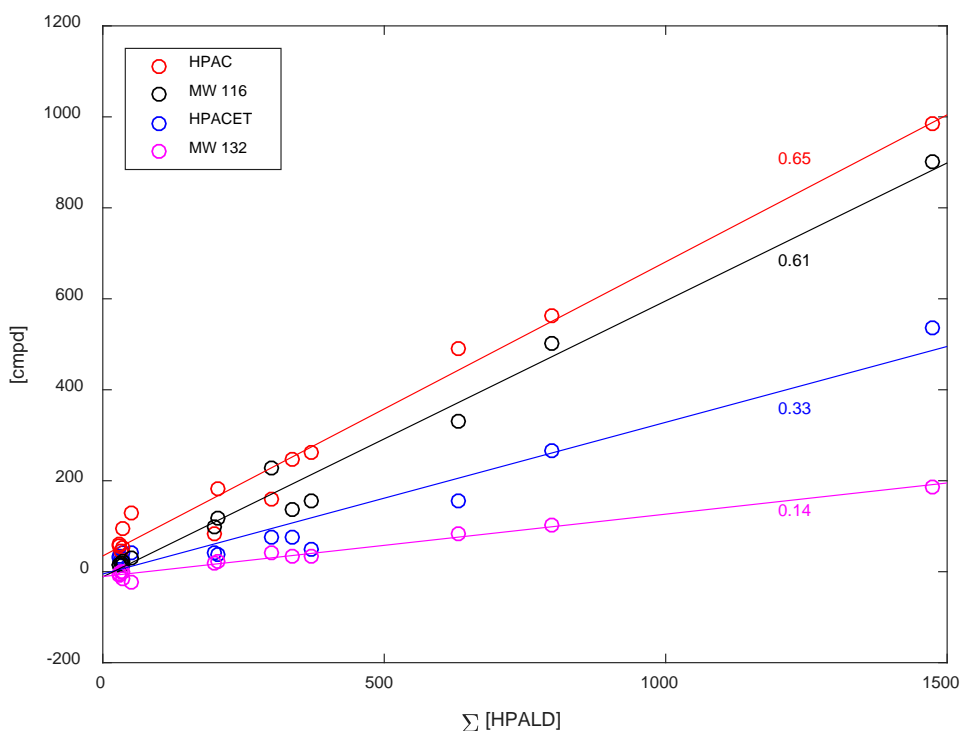


**Figure S14** – Product yields at 297 K for the unimolecular channel products other than HPALDs are derived by best fits against the sum of HPALDs. The signal for each compound and the sum of all  $m/z$  201 compounds are for the times when the CIMS sampled directly from the chamber (i.e. not through gas chromatograph). To derive the signal arising from the HPALDs, the total  $m/z$  201 signal is multiplied by the fraction of HPALDs determined in the subsequent GC samples. Only data above  $\tau_{\text{bimolecular}} 1$  s is used in this analysis. The units for both axes are pptv.

### 6c. Uncertainty in the rate of peroxy radical H-shift chemistry

**$k_{\text{isom}4}$  and  $k_{\text{isom}1}$**  As described in the manuscript, the rate constant of isomerization of the Z- $\delta$  peroxy radical isomers is estimated from the intercept (Figure 6, main body). Error in this estimate arises from several sources:

- Error in determining intercept.** The intercept is insensitive to  $\tau_{\text{bimolecular}}$  and the assumed HPALD yield. Primarily it results from fit uncertainty ( $\pm 20\text{-}40\%$ ). For the 1-OH system, for example, excluding the poorly replicated results at  $\tau \approx 90$  s results in a 30% increase in the inferred intercept.
- Error in  $F_{Z\delta}$  (kinetic).** Error in  $F_{Z\delta}$  (kinetic) arises from the scatter in nitrate ratio determination (and number of points) in Figure 3 (main body,  $\pm 30\%$ ) and from uncertainty in nitrate yields / calibration ( $\delta$  vs  $\beta$  yield and calibration differences,  $\pm 20\%$ ). Thus, we estimate that  $F_{Z\delta}$  (kinetic) is accurate to  $\pm 40\%$ .
- Error in total lifetime of the Z- $\delta$  isomers.** This is the uncertainty in identifying the inflection point in Figure 3 (main body,  $\pm 50\%$ ).

Summing these components yields an estimate of the uncertainty in  $k_{\text{isom}}$  of a factor of 3.5.

**$k_{\text{isom}} \times F_{Z\delta}$  (steady-state)** The product  $k_{\text{isom}} \times F_{Z\delta}$  (steady-state) is derived from the slope of  $[\text{HPALD}]/\Sigma[\text{bimolecular products}]$  vs  $\tau$ . Uncertainty in this estimate is very similar to that described above in 6a for  $F_{\text{isom}}$  (40%) and is limited by uncertainty in  $\tau_{\text{bimolecular}}$ .

**$F_{Z\delta}$  (steady-state)** Derived from  $k_{\text{isom}}$  and product  $k_{\text{isom}} \times F_{Z\delta}$  (steady-state). Uncertainty is dominated by error in  $k_{\text{isom}}$  (factor of 3.5).

**$F_{Z\delta}$  (equilibrium) and  $\Delta G$  (T=297)** For 1-system,  $F_{Z\delta}$  (steady-state) =  $F_{Z\delta}$  (equilibrium) and so inherits the same uncertainty (factor of 3.5). For 4-system, error is somewhat larger as it is correlated with uncertainty in the total lifetime of the  $Z\delta$  isomer. Uncertainty in  $\Delta G$  (T=297) is propagated from uncertainty in  $F_{Z\delta}$  (equilibrium).

#### **6d. Comparison with bulk isomerization rate from Crouse, *et al.*, 2011**

Several advances in our understanding of instrumental sensitivities to ISOPOOH and HPALDs have been achieved since the work of Crouse, *et al.*<sup>2</sup> With the addition of gas chromatography, we have found that only 50 and 85% of the ion signal arising from ISOPOOH and HPALD, respectively, are the  $\text{CF}_3\text{O}^-$  clusters ( $m/z$  203 and  $m/z$  201). Crouse *et al.*<sup>2</sup> had assumed all signal from these compounds was found at these  $m/z$ . Calibration using isomerically pure ISOPOOH, ISOPN, and IEPOX standards (St Clair *et al.*<sup>17</sup>, Lee *et al.*<sup>1</sup>, Bates *et al.*<sup>23</sup>) demonstrate that when all product ions are included, sensitivity between across these isomers nominally scales with the calculated ion-molecule collision rate (Garden *et al.*<sup>24</sup>). Consistent with this finding, we apply HPALD and ISOPOOH sensitivities using calculated collision rates with  $\text{CF}_3\text{O}^-$  after accounting for all observed product ions.

To derive their estimate of the bulk isomerization rate, Crouse, *et al.*<sup>2</sup> assumed that all the  $m/z$  201 signal was from HPALD and that the yield of HPALD was 100% following H-shift. Here, using the carbon balance method, we estimate the HPALD yield to be 25% for the 4-OH system. In analogy with HC<sub>5</sub> yield, we assume that the HPALD yield from the 1-OH system is the same as the 4-OH system.

Together, the different sensitivity and HPALD yield explain the difference in the bulk isomerization rate calculated by Crouse, *et al.*<sup>2</sup> and those determined here. Applying the CF<sub>3</sub>O<sup>-</sup> CIMS sensitivity ratio of ISOP<sub>OOH</sub> to HPALD (Table S1) and an HPALD yield of 25% and a MW116 yield of 30% to the data presented in Crouse *et al.*, the calculated bulk RO<sub>2</sub> isomerization rate constant,  $k_{\text{bulk\_isom}}(297 \text{ K})$ , at  $\tau_{\text{biomolecular}} = 65 \text{ s}$ , is  $0.0032 \text{ s}^{-1}$  – identical, within uncertainties, to that determined here for the same RO<sub>2</sub> lifetime (Figure S15).

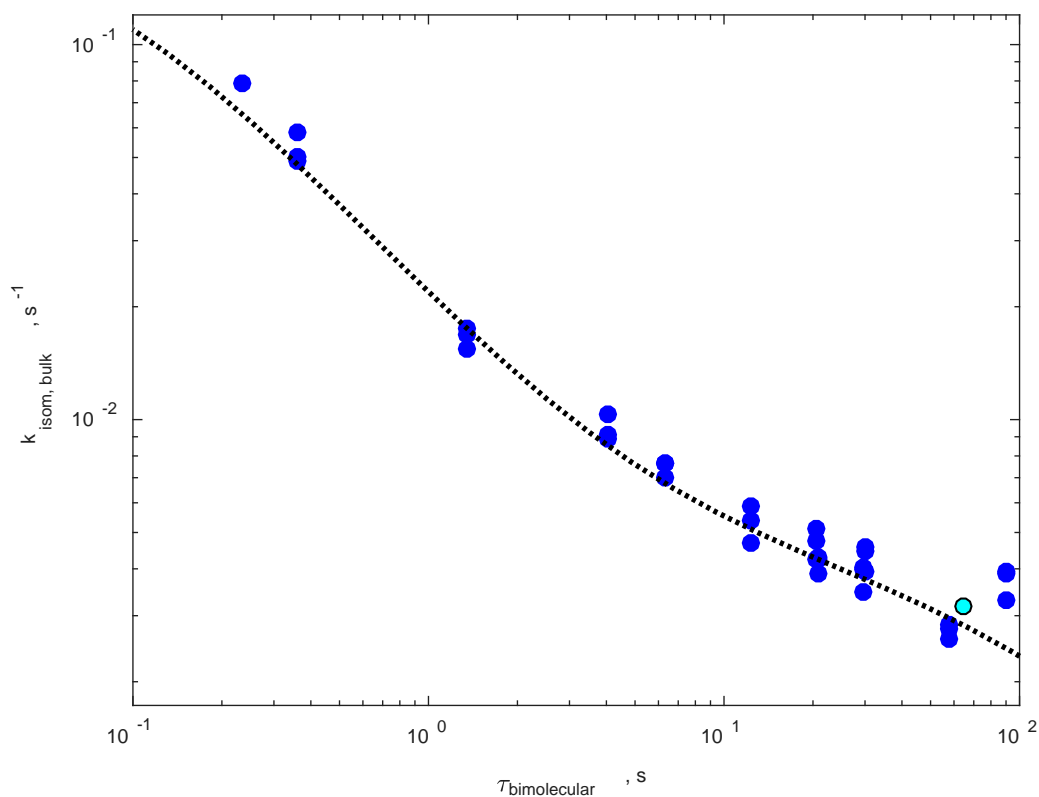


**Figure S15** –  $k_{\text{isom,bulk}}$  at 297 K is estimated as  $([\Sigma \text{HPALD}]/Y_{\text{HPALD}})/\{([\text{ISOPN}]/Y_{\text{ISOPN}} + [\text{ISOPOOH}]/Y_{\text{ISOPOOH}})^* \tau_{\text{bimolecular}}\}$  (blue points). The dashed line represents the model output. A  $k_{\text{isom,bulk}}$  is calculated for Crouse *et al.*, 2011 using  $Y_{\text{ISOPN}}$ ,  $Y_{\text{ISOPOOH}}$ ,  $Y_{\text{HPALD}}$  of 13%, 95%, and 25% respectively, and assuming 70% of the  $m/z$  201 signal is HPALDs (teal point).

## 6e. Derivation of a linear approximation of products vs. $\tau$

In the main body, in the graphical analysis shown in Fig. 6, the dependent variable contains the ratio  $\tau / \tau_{\text{bimolecular}}$ . This factor arises from the integration of  $[\text{NO}] + [\text{HO}_2]$   $d\tau$  as described here.

Stable product formation for the bimolecular products can be expressed:

$$\frac{[\text{ISOPN}]}{Y_{\text{ISOPN}}} + \frac{[\text{ISOPOOH}]}{Y_{\text{HPALD}}} = \int_0^\tau [\text{RO}_2] (k_{\text{NO}+\text{RO}_2}[\text{NO}] + k_{\text{HO}_2+\text{RO}_2}[\text{HO}_2]) d\tau = \int_0^\tau \frac{[\text{RO}_2]}{\tau_{\text{bimolec}}} d\tau = \frac{\tau}{\tau_{\text{bimolec}}} [\text{RO}_2] \frac{[\text{HPALD}]}{Y_{\text{HPALD}}}$$

$$= \int_0^\tau [\text{RO}_2] F_{Z,\delta} k_{\text{isom}} d\tau$$

where  $\tau_{bimolec} = \frac{1}{k_{NO+RO_2}[NO] + k_{HO_2+RO_2}[HO_2]}$ , and  $F_{Z,\delta}$  is the fraction of Z  $\delta$  peroxy radicals.

We simplify the expression for the formation of HPALD by expressing the integral as two parts, the first being during the relaxation of the nascent (kinetic) Z  $\delta$  peroxy radical population, and the second during the steady state  $F_{Z,\delta}$ :

$$\int_0^\tau [RO_2] F_{Z,\delta} k_{isom} d\tau = \left( F_{Z,\delta,kinetic} \frac{k_{isom}}{k_{isom} + k_{Z,\delta \rightarrow \beta}} + F_{Z,\delta,steady\ state} k_{isom} \tau \right) [RO_2]$$

where  $k_{Z,\delta \rightarrow \beta}$  is

We can then express the ratio of the stable products as:

$$\frac{\frac{[HPALD]}{Y_{HPALD}}}{\frac{[ISOPN]}{Y_{ISOPN}} + \frac{[ISOPOOH]}{Y_{HPALD}}} = \frac{\left( F_{Z,\delta,kinetic} \frac{k_{isom}}{k_{isom} + k_{Z,\delta \rightarrow \beta}} + F_{Z,\delta,steady\ state} k_{isom} \tau \right) [RO_2]}{\frac{\tau}{\tau_{bimolec}} [RO_2]}$$

Rearranging:

$$\frac{[Unimolecular]}{[Bimolecular]} \frac{\tau}{\tau_{bimolec}} = F_{Z,\delta,kinetic} \frac{k_{isom}}{k_{isom} + k_{Z,\delta \rightarrow \beta}} + F_{Z,\delta,steady\ state} k_{isom} \tau$$

where  $[Unimolecular] = \frac{[HPALD]}{Y_{HPALD}}$  and  $[Bimolecular] = \frac{[ISOPN]}{Y_{ISOPN}} + \frac{[ISOPOOH]}{Y_{HPALD}}$ .

## 7. Experiments Constraining $k_{2r}$

OH oxidation experiments of 1-OH, 2-OOH ISOPOOH were performed in the presence of NO to constrain the reverse rate constant of the 1-OH, 2-OO ISOPO<sub>2</sub>. A minor product of OH oxidation of 1-OH, 2-OOH ISOPOOH is the peroxy radical 1-OH, 2-OO ISOPO<sub>2</sub>.<sup>17</sup> Synthesized standard of 1-OH, 2-OOH ISOPOOH is added to a Teflon chamber, along with CH<sub>3</sub>ONO and varying concentrations of NO. Approximately 12% of the subsequent OH oxidation proceeds through abstraction of the H on the peroxide, leading to formation of 1-OH, 2-OO. Subsequent reaction with NO will then form ISOPN. At

bimolecular lifetimes in which  $O_2$  is released and re-adds, *E* 1-OH, 4-OO and *Z* 1-OH, 4-OO will form. This leads to subsequent formation of the  $\delta$  ISOPN isomers. The fraction of  $\delta$  ISOPN isomers (*E* + *Z*) to the 1-OH, 2-N ISOPN provides an independent constraint on the  $O_2$  loss rate constant for 1-OH, 2-OO ISOPN.

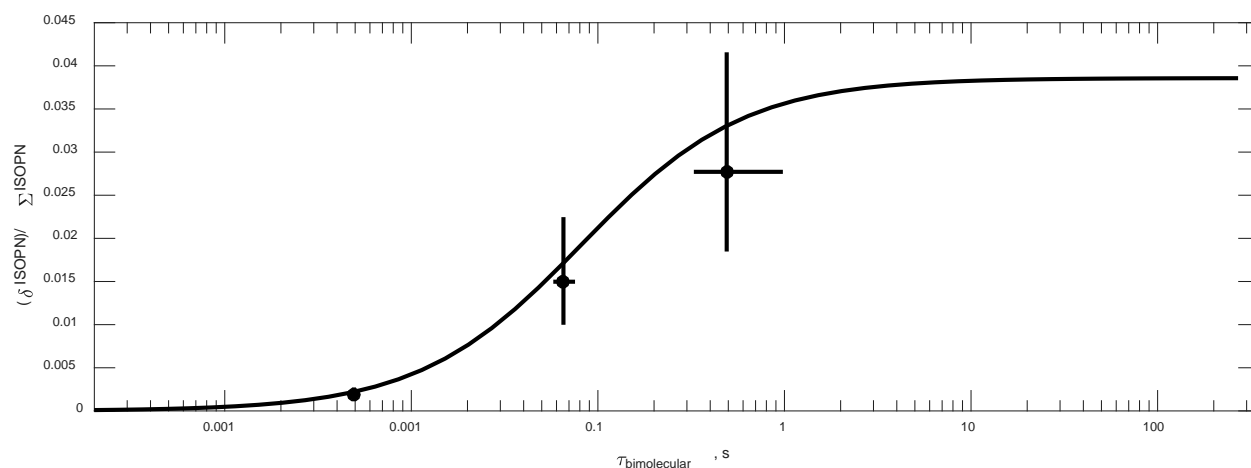


**Figure S16** – The fraction of  $\delta$  ISOPN formed in an experiment in which 1-OH, 2-OOH is oxidized, and ISOPN is formed upon subsequent reaction of the 1-OH, 2-OO radical with NO. The fraction of  $\delta$  ISOPN formed is only possible once  $O_2$  cleaves from 1-OH, 2-OO to form either *Z* 1-OH, 4-OO or *E* 1-OH, 4-OO. The measurement of  $\delta$  ISOPN as a function of  $\tau_{\text{bimolecular}}$  constrains the possible values of  $k_{2r}$ . The black line is the optimized model output of the fraction of  $\delta$  ISOPN formed 297 K for a model run in which 1-OH, 2-OOH is oxidized to form 1-OH, 2-OO.

## 8. Temperature dependence of the RO<sub>2</sub> kinetics.

To estimate the temperature dependence of the underlying kinetics, we performed a series of isoprene oxidation experiments similar to the other experiments in all respects except at elevated chamber temperature (50 C). The data from those experiments (shown in Figure S17) indicate that, as expected, the reverse  $O_2$  rate constants increase with temperature. At elevated temperature, the transition to the kinetic limit occurs at RO<sub>2</sub> lifetimes <0.01 s. Unfortunately, the chromatography at  $\tau_{\text{bimolecular}} > 10$  s and  $T = 50$  C is significantly impacted by conversion of 1-OH, 2-N from hydrolysis due to increased rate of diffusion of water into the chamber from the laboratory at the elevated temperatures.

Recommendation for the temperature dependence of the reverse O<sub>2</sub> rates and the 1,6 H-shifts listed in Tables S7 and S8 are derived utilizing the experimental data at 297 K and 323 K and theoretical calculations from the literature. For the loss of O<sub>2</sub> from the peroxy radicals, the pre-exponential values are taken from Peeters et al.<sup>21</sup> divided by the ratio of the calculated O<sub>2</sub> addition rate from Peeters et al.<sup>21</sup> to those listed in Table S9. The experimentally derived reverse rates shown in Table S7 are used to determine  $\Delta H$  in the Van't Hoff equation. This method is sensitive to error in the O<sub>2</sub> addition rates and is therefore dependent on three assumptions: 1) the *cis* / *trans* OH isoprene adduct formation ratios are taken from calculations by Peeters et al.<sup>2</sup>, 2) the absolute rate for addition of O<sub>2</sub> is assumed to be  $2.0 \times 10^{-12} \text{ cm}^3 \text{ molec}^{-1} \text{ s}^{-1}$ , and 3) the addition rates at the  $\beta$  position are equal for *cis* and *trans* OH adducts. Alteration of these assumptions would result in different temperature dependencies.

Derivation of the recommendation for the temperature dependence of the 1,6 H-shift is more complicated as we must additionally consider the role of the 1,5 H-shift of the  $\beta$  isomers. At room temperature, the calculated rate of the 1,5 H-shifts are very slow and do not impact the lifetime of the peroxy radicals (Crouse et al.<sup>2</sup>). At 323 K, however, this chemistry is calculated to significantly alter the peroxy radical fate at longer RO<sub>2</sub> lifetimes. Therefore, the best fit 1,6 H-shift isomerization rate found from the 323 K experimental data depends on the assumed 1,5 H-shift rates. Assuming no 1,5 H-shift, the best fit values for the 1,6 H-shift are  $k_{\text{isom1}} = 6 \text{ s}^{-1}$ , and  $k_{\text{isom4}} = 11 \text{ s}^{-1}$ . Incorporating da Silva et al.'s<sup>26</sup> rates for the 1,5 H-shift reduces  $k_{\text{isom1}}$  best fit rate to  $5.25 \text{ s}^{-1}$  while using the rate from Peeters et al.<sup>21</sup> yields  $k_{\text{isom1}} = 4.2 \text{ s}^{-1}$ . The values listed in Tables S8 assume a 1,5 H-shift rate as calculated by Peeters et al.<sup>21</sup>. The temperature dependence of the tunneling (C value for the

1,6 H-shifts listed in Table S8) are both assumed to be  $1 \times 10^8$  based on Peeters et al.<sup>21</sup>. A and B values are then calculated from a fit between the 297 K and 323 K  $k_{\text{isom}}$  rates.

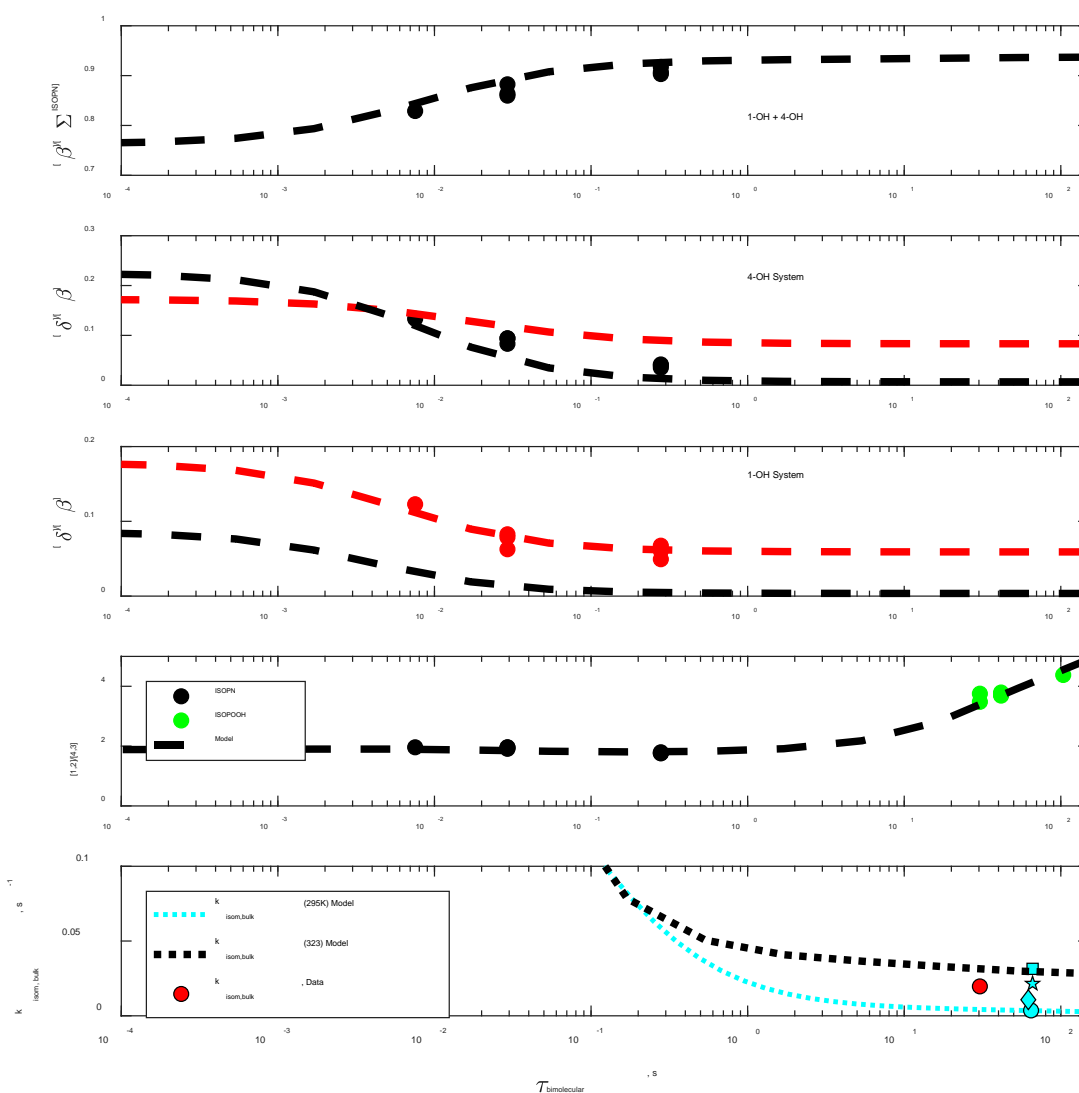


**Figure S17** – A model at elevated temperature (323 K) is matched against the ISOPN isomer distribution at bimolecular lifetimes less than 1s, the ratio of ISOPN isomers at elevated temperatures. The bulk isomerization (filled red circle) at elevated temperatures is estimated from direct, unspeciared measurements of ISOPN ( $Y_{\text{ISOPN}} = 0.09$  at 323 K), ISOPN ( $Y_{\text{ISOPN}} = 0.95$ ), and HPALDs ( $Y_{\text{HPALD}} = 0.25$ , with 0.3 of the bulk signal attributed to unknown compounds MW 116). This agrees well with the estimated bulk isomerization rate constant from Crouse *et al.*, 2011 assuming  $Y_{\text{HPALD}} = 0.25$  is similar to the 323 K value (blue square). Measured bulk isomerization rate constants from Crouse *et al.*, 2011 at 318 K, 310 K, and 295 K are shown as a blue star, blue diamond, and blue circle, respectively.

**Table S6** – Rate constants used to produce model curves shown in Figure S17 to simulate the elevated temperature experiments.

	Rate constants (323 K), s <sup>-1</sup>
<b>k<sub>1r</sub></b>	<b>180</b>
<b>k<sub>2r</sub></b>	<b>27</b>
<b>k<sub>3r</sub></b>	<b>5.5</b>
<b>k<sub>4r</sub></b>	<b>240</b>
<b>k<sub>5r</sub></b>	<b>48</b>
<b>k<sub>6r</sub></b>	<b>5.7</b>
<b>k<sub>7r</sub></b>	<b>2.9</b>
<b>k<sub>8r</sub></b>	<b>117</b>
<b>k<sub>isom1</sub></b>	<b>4.2</b>
<b>k<sub>isom4</sub></b>	<b>11</b>

**Table S7** – First order rate constants for the loss of O<sub>2</sub> from the peroxy radicals used in the model for isoprene oxidation. Temperature dependence for all rates are derived from a fit to very limited dataset at elevated temperatures, and therefore are highly uncertain.

	Rate constants (297 K), s <sup>-1</sup>	A exp(-B/T)	
		A, s <sup>-1</sup>	B, K
<b>k<sub>1r</sub></b>	<b>16</b>	<b>1.83 x 10<sup>14</sup></b>	<b>8930</b>
<b>k<sub>2r</sub></b>	<b>1.6</b>	<b>2.22 x 10<sup>15</sup></b>	<b>10355</b>
<b>k<sub>3r</sub></b>	<b>0.29</b>	<b>2.24 x 10<sup>15</sup></b>	<b>10865</b>
<b>k<sub>4r</sub></b>	<b>22</b>	<b>1.79 x 10<sup>14</sup></b>	<b>8830</b>
<b>k<sub>5r</sub></b>	<b>3.7</b>	<b>2.08 x 10<sup>14</sup></b>	<b>9400</b>
<b>k<sub>6r</sub></b>	<b>0.30</b>	<b>2.49 x 10<sup>15</sup></b>	<b>10890</b>
<b>k<sub>7r</sub></b>	<b>0.14</b>	<b>2.49 x 10<sup>15</sup></b>	<b>11112</b>
<b>k<sub>8r</sub></b>	<b>10</b>	<b>1.75 x 10<sup>14</sup></b>	<b>9054</b>

**Table S8** – First order rate constants used in the model for isoprene oxidation for 1,6 H-shifts. Temperature dependence for all rates are derived from a fit to very limited dataset at elevated temperatures, and therefore are highly uncertain.

	Rate constants (297 K), s <sup>-1</sup>	A exp (-B/T) exp (C/T <sup>3</sup> )		
		A, s <sup>-1</sup>	B, K	C, K <sup>3</sup>
<b>k<sub>isom1</sub></b>	<b>0.36</b>	<b>5.47 x 10<sup>15</sup></b>	<b>12200</b>	<b>1 x 10<sup>8</sup></b>
<b>k<sub>isom4</sub></b>	<b>3.7</b>	<b>2.40 x 10<sup>9</sup></b>	<b>7160</b>	<b>1 x 10<sup>8</sup></b>

**Table S9** – Implied forward rate constants calculated from the observed ISOPN isomer distribution at high levels of NO, assuming thermalized distribution ratios for isoprene-OH allylic radicals from Peeters *et al.*<sup>5</sup> (see Figure 1), and a total R. + O<sub>2</sub> rate constant of  $2.0 \times 10^{-12} \text{ cm}^3 \text{ molec}^{-1} \text{ s}^{-1}$  in each system.<sup>25</sup>

	Rate constants ( $\text{cm}^3 \text{ molec}^{-1} \text{ s}^{-1}$ )
<b>k<sub>1f</sub></b>	<b><math>3.2 \times 10^{-13}</math></b>
<b>k<sub>2f</sub></b>	<b><math>7.8 \times 10^{-13}</math></b>
<b>k<sub>3f</sub></b>	<b><math>7.8 \times 10^{-13}</math></b>
<b>k<sub>4f</sub></b>	<b><math>1.2 \times 10^{-13}</math></b>
<b>k<sub>5f</sub></b>	<b><math>4.9 \times 10^{-13}</math></b>
<b>k<sub>6f</sub></b>	<b><math>7.1 \times 10^{-13}</math></b>
<b>k<sub>7f</sub></b>	<b><math>7.1 \times 10^{-13}</math></b>
<b>k<sub>8f</sub></b>	<b><math>2.1 \times 10^{-13}</math></b>

## 9. Isoprene oxidation: Additional simulations

The simulations shown below (Figures S18-S25) use rate constants (Tables S7, S8, and S9) for the isoprene RO<sub>2</sub> system (Scheme 1) tuned to fit experimental data at 297 K. The model uses the calculated thermalized distribution of isoprene-OH allylic radicals from Peeters *et al.*<sup>5</sup> and an experimentally derived split of 63.5 to 36.5% between the 1-OH system and the 4-OH system.

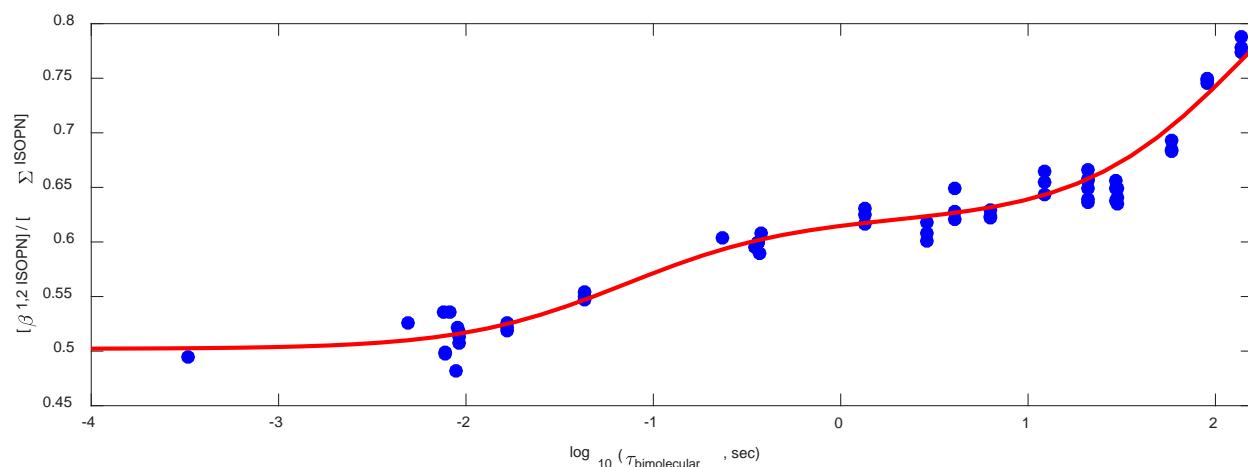


**Figure S18** – Model (solid red line) simulations and experimental room temperature data (297 K) for 1-OH, 2-N distribution.

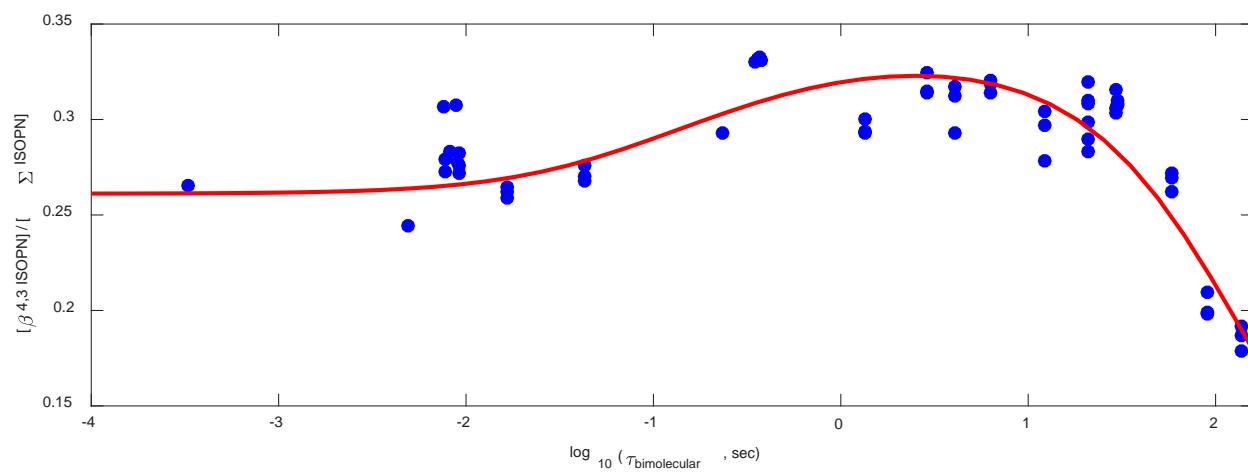


**Figure S19** – Model (solid red line) simulations and experimental room temperature data (297 K) for 4-OH, 3-N distribution.

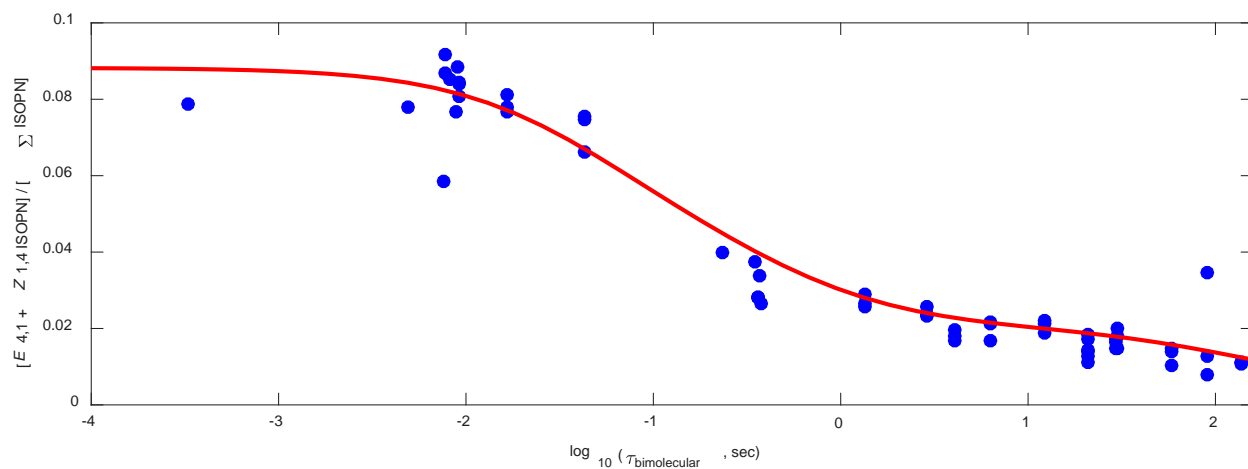


**Figure S20** – Model (solid red line) simulations and experimental room temperature data (297 K) for the sum of *E* 4-OH, 1-N and *Z* 1-OH, 4-N distribution.

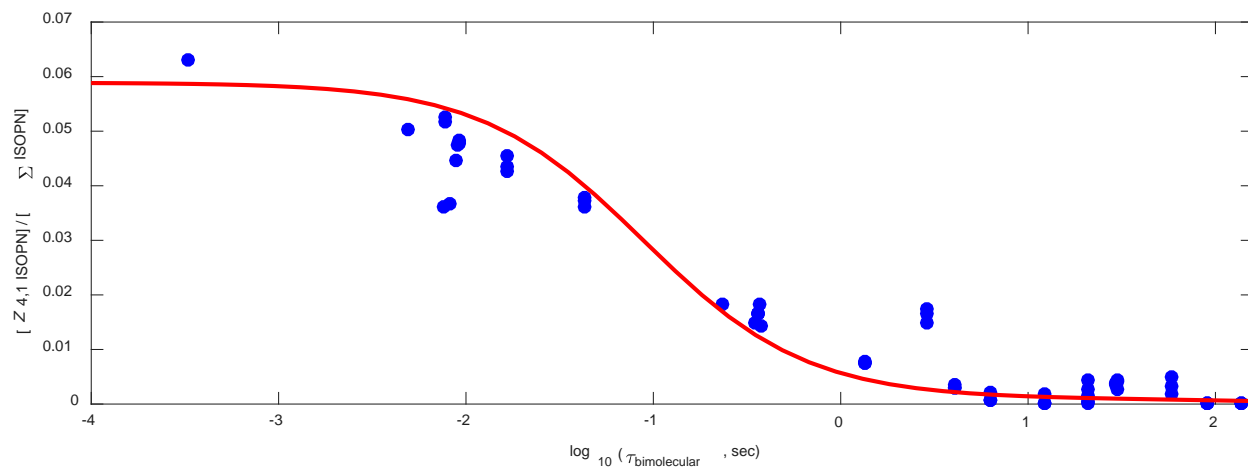


**Figure S21** – Model (solid red line) simulations and experimental room temperature data (297 K) for Z 4-OH, 1-N distribution.

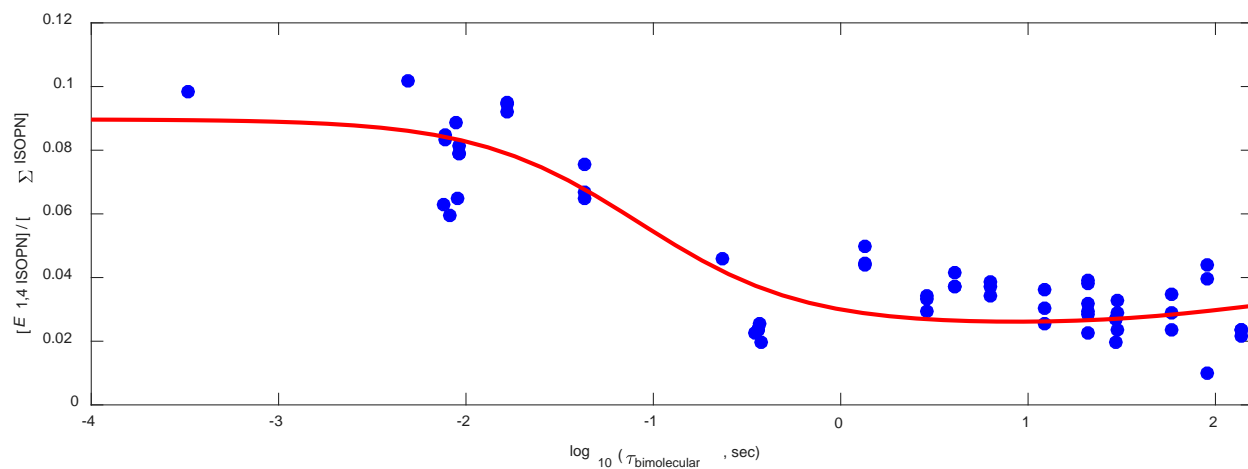


**Figure S22** – Model (solid red line) simulations and experimental room temperature data (297 K) for E 1-OH,4-N distribution.

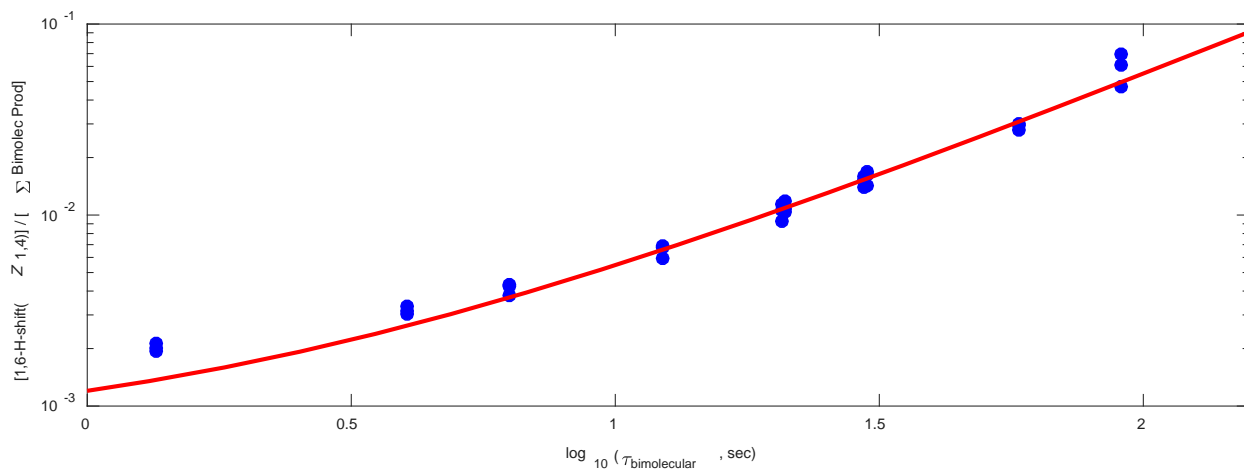


**Figure S23** – Model (solid red line) simulations and experimental room temperature data (297 K) for [1-HPALD (4-OOH, 1-(O))]/ $Y_{\text{HPALD}}$  divided by  $[\text{ISOPN}]/Y_{\text{ISOPN}} + [\text{ISOPPOOH}]/Y_{\text{ISOPPOOH}}$ .

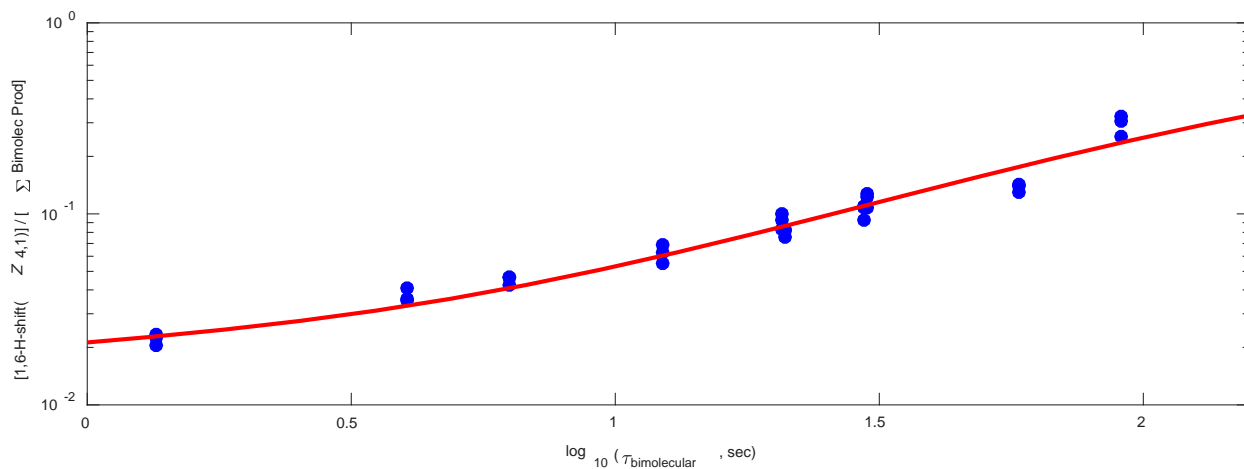


**Figure S24** – Model (solid red line) simulations and experimental room temperature data (297 K) for [4-HPALD (1-OOH, 4-(O))]/ $Y_{\text{HPALD}}$  divided by  $[\text{ISOPN}]/Y_{\text{ISOPN}} + [\text{ISOPPOOH}]/Y_{\text{ISOPPOOH}}$ .

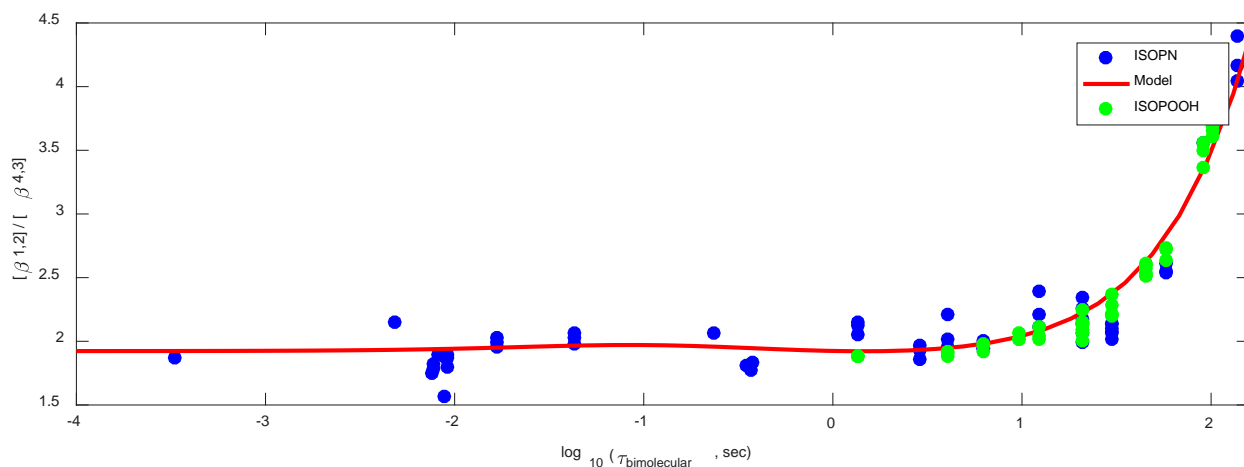


**Figure S25** – Model (solid red line) simulations and experimental room temperature data (297 K) for the ratio of 1-OH, 2-X to 4-OH, 3-X. Blue and green are ISOPN and ISOPOOH measurements, respectively.

### 9a. Comparison with Peeters *et al.*, 2014

Using similar forward rate constants listed in Section 10, and adjusting the reverse rate constants (Table S9) to match the calculated Peeters *et al.*, 2014  $\Delta G$  values shown in Table 4 (main body) demands a much lower  $k_{\text{isom}}$  to nominally match the HPALD formation. As shown in the Figure S26, the thermochemistry from Peeters, *et al.* significantly overpredicts the Z 4-OH, 1-OO isomer abundance. Note, the comparison using the unadjusted rates of Peeters, *et al.*, 2014 with the data of this work is significantly less favorable. As a result of the much lower specific isomerization rate required to match HPALD at long bimolecular lifetimes, HPALD produced via isomerization of the nascent Z- $\delta$  population is minimal and so its production is substantially underestimated at short bimolecular lifetime.

**Table S10** – Rate constants of oxygen loss calculated from Peeters *et al.*, 2014 thermochemistry (Table S11), adjusted fit to observations of measured isomer distributions.

	<b>Rate constants (297 K), s<sup>-1</sup></b>
<b>k<sub>1r</sub></b>	<b>16</b>
<b>k<sub>2r</sub></b>	<b>1.4</b>
<b>k<sub>3r</sub></b>	<b>2</b>
<b>k<sub>4r</sub></b>	<b>22</b>
<b>k<sub>5r</sub></b>	<b>3.7</b>
<b>k<sub>6r</sub></b>	<b>0.08</b>
<b>k<sub>7r</sub></b>	<b>1.12</b>
<b>k<sub>8r</sub></b>	<b>10</b>
<b>k<sub>isom1</sub></b>	<b>0.07</b>
<b>k<sub>isom4</sub></b>	<b>0.5</b>

**Table S11** –  $\Delta G$  values ( $G_\delta - G_\beta$ ) calculated from the rate constants tabulated in Peeters *et al.*, 2014.

<b><math>\delta</math> Isomer</b>	<b><math>\Delta G</math> (297K) (kcal/mole)*</b>
<b><i>E</i> 1-OH, 4-O<sub>2</sub></b>	<b>2.0</b>
<b><i>Z</i> 1-OH, 4-O<sub>2</sub></b>	<b>2.5</b>
<b><i>Z</i> 4-OH, 1-O<sub>2</sub></b>	<b>2.5</b>
<b><i>E</i> 4-OH, 1-O<sub>2</sub></b>	<b>2.0</b>

\*Calculated from Peeters *et al.*, 2014

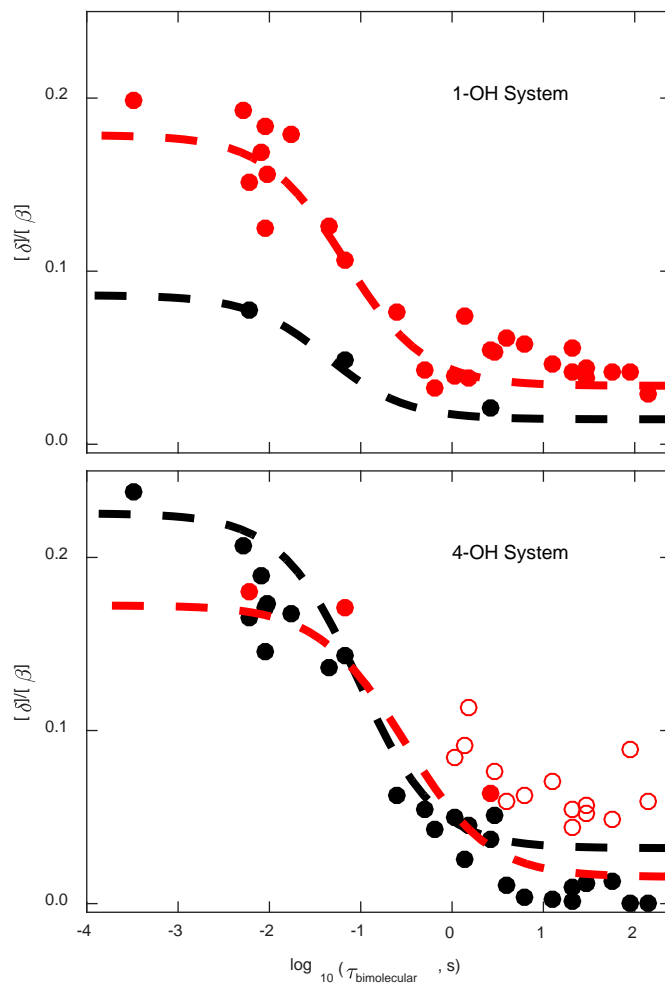


**Figure S26** – Simulations using rates from Tables S9 and S10 compared to ISOPN isomer data at 297 K show that the *E* 1-OH, 4-OO data is slightly higher than predicted, *E* 4-OH, 1-OO is under predicted, and *Z* 4-OH, 1-OO is over predicted using the thermochemistry from Peeters *et al.*, 2014.

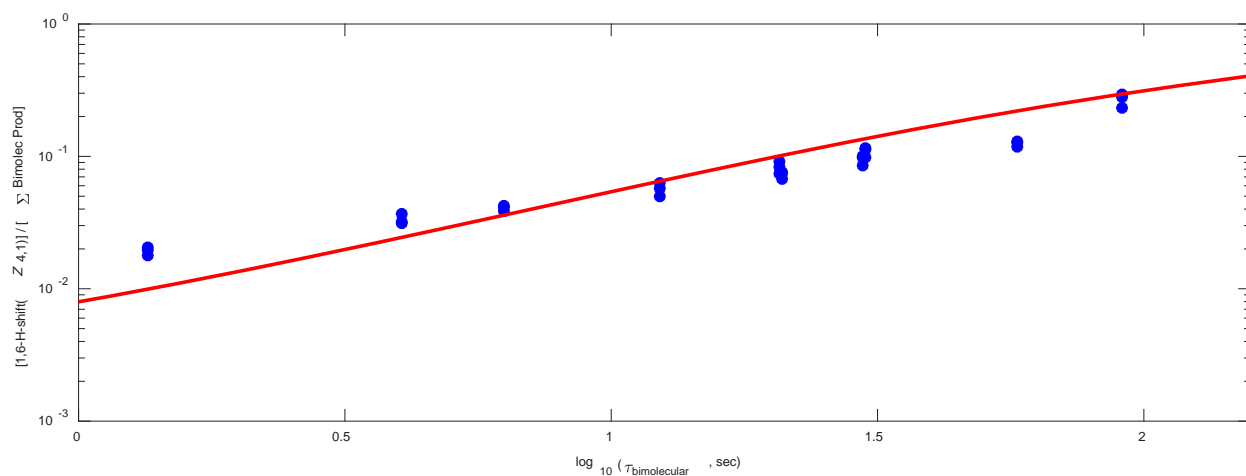


**Figure S27** – Simulations using the rates in Tables S9 and S10 compared to data at 297 K show that the 4-HPALD (1-OOH, 4-O) is not well predicted at short bimolecular lifetimes.

## 10. 1,3-Butadiene and 1,3-Dimethyl-1,3-Butadiene

In the kinetic limit, the ratio of  $\delta$  to  $\beta$  hydroxy nitrates formation decreases from 1,3 butadiene to isoprene to 2,3 dimethyl 1,3 butadiene (Figure S28). This likely reflects the decrease in electron density in the  $\delta$  position of the allylic radical as compared to the  $\beta$  position. Following OH addition, methyl substitution  $\beta$  to the OH produces a tertiary radical center drawing electron density away from the  $\delta$  position.

The methyl groups also affect the yield of hydroxy carbonyls upon formation of alkoxy radicals from the reaction of NO with  $\delta$  peroxy radicals. For butadiene and dimethylbutadiene, we observe the formation of only one hydroxy carbonyl isomer, indicating the fast isomerization between *E* and *Z* for the alkoxy occurs in these systems as well as in isoprene. Assuming the CIMS sensitivities for the hydroxy nitrates are similar to ISOPN, we find that the nitrate yield for butadiene is 9% and for dimethylbutadiene is  $10 \pm 5\%$ . Assuming the CIMS sensitivities for the  $\delta$  hydroxy carbonyls is similar to HC<sub>5</sub>, the yield of hydroxy carbonyls from reaction of NO with the  $\delta$  hydroxy peroxy radicals from

butadiene is  $80 \pm 10\%$ ,  $45 \pm 10\%$  from isoprene, and only  $13 \pm 8\%$  from dimethylbutadiene. The lower yield in isoprene and dimethylbutadiene suggests that  $O_2$  addition is substantially favored at the  $\gamma$  position when the allylic radical encompasses the methyl-substituted center. It is somewhat surprising, then, that the yields of  $HC_5$  are so similar for OH addition at  $C_1$  vs  $C_4$  in isoprene.

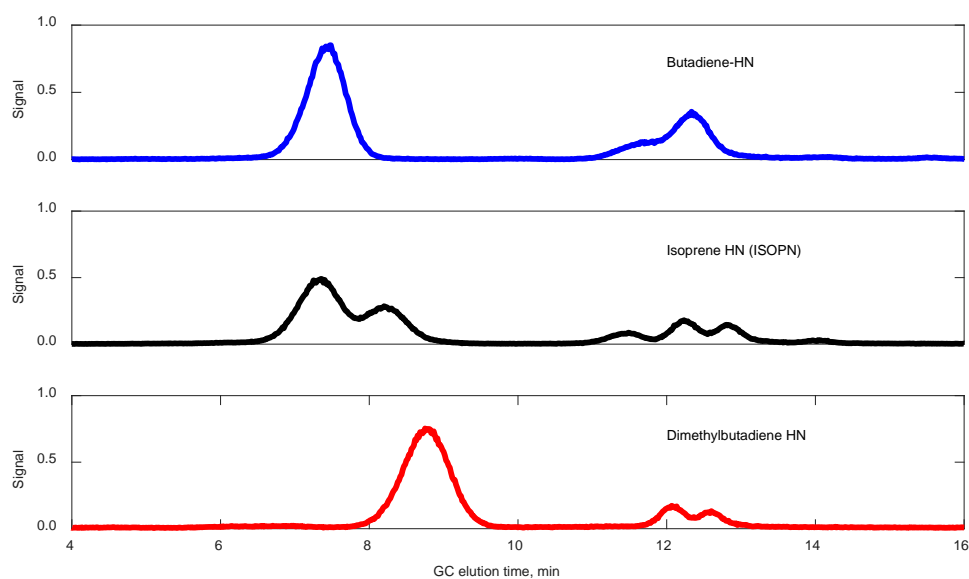


**Figure S28** – Hydroxy nitrates formed from 1,3 butadiene, isoprene, and 2,3 dimethyl 1,3 butadiene (297 K) at bimolecular lifetimes less than 0.01 s. The chromatograms have been normalized to the size of the  $\beta$  peak(s).

## 11. References

- (1) Lee, L.; Teng, A. P.; Wennberg, P. O.; Crouse, J. D.; Cohen, R. C. *J. Phys. Chem. A* **2014**, *118*, 1622.
- (2) Crouse, J. D.; Paulot, F.; Kjaergaard, H. G.; Wennberg, P. O. *Phys. Chem. Chem. Phys.* **2011**, *13*, 13607.
- (3) Paulot, F.; Crouse, J. D.; Kjaergaard, H. G.; Kroll, J. H.; Seinfeld, J. H.; Wennberg, P. O. *Atmos. Chem. Phys.* **2009**, *9*, 1479.
- (4) Lei, W.; Zhang, R.; Sean McGivern, W.; Derecskei-Kovacs, A.; North, S. W. *Chem. Phys. Lett.* **2000**, *326*, 109.
- (5) Peeters, J.; Nguyen, T. L.; Vereecken, L. *Phys. Chem. Chem. Phys.* **2009**, *11*, 5935.
- (6) Peeters, J.; Boullart, W.; Pultau, V.; Vandenberg, S.; Vereecken, L. *J. Phys. Chem. A* **2007**, *111*, 1618.
- (7) Park, J.; Jongsma, C. G.; Zhang, R.; North, S. W. *Pccp* **2003**, *5*, 3638.
- (8) Teng, A. P.; Crouse, J. D.; Lee, L.; St. Clair, J. M.; Cohen, R. C.; Wennberg, P. O. *Atmos. Chem. Phys.* **2015**, *15*, 4297.
- (9) Sprengnether, M.; Demerjian, K. L.; Donahue, N. M.; Anderson, J. G. *J. Geophys. Res. Atmos.* **2002**, *107*, 4268.
- (10) Liu, Y. J.; Herdlinger-Blatt, I.; McKinney, K. A.; Martin, S. T. *Atmos. Chem. Phys.* **2013**, *13*, 5715.
- (11) Tuazon, E. C.; Atkinson, R. *Int. J. Chem. Kinet.* **1990**, *22*, 1221.
- (12) Paulson, S. E.; Flagan, R. C.; Seinfeld, J. H. *Int. J. Chem. Kinet.* **1992**, *24*, 79.
- (13) Miyoshi, A.; Hatakeyama, S.; Washida, N. *J. Geophys. Res.* **1994**, *99*, 18779.
- (14) Ruppert, L.; Heinz Becker, K. *Atmos. Environ.* **2000**, *34*, 1529.
- (15) Karl, M.; Dorn, H. P.; Holland, F.; Koppmann, R.; Poppe, D.; Rupp, L.; Schaub, A.; Wahner, A. *J. Atmos. Chem.* **2006**, *55*, 167.
- (16) Galloway, M. M.; Huisman, A. J.; Yee, L. D.; Chan, A. W. H.; Loza, C. L.; Seinfeld, J. H.; Keutsch, F. N. *Atmos. Chem. Phys.* **2011**, *11*, 10779.
- (17) St. Clair, J. M.; Rivera-Rios, J. C.; Crouse, J. D.; Knap, H. C.; Bates, K. H.; Teng, A. P.; Jorgensen, S.; Kjaergaard, H. G.; Keutsch, F. N.; Wennberg, P. O. *J. Phys. Chem. A* **2016**, *120*, 1441.
- (18) Rivera-Rios, J. C.; Nguyen, T. B.; Crouse, J. D.; Jud, W.; St. Clair, J. M.; Mikoviny, T.; Gilman, J. B.; Lerner, B. M.; Kaiser, J. B.; De Gouw, J.; Wisthaler, A.; Hansel, A.; Wennberg, P. O.; Seinfeld, J. H.; Keutsch, F. N. *Geophys. Res. Lett.* **2014**, *41*, 8645.
- (19) Nguyen, V. S.; Peeters, J. *J. Phys. Chem. A* **2015**, *119*, 7270.
- (20) Peeters, J.; Nguyen, T. L. *J. Phys. Chem. A* **2012**, *116*, 6134.
- (21) Peeters, J.; Müller, J. F.; Stavrakou, T.; Nguyen, V. S. *J. Phys. Chem. A* **2014**, *118*, 8625.
- (22) Jørgensen, S.; Knap, H. C.; Otkjær, R. V.; Jensen, A. M.; Kjeldsen, M. L. H.; Wennberg, P. O.; Kjaergaard, H. G. *J. Phys. Chem. A* **2016**, *120*, 266.
- (23) Bates, K. H.; Crouse, J. D.; St. Clair, J. M.; Bennett, N. B.; Nguyen, T. B.; Seinfeld, J. H.; Stoltz, B. M.; Wennberg, P. O. *J. Phys. Chem. A* **2014**, *118*, 1237.
- (24) Garden, A. L.; Paulot, F.; Crouse, J. D.; Maxwell-Cameron, I. J.; Wennberg, P. O.; Kjaergaard, H. G. *Chem. Phys. Lett.* **2009**, *474*, 45.
- (25) Ghosh, B.; Park, J.; Anderson, K. C.; North, S. W. *Chem. Phys. Lett.* **2010**, *494*, 8.
- (26) da Silva, G.; Graham, C.; Wang, Z.F.; *Environ. Sci. Technol.* **2009**, *44*, 250.

*Appendix B***SUPPORTING INFORMATION FOR CHAPTER 5: FORMATION  
AND FATE OF ORGANIC NITRATES IN THE SOUTHEASTERN  
UNITED STATES**

At the SOAS site, ISOPN measurements were taken by two instruments: the Caltech  $\text{CF}_3\text{O}^-$  CIMS and the Purdue  $\text{I}^-$  CIMS. The Purdue instrument was located inside a trailer on the ground, whereas the Caltech instrument was located on top of the walk up tower. The sensitivity of the Purdue instrument was significantly different than that of the Caltech instrument. The Purdue instrument had strong sensitivity dependencies to the various ISOPN isomers, and a particularly low sensitivity to the dominant ISOPN 1-OH, 2- $\text{ONO}_2$  isomer. This necessitated a correction to the raw signal for the ISOPN isomer distribution in the Xiong et al., 2015 measurements, which relied on modeling to determine this specific distribution. The Caltech CIMS measurements were not impacted by a large sensitivity difference, as noted in A. P. Teng, Crouse, and Paul O Wennberg, 2017. The two ISOPN measurements show a strong correlation when the uncorrected (to a 4-OH, 3- $\text{ONO}_2$  sensitivity only) Purdue measurements are compared to the Caltech measurements. Using the model-based results from the Purdue measurements decreases the correlation between these two measurements. This may be due either to an underestimation of the Purdue sensitivity to the 1-OH,  $\text{ONO}_2$  ISOPN isomer or that the 1-OH,  $\text{ONO}_2$  isomer is significantly less abundant than implied by the modeling in Xiong et al., 2015.

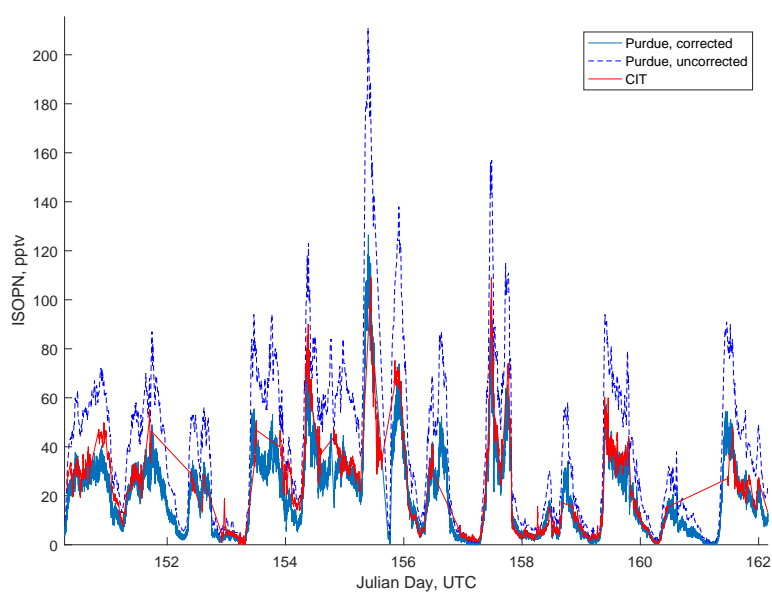


Figure B.1: The Purdue instrument correlates well to the CIT instrument using just raw, unadjusted data. The modeled data, which uses a kinetic model to estimate the ISOPN isomer distribution and then applies a correction for individual ISOPN isomers, correlates less well with the CIT instrument measurement for ISOPN.